INVESTIGATIONS OF MOUNTAIN LEE WAVES AND THE AIR FLOW OVER THE SIERRA NEVADA

JÖRGEN HOLMBOE
Project Director

HAROLD KLIEFORTH
Associate Project Director

Department of Meteorology
UNIVERSITY OF CALIFORNIA
Los Angeles

FINAL REPORT
MARCH 1957
CONTRACT NO. AF [redacted]

Sponsored by
THE GEOPHYSICAL RESEARCH DIRECTORATE
U. S. AIR FORCE

PREFACE

The investigations of the air flow across the Sierra Nevada were started at UCLA in the late summer of 1950. Preliminary experimental field investigations with sail planes were made in the Owens Valley during the winter of 1950-51, and a more fully developed field program was carried out during the following season, 1951-52. This work was undertaken jointly by a number of cooperating agencies. The technical aspects of the work have been described in earlier technical reports. A summary is given in the final report of the Sierra Wave Project, Contract No. AF 19(122)-263 which was issued in July 1954. This report also discussed the evaluation and reduction of the observational data as far as it had been completed at the time.

The further analysis of the observations and the synoptic analysis of the cross-mountain flow patterns were continued under the present contract and the results are discussed in this final report. Also included (Chapter 6) is a discussion of the observations from a later field investigation in the spring of 1955, which was undertaken under a separate project, Contract No. 19(604)-1308. The analysis was carried out jointly by Harold Klieforth and Einar Hovind. The major part of the report which describes and discusses the data reduction and the analysed flow patterns has been written by Klieforth. The observed turbulence and the flight hazards of mountain waves are discussed by Kuettner in Chapters 10 and 11. A review of the linear theory of stationary cross-mountain flow, including comparison of the theoretical models with the observed flow patterns is given in Chapter 12 by Holmboe.

TABLE OF CONTENTS

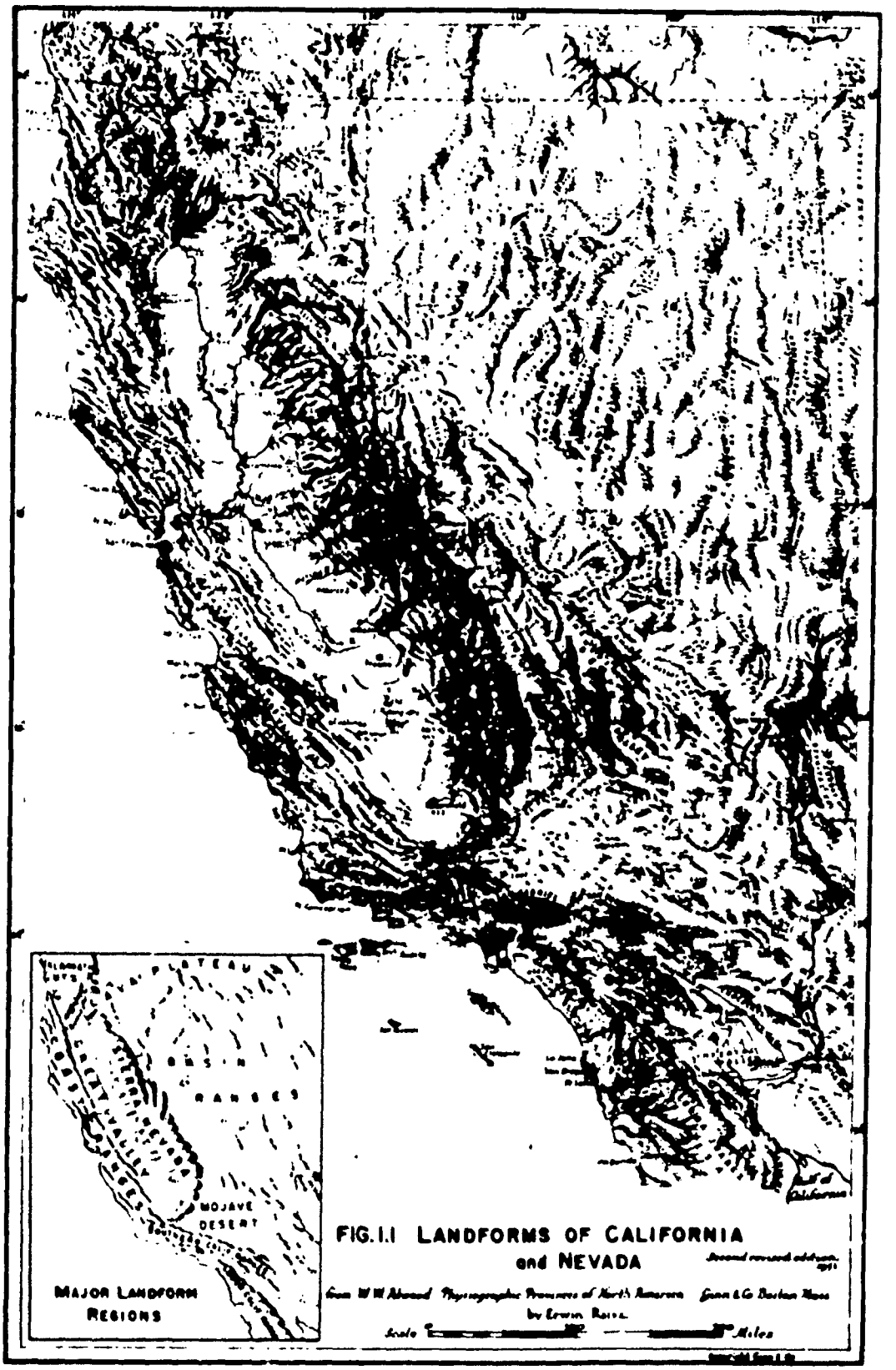

FIG. I.I LANDFORMS OF CALIFORNIA and NEVADA

Second revised edition, 1951

From W.W. Atwood Physiographic Provinces of North America Ginn & Co. Boston Mass.

by Erwin Raisz

Scale 0 Miles

1. THE OBSERVATIONAL DATA

Introduction.

In this chapter is presented a review of the observations made on the three field expeditions of the Mountain Wave Project from 1951 to 1955, inclusive. All of the explorations were conducted over and in the vicinity of the southern or High Sierra in eastern California. The various equipment and observational techniques, particularly the use of sailplanes, have been discussed in detail in previous reports of The Southern California Soaring Association (S.C.S.A.) in 1952 and the Meteorology Department of the University of California at Los Angeles (U.C.L.A.) in 1954 and 1955. In the following sections are summaries of the data with mention of where they are treated in later chapters. A brief description of the study region is given first.

Physiography of the Southern Sierra and Owens Valley region.

The Sierra Nevada is a single, unbroken mountain range with a length of about 400 miles and a width varying from 50 to 80 miles (Fig. 1.1). Although the range extends roughly northwest-southeast between latitudes 35° and 40° North, the main crest of the High Sierra which borders on Owens Valley is only about 14° from a north-south orientation. In this southern portion of the range the crest is the highest, generally about 12,000 feet, and with numerous peaks rising over 14,000 feet. There the eastern scarp is most abrupt, it is remarkably straight, and the Owens Valley, to the east at an average elevation of about 4,000 feet, is of nearly uniform width (Fig. 1.2).

In form, the southern Sierra profile is strongly asymmetric; its appearance has been likened to that of a huge ocean wave rolling in from the west. The western slope rises gradually in rolling foothills from the San Joaquin Valley to the jagged peaks which form the crest of the range. The eastern front, one of the greatest escarpments in the world, towers high above the Owens Valley. The San Joaquin, Kings, the Kern, and other rivers have cut deep canyons on the western slope while on the eastern slope there are shorter, steeper canyons. The high country has been sculptured by glaciation and in many of the eastern valleys glacial moraines reach nearly to the Valley floor. Volcanic activity has formed a slight constriction of lava flows and cinder cones in the central portion of the Owens Valley.

The east wall of Owens Valley is the large fault-block range known as the Inyo Mountains to the south of and the White Mountains to the north of 7,000 foot Westgard Pass. The Inyo Mountains have an average elevation of 9,000 to 11,000 feet, while the White Mountains, rivaling the Sierra in height, culminate in 14,254 foot White Mountain Peak just northeast of Bishop. The western slope of these desert mountains is a fault scarp at the base of which the Valley reaches its lowest elevation. The floor of the eastern side of the Valley is fairly level but on the western side it rises in a broad alluvial apron to about 6,000 feet where it meets the steep flanks of the Sierra (Fig. 1.3).

Near Bishop there is a jog in the Sierra crest; the highest peaks are much farther west and the Valley widens considerably. In this, the northern

Fig. 1.2. Topographic map of the Sierra Wave Project field area showing the tracking network and the location of the barograph stations (From the U. S. G. S.)

Fig. 1.3 - An aerial view of the High Sierra from the east. Mt. Whitney is in the center.

Fig. 1.4 - One of the Pratt-Read sailplanes at the Bishop Airport with wave and roll clouds to the north.

end of Owens Valley, the Sierra crest is about 25 miles west and the White Mountains about 10 miles east of the center of the Valley. In the central portion of the Valley near Independence - the region in which the aerial explorations of the Project were made - the width of the Valley is about 10 miles and the distance from the crest of the Sierra to the crest of the Inyo Mountains is about 18 miles (Fig. 1.2). In the latter region the relative uniformity and simplicity of the topographic profile make it nearly ideal for the investigation of lee wave phenomena. For an east-west canyon along which to measure lee side pressures and down-slope winds, the topography was less favorable; the valleys which drain the east side of the Sierra are narrow, steep, curving, and quite unlike the broad, straight glacial valleys of the Alps where the classical föhn observations were made. The valley of Independence Creek, west of Independence and east of Kearsarge Pass, was chosen.

Sailplane measurements.

The principal tool of research on all of the field projects of this investigation has been the instrumented sailplane. The greatest assets of the sailplane for this work are its relatively slow flying speed, its independence of power, and its consequent ability to measure to a satisfactory degree of accuracy the vertical and horizontal components of the wind velocity. It was the science and sport of soaring flight that first explored and made known the gross structure of the Sierra Wave and whose observations instigated the initial Sierra Wave Project. The use of the sailplanes in project operations, their instrumentation, and the data obtained from these flights have been discussed in detail in earlier reports given as references at the end of this chapter. Only a summary of that information is given here.

In the fall and winter of 1951-2 sailplanes were tracked in flights in the lee flow of the Sierra by a network of 3 photo-theodolites, a radar set, and a Raydist system. Upwind, downwind, crosswind, and hovering runs and combinations of these were chosen to traverse the various parts of the lee wave flow according to their practicability under different wind and weather conditions. The locations of the tracking devices and the region over which the flights were made are shown in Fig. 1.2. The Pratt-Read sailplanes used (Fig. 1.4) were two-place, had a wingspread of 50 feet, and a gross weight of about 1,400 pounds. The principal instruments borne by the sailplane were a clock, altimeter, rate of climb indicator, outside air thermometer, airspeed indicator, direction indicator, and accelerometer (Fig. 1.5). The dial of these instruments in the panel of the sailplane were photographed at intervals of one or two seconds by 16 mm cameras mounted behind and to one side of the heads of the two-man crew (Fig. 1.6). Basic equipment of the sailplanes included a pressure oxygen breathing system, instrument-flight equipment, radio communication, barograph, and, for the crew, warm flying suits, parachutes, and oxygen masks. The ground tracking measurements of the 3 theodolites and the radar set were recorded as synchronous photographs at 5-second intervals of the corresponding time and instrument dial readings. The Raydist tracking data were recorded as brush recordings of the Raydist system's electronic signals. From 26 November, 1951 to 30 March, 1952 there were 24 tracking operations and of these about 50 per cent of the cases have yielded useful data for analysis. A complete description of these data and their reduction are given in Chapter 2, and the meteorological analyses in Chapter 3.

Fig. 1.5 - Cabin of Pratt-Read sailplane showing instrument panel, plexiglass canopy, and control stick.

Fig. 1.6 - Rear of sailplane cabin showing two 16 mm cameras, barographs, battery boxes, seat backs and shoulder straps.

The very brief field season from 22 March to 6 April, 1954 accomplished two important results which laid the groundwork - or, more appropriately, "airwork" - for the 1955 investigation. First, a combined wave exploration by a B-29 and a sailplane on 29 March proved the feasibility of a new measuring technique. Secondly, a sailplane flight on 4 April to 35,000 feet altitude over the Owens Valley and the subsequent cross-country flight to Las Vegas established the existence and movement of "jetlets" or travelling wind speed maxima. The decisions to use powered aircraft in a more extensive field program and to investigate the relationship of the mountain wave to wind velocity maxima formed the basis of the plan for the new project.

In the spring of 1955 sailplanes were again employed for lee wave observations, some of which were made in conjunction with traverses by the instrumented powered aircraft. The sailplane flights, which were not tracked, obtained vertical velocity measurements to be combined with the measurements of temperature, air speed, pressure, and wind obtained by the powered planes. There were three such combined operations and several other days on which lee waves were explored by sailplanes alone and for which soundings and observations were thus obtained. The majority of these flights reached altitudes higher than 40,000 feet. In all the flights of all seasons the sailplane data consist of films of the instrument panel and the reports and observations of the crew.

Powered aircraft data.

During the last two months of the 1952 season power plane flights with an attached meteorograph were made in the lee of the Sierra. The BT-13 towplane was used, taking off before a planned sailplane tracking flight, to serve the dual purpose of ascertaining the strength of the developing updrafts and collecting data in soundings and cross sections of the roll cloud region. The standard aircraft instruments were included in the observer's cockpit panel. Other equipment installed were an oxygen breathing system, radio communication, an intervalometer for recording time marks on the meteorogram, and a special thermistor-type thermometer with sensing element mounted in the leading edge of one wing. Although it was attempted to track these flights with radar, the method proved impracticable and knowledge of space positions was almost entirely dependent on the notes of the observer. There were 22 such flights made from mid-February to the end of March 1952 and of these about 6 provide data from lee wave and roll cloud developments. The basic data are the meteorograms with supplementary notes by the observer giving synoptic records of time, altitude, temperature, air speed, rate of climb, compass heading, positions over the terrain, and information as to when time marks were made, the positions of clouds, and photographic data. These observations are treated in Chapter 4.

In 1955 meteorograph flights were also used, but the principal contributions of powered aircraft to wave exploration were the techniques employed by the B-29 and B-47 of Project Jet Stream. These instrumented weather aircraft, earlier used for hurricane reconnaissance and jet stream exploration, made coordinated flights with the sailplanes in strong lee waves on three days in April, 1955. The traverses of these aircraft through the mountain flow at altitudes from 20,000 to 40,000 feet have provided the most complete nearly-synoptic cross sections of the mountain wave including important and hitherto missing data on the structure of the flow upwind of the

mountain range, in the roll cloud region, and in the stratosphere. Both aircraft were equipped with the new automatic navigation equipment which gives continuous readings and recordings of the true wind. The raw data are in the form of aerograms, films of the instrument panels, wind measurements, and notes of the co-pilots. These have been made available to the Project for integration with the sailplane measurements and the large-scale surface and upper air observations of the region. Chapters 6 and 8 are devoted to the meteorological results of the 1955 field work.

Cloud photography.

A valuable supplement to the aerial measurements and synoptic observations is the file of motion pictures and still photographs of cloud formations and developments. Most of the motion pictures were taken by time-lapse cameras in which frames were exposed at one or two second intervals thus artificially speeding up the projected rate of cloud movement by 16 or 32 times. Studies of these films of wave and roll cloud developments give much insight into the time variations of the air flow. Also, the best sequences of these films have been combined into documentary films which have been shown to thousands of military and civilian pilots and thus have provided an educational service of inestimable value. The still photographs - both black and white and color transparencies - have been used as an integral part of the complete synthesis of the available meteorological data for all the cases studied. Since these photographs were supplemented by pertinent notes and are applicable to elementary techniques of photogrammetry, they provide information that is also of quantitative value. Illustrations of cloud phenomena appear in Chapters 3, 4, and 6.

Other meteorological observations.

Several types of observations and measurements other than aircraft flights and cloud photography were made in the Sierra Nevada and Owens Valley region for the purposes of the Mountain Wave Project. Observations which were of great importance to the synoptic studies were available from the network of Weather Bureau and military weather stations in the surrounding region. These various types of data are listed and briefly discussed below.

Pilot balloon soundings. One of the many valuable contributions of the Weather Bureau to the Project was the program of double-theodolite pilot balloon wind measurements at the Bishop Airport. These soundings were begun in 1951, were taken twice daily (at 0700 and 1200 PST) during the 1951-2 season, and once daily (1200 PST) in the spring of 1955. The data have been used for the synoptic study of the air flow over the Sierra, the change of the vertical wind profile in the mountain flow, and as exhibit "A" of the errors inherent in single-theodolite computations in regions of large vertical air currents. The latter subject has been treated by De Ver Colson (1952) of the Weather Bureau, using some of the Bishop observations. Several Bishop wind soundings are reproduced in Chapter 3 and an example of the effect of the lee wave on the balloon's path is shown in Chapter 4.

Radiosonde ascents from Sequoia. Measurements of the upper air temperature, pressure, and relative humidity over the windward slope of the Sierra were made at 1000 local time (PST) on 70 days of the period 5 December, 1951 to 30 March, 1952. The balloons were released from a station at Lodgepole at an elevation of 6,760 feet in Sequoia National Park by a team of two Weather Bureau observers. During the latter half of the period wind measurements were made on days when the observer could follow the radiosonde balloon with a theodolite. Several of the ascents were made near the time of tracked sailplane flights and have been treated in the study of the disturbed flow rather than as being representative of "upwind," i.e., "undisturbed," conditions. All of the 70 soundings have been studied carefully and analyzed with other observations from surrounding stations since they provide rarely obtainable data from a high elevation for a general investigation of mountain flow and in particular the flow over the Sierra. Lodgepole soundings are shown and discussed in Chapters 3 and 4 and the observations are plotted on the synoptic charts of Chapter 5.

Surface measurements from recording instruments. Surface pressures were measured in 1951-2 by seven barographs placed in various cabins in a cross section of the floor of Owens Valley and the eastern Sierra slope in the sailplane tracking area. These provide continuous barograms for the period 18 November, 1951 to 1 April, 1952, with the exception of a few lapses in the records of the highest stations when these were inaccessible because of severe snow storms. Other data from recording instruments of the 1951-2 season are anemograms from Manzanar near the center of Owens Valley and, for the last six weeks of the season only, thermograms from Manzanar. It may also be added here that barograms and thermograms were available from the Weather Bureau station at the Bishop Airport and have been used for every season of field operations. Surface measurements for selected cases are analyzed in Chapter 4.

During the Mountain Wave-Jet Stream Project of 1955, no special barographs were employed because of the unavailability of the instruments and the lack of additional personnel to tend them. However, for the period 24 April to 24 May, 1955 a special network of five sensitive pressure variographs was placed in the form of a large cross with the center at the Bishop Airport. Two of the other stations were on the eastern Sierra slope, one west of Bishop, the other west of Big Pine, another was in the Chalfant Valley north of Bishop just west of White Mountain Peak, and the fifth was east of Bishop at Deep Springs in the lee of the White Mountains. These instruments recorded changes of pressure at a frequency of the order of 10 to 20 minutes, filtering out both local gusts and pressure changes associated with the movement of large-scale synoptic systems. While these variograms which are the property of Project Jet Stream have not been analyzed yet, they may later provide some interesting information on travelling waves associated with strong wind velocities aloft and, perhaps, on non-steady conditions of lee waves and the interaction of travelling and stationary waves.

Surface measurements from mobile observations. For the same period in the spring of 1952 during which the meteorgraph flights were inaugurated and the number of barographs were increased, special observations at half mile intervals were made across Owens Valley to about 7,000 feet altitude on the Sierra slope. These observations were made by Dr. Joseph Knox on 11 days of February and March, 1952, and, since they were selective with respect to the

synoptic situation, all of the cases provide valuable data to be used in conjunction with aerial measurements and/or other meteorological observations. The data consist of readings of altimeter, aneroid barometer, thermometer, anemometer, and notes and photographs of the cloud phenomena. The value of these measurements has increased since the re-survey of the area and the recent publication by the U. S. Geological Survey of detailed topographic maps with 40 foot contour interval and a scale of 1:62,500. Analyses of these observations are included in Chapter 4.

Weather logs. Daily records of local meteorological observations were kept by the meteorologist in each of the three field seasons. These records contain notes on cloud development, special phenomena, and information of the overall synoptic events. On the days of project flights these notes were expanded and formalized into weather reports with sections on the upper air and surface synoptic situation and development derived from analyzed maps, and significant local observations. They also include lists of photographs or time-lapse motion pictures taken, and the number and times of flights, thus providing both a brief description of the weather phenomena and the data available for study. Since these observations extend over longer periods than those of the actual field work - the whole year of 1955 is thus covered - the logs provide additional records of the frequency and seasonal distribution of storms, lee wave occurrences, and other weather phenomena.

Synoptic data. The project had access to the daily observations made at the Bishop Airport and retained for special days the circuit "A" teletype records received at Bishop. The teletype data giving hourly and 3-hourly surface observations from California and Nevada stations were used for analyses of synoptic maps and cross sections. Many of these data were also retained in the form of plotted and analyzed surface maps prepared daily by the project and/or Weather Bureau meteorologists at the Bishop Airport. Other analyzed maps, such as the facsimile charts received at the Bishop Airport during the 1951-2 and 1955 field operations and the Daily Weather Maps, were saved for knowledge of the large-scale situations and their evolution. Some climatological data have been used for detailed case histories of particular storms, particularly the precipitation records for studies of orographic rain and snowfall. An example of the latter is given in Chapter 5 in a section entitled "The Effect of the Sierra Nevada on a Pacific Storm."

Some valuable observations at non-synoptic times were provided by the Navy. At the two White Mountain Research Laboratories of the Navy and the University of California at 10,500 and 12,470 feet, respectively, about 10 miles northeast of Bishop, daily records of pressure, temperature, humidity, wind, and weather at 0800 PST were recorded. At the Naval Ordnance Test Station near Inyokern, about 130 miles south-southeast of Bishop, once or twice daily radiosonde and pibal soundings were made. These data, taken at 0500 PST and sometimes also at 1000 PST, were used with those from 1000 PST at White Mountain on the appropriate 0700 PST (1500 GCT) isobaric upper air charts of Chapters 5 and 6 as aides in synthesizing the contour field in the area of high mountains.

The primary source of data for the large-scale synoptic studies were the Upper Air Bulletins and teletype records of raobs and rawins received and filed at U.C.L.A. The region of interest for periods chosen for careful analysis was the whole western United States with emphasis on the area enclosed by

the Weather Bureau upper air sounding stations at Medford, Oakland, Santa Maria, Las Vegas, and Ely (Fig. 1.7). These upper air data for the 1951-2 analyses are from 1500 GCT (0700 PST) and 0300 GCT (1900 PST), and the more nearly synoptic of these with respect to the time of the flight usually preceded or followed the flights by three to six hours. From 1 December, 1951 to 1 March, 1952 6-hourly radiosonde and rawin soundings from Castle Air Force Base at Merced provided extremely important measurements of the air flow over the Great Valley immediately west of the Sierra Nevada.

However, the most complete overall synoptic upper air coverage was that of the spring of 1955 when the flight operations fortuitously coincided with the series of atomic bomb experiments at the Nevada Test Site of the Atomic Energy Commission (A.E.C.). During the period from mid-February to mid-May, 1955, the five Weather Bureau stations mentioned above took observations thrice daily at 1500, 2100, and 0300 GCT as did the additional stations in the A.E.C. network - Stead Air Force Base at Reno, Tonopah, Fresno, and Camp Mercury. The network was further augmented by other radiosonde stations such as Yuma and Edwards Air Force Base and six special A.E.C. pilot balloon stations at Furnace Creek, Needles, Round Mountain, Beatty, Caliente, and St. George. (See map, Fig. 1.7.) In addition to the greater density of the network and the more frequent observations in comparison with the relatively sparse upper air coverage of 1951-2, the far greater number of wind data as a result of improved equipment is strikingly evident. Thus the most complete data for the synthesis of the large-scale patterns of air flow over the Sierra Nevada are those from the 1955 season.

References.

Colson, D. (1952): Results of Double-Theodolite Observations at Bishop, Cal., in Connection with the "Bishop-Wave" Phenomena. Bull. Amer. Met. Soc., Vol. 33, No. 3, pp. 107-116.

Holmboe, J., and Klieforth, H. (1954): Final Report, Sierra Wave Project. Meteorology Department, University of California, Los Angeles. A.F.C.R.C. Contract AF 19(122)-263.

Klieforth, H. (1955): Final Report, Mountain Wave-Jet Stream Project. Meteorology Department, U.C.L.A. A.F.C.R.C. Contract AF 19(604)-1308.

Saudek, V., et al (1952): Mountain Wave Project Report No. 3, October, 1951, to October, 1952. Southern California Soaring Association, Inc. Meteorology Department, U.C.L.A. Contract AF 19(122)-263.

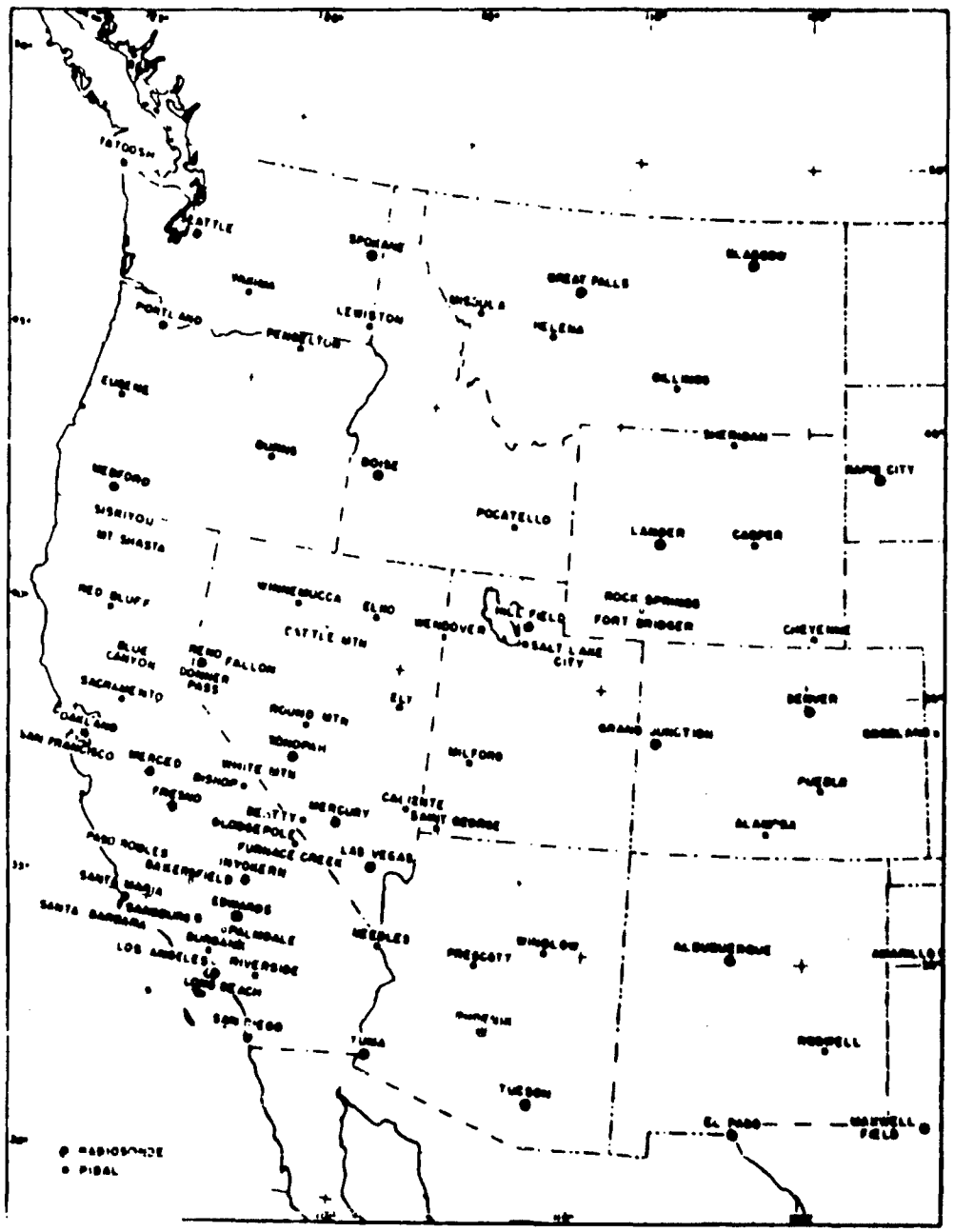

Fig. 1.7 - Map of western United States showing weather stations reporting in 1951-52 and/or 1955.

2. DATA REDUCTION PROCEDURE

Introduction.

This chapter deals primarily with the reduction of the flight and tracking data from the 1951-2 season although the discussion of sailplane data reduction is equally applicable to that of the later field seasons. The first part of the story dealing with the tracking data from phototheodolites, radar, and Raydist has been placed in an Appendix at the end of this report. Procedures and sources of error are discussed there with some detail as the experiences gained with this kind of meteorological high altitude tracking of erratic targets may be of special value to future research programs. Below are treated the sailplane measurements and the integration and synthesis of tracking and airborne data into primary meteorological fields. The relatively simple and straightforward reduction and correction of other data such as that from the meteorograms, barograms, and soundings will be discussed briefly in later chapters where pertinent.

Airborne measurements.

Instruments and data. A photograph of the sailplane instrument panel is shown in Fig. 1.5 and in Fig. 2.1 is shown a sample frame from the film exposed during one of the flights. The instrumentation and flight procedures of the sailplanes have been discussed at length in previous reports; as a resumé of the meteorologically significant instruments, their indicated readings, and the degree of accuracy to which it was possible to record the readings from the film, the following table is presented:

Instrument	Indicated reading	Units	Read to nearest
air speed indicator	air speed	knots, mph	± 1.0 knot
clock	time	hr, min, sec	± 0.5 s
altimeter	altitude	feet	±20.0 ft
rate of climb (or sink) indicator	rate of climb (or sink)	feet min^{-1}	±50.0 ft min^{-1}
direction indicator	magnetic heading	degrees	± 1.0 deg
thermometer	air temperature	^{o}C	± 0.5 ^{o}C

All of the sailplane films for which there were corresponding tracking data were read and recorded. The total flight time of the sailplane was limited by the oxygen supply of 4½ hours and the time during tracking operations by the 1½ hour film supply in the two cameras. These limitations were allowed for in planning the operation so that where there exist

tracking data without sailplane data the loss of the latter can be ascribed to failures in the photography of the instrument panel; either the film failed to transport or it was unreadable entirely or in part because of poor lighting or because of interference by parts of the clothing of the crew. To each of the above six instrument readings except the time, which was adopted as the standard for the flight, a series of corrections was applied to obtain the quantities needed for integration with the trajectory data.

Symbols and notation. The following symbols and notation apply to the airborne measurements:

t time, indicated and "true" in hours, minutes, and seconds.

V_I indicated air speed.

Z_I indicated altitude.

$(dZ/dt)_I$ indicated rate of climb.

α_I indicated compass heading in degrees.

T_I indicated free air temperature.

Z_p pressure altitude in the U. S. Standard Atmosphere.

T temperature.

α geographical heading in degrees (true north = 360^o).

V_A true speed of the sailplane with respect to the air.

w_A sinking speed of the sailplane with respect to the air.

w_I "indicated" sinking speed of the sailplane corresponding to V_I.

A altimeter setting in inches of mercury.

c_1 altimeter correction for instrument error and hysteresis, a function of altitude and direction of vertical motion.

c_2 altimeter correction for static errors, dependent upon altitude and air speed.

ρ density.

ρ_o density at sea level corresponding to STP: 760 mm, 0^oC.

Time. While the reading of the instrument panel clock gave the official time to which all the other instrument readings were referenced, correlation with the 5-second pulses of the tracking network depended on the time of the blackouts. The latter, given usually every two minutes, were indicated on the instrument panel by a small light which was turned on by the observer on the count down from the tracking control operator. Since the cameras took

photographs at either one or two second intervals, there was the possibility of a maximum absolute error of one or two seconds, depending on which camera was used, in correlating the sailplane measurements with those of the theodolites.

Pressure altitude. Determination of pressure altitude from indicated altitude required knowledge of the altimeter setting used, the instrument calibration curves--two, according to whether the altitude was increasing or decreasing--and the corrections for static pressure effects which were related to the air speed. Accordingly, the formula used was:

$$Z_p = Z_I + c_1 + c_2 + 925\ (29.92 - A)$$

The altimeters were calibrated at U.C.L.A. immediately after the field work. Static pressure corrections were determined in calibration flights by the Southern California Soaring Association (S.C.S.A.) and by laboratory tests of the calibration equipment. Altimeter settings were recorded by the observer and/or could be read from the altimeter dial on the film. There were then three calibration curves for the altimeter, two for c_1, and one for c_2; the correction for altimeter setting was constant for the entire flight. In order of magnitude, c_1, which was as large as $\pm$300 feet at 40,000 feet, was generally larger than c_2 which varied from 0 to $\pm$30 feet. The difference in hysteresis correction between ascent and descent was of the order of 250 feet at high altitudes. The correction for altimeter setting was sometimes of the order of 300 feet. Accuracy of the final result could not be definitely known but a careful estimate of possible random errors and the reading accuracy suggest that the largest absolute error would be $\pm$40 feet at sea level and increasing to $\pm$100 feet at 40,000 feet. Relative errors from point to point were negligible except where the sailplane changed from ascent to descent or vice versa, and these discontinuities were largely eliminated by smoothing.

Temperature. One of the deficiencies of the sailplane instrumentation was the lack of a very accurate and precise thermometer. Those used in the project flights were of the thermocouple type consisting of a copper-constantin sensing element placed on the fuselage where dynamic heating was negligible, a thermos ice-in-water bath, and an indicator dial which could be read to the nearest 0.5°C. There were three such units used, all of which were calibrated while removed from the aircraft during and after the flight season. Some uncertainty, of course, exists about the effects of airspeed, radiation, and low temperatures of the indicating mechanism. During the first few flights of the season a 40-pound thermistor-type unit was used before its weight caused it to be removed from the sailplane. It was considered accurate to $\pm$0.2°C and on one flight was used together with the most frequently used thermocouple unit. These data provided a further check and flight calibration of the latter. Considering the overall accuracy, it is estimated that the corrected temperature is known to $\pm$1.5°C absolute error; it is possible that in extreme cases the absolute accuracy was less than this, say $\pm$3.0°C, but the internal consistency of the readings was better than this--probably $\pm$1.0°C--and the relative accuracy $\pm$0.5°C.

Heading. The magnetic direction indicators used in the sailplanes were calibrated at the Bishop Airport by swinging the sailplane on an accurately marked magnetic compass rose. Several calibrations were made for the different instrument panel ensembles used for various periods of the season. Since the compass was affected by banking or turning in flight it could not give reliable readings of the direction of the aircraft except in straight flight. The correction curves combined corrections for effects of the metal parts in the vicinity of the compass with corrections for magnetic variation and declination (17° E of N at Bishop). Theoretically, the absolute accuracy of the corrected readings should be about ±2 degrees or perhaps ±3 degrees. It should be pointed out that if there was any yawing in the flight the error would be augmented by the angle of yaw since the direction of travel relative to the air would be different from the direction of alignment of the fuselage. However, in straight flight the pilots attempted to eliminate this effect.

True air speed and velocity. A calibration curve for the air speed indicators combined corrections for instrument errors and errors in the static and dynamic pressure sources. True air speed is a function of density, ρ, and thus of Z_p and T, or:

$$V_A = V_I \left(\rho_o/\rho\right)^{\frac{1}{2}} = V_I \, f(Z_p, T)$$

The total velocity of the sailplane with respect to the air was described by combining the speed V_A with the geographic heading, α. The accuracy of the velocity computations was primarily dependent on the accuracy of the compass readings. As a further reduction, V_A was also interpreted as being practically equal to its horizontal component since the glide angle was small; the glide ratio which is constant with altitude was never smaller than 10:1.

Sinking speed. Two effects contribute to the effective glide angle of a sailplane in flight: the first and greater is the natural sinking speed in still air at a given air speed and the second is a dynamic rise which may accompany any dynamic soaring maneuver. The latter effect is absent in a steady glide and could not be corrected for in the turns. A third effect, a dynamic inertia reaction, could be expected to occur where there were large accelerations; this could not be measured well enough to apply corrections but was important to note in those rather brief periods when turbulence was experienced. The principal dependence is on air speed, and these calibrations were performed in relatively still air over the Pacific Ocean near Santa Monica. A conservative estimate of the maximum effect of some varying vertical motion in the air--probably general subsidence rather than convection--is ±0.3 feet per second. Calibration curves were prepared for the determination of the "indicated" sinking speed corresponding to a given indicated air speed. Then the true sinking speed of the sailplane with respect to the air was determined in the same manner as the true air speed given w_I, Z_p, and T:

$$w_A = w_I \left(\rho_o/\rho\right)^{1/2} = f(Z_p, T)$$

Summary. The corrected quantities derived from the airborne measurements and their estimated accuracies are:

Corrected flight data	Symbol	Estimated accuracy
time	t	±0.5 second
pressure altitude	Z_p	±40 ft msl to ±100 ft at 40,000 ft (relative accuracy ±20 ft)
true air speed	V_A	±3 ft s^{-1}
heading	α	±3 degrees
sinking speed	w_A	±0.3 ft s^{-1}
temperature	T	±1.5° C. (relative accuracy ±0.5°C)

Comparing these accuracies, temperature measurement appears to be the weakest link of the airborne data.

Synthesis of tracking and airborne data.

General considerations. Given the basic data one had to decide upon the manner in which to treat them in order to derive the most meaningful patterns of the pertinent meteorological fields--those of motion, temperature, and pressure--in the leeward flow. The choice was influenced first of all by the limitations and coverage of the data: a thread of measurements taken during a finite period of time through a volume of the atmosphere. Secondly, for comparison with theory, hydrodynamical models, and other lee wave observations, it was important to obtain a synoptic picture of the air flow in the vertical plane perpendicular to the mountain range. To satisfy both of these considerations, it was decided to analyze the field of motion in the form of streamlines in the plane perpendicular to the Sierra crest in the Independence-Manzanar tracking area. The other important meteorological variables, temperature and pressure, were analyzed as isotherms, isolines of potential temperature, and D values in the same cross section.

In order that these results can be considered as representing "synoptic" conditions, two assumptions are implied: 1) There was a steady state or $\partial/\partial t = 0$; 2) the flow was two-dimensional, i.e., $\partial/\partial y' = 0$ where y' is the coordinate parallel to the Sierra crest. We thus are forced to consider as negligible actual changes in the variables in time and "latitude" (y') but commit the assumptions to mind in order that they may later be examined for their effect on the representativeness of the results.

Symbols and notations.

t	time.
Z_p	pressure altitude.
$\underset{\sim}{V}_A$	horizontal velocity of the sailplane with respect to the air.
V_A	horizontal speed of the sailplane with respect to the air. $V_A = \lvert \underset{\sim}{V}_A \rvert$.
α	geographic heading of the sailplane.
w_A	true sinking speed of the sailplane with respect to the air.
T	corrected free air temperature.
$P(x,y,z)$	position of sailplane determined by tracking system.
Z	geometric altitude above mean sea level.
$\underset{\sim}{V}_G$	velocity of sailplane with respect to the ground.
V_G	speed of the sailplane with respect to the ground. $V_G = [d(x,y)/dt]_S = \left((dx/dt)_S^2 + (dy/dt)_S^2\right)^{1/2}$
$\underset{\sim}{V}_H$	horizontal component of the wind velocity. $\underset{\sim}{V}_H = \underset{\sim}{V}_G - \underset{\sim}{V}_A$.
V_H	horizontal wind speed. $V_H = \lvert \underset{\sim}{V}_H \rvert$.
β	angle between $\underset{\sim}{V}_H$ and the x' axis.
x', y'	coordinates of reference system rotated and translated to origin O' on Sierra crest; x' along 70°, y' along 340°.
U	horizontal wind speed component along x'. $U = V_H \cos \beta$.
w_G	vertical speed of the sailplane with respect to the ground. $w_G = (dZ/dt)_S$.
S	distance measured along path of sailplane; as a subscript it refers to quantities measured along the flight path.
w	vertical wind speed. $w = w_G - w_A$.
ε	slope of a streamline in the (x',z)-plane. $\varepsilon = \arctan w/U$.
ε'	slope of streamline in exaggerated cross section. $\varepsilon' = \arctan 3w/U$.
V	total wind speed component in (x',z)-plane. $V = \left(U^2 + w^2\right)^{1/2}$
V'	total wind speed component in exaggerated cross section.

ρ	density. $\rho = p/R_dT$.
Δz	thickness of streamline channel on plotted cross section.
p	pressure.
F	mass flux.
$\Delta y'$	width of streamline channel.
C	constant.
R_d	gas constant for dry air. R_d = 287 kj per ton per °K.
$\varkappa_d$	Poisson constant. $\varkappa_d = R_d/c_{pd} = 2/7$.
θ	potential temperature in °K. $\theta = T(100/p)^{\varkappa_d}$.
D	"altimeter correction." $D = Z-Z_p$.

The basic charts. The primary quantities were the corrected airborne data, t, Z_p, V_A, α, w_A, and T; the space positions from the theodolites, P(x,y,z,t); and the positions from Raydist, P(x,y,t). The other meteorological variables were obtained as derivatives and combinations of these basic quantities by the procedures outlined below.

On centimeter graph paper the flight path was plotted in the (x,y)- and (x,z)- planes with every tenth point identified by its frame number. The scale in the horizontal was 1 centimeter = 1000 feet and in the vertical 3 centimeters = 1000 feet. Plotting accuracy was to the nearest 50 feet in the horizontal and to the nearest 20 feet in the vertical.

A time section of Z and Z_p was prepared on a continuous roll of graph paper. The scale was 1 cm = 5 or 10 seconds in the horizontal and 1 cm = 100 or 200 feet in the vertical. The time was labeled in frame numbers at the top and in hours, minutes, and seconds at the bottom. Different symbols were used for the points of both curves and in analyzing them the data was smoothed to reduce random errors in the tracking data and to minimize small discontinuities in the Z_p curve when the sailplane changed from ascent to descent or vice versa.

The third basic chart was the tephigram on which soundings of T,p were plotted to obtain an average lapse rate and an average density-height curve for use in depicting the field of motion as described below.

The horizontal wind. On the (x,y) chart of the flight path V_G was measured graphically for overlapping 50-second (10-frame) intervals. It was thought that this time interval would eliminate the effect of errors in the 5-second theodolite fixes and, especially, increase the probability of measuring the quasi-steady wind rather than short period gusts. These V_G values were measured only in essentially straight sections of the flight path. The graphical velocities were determined to ±1 foot per second and ±1 degree. The values were considered to apply at the midpoint of the time

interval. (It would have been possible to compute $V_G = [d(x,y)/dt]_S = [(dx/dt)_S^2 + (dy/dt)_S^2]^{1/2}$ on SWAC* but it was desired to use smoothed and adjusted trajectory data.)

On the sailplane computation sheets V_A was determined for the same 50-second intervals as V_G. This was done by averaging V_A and α separately for the interval. By inspection an estimate was made of the average value, the column of recorded values at one or two second intervals was scanned, residuals were added algebraically, and the estimated value was corrected by the appropriate amount. Since these calculations were made over essentially straight portions of the flight path during which V_A and α were nearly constant, the difference in the result between averaging by vectorial addition and division and that by determining separately the average magnitude and direction was negligible.

Using an accurate protractor and a metric ruler $\underline{V}_A$ was subtracted graphically from $\underline{V}_G$ to obtain $\underline{V}_H = \underline{V}_G - \underline{V}_A$.

A preliminary inspection of the w field of the first flight revealed the anticipated fact that the crests and troughs of the air flow lay roughly parallel to the direction of the Sierra crest upwind of the flight. Thus, for the reasons stated above, the coordinate system** was rotated counter-clockwise 20° and translated 50,000 feet along its new -x' axis to a center O' approximately at University Peak on the Sierra crest. The y' axis then lay along the mean line of the Sierra crest between Mt. Keith and Diamond Peak, a distance of approximately 10 miles. All data for analysis in the vertical plane were then re-referenced to their new positions with respect to the x' axis. The horizontal wind component perpendicular to the Sierra crest in the tracking area was obtained from $\underline{V}_H$ by the formula $U = V_H \cos \beta$.

Vertical motion. On the time section $(dZ/dt)_S = w_G$ was computed graphically from the slope of the Z,t curve. Where Raydist data were used or where the residuals in the computation of Z were large, $(dZ_p/dt)_S \approx w_G$ was computed graphically. For all practical purposes $(dZ/dt)_S = (dZ_p/dt)_S$. The curve of w_G,t was plotted on the same time section on a scale of 1 cm = 2 ft s^{-1}. (See Fig. 2.2.)

From the sailplane computation sheets the values of w_A were plotted on the time section and added graphically (subtracted algebraically) from w_G to obtain $w = w_G - w_A$ and a curve of w,t. (Fig. 2.2)

A continuous record of w,t then was had for all periods of continuous airborne measurements; and computations of U,t were listed for periods of essentially straight flight for which both airborne and tracking data existed.

---

*SWAC (Standards Western Automatic Computer) was used to compute the space positions (x,y,z) from the tracking data. See Appendix A.

**A rectangular coordinate system with the origin at a point in Independence, x east, y east, and z vertical. See p. of Appendix A.

Fig. 2.1 - Sample frame of 16 mm film of sailplane instrument panel. Instruments shown are air-speed indicator (upper left), outside air thermometer (upper right), altimeter (middle row, left) clock (center), compass (lower left), accelerometer (far right), and 2 rate-of-climb indicators (left of and below temperature indicator).

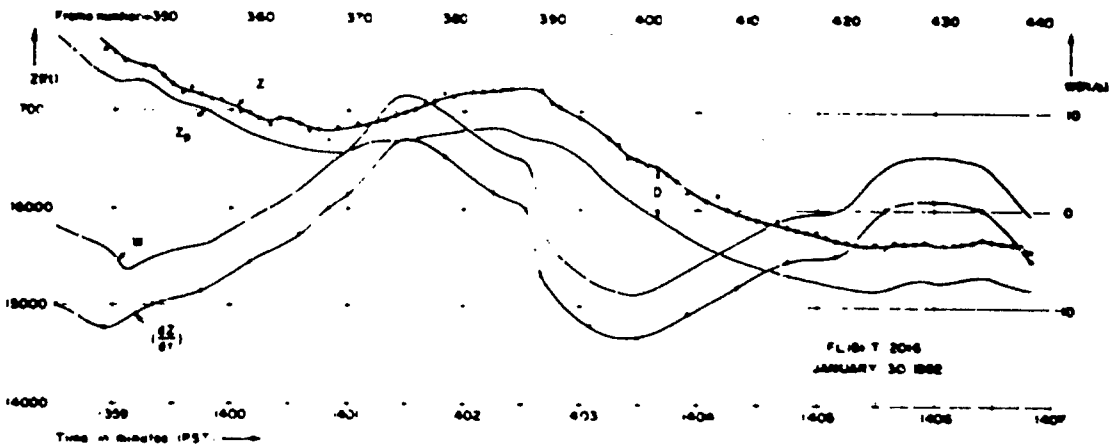

Fig. 2.2

In selecting the critical points to be represented in a vertical cross section, the w,t curve was examined and the maxima, minima, and zero values of w were listed with the corresponding frame numbers; these values represented the inflection points (maximum up- and down-drafts) and the crests and troughs ($w = 0$) of the flow pattern in the vertical plane. Other intermediate values were added as required by the analysis.

Streamlines. The slope of the streamlines*, w/U, was computed as the angle $\varepsilon = \arctan w/U$. In the cross section the vertical scale was exaggerated over the horizontal by 3:1 so that the exaggerated slope was computed as the angle $\varepsilon' = \arctan 3w/U$. Consistent units were employed; both w and U were converted to meters per second for this and later computations.

In order that the streamlines should represent the speed as well as the direction of the wind in the (x',z)-plane, it was decided that the speed should be indicated graphically by means of varying the distance between adjacent streamlines rather than by isotachs (isovels), vectors, or other methods. To do so one invokes the concept of "channels of flow" and assumes:

1) $\partial/\partial t = 0$ (steady state).

2) $\partial/\partial y' = 0$ (no variation parallel to the Sierra crest).

Then the equation of continuity:

$$\partial\rho/\partial t = -[\partial(\rho u)/\partial x' + \partial(\rho V)/\partial y' + \partial(\rho w)/\partial z]$$

reduces to $\partial(\rho V)/\partial S = 0$ which states that the mass transport through any streamline channel is constant.

Consider now the following schematic drawing and the geometric relationships:

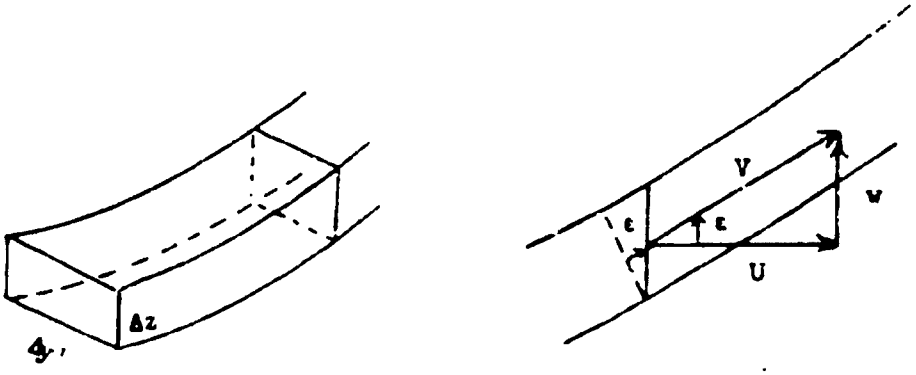

The mass flux $F = \rho V \Delta y' \Delta z \cos \varepsilon$ (or $F = \rho V' \Delta y' \Delta z \cos \varepsilon'$). Since $U = V \cos \varepsilon$ (or $U = V' \cos \varepsilon'$), $F = \rho U \Delta y' \Delta z$. From the reduced equation of

*It is to be noted that these are streamlines of V, the wind component in the vertical plane perpendicular to the Sierra crest.

continuity equation: $\rho U \Delta z = \Delta\psi' = C$ = a constant of dimensions $[M L^{-1} T^{-1}]$*. The thickness of the channel at any point is $\Delta z = C/\rho U$ in meters where C is in ton $m^{-1}sec^{-1}$. Since in the cross section 3 cm represents 1,000 ft, 1 cm in the certical scale of the cross section = 101.6 m in the atmosphere, so $\Delta z = C/101.6(\rho U)$cm where ρ is in ton m^{-3}.

The constant C chosen depended on the average speed of the wind for each lee wave, but, of course, was kept constant for each flight. The values used were 7.5, 5, and 2. Thus, for a given flight cross section, if ρ is expressed in kg m^{-3}, Δz in cm was approximately $75/\rho U$, $50/\rho U$, or $20/\rho U$, depending on whether the average wind U was relatively strong, moderate, or weak. While this technique sacrifices the opportunity to compare wind speeds from one flight to the next - except where C is the same for both - it satisfies the more important requirement of having each lee wave represented by a sufficient and convenient number of streamlines to describe the flow pattern, and it allows comparison of relative speeds within each cross section.

In the vertical (x',z) cross section were plotted the values of ψ' as slopes and the corresponding values of Δz as numbers for all critical values of w along the flight path and at a sufficient number of intermediate points to ensure as complete a coverage as practicable. The streamline analysis was then performed as an objective attempt to best satisfy the requirements of the data.

Other variables. From Z_p, p was obtained directly from Bellamy's (1945) tables, and from p and the corresponding T were computed density ρ and potential temperature θ by the formulas:

$$\rho = p/R_d T$$

and

$$\theta = T(100/p)^{\kappa_d}$$

in practice, both of these quantities were obtained by referring to the Smithsonian Meteorological Tables (1951). For the computation of Δz it was sufficient to plot all values of p,T on the adiabatic chart, thus obtaining an average sounding for the flight and an average curve of ρ, Z_p or ρ, Z. These values were quite accurate enough for the determination of Δz, the probable error in ρ being less than that of U.

The computation of θ was somewhat more sensitive to errors and space differences, however, and it was desired to use the Tables based on the accurate formula rather than the graphical determination on the adiabatic chart, which method introduces further errors of chart construction and of reading. It is obvious that the accuracy of θ is that of T compounded, perhaps, by a somewhat smaller error in p. The overall absolute accuracy of θ is probably $\pm 2.0^{\circ}K$ while the internal consistency is probably $1.0^{\circ}K$ and the maximum relative error $\pm 0.5^{\circ}K$.

On the time section the values of $D = Z - Z_p$ were obtained graphically from the smoothed curves of Z and Z_p. The field of D was analyzed from the

*Here M refers to mass, L to length, and T to time.

plotted values along the projected flight path in the (x',z)-plane together with those from the surface barograms referenced to the same plane.

The fields of T and θ were similarly plotted and analyzed. T was often graphed on the time sections on which it likely indicated inversions encountered along the flight path.

Concluding remarks. The accuracy of the results as dependent only on the errors of the instrumentation and of the reduction procedure, as distinct from those resulting from the imperfect fulfillment of the assumptions, can be estimated. Some of the errors depend on the magnitude of the quantity and so are more adequately expressed as percentages. In summary these are as follows:

Quantities	Estimated accuracy
U, v	± 5%
Δz	± 5%
ε'	± 10% maximum
θ	± 1 °K (±0.5° relative)
T	± 1.5 °C (±0.5° relative)
P	± 100 ft to ±200 ft (±100 ft maximum relative)

Considering the meaning of the results represented by the analyzed data, it must be remembered that ε and V refer to that component of the wind perpendicular to the Sierra crest. ε_p of the path of an air parcel and V_H of the total wind would be related to the quantities in the cross sections in the following manner: $\varepsilon_p \leq \varepsilon$ and $V_H \geq U$. The greater is β, the angle between V_H and the x' axis taken normal to the mountain crest, the less the streamlines approximate the paths of air parcels and the greater discrepancy one should expect in the fields of θ, D, and T as analyzed on the (x',z) cross section. It is reasonable to assume adiabatic flow so that the temperature pattern along the streamlines will be a result of differential vertical motion with coolest temperatures in the crests and warmest temperatures in the troughs at any level. Since the principal component of the horizontal temperature gradient, that of the overall synoptic situation, is directed to the left of V_H, only if the flight has been made essentially along the streamline of the true wind can one expect to measure the temperature field due to the wave perturbation. Similarly, the field of θ in the vertical should resemble that of the true streamlines where the vertical plane is taken along the wind; and there each isoline of θ should nearly exactly represent a true path. Also, there is advection of temperature to be considered: $\partial T/\partial t \neq 0$. The effects of this will be greater the longer the flight. Finally, the greater the north-south range of the flight path, the less well defined all of the fields should be as a consequence of the condition $\partial/\partial y' \neq 0$. The errors resulting from the variations in the third dimension derive less from the normal gradients of the variables than from variation of the Sierra crest from the y' axis.

References.

Bellamy, John (1945): The Use of Pressure Altitude and Altimeter Corrections in Meteorology. J. Meteor., Vol. 2, pp. 1-7.

Holmboe, J., and Klieforth, H. (1954): Final Report, Sierra Wave Project. Department of Meteorology, University of California, Los Angeles. Air Force Cambridge Research Center Contract AF 19(122)-263.

Klemperer, W., et al (1951): Report on the Activities of the Southern California Soaring Association, Inc. in Phase I of the Sierra Wave Project October 1950 to October 1951.

Saudek, V., et al (1952): Mountain Wave Project Report No. 3, October 1951 to October 1952, Southern California Soaring Association, Inc. Department of Meteorology, U.C.L.A. Contract AF 19(122)-263.

Smithsonian Meteorological Tables, Sixth Revised Edition (1951). Smithsonian Institution, Washington, D. C.

3. VERTICAL CROSS SECTIONS AND SOUNDINGS

Graphical presentation of results.

After all of the 1951-2 airborne and tracking data had been analyzed, results from 11 flights on 9 separate days were considered to have sufficient coverage to be worthy of publication in the form of vertical cross sections.* The 9 lee wave examples are treated below in chronological order. Each case is presented according to the following order of subject headings:

i. Clouds and weather. Significant observations of cloud and weather phenomena at the time of the flight are briefly described. When applicable, one or two photographs illustrating the cloud phenomena are shown.

ii. Flight summary. A plan view of the path of the flight is shown in relation to the topography and the tracking network. Specific accomplishments of the flight and particular limitations of the tracking runs are noted.

iii. Streamlines. The field of motion is presented in the form of streamlines constructed according to the manner described in Chapter 2. A projection of the flight path on the vertical plane--the thread along which data were measured--is drawn on the cross section. Pertinent measurements such as wave length, vertical displacement, maximum horizontal and vertical velocities, turbulence, etc., are included on the cross sections. A brief discussion of these results is given.

iv. Other fields. The fields of temperature, potential temperature, and pressure (D values), while not of sufficient coverage for cross section analysis, are discussed with respect to the streamline pattern and the mean flight sounding.

v. Soundings and velocity profiles. With each flight cross section are presented an "up-wind" temperature sounding and wind velocity profile. The latter is that of the U (250 degree) component of the true wind. The data used for the period of 1 December 1951 to 29 February 1952 were from Castle Air Force Base, Merced, California. For the months of November, 1951 and March, 1952, the data used were from Oakland or from interpolated values between Oakland and Santa Maria depending on the direction of the upper air flow. For several of the cases upper air data from Lodgepole in Sequoia National Park are included. Together with the sailplane flight soundings are shown the U components of the Bishop double-theodolite pibal wind sounding representing a synoptic vertical profile in the leeward flow.

In Chapter 5 the surface and upper air synoptic charts corresponding to these vertical sections are shown and discussed.

Additional symbols and notations. Besides the symbols defined earlier, some others are introduced here for abbreviated notation on the

---

*Data from two additional flights were used for special roll cloud studies, the results of which are presented in Chapter 4.

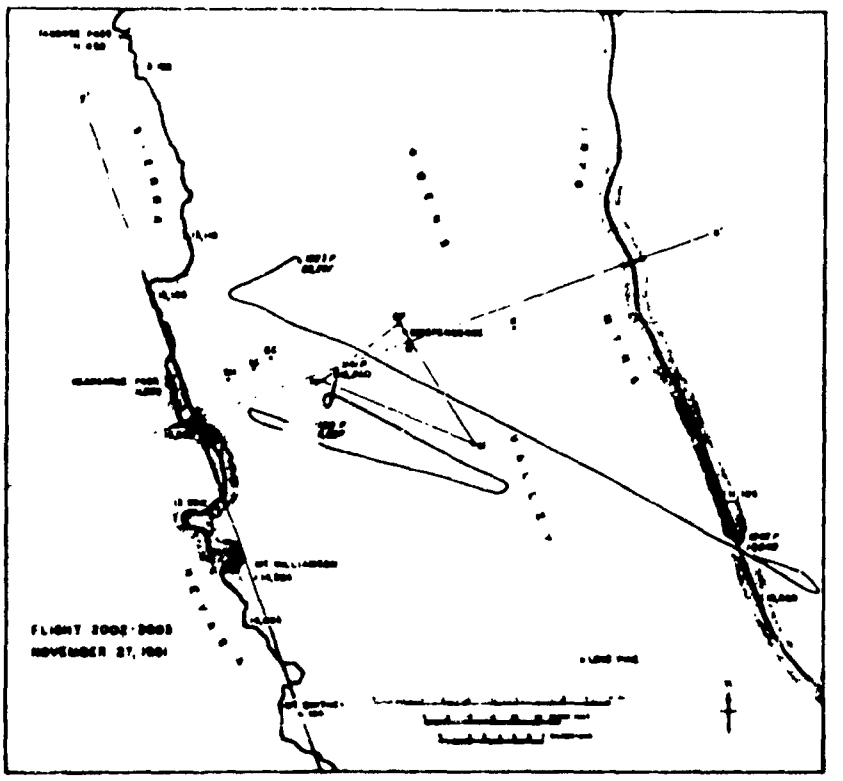
FLIGHT 2002-2003
NOVEMBER 27, 1951

Fig. 3.1

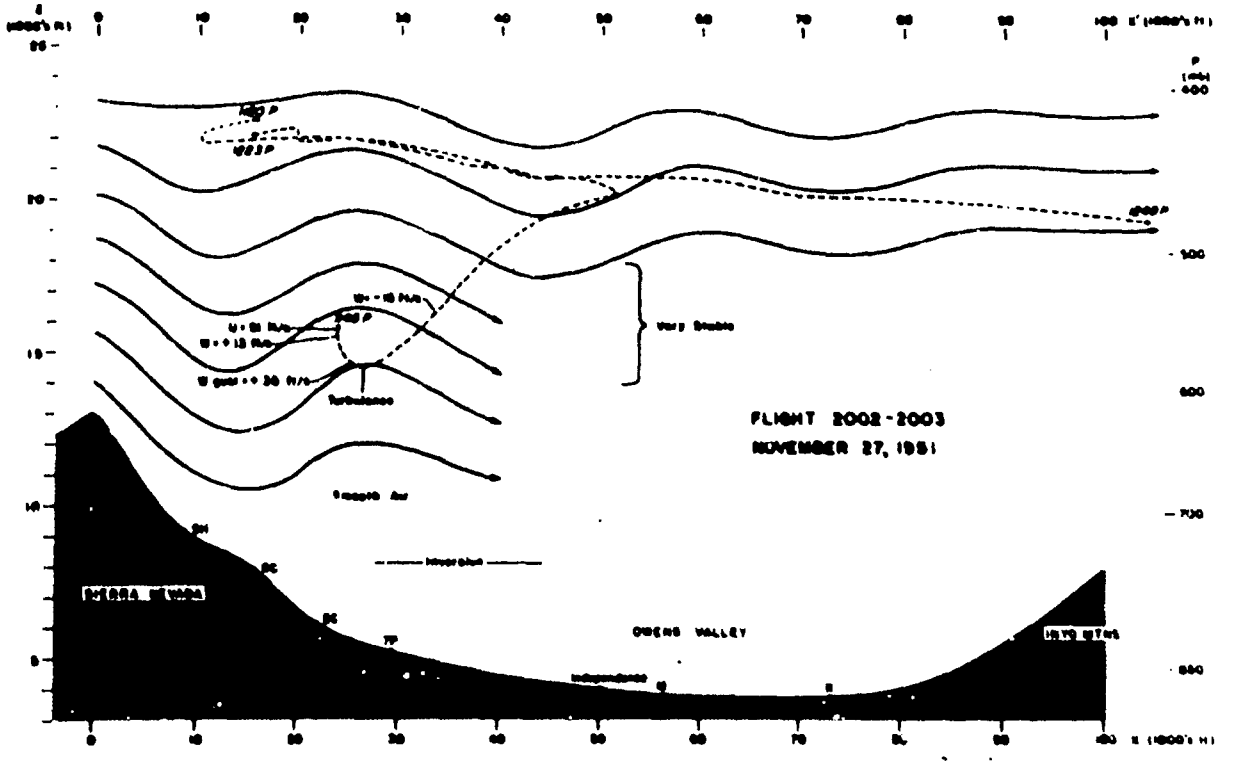
FLIGHT 2002-2003
NOVEMBER 27, 1951
Very Stable
Turbulence
Inversion
OWENS VALLEY

Fig. 3.2

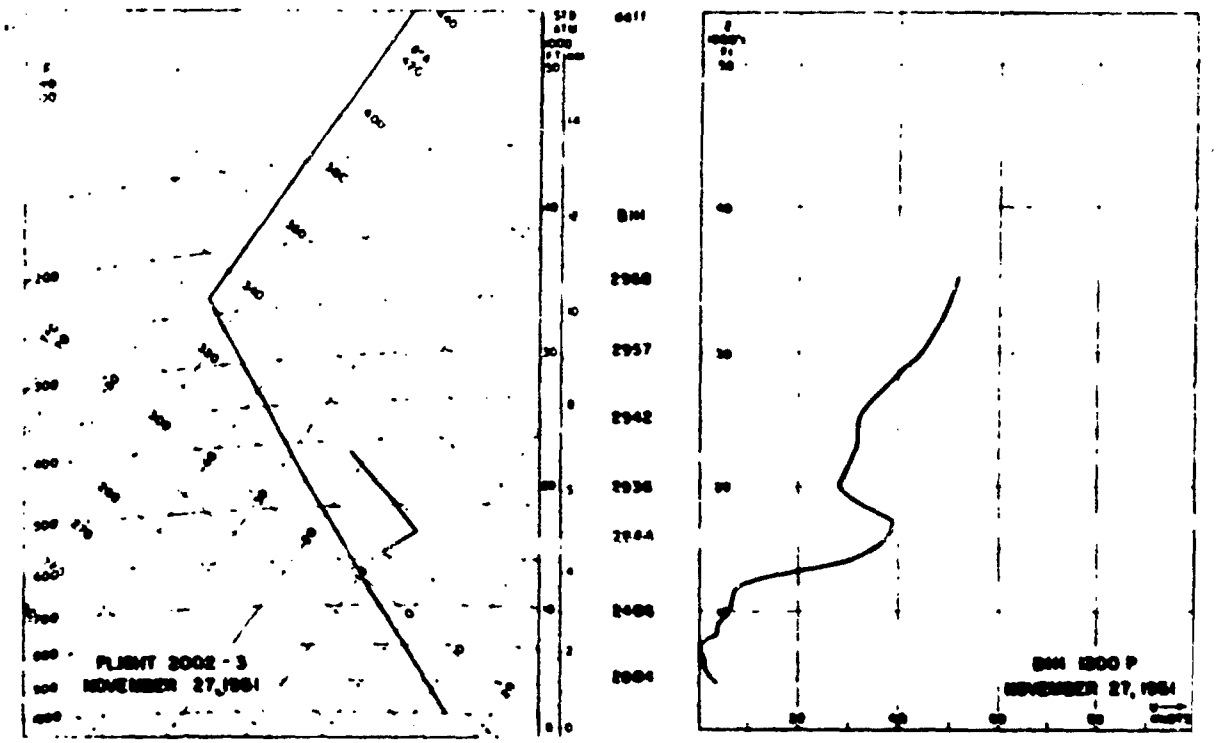
FLIGHT 2002 - 3
NOVEMBER 27,1951
BIH 1500 P
NOVEMBER 27, 1951

Fig. 3.3

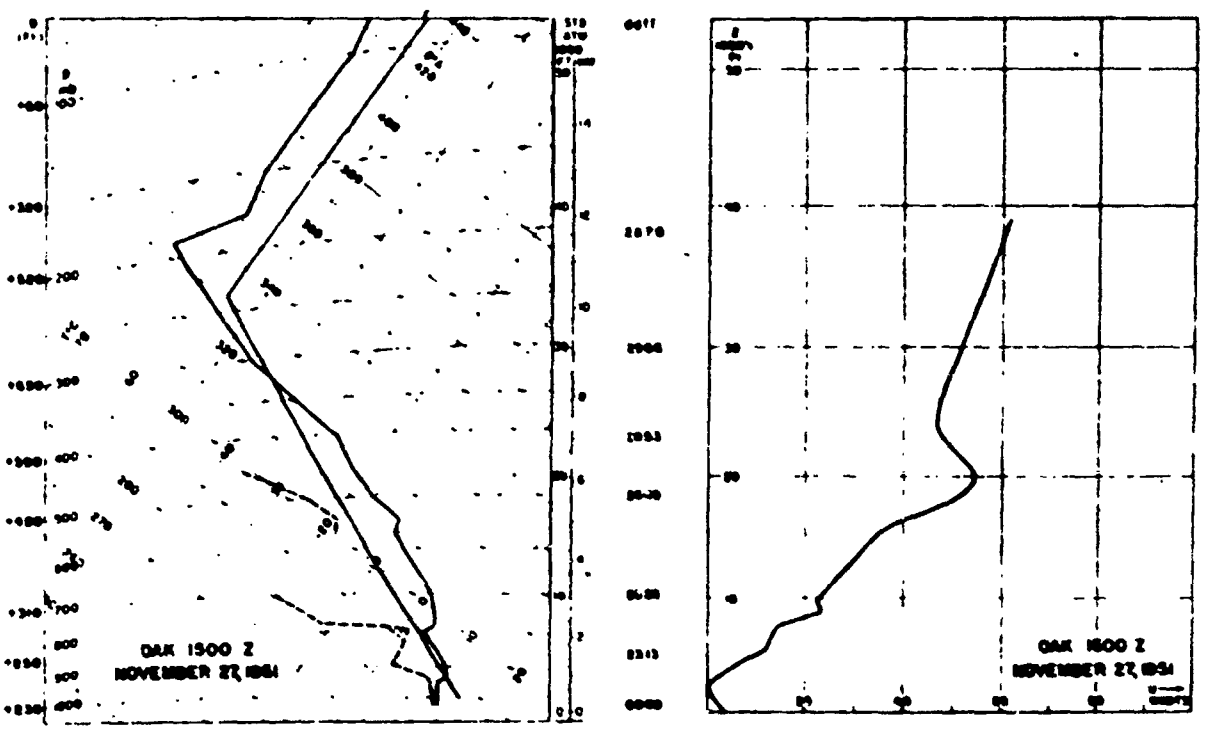
OAK 1500 Z
NOVEMBER 27, 1951
OAK 1500 Z
NOVEMBER 27, 1951

Fig. 3.4

charts and in the text. These are:

L	wave length of the perturbation in the (x',z)-plane.
ζ	displacement of a streamline from its mean height; amplitude of the wave flow in the vertical plane.
$2\zeta_{max}$	the maximum total height variation of any streamline in the vertical plane.
BIH	Bishop Weather Bureau station. 4,110 ft.
BP	Ball Park, Independence. Theodolite. 3,904 ft.
CC	County Cabin, Independence Creek. Barograph. 7,886 ft.
EC	Eckert's Cabin, Independence Creek. Barograph. 6,166 ft.
I	Independence. Barograph. 3,934 ft.
K	Kearsarge Station. Barograph. 3,760 ft.
LP	Lodgepole, Sequoia National Park. Radiosonde and barograph. 6,700 ft.
M	Manzanar Barograph and theodolite. 3,831 ft.
SH	Ski Hut, Owens Valley. Barograph. 9,201 ft.
7P	Seven Pines Theodolite. Theodolite and barograph. 7,992 ft.
1500 Z	Here Z refers to Greenwich Civil Time (GCT).
0700 P	P refers to local time i.e., Pacific Standard Time or 120th meridian civil time

1. Flights 2002 and 2003, 27 November 1951: a moderate lee wave

Clouds and weather. There were a few cirrus and altostratus clouds visible, none of which showed wave form. Visibility was unlimited.

Flight summary. In Fig. 3.1 are shown the flight paths over the ground and in Fig. 3.2 are shown the projections of the paths on the (x',z)-plane. On Flight 2002 the air was found to be smooth up to 11,500 ft* on the tow; turbulence was experienced at 14,500 ft over 7P; and release was made at 15,500 ft. A maximum altitude of 22,000 ft was attained. The long downwind run (Flight 2003) encountered three waves across the Owens Valley and a fourth over the south rim of Saline Valley in the lee of the Inyo Mountains. The subsequent upwind run, which was not

*All altitudes refer to mean sea level.

tracked, encountered turbulence over 7P at an altitude of 10,000 ft but insufficient lift there to regain altitude. No roll clouds appeared but moderate turbulence was encountered in those zones where they normally formed.

Streamlines. The air flow in the vertical plane is shown in Fig. 3.2. It should be mentioned here that in this drawing and in all subsequent sections, the upwind velocity profile has been used as a guide in drawing the streamlines above the crest of the Sierra at altitudes where no flight data exist. The constant* used in determining the thickness of the channels was C = 7.5. The wave length varies somewhat depending on where it is measured but the average value is 29,000 ft or 8.8 km. The average altitude variation of a streamline is 2,100 ft or 640 m. There is indication of a slight upwind tilt with height.

A predominantly northwest wind is evident in the flight path. The average vector wind measured on Flight 2002 was 281 deg, 40 knots and that on Flight 2003 was 291 deg, 47 knots. The maximum U component measured was 91 ft s^{-1} (54 knots). Vertical velocities were moderate: +13 and -16 ft s^{-1} were maximum sustained values. A shorter period (10 second) measurement of +35 ft s^{-1} was made in the first wave updraft near mountain top level.

Other fields. A flight sounding is plotted in Fig. 3.3. The maximum deviation of the plotted points from the curve shown is ±1°C. An inversion was passed through at 8,200 ft on tow. A 4°C temperature inversion existed between 590 and 550 mb (14,000 to 16,000 ft). It was in this zone that turbulence and the maximum vertical velocities were found. The only other significant temperature change along the flight path was a 1°C drop at the same level between the first lee trough and the following crest.

Potential temperature varies from 307° to 322° K. The field of θ in the cross section agrees with that of the streamlines but the data are not dense enough to allow an independent analysis.

The D values are all positive and large. The mean surface values for the flight period are: M = 290 ft, EC = 340 ft, and OC = 380 ft. There is a general increase upward since the sounding is warmer than that of the U. S. Standard Atmosphere. The values vary from +320 ft to + 720 ft. Those determined from the "sounding and the barograms agree rather well with those derived from $Z-Z_p$ on the time section.

Sounding and wind profiles. Upwind conditions are represented by the 1500 GCT Oakland sounding and rawin (Fig. 3.4). The sounding is seen to be quite stable below 540 mb. Above 20,000 ft there is a decrease in U as the upper winds shift to slightly north of west. The Bishop U profile at 1200 PST (2000 GCT) is shown in Fig. 3.3.

2. Flight 2004, 28 November 1951: a moderate lee wave.

Clouds and weather. Cirrus clouds were observed in all quadrants with

*See Chapter 2.

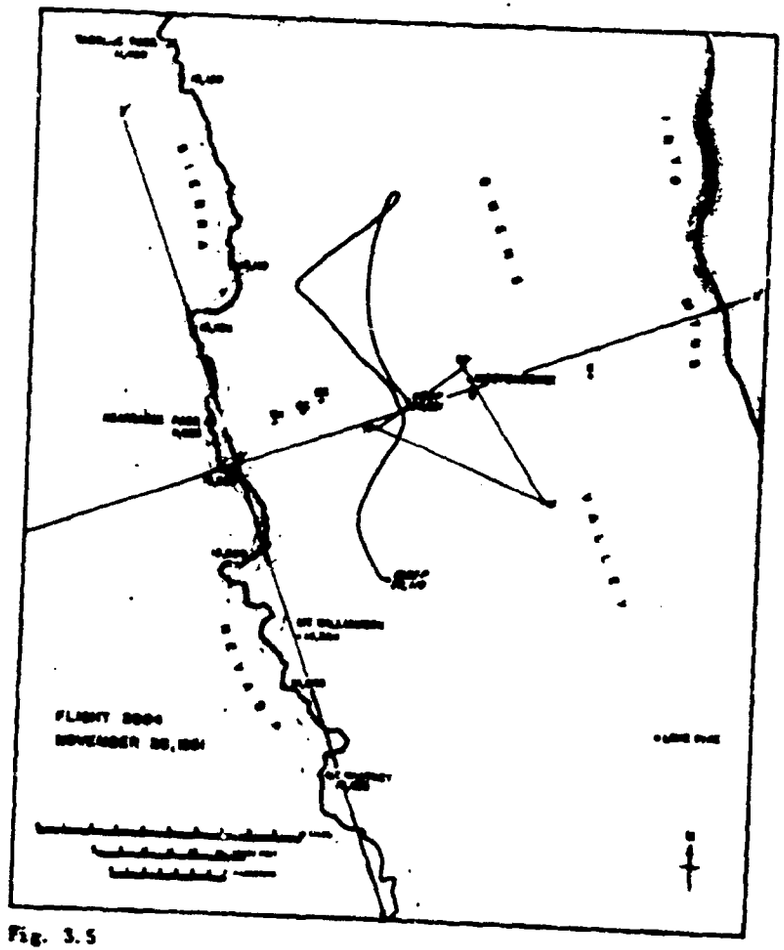
FLIGHT 2004
NOVEMBER 28, 1951

Fig. 3.5

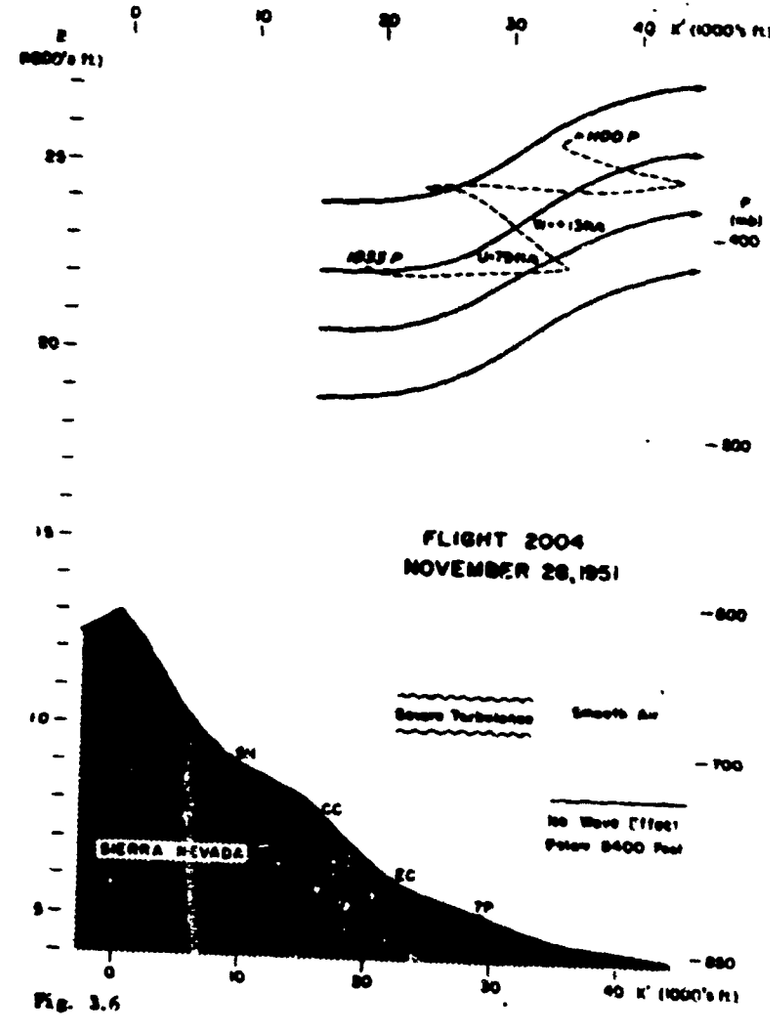
FLIGHT 2004
NOVEMBER 28, 1951
SIERRA NEVADA
Severe Turbulence
Smooth Air
SN
CC
SC
TP

Fig. 3.6

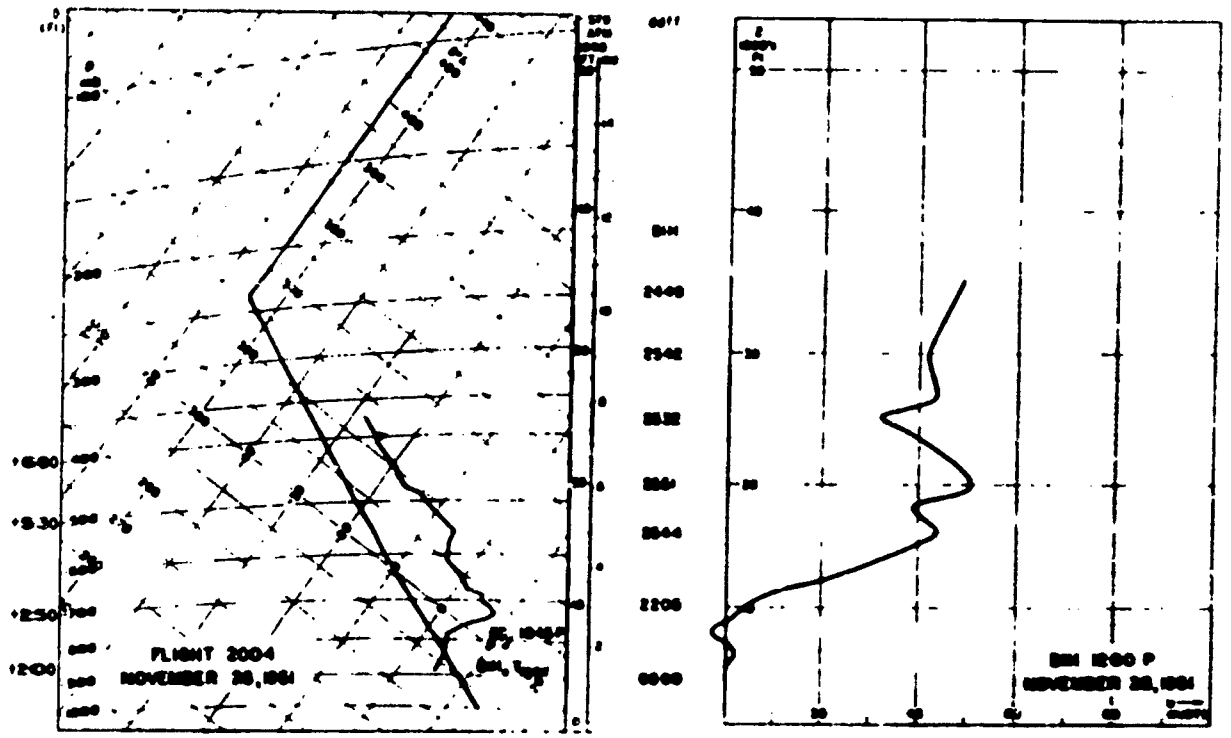
FLIGHT 2004
NOVEMBER 28, 1961
BMI 1200 P
NOVEMBER 28, 1961

Fig. 3.7

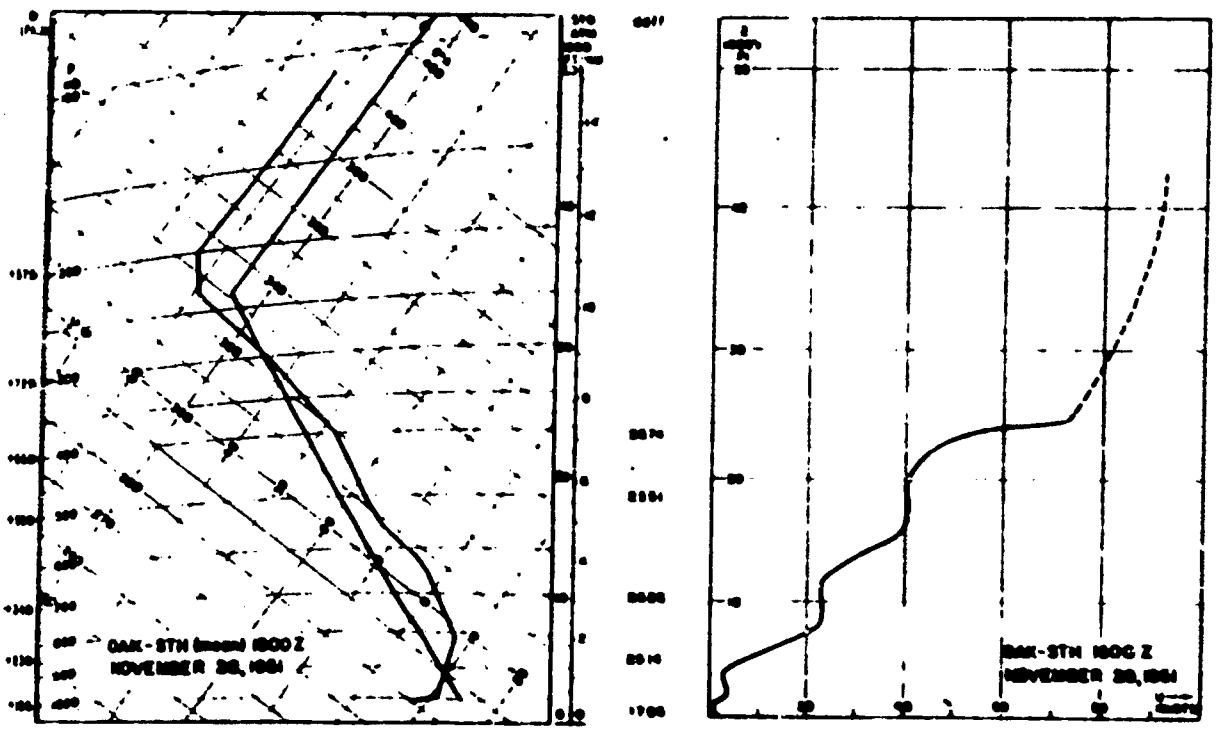
OAK-STH (noon) 1800 Z
NOVEMBER 28, 1961
OAK-STH 1800 Z
NOVEMBER 28, 1961

Fig. 3.8

altocumulus lenticularis to the northeast over the White Mountains. This was known as a "dry" wave with ceiling and visibility unlimited. In Onion Valley, below Kearsarge Pass, wave form was observed in cirrus clouds, snow banners were seen blowing from the peaks, and a warm föhn wind was felt. Toward evening the sky cleared.

Flight summary. Slight turbulence was encountered from 10,000 to 12,000 ft and the release was made at 12,500 ft. The flight path is shown in Fig. 3.5. The air was considered smooth up to 10,000 ft. The maximum altitude attained was 25,500 ft. A downwind run and the subsequent upwind run were nullified by failures of the sailplane camera. What remains is a long run parallel to the Sierra crest in the updraft region of the first wave. On the downwind run three waves were penetrated; the downdraft of the second wave was above the slope of the Inyo Mountains and the third crest was east of that range.

Streamlines. In Fig. 3.6 the constant used for channel thickness was 5. The average values of U and w were 68 ft s^{-1} (40 knots) and +8 ft s^{-1}, respectively. Maximum values of U and w were 79 ft s^{-1} (47 knots) and +13 ft s^{-1}, respectively. Since the streamlines show only the updraft section of the wave, the wave length cannot be measured. However, the half-wave length appears to be 26,000 ft, indicating a complete wave length of 52,000 ft (16 km). $2\ell_{max}$ is approximately 3,500 ft.

Other fields. The flight sounding is much warmer than the Standard Atmosphere as shown in Fig. 3.7. It is rather stable with a strong inversion below 730 mb (about 9,000 ft) and a near-isothermal layer between 615 and 550 mb (14,000 and 16,000 ft). That the lower inversion disappeared by midday is indicated by the fact that three stations in Owens Valley--Bishop, Independence, and Haiwee--all had a maximum temperature of 58°F (14.5°C) and by the measurement of 53.9°F (12.2°C) at BC at 1125 PST.

D values were in agreement with the temperature sounding. Surface measurements were: M = +275 ft, BC = +320 ft, CC = +355 ft, and SH = +285 ft. In the flight section the values increased to +840 ft at 25,500 ft, the maximum altitude reached.

Soundings and wind profiles. A mean 1500 GCT sounding for Oakland and Santa Maria (Fig. 3.8) was used for a representative sample of the west-southwest flow over the Sierra. The dashed line in the wind profile indicates where geostrophic values were used. The 1200 PST Bishop U profile is shown in Fig. 3.7.

3. Flights 2006 and 2007, 18 December 1951: a strong lee wave.

Clouds and weather. At dawn the lee wave was fully developed; a large, dark roll cloud had formed to the south over the center of the Valley surmounted by one, and later two, decks of high wave clouds (Fig. 3.9). Low clouds and blowing snow trailed in a "cloudfall" far down the Sierra slope in the downdraft area while another wave crest was marked by stationary cumuloform clouds over the Inyo Mountains. By afternoon a long, ragged roll cloud was

visible extending from the Mono Lake area in the north to Inyokern far to the south. In the Bishop area the föhnwall hung over the Sierra and the roll cloud hovered over the western slope of the Valley with clear sky immediately overhead. These phenomena persisted with some change throughout the day.

Over the tracking area south of Bishop the roll cloud, extending over Big Pine, Independence, and Lone Pine, covered about 20 per cent of the width of the Valley. Its base and top were at about 15,000 and 18,-20,000 ft respectively. Smaller roll clouds marked the second wave crest over the Inyo Mountains. A solid cloud deck at about 16,000 ft covered the Sierra and the San Joaquin Valley. As seen from the sailplane on Flight 2006, "the downwash of the cap cloud in the lee of the Sierra was very steep and at high velocity resembling water overflowing a dam." There were two lenticular cloud arches above the roll cloud; the highest wave cloud in the tracking area was passed at 35,-36,000 ft. To the north a higher deck could be seen at about 38,-40,000 ft.

Surface winds ranged from calm in some areas to gusts of 50 or 60 knots elsewhere. Strong winds north of Bishop blew a bus off the road and blew snow from previous storms into deep drifts which covered the highway 8 feet deep in places. Dense clouds of dust filled the air high over Owens (dry) Lake while north of Lone Pine sand was propelled at 60 knots in northwesterly gusts.

Flight summaries. On Flight 2006 the sailplane took off on tow from Bishop at 0910 PST, headed southeast, and encountered the second wave updraft over the western slope of the Inyo Mountains. Turning southwest it flew under the roll cloud and released from tow at 18,500 ft just upwind of the roll cloud and lower Sierra slope and southwest of Big Pine. Over the tracking area the sailplane encountered severe turbulence at 39,000 ft, rose to a maximum indicated altitude of 42,000 ft, then countinued northward in the lift zone landing at Bishop at 1200 PST. There was no theodolite tracking of the flight because of pulse failures in the ground equipment. The flight notes of the observer, the notes recorded in the control van, and about 3 minutes of film showing the instrument panel readings between 35,000 and 42,000 ft provide data for analysis.

Flight 2007 reached a maximum altitude of 39,000 ft and was tracked by two theodolites from 1538 to 1650 PST in the altitude range of 32,000 to 38,000 ft. The path, shown in Fig. 3.10, is one of large range, particularly in the region west of the Sierra crest. Unfortunately, the apparent malfunctioning of the direction indicator and the fact that the thermometer dial was off scale for most of the flight, placed severe limitations on the analysis of the data.

Streamlines. As Flight 2006 was not tracked, a conventional streamline analysis was impossible. However, by invoking the assumption of adiabatic flow, it was possible to construct a potential temperature cross section which may be regarded as an approximate representation of the field of motion in the (x',z)-plane. Fig. 3.11 shows the cross section constructed from the 1000 PST radiosonde ascent from Lodgepole and the "sounding" from Flight 2006; since the flight data used were measured in the period 0930 to 1045 PST, these were nearly synoptic. The Lodgepole sounding was plotted

Fig. 3.9a - Southward from Bishop Airport, 0900 PST, 18 December 1951. High lenticular deck, dark roll cloud, foehnwall, cloud-fall, and Rhinegap.

Fig. 3.9b - 1200 PST, 18 December 1951. Westward from Bishop Airport. Foehnwall pouring over Sierra in cloud-fall, and rotor cloud fragments.

Fig. 3.9c - 1200 PST, 18 December 1951. Southward from Bishop Airport. Upper wave cloud smaller with short, transient waves near trailing edge.

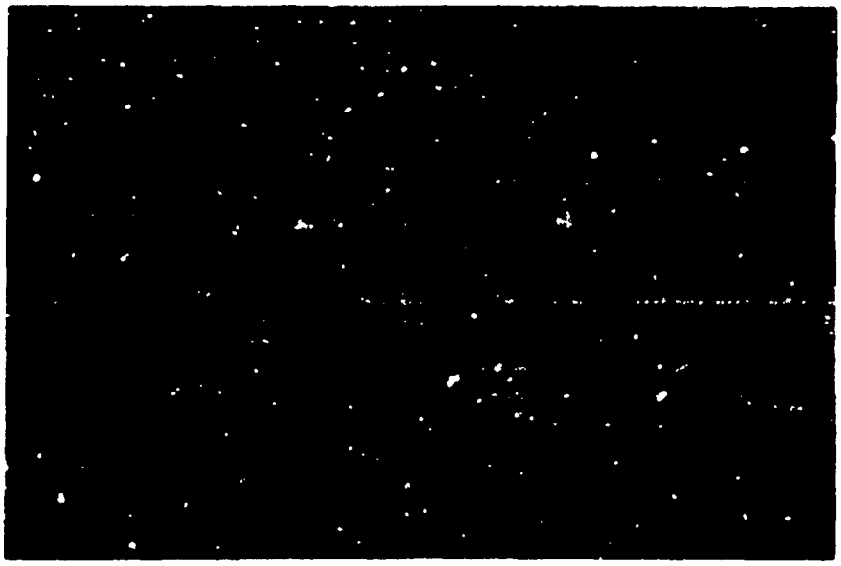

Fig. 3.9d - 1350 PST, 18 December 1951. Southward from Bishop Airport. Wave and roll cloud dense and continuous northward over Bishop.

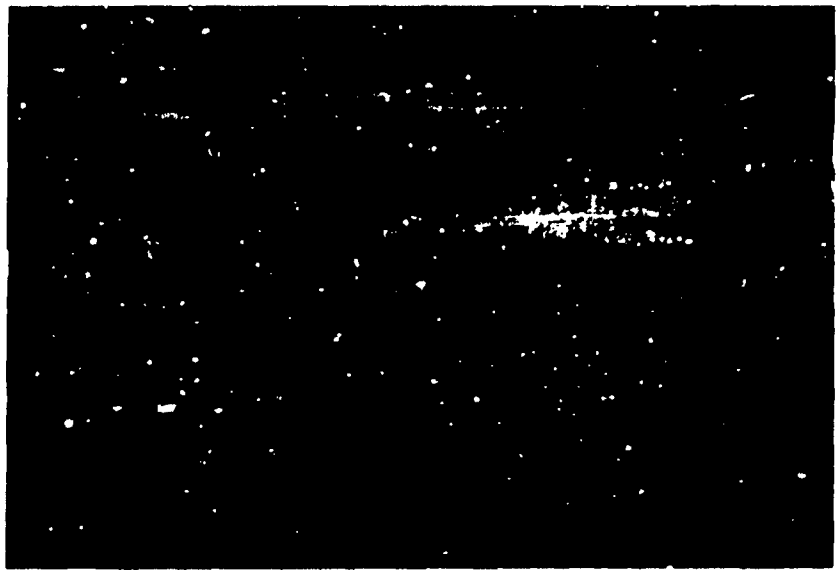

Fig. 3.9e - 1443 PST, 18 December 1951. Toward SSW from 14,000 ft altitude, under rotor cloud base. Cloud-fall pours over Sierra.

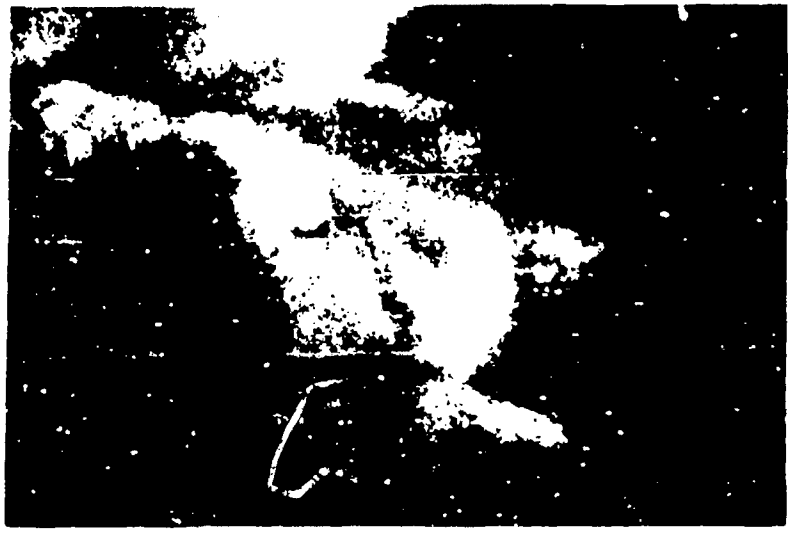

Fig. 3.9f - 1447 PST, 18 December 1951. Southeastward from 15,000 ft. Sailplane in 4000 ft min^{-1} updraft at leading edge of rotor cloud.

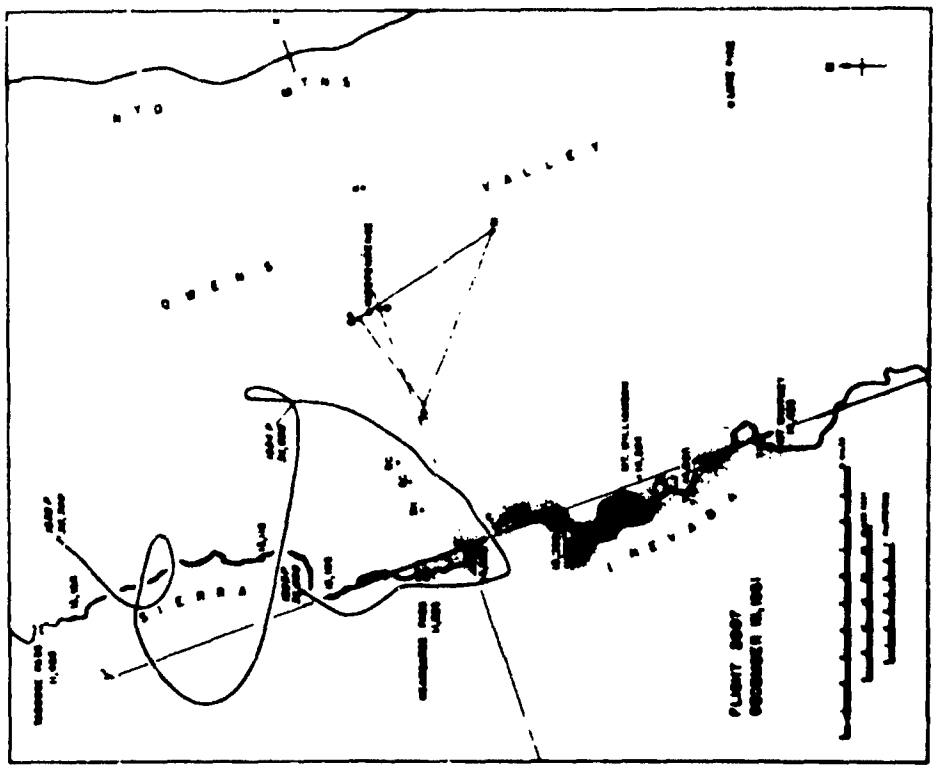

Fig. 3.10

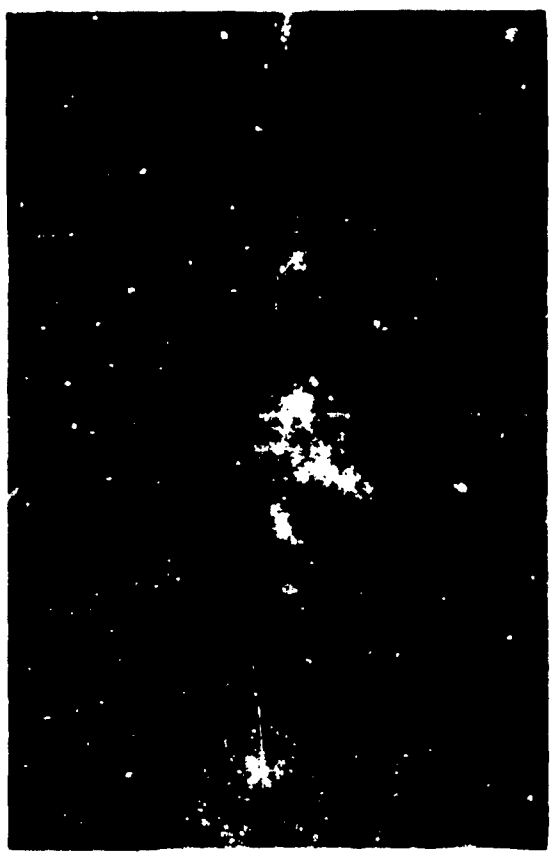

Fig. 3.9a - 1450 PST, 18 December 1951. Southward from 16,000 ft. Southern end of Owens Valley; Independence; Kaiser Pine, Alabama Hills, and Owens (dry) Lake. Altocumulus wave deck above and apparently somewhat upwind of the roll cloud.

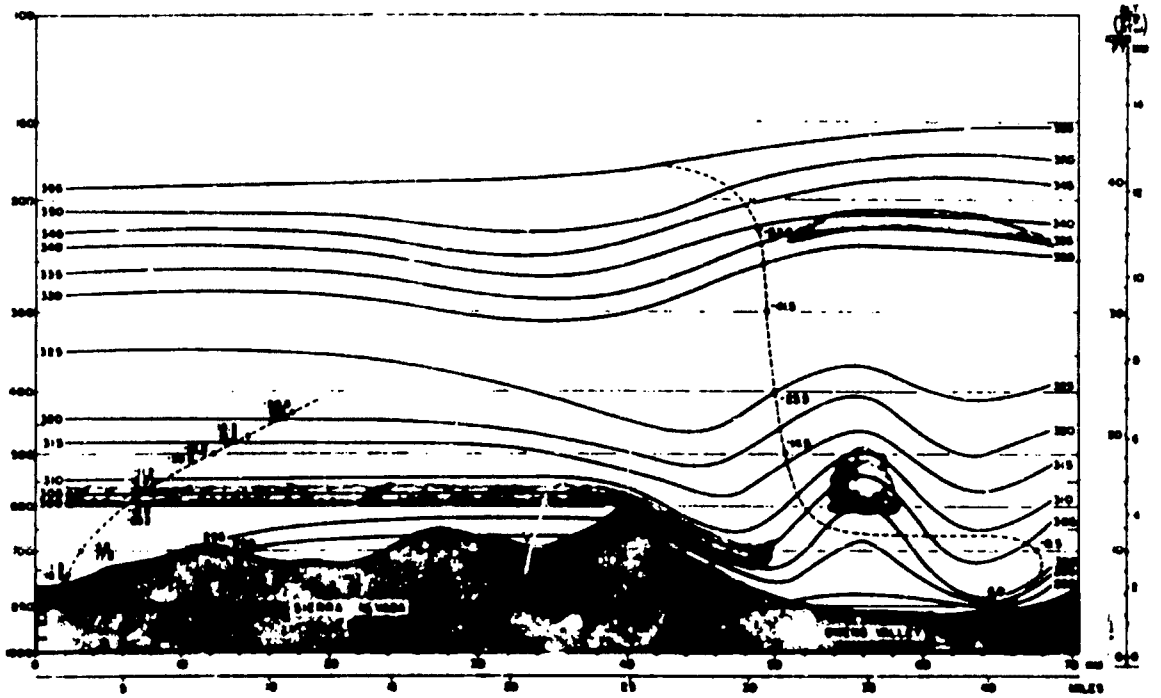

Fig. 3.11

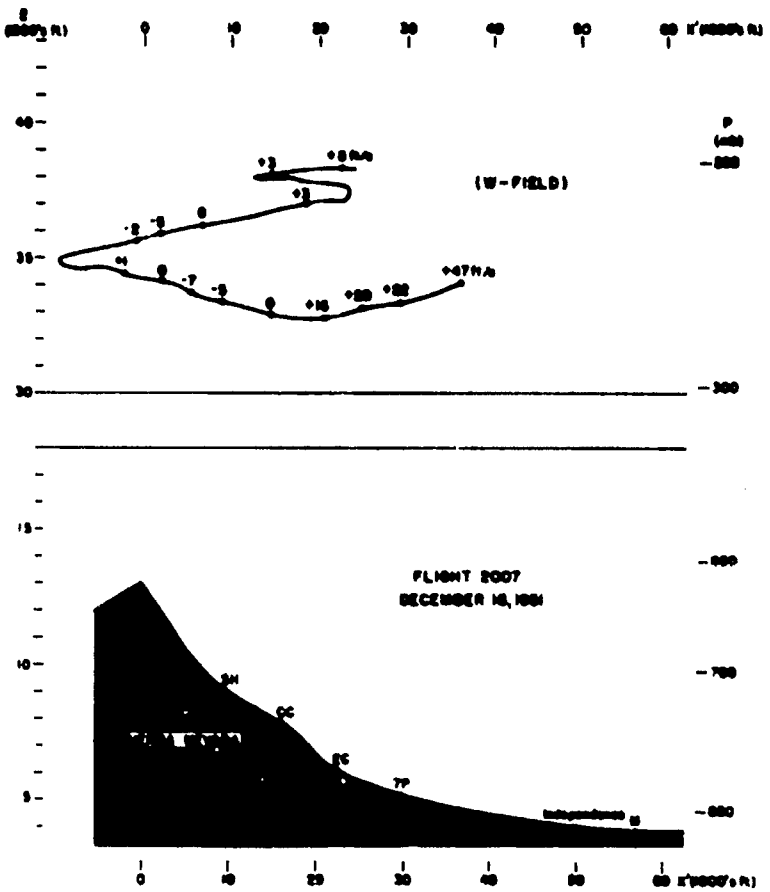

Fig. 3.12

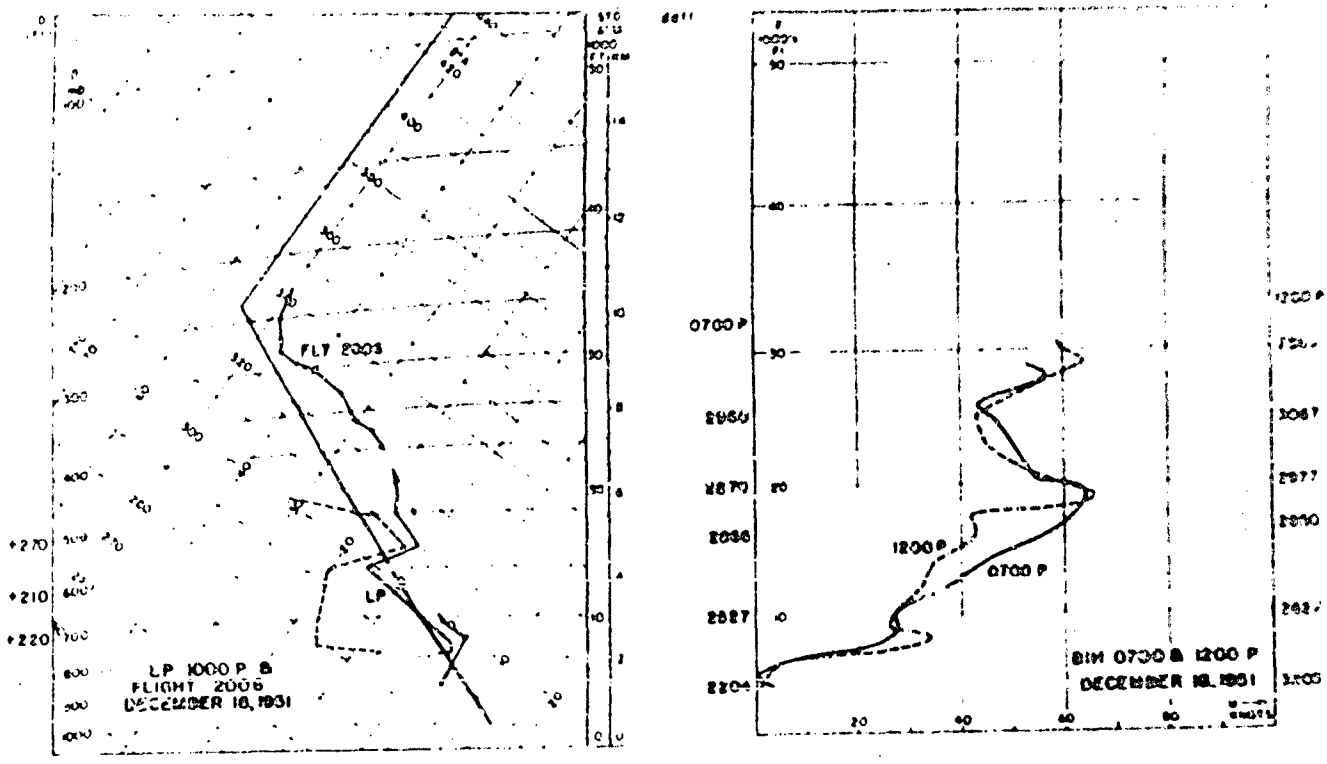

Fig. 3.13

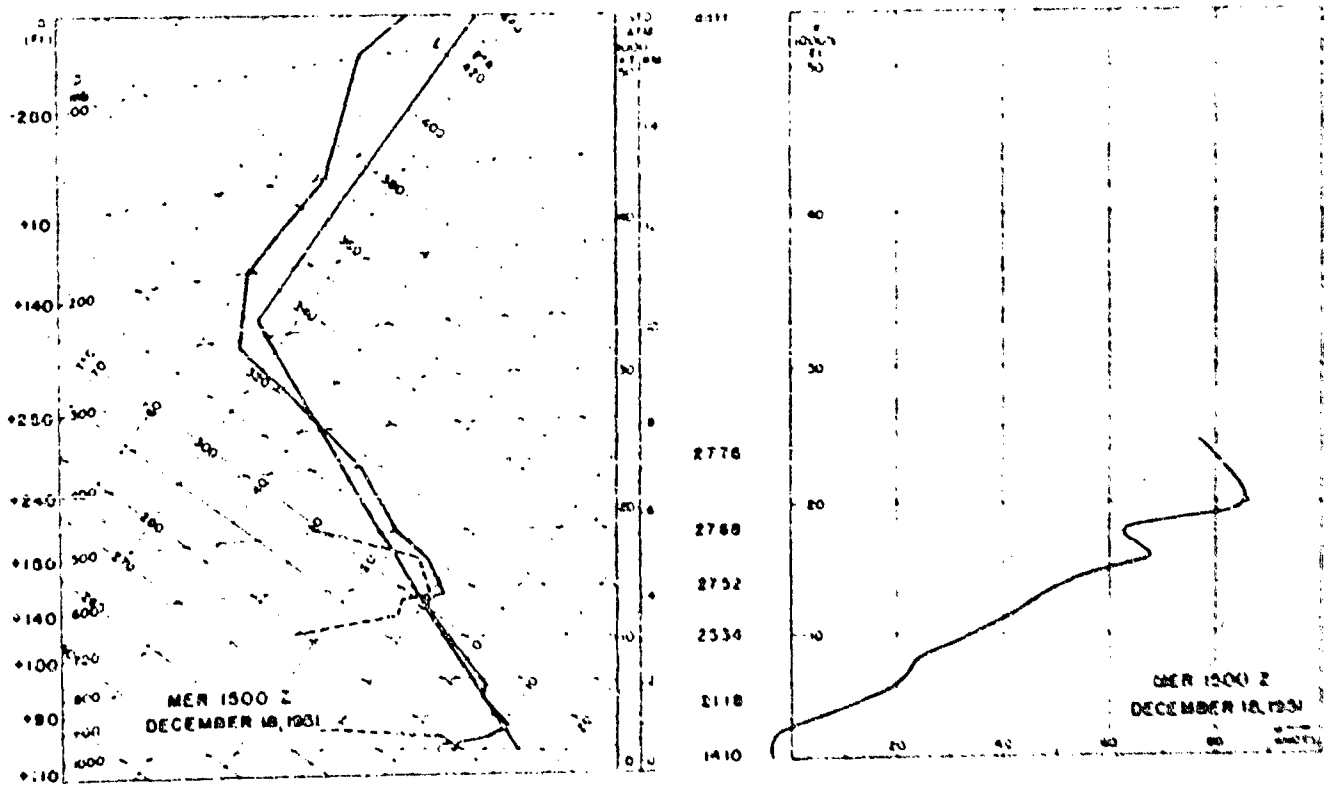

Fig. 3.14

according to its calculated downwind drift with height and the sailplane measurements were plotted according to the path of the flight as reconstructed from the observer's notes. From photographs and observational notes the föhnwall, cloudfall, roll cloud, and lenticular deck were sketched. It was assumed that the inversion of the föhnwall was the same as that of the roll cloud and that the air flow was isentropic except within the clouds. It was further assumed that the streamlines could be approximated by the isentropes except within the cloudfall and the roll cloud where the actual streamlines would have steeper slopes. A rough calculation of the slope of the streamlines was made from the ratio of the vertical wind speed w ($=dZ_p/dt-w_A$) to the horizontal wind speed (equal to V_A in the hovering flight). The wave length of the flow can be seen to vary from 46,000 to 59,000 ft (14 to 18 km or 9 to 11 miles). Since the analysis for the whole section was made from data taken along two threads in space, such a drawing should be regarded only as an attempt to create an approximate picture of the flow pattern.*

In the course of the ascent a maximum U of 85 knots was found at 24,000 ft. Maxima of w occurred in the roll cloud layer (± 70 ft s^{-1}) and at about 32,000 ft (± 40 ft s^{-1}). Severe turbulence was encountered near the roll cloud and again at about 31,000 ft to 39,000 ft. Of interest in the drawing is the suggestion of a much longer wave length in the stratosphere and the upwind tilt with height of the region of maximum updraft. Drifting eastward at 38,000 ft, the sailplane lost altitude above the region in which updrafts were encountered in lower levels, and it was necessary to head westward with altitude in order to remain in the lift area. On the return flight the wind speeds had increased by about 15 knots at 24,000 ft, and reached an estimated maximum of 120 knots near 32,000 ft.

The path of Flight 2007 in the (x',z)-plane is plotted in Fig. 3.12, together with some significant measurements and observations. No streamlines have been constructed because of serious doubts of the reliability of horizontal wind measurements. These indicate wind velocities with large northerly components which appear unlikely even though the synoptic charts (Figs. 5.7 and 5.16) show the upper flow to be west-northwest. The most damning evidence for this contention is the comparison of corrected heading and flight path; the angle varies from 45° to 90° for much of the run. The field of vertical motion was determined, however, and is indicated in Fig. 3.12.

Other fields. A sounding curve for Flight 2006 is drawn in Fig. 3.13. Some isolated temperature observations from Flight 2007 indicate cooling aloft during the day. The potential temperature field has been discussed above in relation to streamlines. The temperatures are warm with respect to the Standard Atmosphere and D values are large and positive. However, none could be determined on Flight 2006 for lack of Z values and those from Flight 2007 involve too large maximum errors in Z to permit listing of absolute values.

*It is to be noted that this was the only case for which the airborne data lent itself to this form of analysis. The reason for this was that it fortuitously satisfied the requirements: 1) that the flight be nearly synoptic with the radiosonde ascent; 2) that it be made approximately downwind of the radiosonde ascent; and 3) that data be obtained through a great depth of the atmosphere.

Soundings and wind profiles. Fig. 3.14 shows the sounding and U profile from Merced at 1500 GCT. The sounding indicates a lower inversion at about 3,000 ft--the typical winter subsidence inversion of the Great Valley--and a higher inversion at about 13,000 ft (615 mb). The greatest vertical shear in the wind profile occurs at about 14,000 ft, just above the top of the inversion. At 1500 GCT and 2100 GCT the Merced wind profiles indicated maximum speeds at about 20,000 ft and 25,000 ft, respectively; this fact was confirmed by Bishop pibal measurements (Fig. 3.13) and by the flights, although the latter suggest that even stronger speeds occurred near the tropopause in the lee wave. The Lodgepole sounding is presented in Fig. 3.13. The inversion associated with the cap cloud can be identified with that over Merced and was apparently intensified by the flow over the Sierra.

4. Flight 2015, 29 January 1952: a weak lee wave.

Clouds and weather. In the morning much of the sky was covered by cirrus and altostratus becoming altocumulus. In the afternoon there were patches of altocumulus and considerable cirrus. From the air it was clear in the north and east. High clouds were visible in the south stretching over Los Angeles and Las Vegas. The San Joaquin Valley was covered by stratus.

Flight summary. Some turbulence was encountered just prior to release at a rate of climb of 1,000 ft min^{-1} at 13,400 ft. The flight (fig. 3.15) was confined to the rather narrow region of lift between Independence Peak (11,773 ft) and Mt. Bradley (13,280 ft). The flight path was a general descent from the maximum altitude of 15,000 ft.

Streamlines. A single, primary crest is evident in Fig. 3.16. The wind was weak; very little wind was found below 12,000 ft, and in the small zone of lift it was possible to fly cross wind and to spiral without drifting downwind rapidly. The constant used was 2; channel thicknesses are therefore not comparable with those of other flights. The wave length is about 14,000 ft or 4.4 km, $2\ell_{max}$ is 900 ft. A possible explanation for the confinement of the wave motion to that particular region of the crest is that the wind was channeled along the canyon of the South Fork of the Kings River and reached somewhat stronger speeds there. The maximum U was 37 ft s^{-1} (22 knots); maximum vertical velocities were +11 and -7.5 ft s^{-1}. Brief gusts of about ±20 ft s^{-1} were experienced between 13,000 and 14,000 ft. An interesting aspect of the streamline patter. is the tilt of the lee trough upstream with altitude.

Other fields. The temperature sounding (Fig. 3.17) is much warmer than that of the Standard Atmosphere. A 2°C inversion existed below 750 mb (8,000 ft), and above 670 mb the lapse rate was nearly adiabatic. The temperature field is fairly consistent in the (x'-z)-plane, probably because much of the flight path was nearly in the same vertical plane. The potential temperature field would not indicate a lee wave if analyzed independently. θ varies from 308° to 314° K in the tracked portion of the flight. On the return flight to Bishop, the temperatures aloft were cooler by 1° or 2°C.

The D values for the surface were BIH = +320, M = +300, EC = +330,

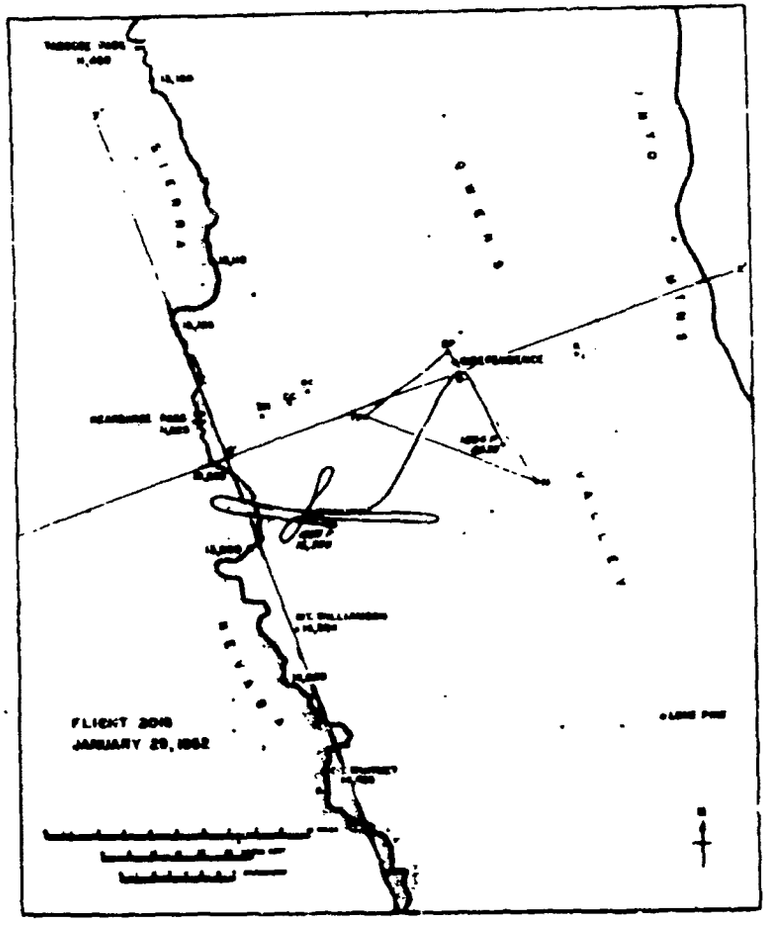

Fig. 3.15

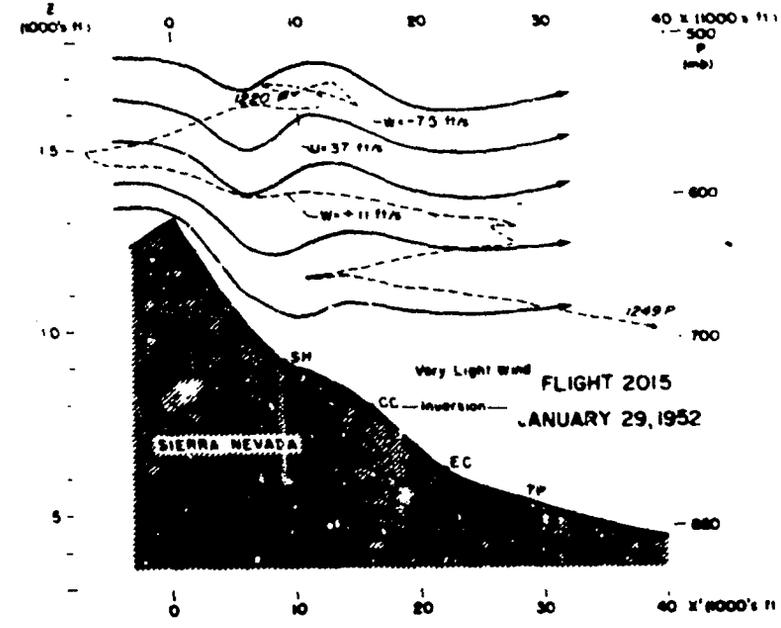

Fig. 3.16

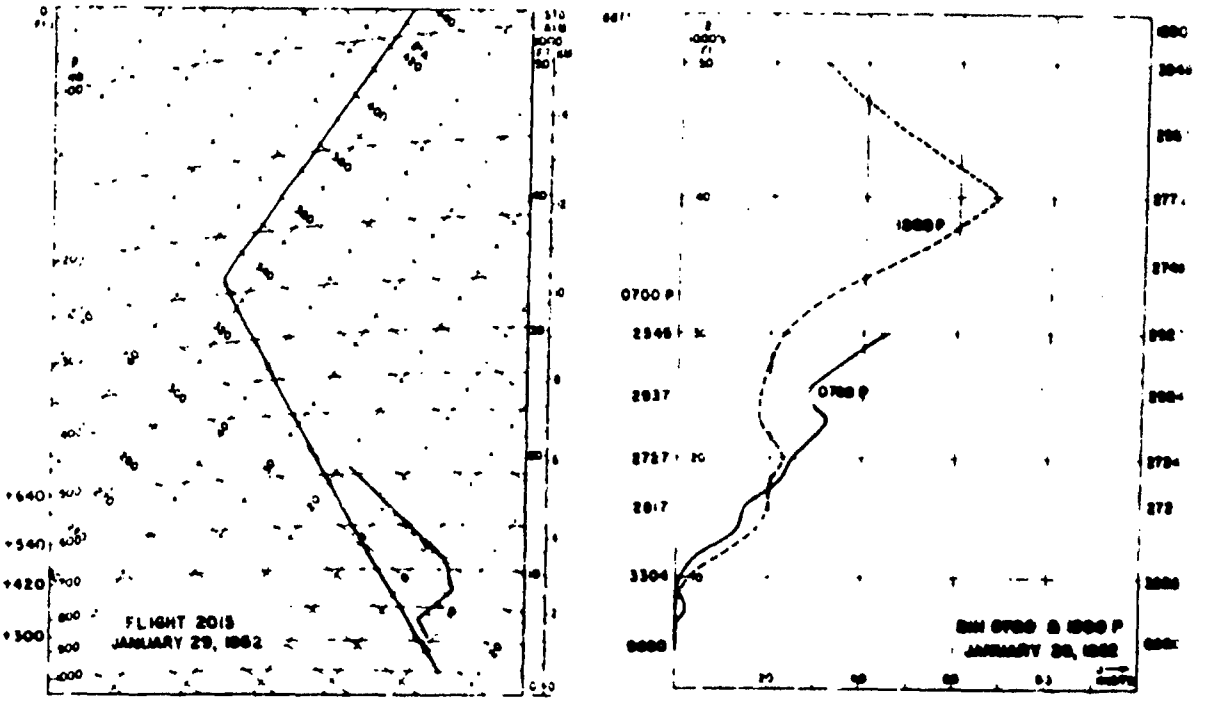

Fig. 3.17

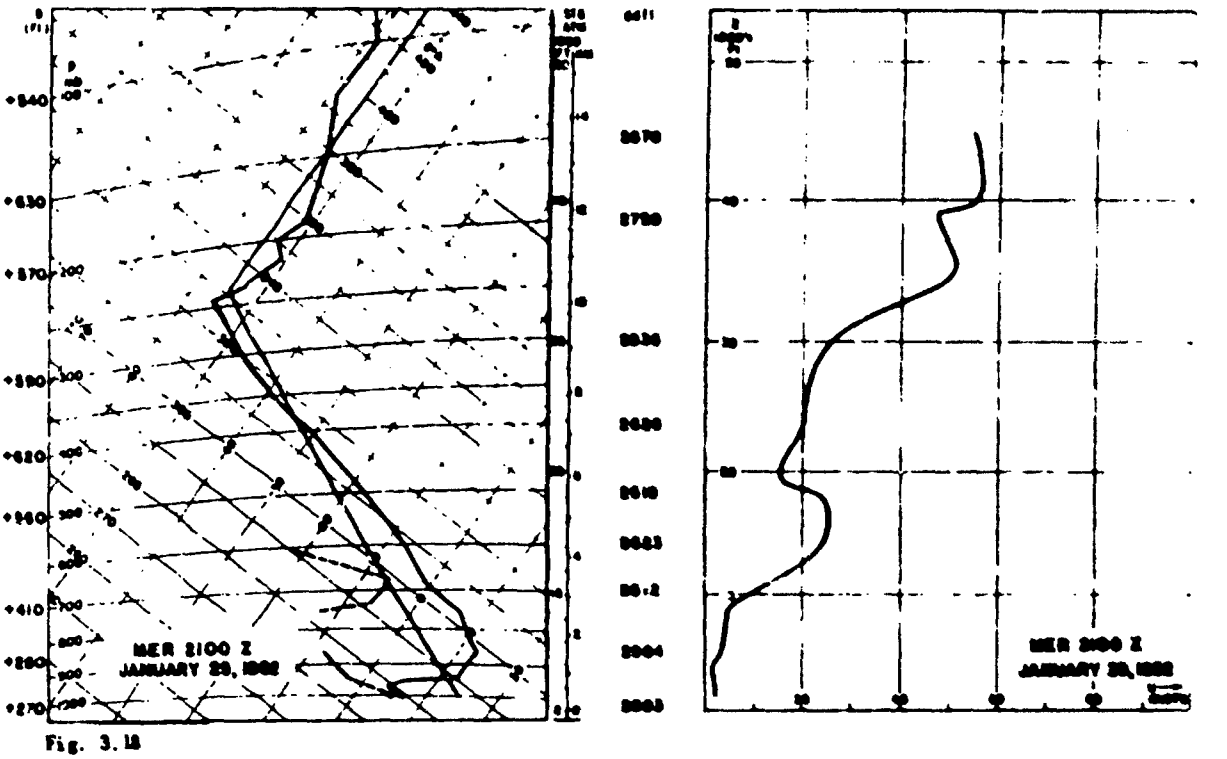

Fig. 3.18

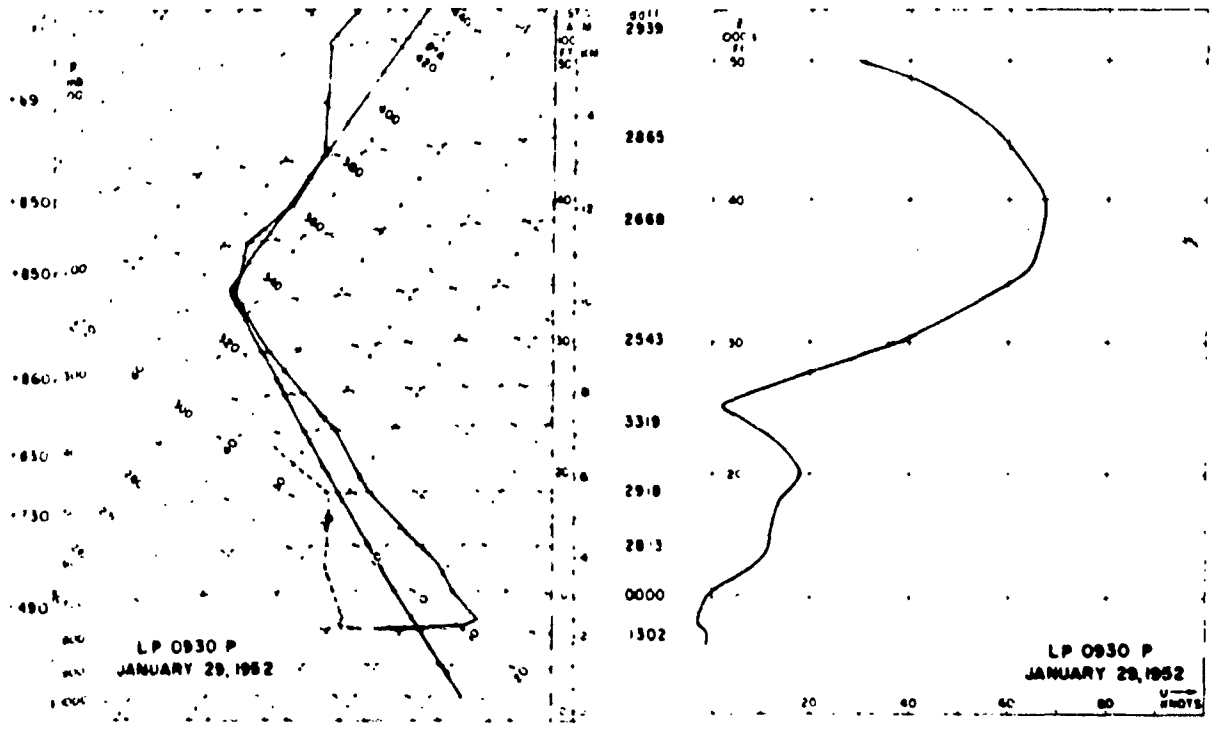

Fig. 3.19

Fig. 3.20 - High wave cloud in lee of Sierra at 1300 PST, 30 January 1952. The view is toward the south with Mt. Williamson on the extreme right.

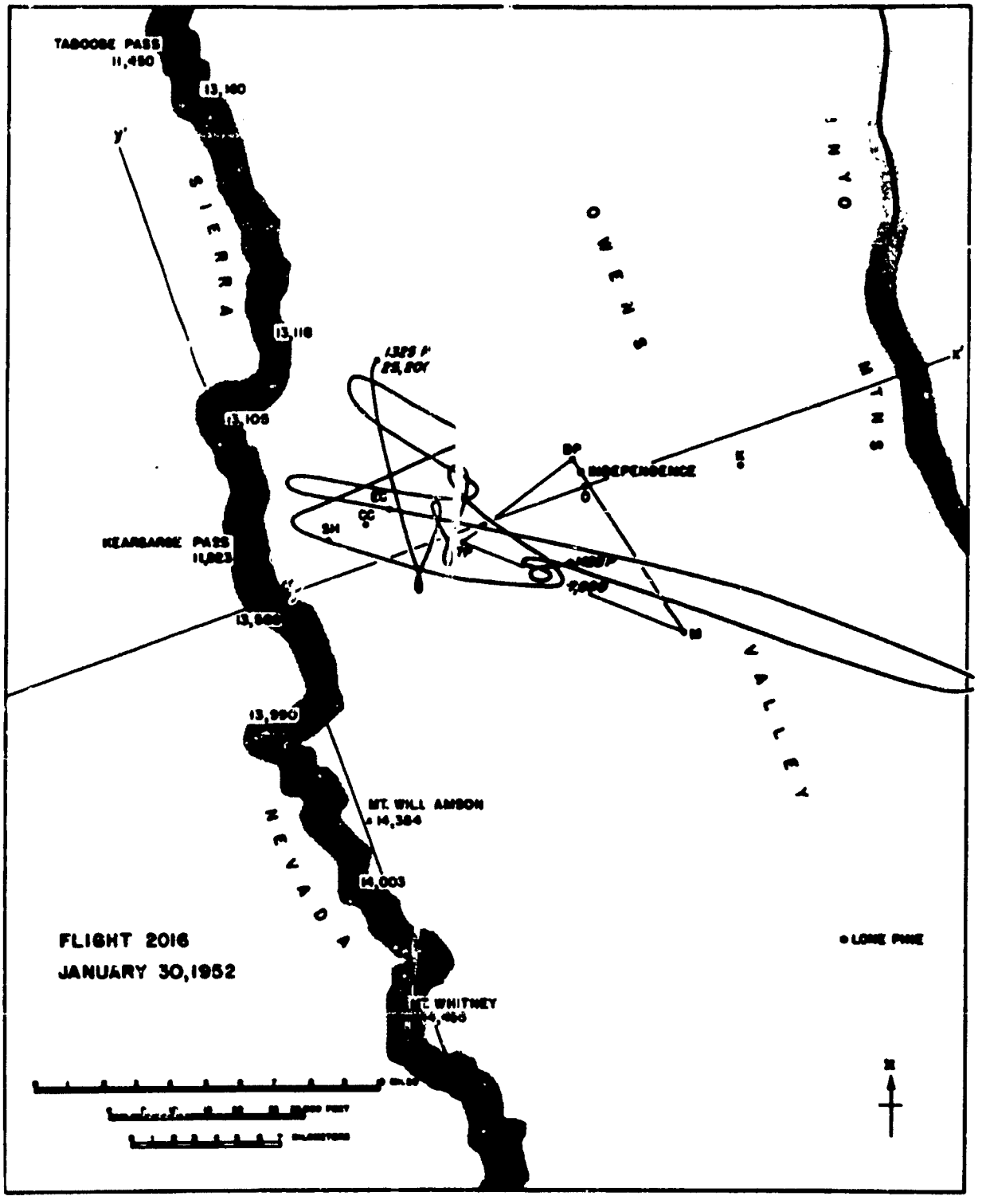
TABOOSE PASS
11,450
13,160
13,118
13,108
KEARSARGE PASS
13,990
MT. WILLIAMSON
14,384
14,003
MT. WHITNEY
INDEPENDENCE
LONE PINE
FLIGHT 2016
JANUARY 30,1952

Fig. 3.21

and SH = +360 ft. The values increased aloft in agreement with the warm sounding. However, there is a rather systematic discrepancy of about 100 ft between D values computed from the sounding and the barograms and those from $Z-Z_p$, the latter being the smaller. It seems likely that this difference can be reasonably attributed to absolute errors in T, Z, and Z_p.

Soundings and wind profiles. The undisturbed flow characteristics are represented in Fig. 3.18. The pronounced low inversion at Merced is related to the stratus layer in the San Joaquin Valley below 4,000 ft. The Lodgepole sounding and wind profile (Fig. 3.19) is similar to that of Merced--a pronounced surface inversion, no high inversion, tropopause near 240 mb, and a rather weak flow at crest level. The Bishop double-theodolite pibal measurements are shown in Fig. 3.17.

5. Flight 2016, 30 January 1952: a moderate lee wave.

Clouds and weather. In the morning there were bands of altocumulus and cirrus overhead and altocumulus lenticularis arches with clear-cut leading edges west of Bishop. Over the Sierra was a mass of cumulus. The San Joaquin Valley was under low strato-cumulus to about 6,000 ft. The lenticular cloud which lay along the Owens Valley in the afternoon (Fig. 3.20) drifted eastward three times during the course of the flight.

Flight summary. Release was made at 17,000 ft, the sailplane reached 26,000 ft, and tracking was begun at 25,000 ft. The flight path (Fig. 3.21) performed in the west-northwest flow included a crisscross run, a long downwind run through three complete wave lengths, and an upwind run prior to descent over Manzanar.

Streamlines. The flow pattern shown in Fig. 3.22 is that of a moderate wave in which three waves formed over the Owens Valley with an average wave length of 25,000 ft (8 km). The values of $2\ell_{max}$ vary from 1500 ft to 2500 ft. The constant used in determining channel thickness was 5. The maximum U measured was 85 ft s^{-1} (50 knots). Maximum vertical velocities were +12 and -21 ft s^{-1} at the locations indicated on the cross section. In the lowest extent of the flight path, near 7,000 ft, a light easterly flow was measured. This suggested that below the wave crests between 7,000 and 9,000 ft were light rotor-like circulations which, however, are not to be confused with the so-called rotors of stronger waves that form at higher altitudes and are usually marked by roll (rotor) clouds. In this case there was neither moisture nor sufficient amplitude of the flow to induce the formation of clouds at the crests of the waves. Only at a higher level, perhaps 30,000 ft, was there a cloud which formed in the principal wave crest.

Other fields. Temperatures measured on this flight were warmer than Standard Atmosphere to 425 mb and cooler above as shown in Fig. 3.23. An inversion appears below 7,000 ft (800 mb) and an isothermal layer between 615 and 580 mb (13,000-15,000 ft). Throughout the remainder of the "sounding" the lapse rate was nearly adiabatic. Deviations of temperatures measured from those of the curve are within ±1°C. The θ field, not unexpectedly, appears somewhat chaotic when analyzed separately and is not indicative of a lee wave. The D

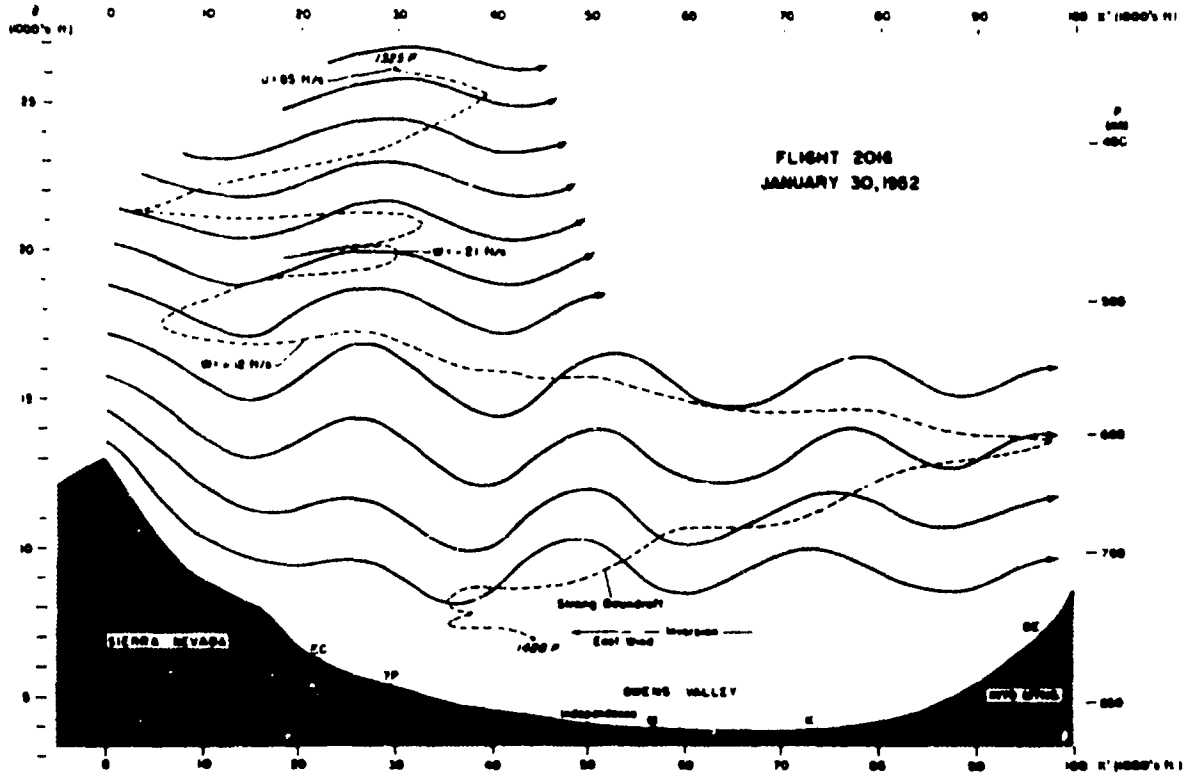

Fig. 3.22

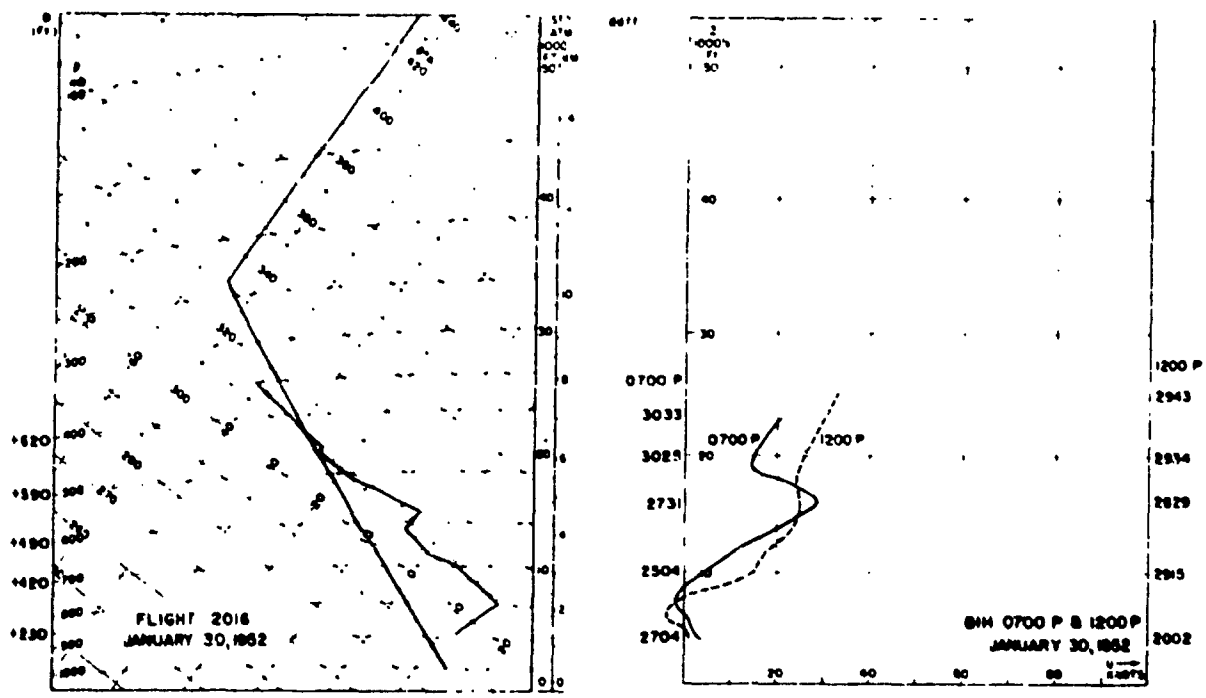

Fig. 3.23

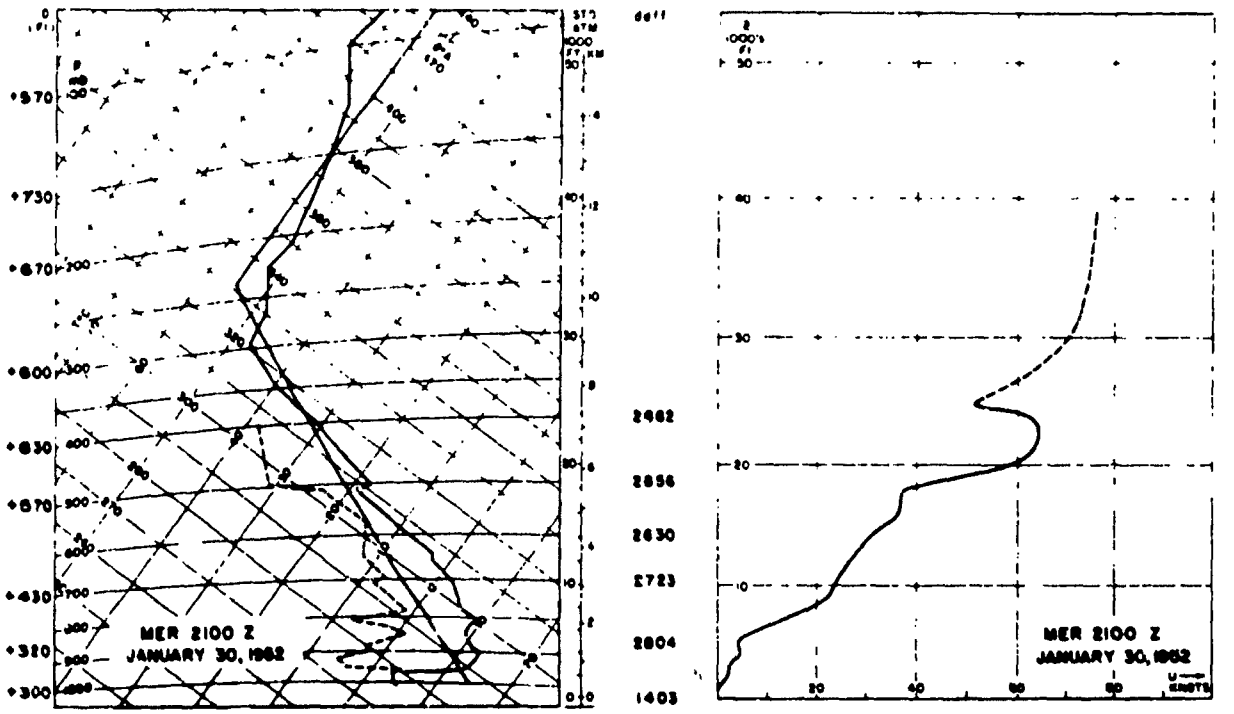

Fig. 3.24

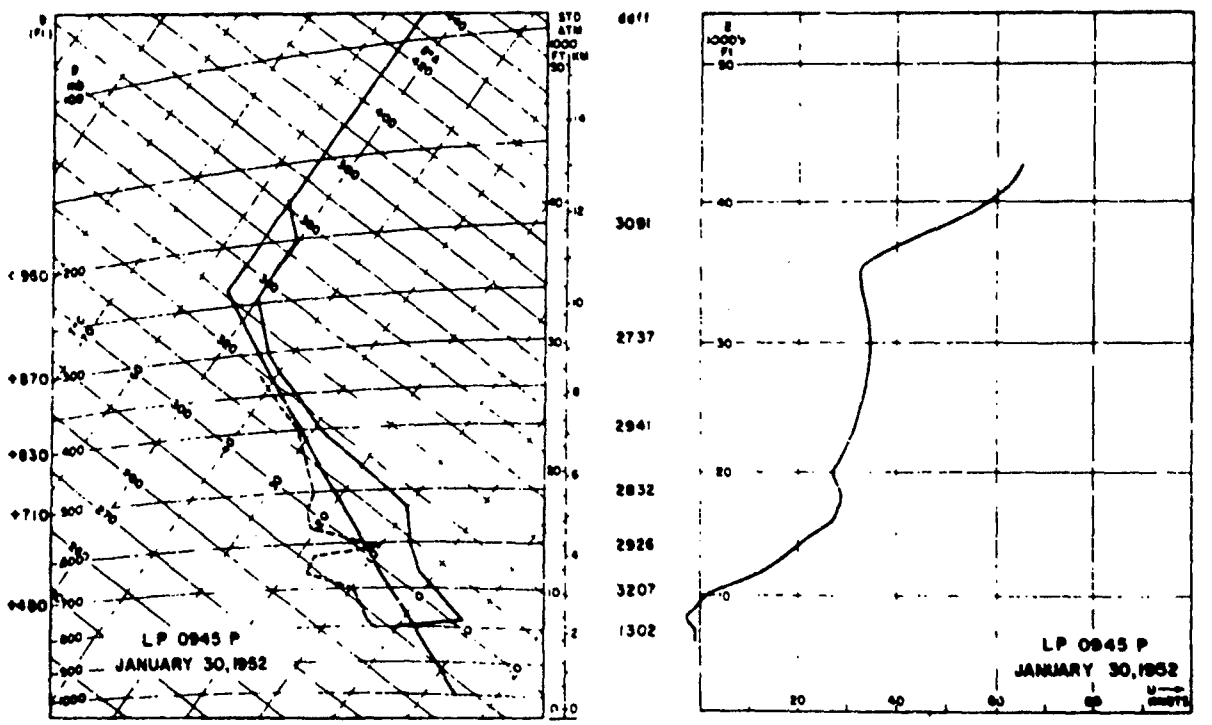

Fig. 3.25

field similarly does not lend itself to a reasonable analysis. The values from the sounding are given in Fig. 3.23.

Soundings and wind profiles. Merced, Lodgepole, and Bishop upper air data are shown in Figs. 3.24, 3.25, and 3.23, respectively.

6. Flight 2018, 16 February 1952: a strong lee wave.

Clouds and weather. The wave cloud phenomena of this day were the best developed and most extensive since those of 18 December 1951. Early in the morning a föhnwall appeared over the Sierra west of Bishop and during the day extended itself along the crest. Fracto-cumulus patches resolved themselves into roll clouds in the south (Fig. 3.26a) and over the Inyo Mountains. By noon the föhnwall had developed to about 4 miles south of Mt. Williamson (14,384 ft) and strato-cumulus clouds were observed moving from west to east over Onion Valley. By 1330 PST the föhnwall extended along the entire crest and the cloud fell covered Onion Valley. A high altostratus wall was seen to the west above and upwind of the föhnwall; from the sailplane its height was estimated to be about 30,000 ft. High cirrus bands formed parallel to the wind in the east, and to the southeast slight wave form was visible in cirrus.

No single, dominant stationary arch cloud formed, only small bands and patches. However, during the time of the flight the roll cloud was well developed (Fig. 3.26b) and extended in a solid chain over the Owens Valley xcept, as is usual, in the Bishop area where there was a break. The base of the roll cloud was observed to be at about 14,500 ft. The second wave crest was well marked by a smaller but continuous cumulus cloud band over the crest of the Inyo Mountains and continuing upwind of the White Mountains.

At dusk the cap cloud (föhnwall) swept far down the eastern Sierra slope but the föhngap never clouded over. No precipitation fell in the Owens Valley.

Flight summary. The data from this flight are the most complete of all the flights and are of especial interest for the study of a strong lee wave. The tracking began at 1217 PST (Fig. 3.27) with an upwind run on tow. Release was made in the strong updraft at 14,200 ft above 7P. About that time the sailplane was lost to view by the theodolites because of the intervening roll cloud but its 45-minute ascent to a maximum altitude of 33,000 ft was followed by the Raydist system. A downwind and an upwind run were performed between 1344 and 1400 PST after the sailplane had again been sighted by the theodolites. Later a crisscross run was tracked except for a gap during which the sailplane was above the roll cloud. The final run was made downwind under the roll cloud. The flight time from beginning to end of tracking data was 3½ hours.

Streamlines. The air flow pattern of the strong lee wave is shown in Fig. 3.28. As the flight was both long in time and extended rather far north of the tracking network, the data provide the most noteworthy examples of the four-dimensional character of the lee wave. The two-dimensional streamline cross section was constructed after data from portions of two of the runs had been deleted. First, the data from the northernmost region of the flight

Fig. 3.26a - 1020 PST, 16 February 1952. Southward from 12,000 ft. Mts. Williamson and Whitney on right. Developing wave and roll clouds.

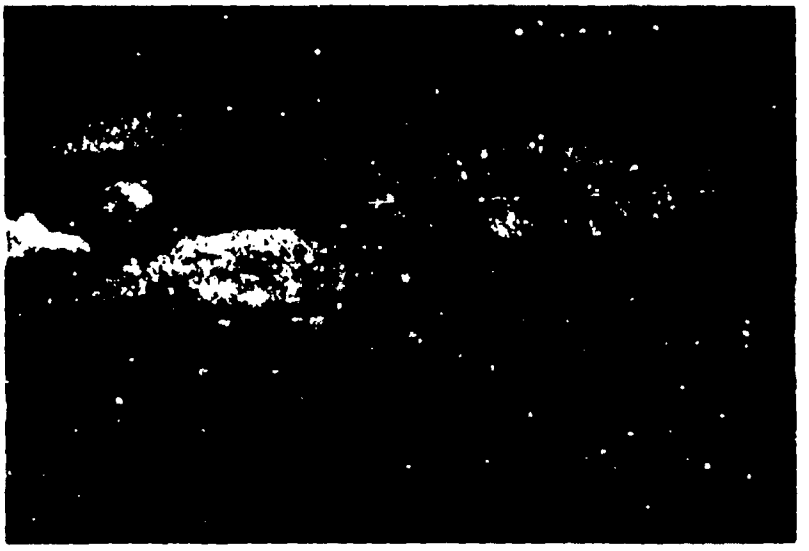

Fig. 3.26b - 1330 PST, 16 February 1952. Southward from Bishop Airport. Roll cloud and cloud-fall well developed. High, tenuous arch cloud. Photo by C. Patterson, U.S. Weather Bureau.

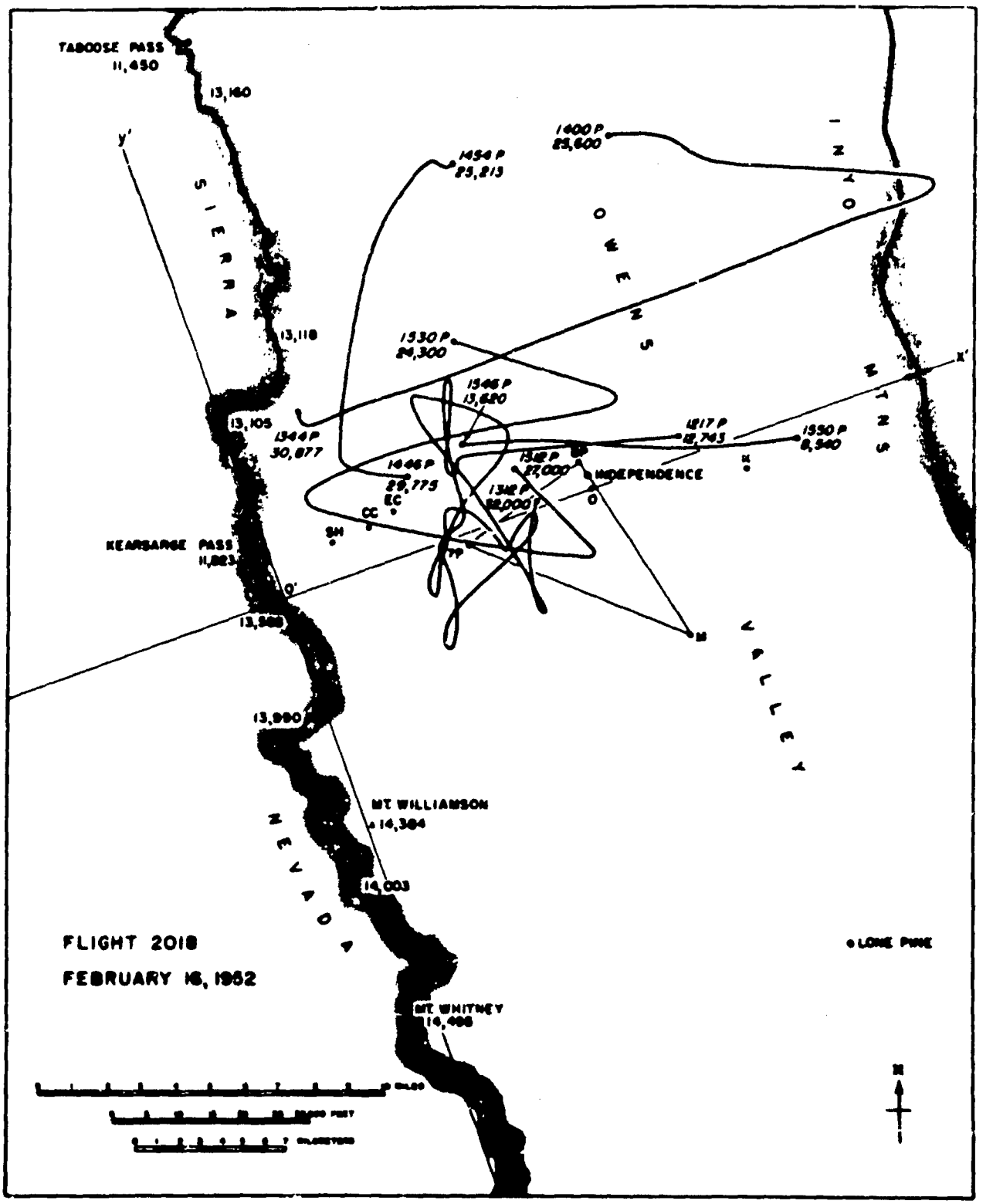
TABOOSE PASS
11,450
13,160
13,118
13,105
KEARSARGE PASS
11,823
13,990
13,990
MT WILLIAMSON
14,384
14,003
MT WHITNEY
14,496
SIERRA
NEVADA
1400 P
85,600
1454 P
85,213
1530 P
84,300
1546 P
13,620
1344 P
30,877
1446 P
88,775
1342 P
88,000
1417 P
88,745
1550 P
8,540
INDEPENDENCE
LONE PINE
FLIGHT 2018
FEBRUARY 16, 1952

Fig. 3.27

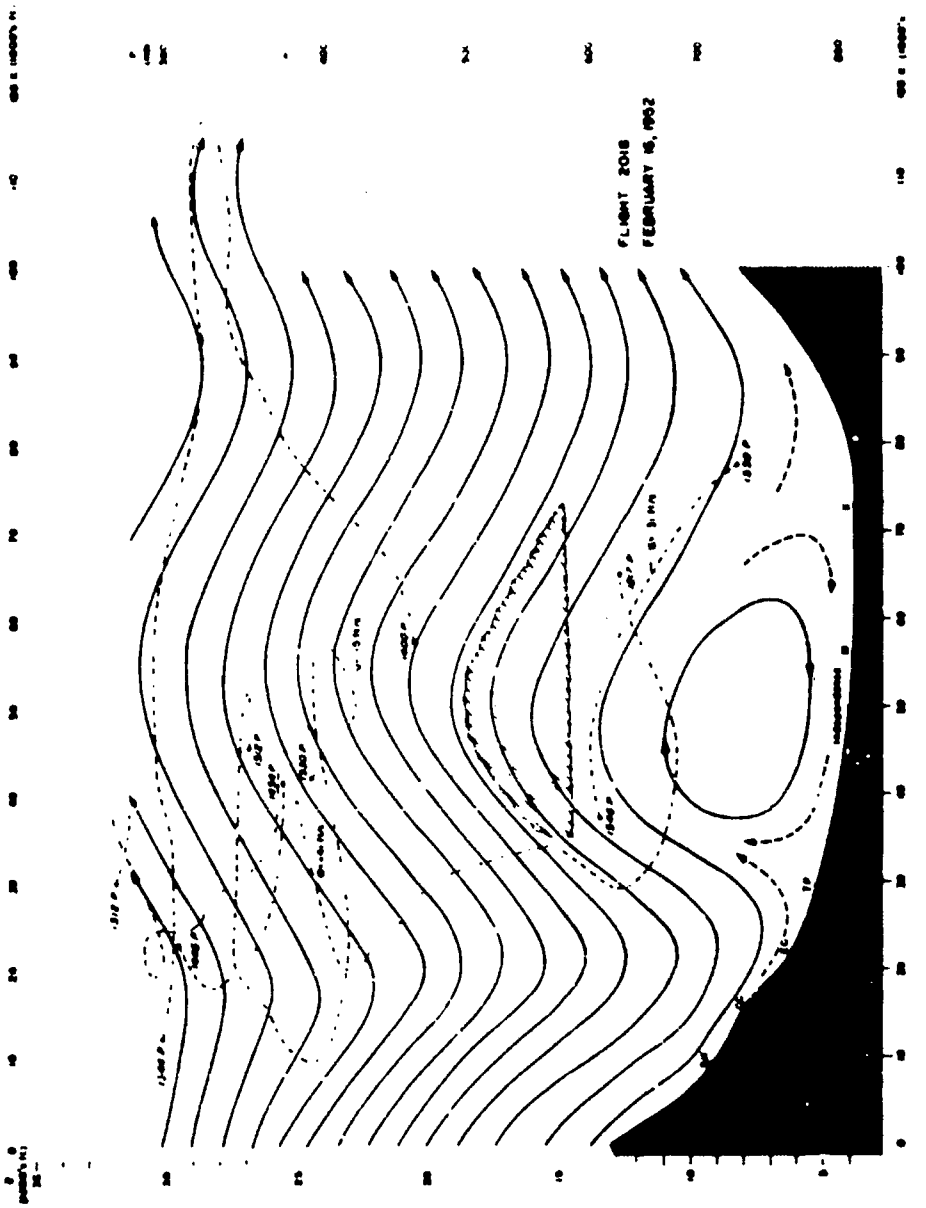

Fig. 3.28

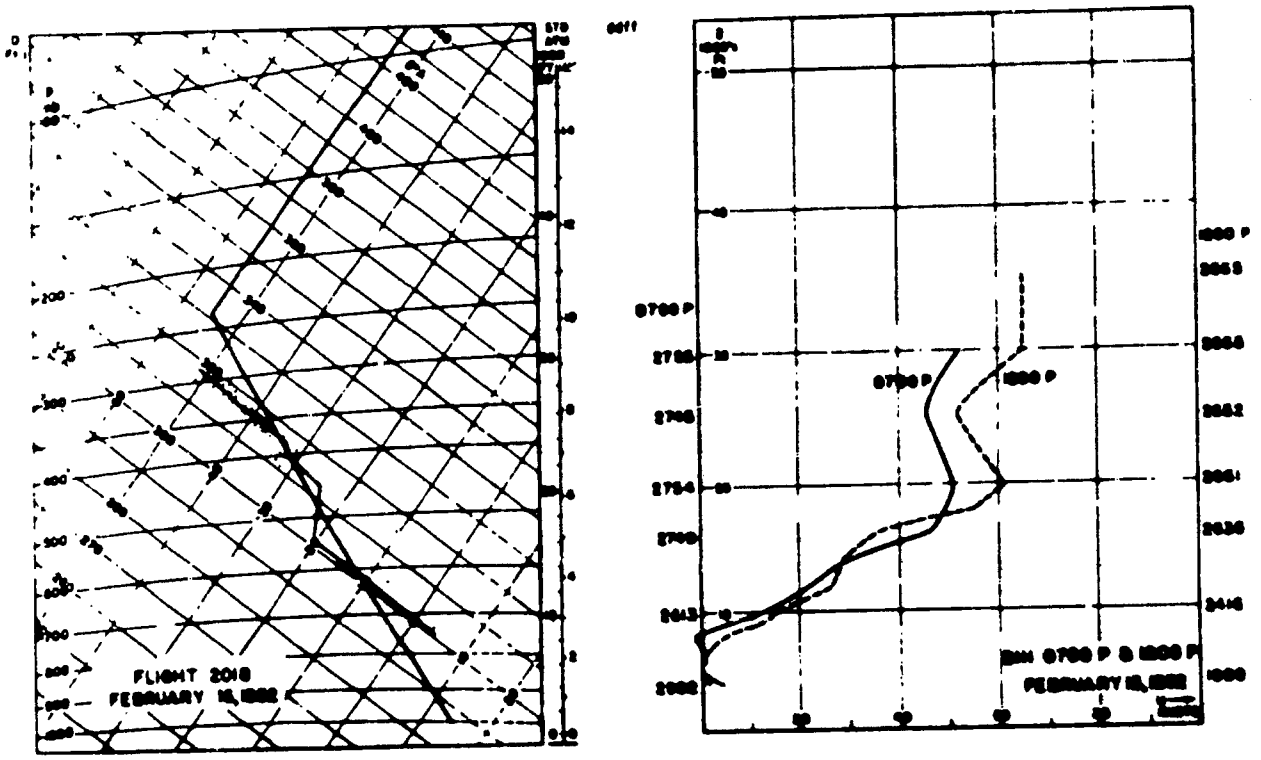

Fig. 3.29

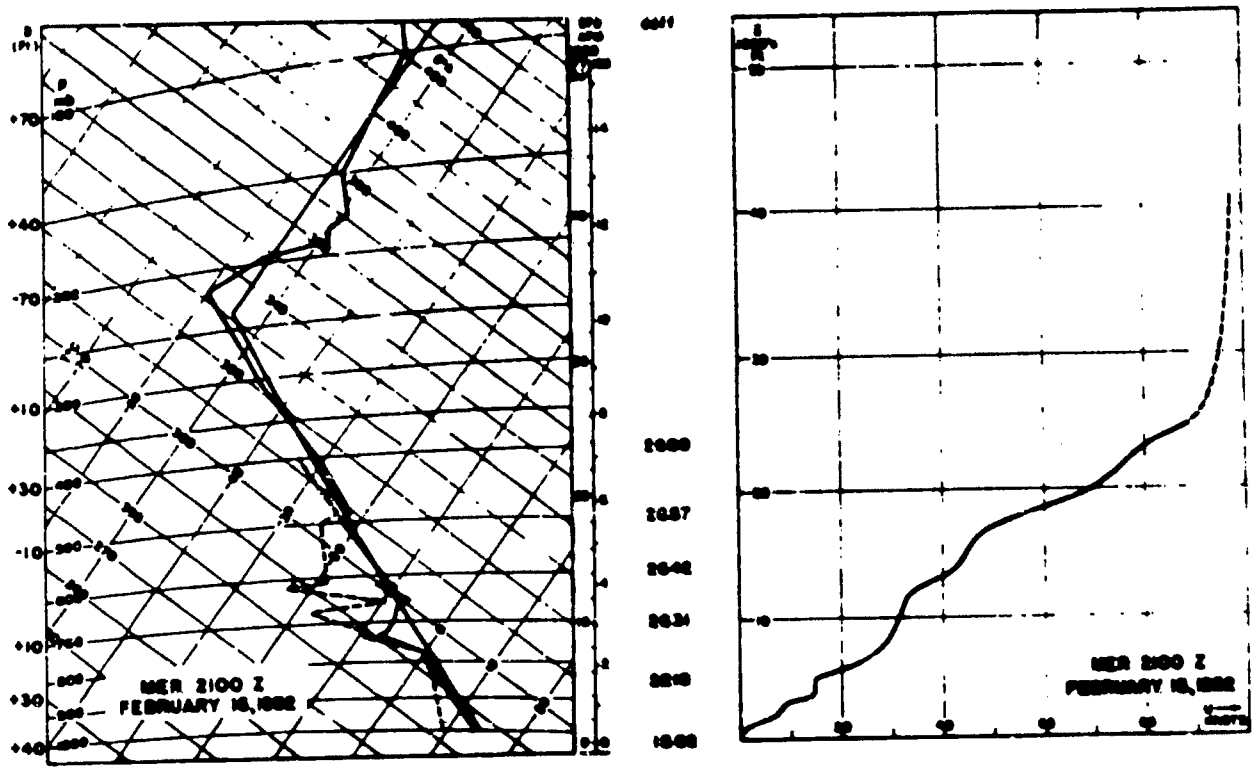

Fig. 3.30

showed the wave crest to be about 10,000 feet east of the crest position indicated by the southern portion of the flight. Examination of Fig. 3.27 reveals that this is undoubtedly a result of the eastward jog in the Sierra crest north of Diamond Peak (13,195 ft). Since the upper flow was roughly from 260 deg, the roll cloud line downwind was similarly displaced.

A second adjustment had to be made for the development which took place during the 3½ hours between the two flights under the roll cloud and the fact that the first, upwind flight was made on tow. With due allowance for probable errors of airborne measurements made while on tow, it was evident that the downdraft below the roll cloud had increased considerably in speed. Consequently, in order that the complete streamline pattern be consistent and quasi-synoptic, the data from only the first run under the roll cloud were used as guides in the analysis of the lower streamlines. The channel constant was 7.5.

The roll cloud sketched in the cross section was carefully constructed by photogrammetry and from the observer's notes. The turbulence below the leading and trailing edges of the roll cloud was rather severe. A narrow zone of comparatively smooth flow existed under the roll cloud over the center of the Valley.

The wave length of the flow appears to increase with height; measured from trough to trough it varies from 60,000 ft (18 km) at Z = 7,000 ft to 70,000 ft (21 km) at Z = 30,000 ft. An average value is 67,000 ft (20 km) which is also that at Z = 15,000 ft. $2\ell_{max}$ = 7,000 ft (2,150 m) at the mean altitude of 13,500 ft. Maximum vertical velocities measured along the flight path were +41 and -31 ft s^{-1}; the locations of these are shown in the cross sections. U_{max} was 115 ft s^{-1} (68 knots) near 24,000 ft at the point indicated. Measuring ϵ' and Δz along a vertical at x' = 32,500 ft through the inflection point of the flow, and computing U and w from the formulas $U = C/\rho\Delta z$ and $w = U/3 \tan \epsilon'$, some interesting results are obtained: maxima of U at the inflection points occur at Z = 15,750 ft where U = 100 ft s^{-1} (59 knots) and at Z = 27,550 ft where U = 96 ft s^{-1} (57 knots), and a single maximum of w = 28 ft s^{-1} occurs at Z = 15,250 ft.

Of greater interest are the synoptic variations of wind speeds between troughs and crests at different levels as measured along the path of Flight 2018 in Fig. 3.28. In the levels above the roll cloud zone the wind speed is least in the trough and greatest in the crest of the flow. Near 300 mb the speed varied from 21 ms^{-1} at the first lee trough to 31 ms^{-1} at the crest to 21 ms^{-1} at the second trough. Near 400 mb a similar difference is found; the speed varies from 24 ms^{-1} at the trough to 34 ms^{-1} at the crest. In the levels below the roll cloud the wind speed is greater in the troughs than in the crests as can be seen by comparing the channel width at the troughs and the crests in those levels. The horizontal wind speeds and values of the other synoptic fields measured at critical points in the vertical plane of the strong lee wave with rotor cloud are listed in Table 3.1 and discussed further below.

Other fields. The mean "sounding" of the flight (Fig. 3.29) straddles that of the Standard Atmosphere. The various temperatures measured along the flight path are also shown. As a first approximation it appears that two nearly adiabatic layers are separated by a rather thick stable layer between 540 and 450 mb (16,000 to 21,000 ft). A smaller stable layer appears between 400 and 385 mb. The two layers of steep lapse rate appear to have potential temperatures of 301° and 317° K respectively. The θ field fits the field of

Table 3.1 LEE WAVE MEASUREMENTS
FLIGHT 2018, 16 FEBRUARY 1952

Time PST	Position	Z ft	x' ft	p mb	T °C	θ °K	v ms-1	U ms-1	D* ft
1345	1st trough	29,790	20,200	304	-46.5	319	0	21	0
1348	wave crest	30,400	54,500	294	-51.0	316	0	31	-120
1350	2nd trough	28,800	86,800	319	-44.5	317.5	0	21	+ 80
1521	1st trough	(23,450)	18,000	402	-32.0	313.5	0	24	----
1525	wave crest	(23,400)	56,000	403	-33.0	312	0	34	----
1217	downdraft	12,420	32,200	632	- 7.0	304	-5	9	- 55
1220	wave crest	10,830	47,100	674	- 4.5	301	0	4	0
1223	updraft	11,070	62,600	665	- 5.0	302	+7	12	-110
1547	wave crest	14,170	45,500	589	-15.0	300.5	0	13	-100
1549	downdraft	11,000	65,400	669	- 5.5	300.5	-10	15	- 40

*At some points D is indeterminate because no independent value of Z was computed, the position in those cases having been determined by Raydist or by one theodolite.

motion fairly well, i.e., it does not contradict the assumption of adiabatic flow, but in places it is inconsistent because of time and space differences. With reference to the values of T and θ listed in Table 3.1, it is found that the lowest temperatures are found in the crests at all levels and the isolines of potential temperature approximate the streamline pattern as should be expected if the temperature changes along a streamline are adiabatic and the lapse rate is less than the dry adiabatic lapse rate.

The D values at the surface changed markedly as a result of the steady pressure fall during the flight. The barogram from Manzanar is shown in Fig. 4.2 of Chapter 4 where special surface observations of this date are discussed. The following values at various stations are given for the beginning and end of the flight:

Station	LP	SH	CC	EC	M	I	K	BIH
1221 PST:	+90	-55	-110	-110	-115	-90	-110	-115 ft
1548 PST:	+45	-125	-205	-210	-235	-225	-255	-205

It is probable that the heights of isobaric surfaces aloft would have decreased by at least 100 ft and probably 200 or 300 ft during the time of the flight. Thus again a quasi-synoptic cross section of the D field is rather unclear and the coverage is incomplete with a large gap in the Raydist-tracked section of the flight where no Z values exist. In general the values increase upward to 610 mb where the sounding crossed that of the Standard Atmosphere and above that level decrease.

Significant values of D measured along the flight path are given in Table 3.1. In the higher levels near 300 mb, D values appear to be highest in the troughs and lowest in the crest although one should temper this conclusion with the observation that since the points are not at the same level, there is undoubtedly some influence by the vertical gradient of D. However, the differences, of the order of 100 ft, are in close agreement with the observed acceleration of the wind from trough to crest at that level as will be demonstrated in Chapter 9. The D values measured directly below the roll cloud at the crest of the flow appear to be somewhat greater than those in either updraft or downdraft-unfortunately, no measurements were made in either trough--but this result is also somewhat inconclusive because of differences in elevation of the points and the consequent effect of the vertical gradient of D.

Sounding and wind profiles. Upwind conditions at Merced are shown in Fig. 3.30. The sounding shows rather moist air up to 400 mb and a stable lapse rate with one inversion near 650 mb (12,000 ft) and another near 480 mb (19,000 ft). The tropopause is at 218 mb (36,800 ft) with a temperature of -60°C. A stratospheric inversion has a maximum temperature of -49°C. The wind profile shows a rather strong shear to 25,000 ft, above which the geostrophic speed appears to be nearly constant. Unfortunately, no Lodgepole upper air data were obtained. The Bishop winds at 0700 and 1200 PST are shown in Fig. 3.29.

7. Flight 2020, 21 February 1952: a weak lee wave.

Clouds and weather. Wispy, veil-like lenticular clouds in irregular patterns appeared over Owens Valley (Fig. 3.31), forming and disappearing at irregular intervals. Stratocumuli lay in the valleys east of the Inyo Mountains with tops at about 9,000 ft. Another band of stratocumulus at about the same altitude stretched along the Sierra west of the Alabama Hills. A high altocumulus band thickening in the northwest showed smooth wave form along its leading edge.

Flight summary. Weak updrafts allowed a maximum altitude of 16,000 ft, from which descending downwind and upwind runs over the Valley were made (Fig. 3.32).

Streamlines. A somewhat abnormal flow pattern resulted from the streamline analysis (Fig. 3.33). The downwind run passed through two wave crests to a third which lay over the Inyo Mountains. However, the measurements of the upwind flight would seem to indicate a single crest of longer wave length in the lower levels. Since this result is not in agreement with either theory or other observations, an explanation is required. It is suggested that a separate wave system was induced on the low level (8,000 to 9,000 ft) inversion by the predominantly northwest wind at and below that level; that that wave system may have oriented itself parallel to the transverse ridges of the eastern Sierra escarpment; and that the sailplane's path may have been along a band of upward motion. Local convection or thermals can be invoked but appear unlikely as an explanation.

In the upward portion of the wave the half-wave length is about 15,000 ft, suggesting a full wave length of 30,000 ft (9.2 km) and the maximum vertical displacement about 1500 ft. The constant used for channel thickness was 5. The wind was weak; the sailplane was able to spiral, fly parallel to the Sierra, and upwind with ease. The lift was somewhat better south of the tracking network. Lift was found at the leading edge of cloud wisps but was not continuous between clouds. The maximum U was 70 ft s^{-1} (41 knots) and the maximum vertical velocities were +10 and -7 ft s^{-1}. As in the streamlines of Flight 2015, the trough tilts upwind with altitude.

Other fields. The sounding was cooler than Standard Atmosphere (Fig. 3.34). Stable layers appeared between 710 and 680 mb and between 605 and 580 mb. The maximum deviation of any individual point from the curve was ±1°C. The temperature field in the cross section is not significant in itself. Similarly, the θ field is reasonable, i.e., it can be analyzed to agree with the streamlines, but it is of insufficient coverage and accuracy to indicate the lee wave when analyzed independently. D values were negative at the surface and decreased with altitude, but their horizontal variation in the vertical plane presented a confused and insignificant pattern.

Soundings and wind profiles. Upper air data from Merced and Lodgepole are shown in Figs. 3.35 and 3.34, respectively. Bishop winds are plotted in Fig. 3.34.

Fig. 3.31 - 1145 PST, 21 February 1952. WSW from Bishop Airport. Photo by C. Patterson, U.S. Weather Bureau.

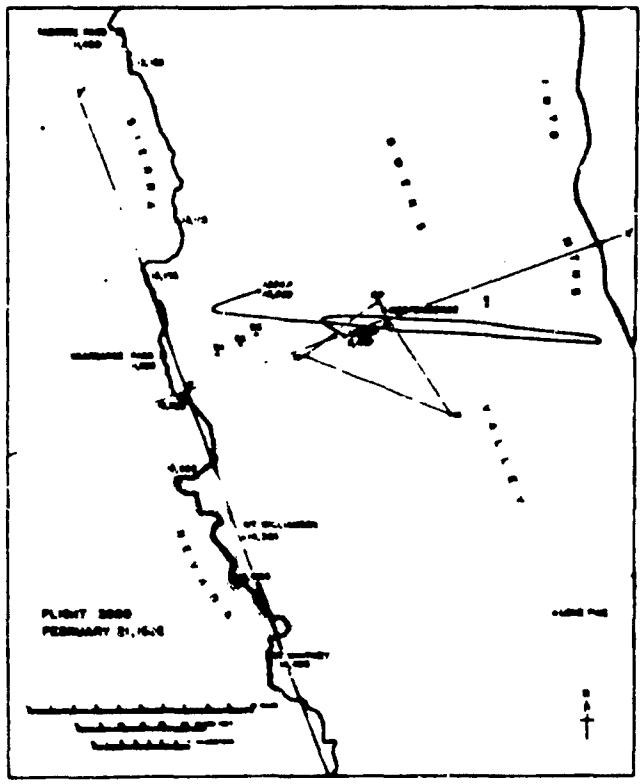

Fig. 3.32

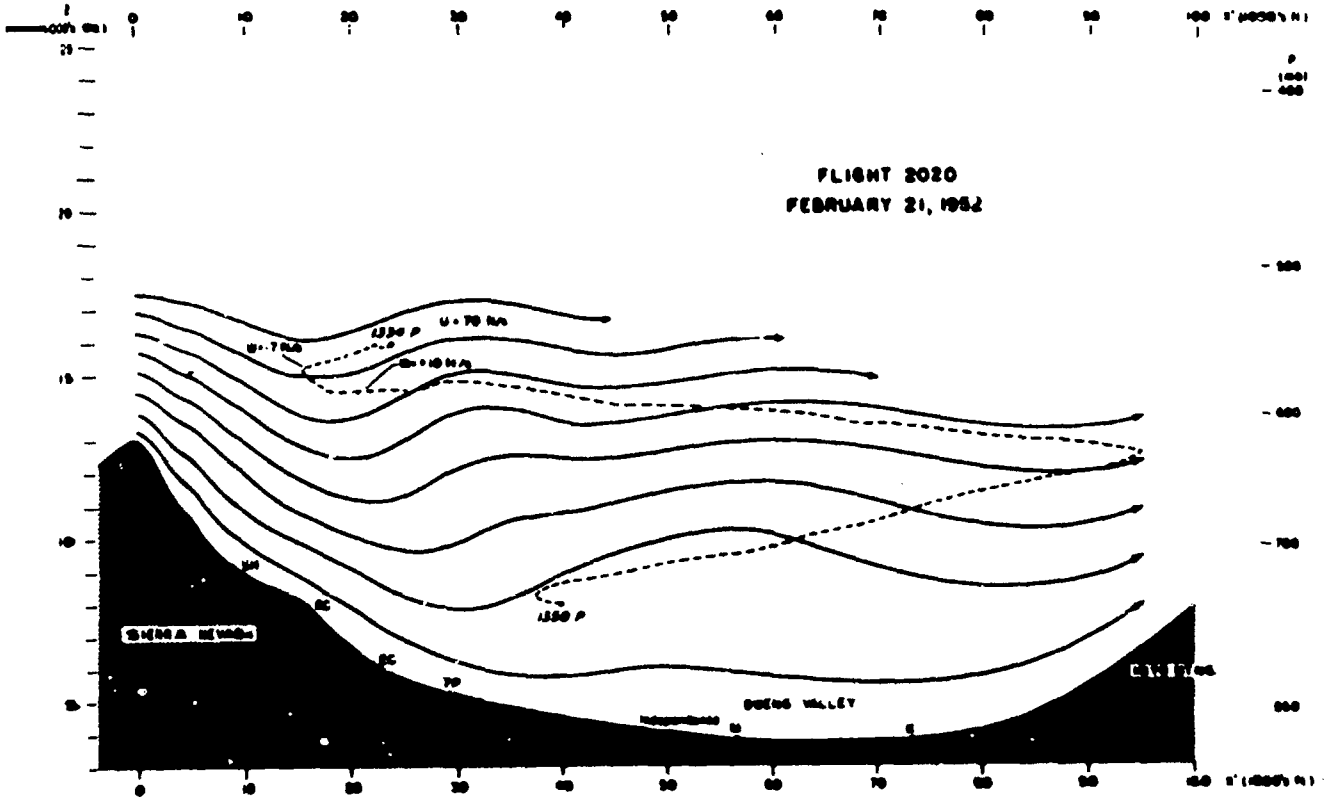

Fig. 3.33

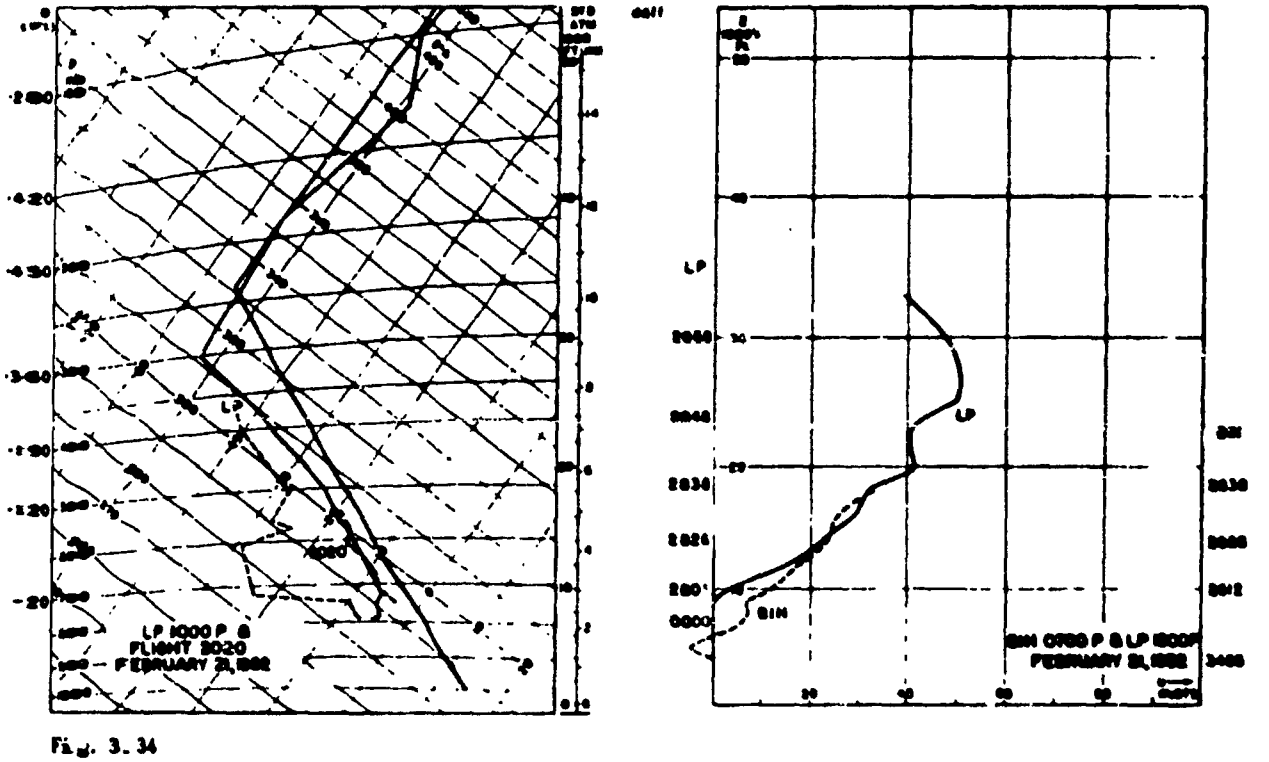

Fig. 3.34

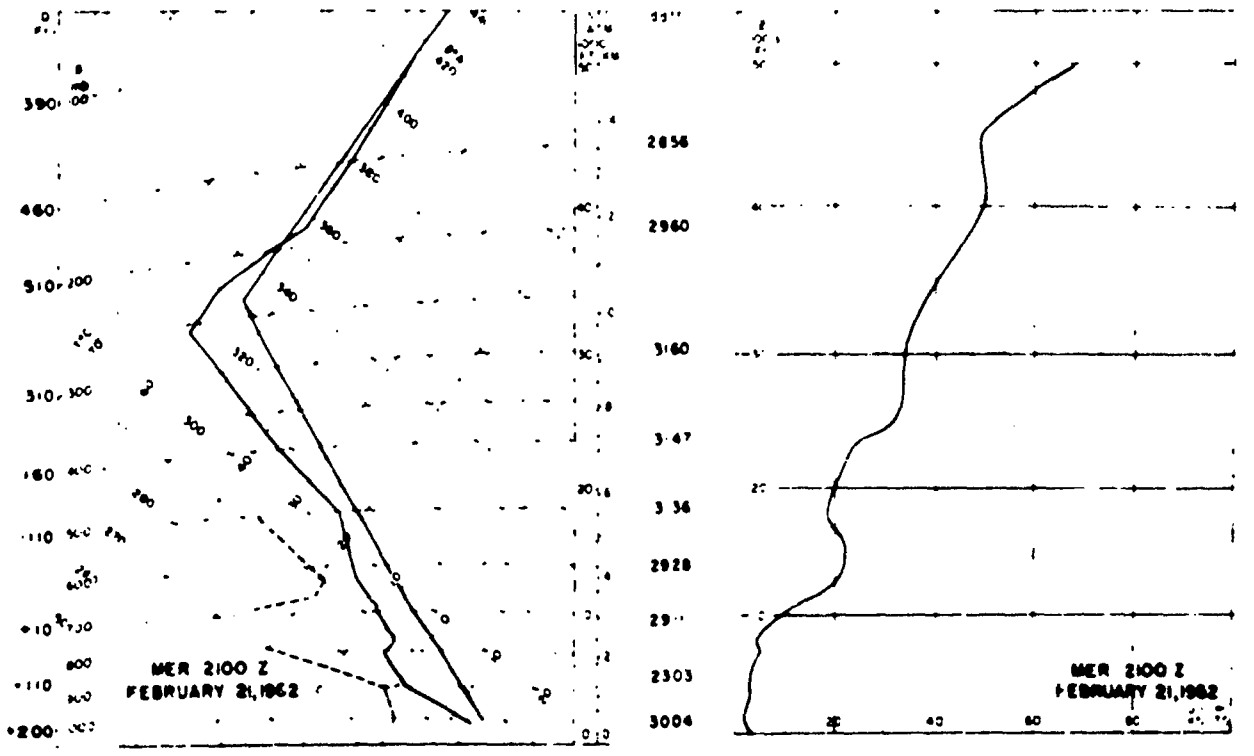

Fig. 3.35

Fig. 3.36 - 1020 PST, 19 March 1952. Southward from Bishop Airport.

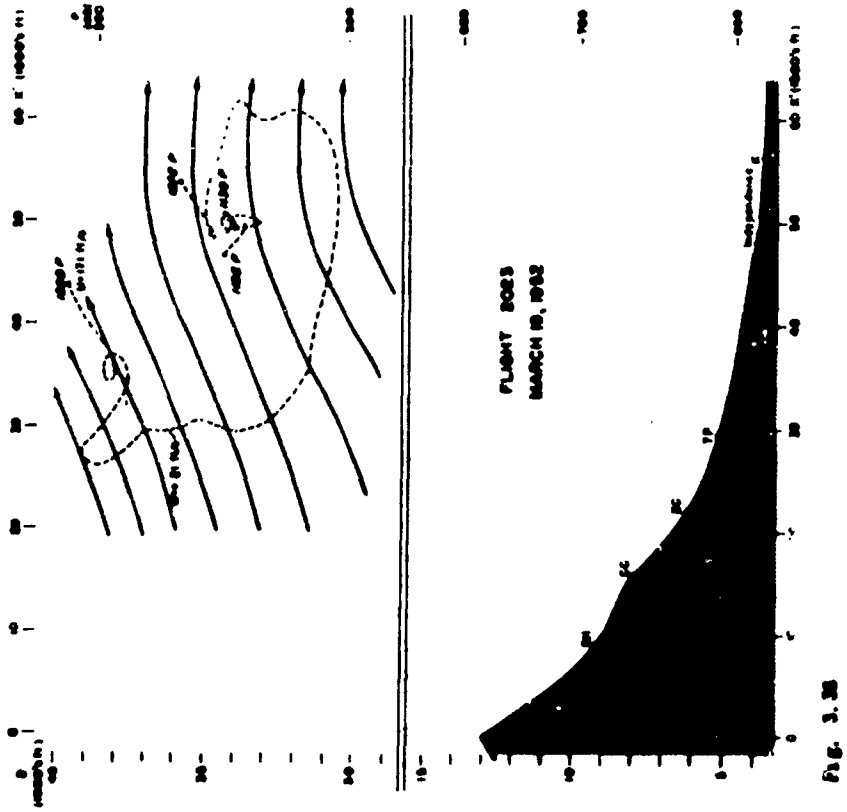

Fig. 3.36

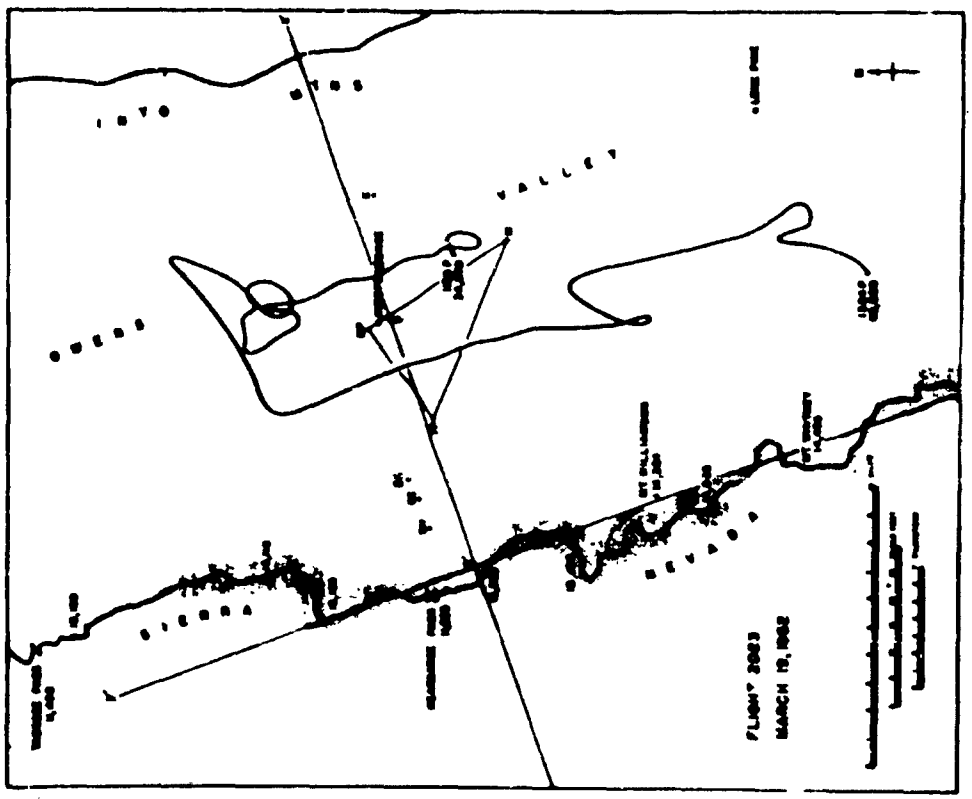

Fig. 3.37

8. Flight 2023, 19 March 1952: a strong lee wave.

Clouds and weather. At sunrise the föhnwall in the west swept in a white blanket down the Sierra slope, to the south was a wide föhngap over a long cloudfall, and a massive smooth-topped roll cloud hovered over the east side of the Valley surmounted by a high, stationary arch cloud (Fig. 3.36). The wave crest, with an apparent downwind tilt with height, lay exceptionally far back from the Sierra and the clouds were higher than usual. The top of the cloud deck over the Sierra was at 17,000 ft, while that of the roll cloud was at 19,000 ft. The base of the roll cloud was at 14,200 ft at its leading edge over the center of the Valley and at 16,500 ft directly over the Inyo Mountains. Lenticular-form clouds were observed as high as 43,000 ft. The wave phenomena persisted all day but by evening were diminishing.

Flight summary. On the tow, moderately turbulent air was encountered at low levels with rates of climb and fall of the order of ±2,000 ft min^{-1} as low as 7,000 ft. The sailplane was forced to release in strong turbulence west of Big Pine at 9,500 ft altitude and continued smoothly upward at a rate of ?,000 ft min^{-1}. In 20 minutes an altitude of 33,000 ft was reached, by which t me the sailplane was over the tracking area. The wind speed being exceptionally strong and the downdraft of the wave apparently east of the Inyo Mountains, no downwind run was made because of the uncertainty of being able to return upwind to the Owens Valley. Exploring the lift zone along the Sierra crest (Fig. 3.37) the sailplane worked southward and continued to rise leeward of Mt. Whitney. The tropopause was penetrated at 39,000 ft as the sailplane continued to soar at 1,000 ft min^{-1} into the stratosphere. A maximal altitude of 44,500 ft* was reached at 1332 PST. A deliberate descent was made from that point though the rate of climb was still +700 ft min^{-1}. The return to Bishop was made by a "crabbing" flight up the Valley in the lift zone. Considerable variations of horizontal wind speed and updrafts were experienced as roll cloud fragments formed and disappeared rapidly in the lee of Coyote Ridge southwest of Bishop. Moderate to heavy turbulence was encountered at 13,500 ft east of Coyote Ridge.

Streamlines. Due to the high altitude at which the tracking run was begun and its limitation to the updraft zone, the streamline pattern (Fig. 3.38) covers a rather small area. Consequently, an exact determination of the wave length was not possible and both the amplitude and vertical velocities are probably less than half the values of those at 20,000 ft. The constant used for channel width was 7.5.

From the half-wave length it appears that the wave length between 30,000 and 40,000 ft altitude was of the order of 90,000 ft (28 km). $2\zeta_{max}$ in the same altitude range in the cross section is about 4,000 ft. The wind at those levels was near 290 deg; the average U component was 117 ft s^{-1} (68 knots) and the maximum U was 171 ft s^{-1} (101 knots) measured near 40,000 ft. No systematic wind gradient along the y' axis was detected, probably because of the inseparability of time and space changes. W_{max} in the cross section was +21 ft s^{-1} at 36,500 ft. At 40,000 ft w exceeded +10 ft s^{-1}. It is probable that vertical

*The present world altitude record for sailplanes.

velocities in the roll cloud region were of the order of ±60 ft s^{-1} with shorter period gusts of the order of ±100 ft s^{-1}. The towplane, exploring the lower levels of the lee wave in level flight attitude after the sailplane's release, experienced steady 3,000 ft min^{-1} rise near the leading edge of the roll cloud and a 6,000 ft min^{-1} fall in the downdraft southeast of Bishop and west of Black Mountain of the Inyo range.

Other fields. A flight sounding is plotted in Fig. 3.39. The air was stable between 550 and 500 mb and approximately dry adiabatic to the tropopause near 200 mb (39,000 ft). A minimum temperature of -78°C was measured there, and at 44,500 ft (154 mb) the temperature had risen to -71°C. Comparison of the ascent and descent temperature curves indicates a considerable cooling aloft during the time of the flight. At 18,000 ft the air had cooled about 10°C in 3 hours. This can be attributed to the passage of the cold front at these levels as can be seen from the large-scale synoptic charts in Chapter 5. (See Figs. 5.46, 5.47, and 5.48.)

The field of potential temperature was chaotic in the cross section; values ranged from 307° to 317° K with no logical pattern. The reasons for this--large $\partial/\partial t$ and $\partial/\partial y'$--are easily seen on examination of the sounding and the horizontal flight path. Another difficulty in θ analysis on vertical cross sections is the small variation of θ in an altitude layer of several thousands of feet whereby actual horizontal variations are of the same order of magnitude as time variations and errors of measurement.

D values measured reflect the synoptic situation and perhaps also the variations caused by the lee wave. The values were generally negative, ranging in the cross section from +170 to -430 ft. The higher values with respect to the (x',z)-plane were found in the trough to the west and in the lower altitudes; the lower values were found in the east at the higher elevations near the crest of the wave flow.

Soundings and wind profiles. As no radiosonde data from Merced were available, and the upper flow was nearly westerly, a mean sounding for Oakland and Santa Maria was constructed (Fig. 3.40). It is similar to the sounding of 18 December 1951 (Fig. 3.14), but with a higher inversion at 480 mb (19,000 ft) and a clear-cut tropopause at 193 mb (39,000 ft). Unfortunately, true winds are lacking above 10,000 ft, so geostrophic winds were used to construct the wind profile.

The Sequoia sounding is shown in Fig. 3.39. No wind measurements could be made because of the strong flow and the presence of the cap cloud. In Fig. 3.39 are also shown the Bishop winds aloft. The 1200 PST ascent reached an altitude of 60,000 ft near the time that maximum altitude was attained by the sailplane. Of great interest are the strong positive vertical shear between 7,000 and 25,000 ft and the large negative shear above 45,000 ft.

9. Flight 2025. 30 March 1952: a moderate lee wave.

Clouds and weather. No lenticular clouds appeared over Owens Valley but wave forms were observed to the north and over the Mojave Desert to the

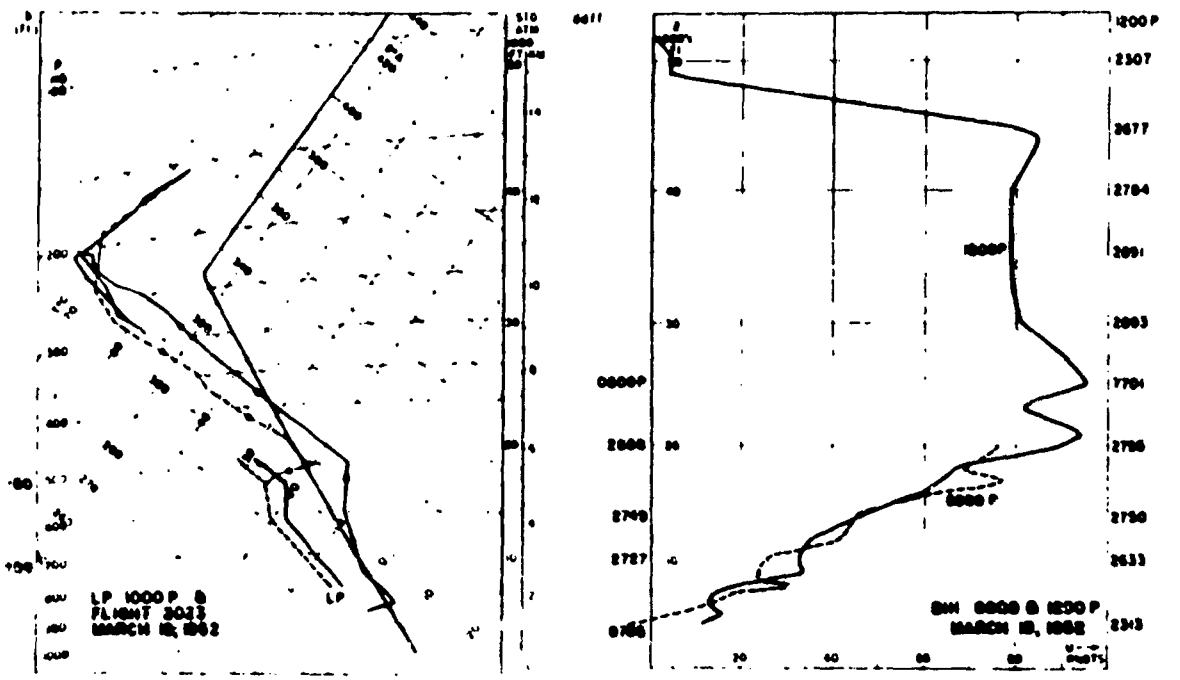

Fig. 3.39

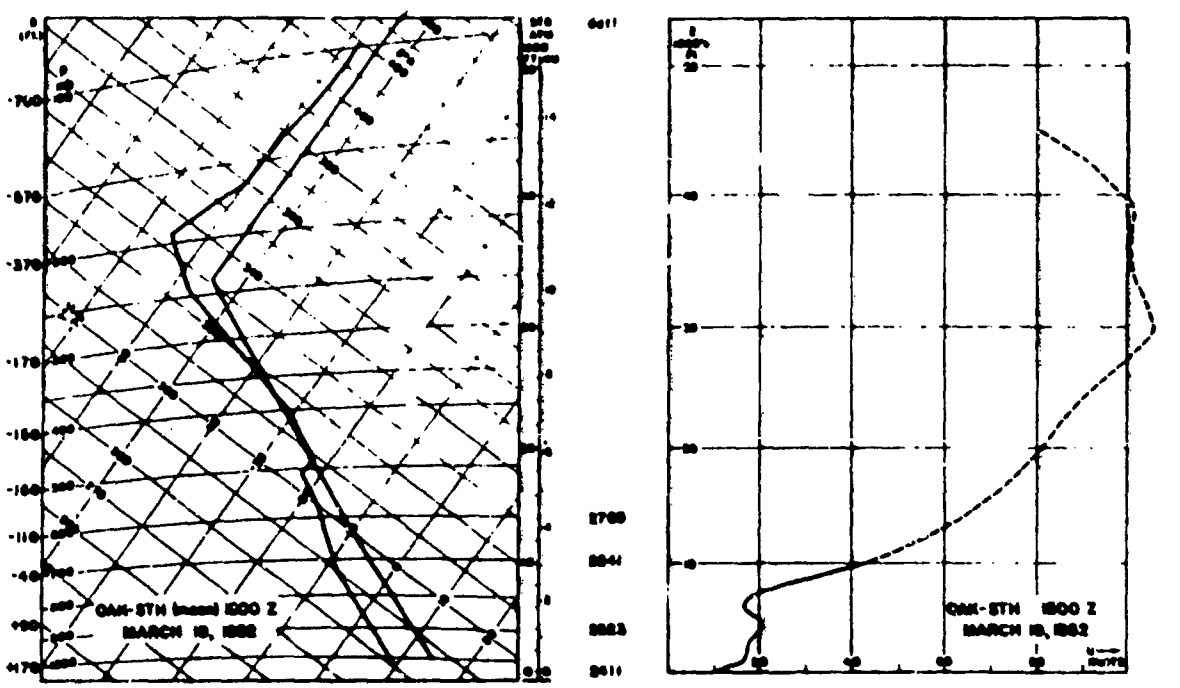

Fig. 3.40

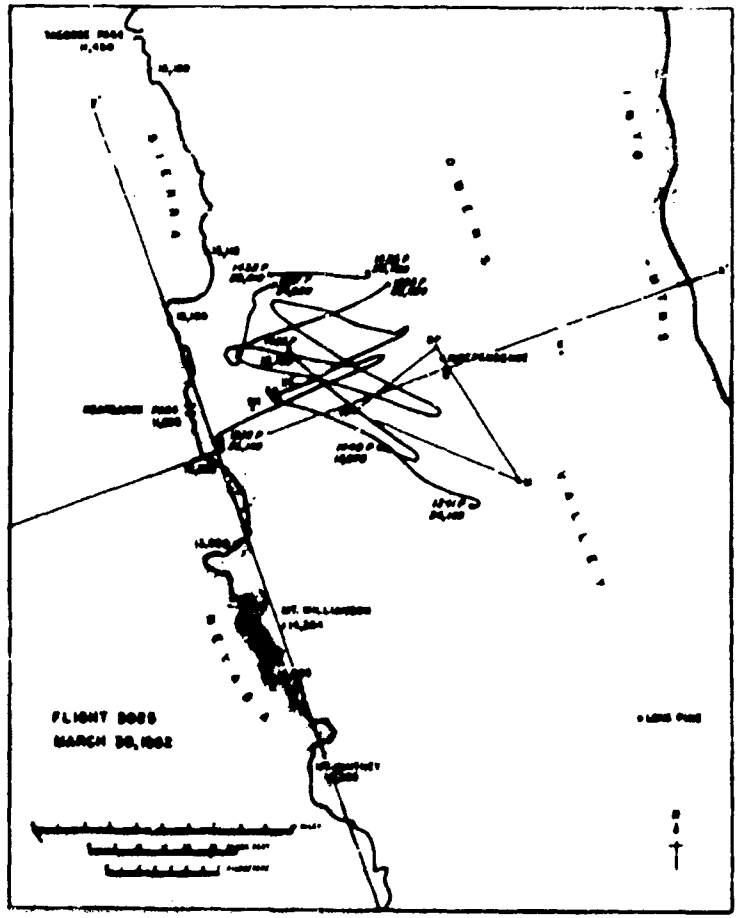

Fig. 3.41

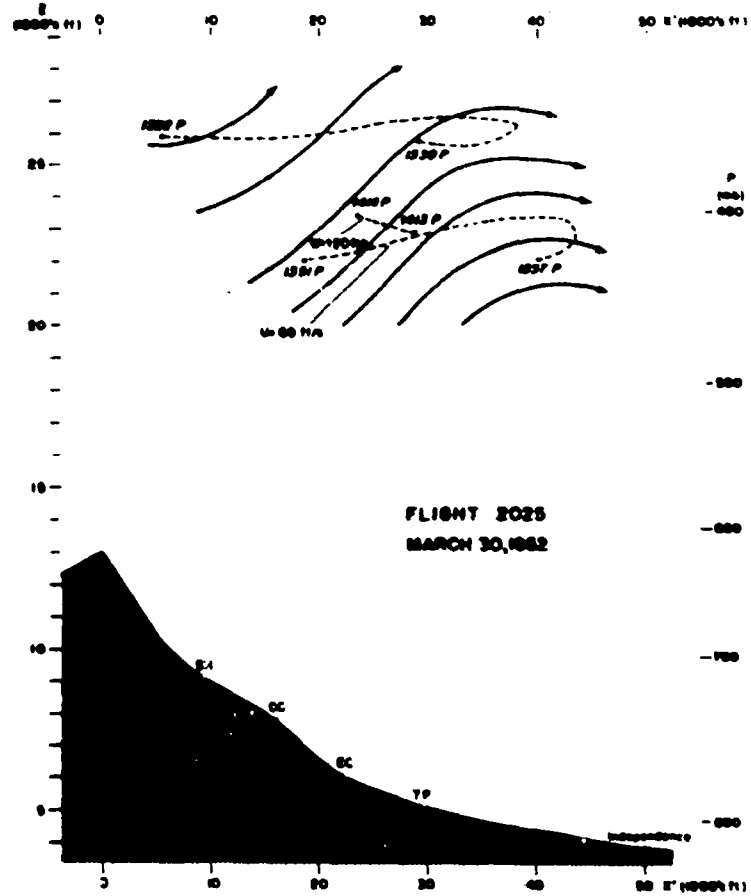

Fig. 3.42

south. There were a few scattered cumuli and a few transitory roll cloud fragments in the Independence area. The San Joaquin Valley was covered with a stratocumulus deck.

Flight summary. A two-sailplane operation was performed but only the data from the theodolite-tracked flight was reducible. The path of this flight is shown in Fig. 3.41. Release was made at 13,700 ft after moderate turbulence (-6, +2 G's) was experienced on tow. It was found that the best area of lift lay between Black Mountain and Kearsarge Pass. The maximum altitude reached was 27,000 ft. A second wave crest was not found on the first downwind run but an updraft zone of a second wave was encountered at a lower level on the second run. Rotor zones were marked by turbulence rather than clouds. Below 8,000 ft only turbulence and downdrafts were encountered.

Streamlines. Because of space differences along the flight path in the y' direction, it was necessary to plot and analyze three separate vertical cross sections. All were quite similar; one of them is reproduced in Fig. 3.42. The principal difference among the three cross sections was the position of the trough and crest of the flow with respect to x'. These varied by approximately 10,000 ft along x' as a consequence of the west-northwest flow and the variation of the Sierra crest. In all three the wave length appeared to be about 25,000 ft and $2\zeta_{max}$ about 3,000 ft. C was 5. The direction of V_H was about 300 deg; U_{max} was 69 ft s^{-1} (41 knots) at 25,000 ft. Vertical velocity maxima were +20 and -8 ft s^{-1} as indicated on the cross section.

Other fields. A flight sounding is shown in Fig. 3.43. D values are positive; they increase from west to east and generally increase with altitude with an apparent minimum value at 24,000 ft.

Sounding and wind profile. Again, no Merced sounding was made but since the flow was west-northwest, the Oakland 1500 GCT data are used to represent upwind conditions (Fig. 3.44). No Lodgepole upper air data were obtained. The Bishop pibal is shown in Fig. 3.43.

Summary of meteorological results.

The streamline cross sections and soundings presented in this chapter summarize the air flow pattern in the lee of the Sierra and the quasi-synoptic upwind temperature and wind profiles in the vertical for 9 selected cases. Considering the empirical results from all the cases, the following conclusions were drawn:

1) Some lee waves appear to have relatively no tilt with height while in others there is rather pronounced upwind tilt. The observed wavelengths ranged from 14,000 ft (4.4 km) in the weak lee wave of 29 January 1952 to 90,000 ft (28 km) in the strong lee wave of 19 March 1952.

2) The flow is adiabatic; temperatures are coolest in the crests and warmest in the troughs at all levels. In general, leeward soundings appear to have steeper lapse rates than those from windward with warmer temperatures in the lower troposphere and cooler temperatures in the upper troposphere.

3) In strong lee waves without appreciable tilt, the maximum wind speed in the horizontal occurs at the trough at levels below the roll cloud zone and at the crest at levels above the roll cloud zone. At a level in the roll cloud zone the vertical velocities appear to reach maximum values.

4) All of the 3 cases of strong lee waves were associated with similar upwind temperature soundings with pronounced inversion layers whose tops lay between 12,000 and 19,000 ft altitude. The other lee wave cases of moderate and weak intensity were associated with varying degrees of stability in the troposphere but generally without big inversion layers near mountain top level.

5) In the 3 strong lee wave cases the wind profiles were similar with large vertical shear in the lower troposphere and with speeds increasing to maximum values of the order of 100 knots near 30,000 and 40,000 ft. Wind profiles for the moderate and weak lee wave examples showed lesser wind speeds at mountain crest level and lesser vertical shear in the troposphere.

6) The principal gradient of D value is that in the vertical due to the sounding being warmer or colder than that of the Standard Atmosphere. Significant horizontal differences in D are detectable only in strong waves. In the only strong wave case* allowing comparison between points at roughly the same level, it was found that in the upper layers there was a gradient of D from trough to crest of the order of 100 ft; this difference was in agreement with the observed increase in wind speed of 10 m s^{-1} from trough to crest at that level.+ In the lower layers of a strong lee wave the gradient of D between trough and crest is either less than, or in the opposite direction to, that in the upper levels. In none of the flights were large negative D values (altimeter errors)** measured.

Conclusions concerning the problems of analysis. Streamlines derived from the horizontal and vertical wind components show most clearly a "synoptic" picture of the lee wave while the analyses of the fields of temperature, potential temperature, and pressure (D values) present more complicated and somewhat confused patterns because of their greater sensitivity to instrument and data reduction errors, "streakiness" of these variables in the atmosphere itself, and to time and space (north-south) variations in the course of the flight. It appears that if a lee wave persists for several hours during a day--and it is usually observed to do that--the wind field, which depends upon the slope of pressure surfaces which in turn depends upon the spatial (horizontal and vertical) gradients of temperature, can remain more nearly the same while the absolute values of T, and, consequently, θ and D, are changing more rapidly. The D field was further limited to theodolite-tracked portions of the flight since no Z values were gotten from Raydist. Finally, analysis of the θ field was nearly impossible throughout deep layers where the lapse rate was nearly adiabatic since in those regions instrument errors, time variations ($\partial\theta/\partial t$), and north-south variations ($\partial\theta/\partial y'$) were all of the same order of magnitude as the vertical variation ($\partial\theta/\partial z$).

---

*Flight 2013, 16 February 1962.

+See Example 1, Chapter 9.

**This subject is discussed more fully in Chapter 9.

Leaving the discussion of other techniques of measurement to a later chapter, refinement of this (sailplane tracking) technique of obtaining quantitative lee wave data would require these improvements:

1) More accurate instrumentation. In particular, it would be desirable to have airborne thermometers accurate to the order of $\pm 0.1^{\circ}C$.

2) The flight should be made along the wind and cover as large a section of the vertical plane as possible within a relatively short time period in order to minimize effects due to non-fulfillment of the steady state condition, $\partial/\partial t = 0$ and the two-dimensional condition, $\partial/\partial y' = 0$.

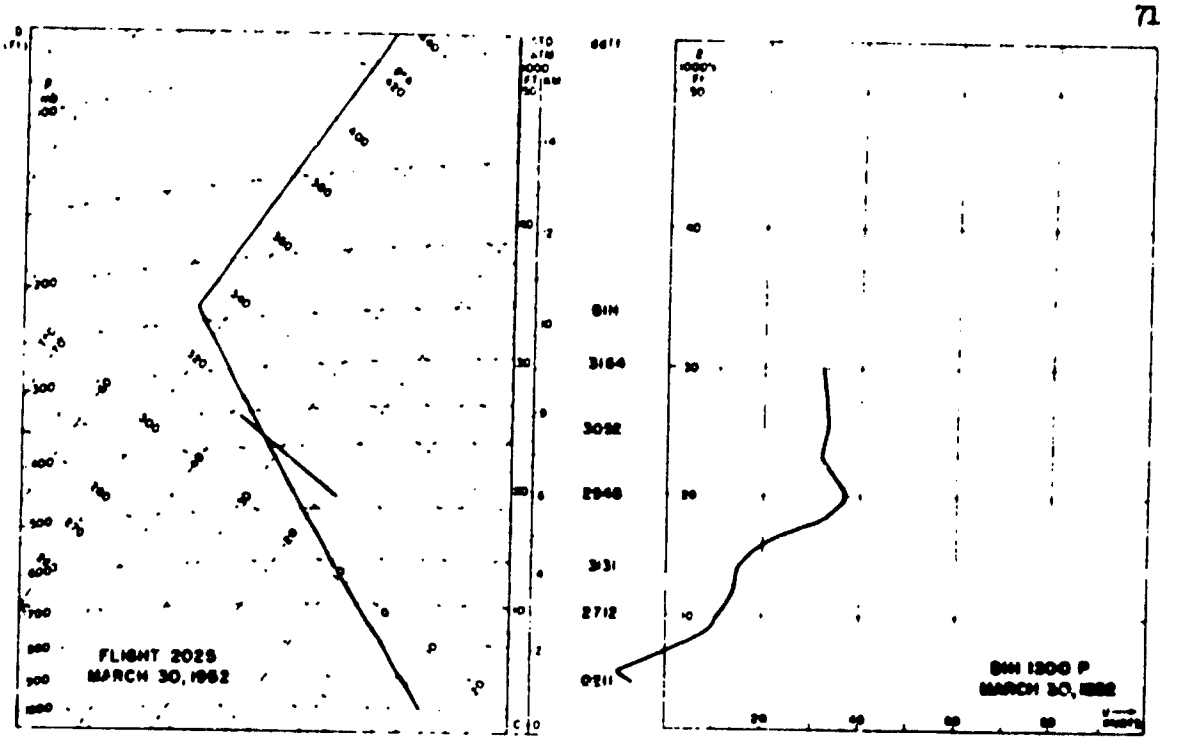

Fig. 3.43

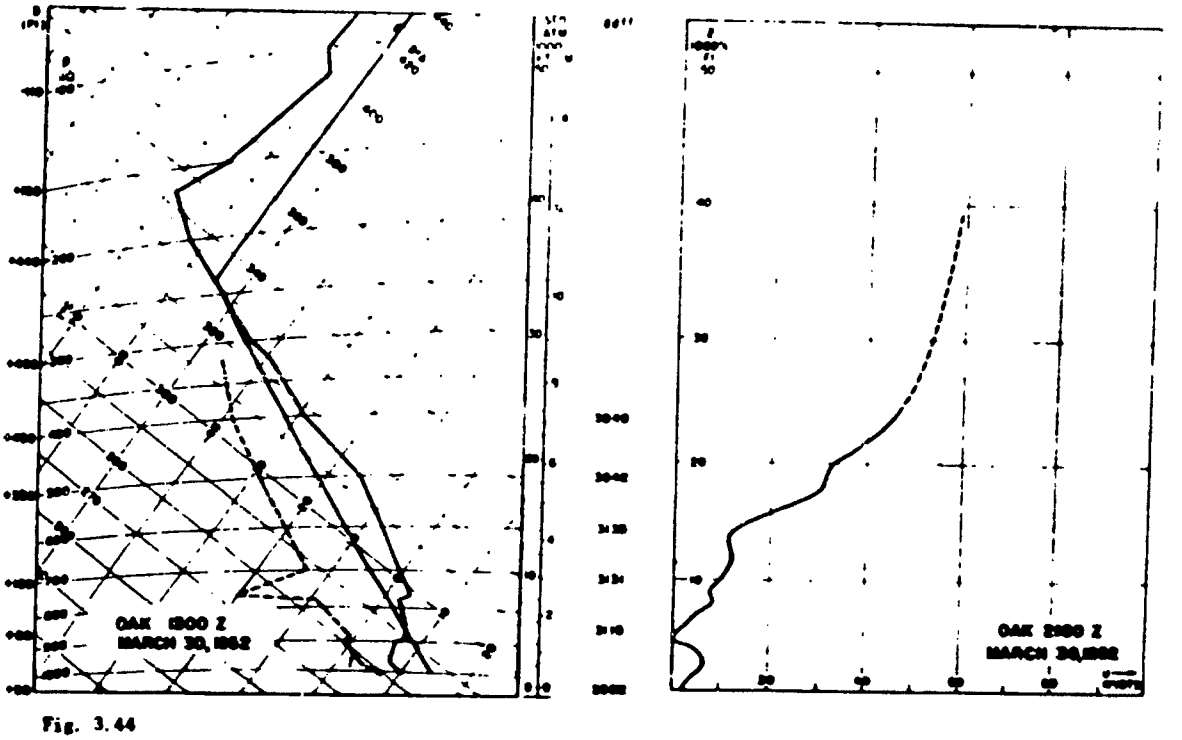

Fig. 3.44

4. ROTOR FLOW STUDIES

Introduction.

What is known as the rotor zone is the layer of the lee wave flow centered near or somewhat above mountain top level and extending downward to the surface and upward through a depth varying from 2,000 to 10,000 ft. It is generally more turbulent than the laminar-like flow of the upper wave and may or may not be marked by rotor (roll) clouds. The air flow within the cloud is not actually rotor-like but gives this illusion because of the strong vertical shear through the layer. For examples see Figs. 3.2, 3.9, 3.28, and 3.36 of Chapter 3.

Awareness of the rotor or roll cloud as an important feature of many Sierra lee waves increased greatly during the latter part of the 1951-2 field project. After a study of the time-lapse motion pictures of the rotor cloud phenomena of 18 December 1951, it was pointed out by Professor J. Bjerknes that the flow pattern resembled that of an hydraulic pressure jump and it was decided that this hypothesis should be tested by obtaining pertinent data from the rotor cloud zone.

Special measurements which were begun in February, 1952, are described in Chapter 1. They include the meteorograph flights, the placement of additional barographs across Owens Valley, and the mobile surface observations of Dr. J. Knox. These data were treated in a preliminary study in 1952 by Knox, who developed a one-dimensional dynamic model of a pressure jump and applied this model to test the observations from the case of 18 March 1952. The results of this investigation were encouraging but further progress was frustrated by serious uncertainties in data reduction and analysis, and the lack of certain critical measurements. Specifically: the ground stations were unsurveyed at the time and an adequate large-scale topographic map of the area did not exist; and there were no quantitative measurements of wind velocity at the mountain crest level, above the cloudfall, and over the rotor cloud.

Having lain fallow for a few years, these data have now been re-examined with the object of organizing them in a coherent fashion. The cases chosen for presentation of analyzed data are the strong waves of 16 February and 19 March, the sailplane data of which were treated in Chapter 3, and two additional cases which, except for unfortunate failures in film transport and processing, would have had complete sailplane coverage as well. These latter two cases are the moderate wave of 3 March and the strong wave of 18 March 1952. The surface and upper air synoptic charts for all four cases treated here are shown and discussed in Chapter 5.

Treatment of the data.

Surface observations and measurements. The locations and altitudes of the barograph stations are listed in Chapter 3 and are shown graphically in the horizontal and vertical flight sections of that chapter. The barographs at the Ski Hut (SH) and Manzanar (M) were set according to the corrected mercurial barometer readings at those stations.* At all the other stations the barographs were set by a precision aneroid barometer which in turn was corrected to a contemporary reading of the mercurial barometer at Manzanar. The barograms were corrected for time and pressure errors by comparing chart readings with notes taken at times of setting and removal of charts. Some random errors are probable due to variable hysteresis in the aneroids and the inability to check and reset the barograms daily or oftener as is usually done at weather stations; the probable maximum absolute error of this type is ±0.03 inch.

Other fixed instruments were a thermograph and an anemograph, both located at Manzanar. The thermogram was corrected for time and mercurial thermometer readings at the beginning and end of each trace. The anemogram, which indicated wind direction and speed graphically, was corrected for chart time errors.

The mobile surface measurements, taken at specified points at half-mile intervals across Owens Valley between Kearsarge (K) and Eckert's Cabin (EC), consist of the following:

1) Pressure measured by a Wallace and Tierman aneroid barometer to the nearest tenth of a millibar, and corrected to the mercurial barometer at Manzanar. Correction for local gravity (minus 1 mb) was also applied.

2) Temperature as measured by a standard sling psychrometer to the nearest tenth of a degree Centigrade.

3) Wind speed measured by a Friez three-cup anemometer to the nearest mile per hour.

4) Wind direction measured by a wind vane and a pocket compass to a sixteen point compass scale.

5) Notes on the development and movement of the rotor zone. These notes are documented as well as possible with photography.

Pressure data from both mobile and fixed instruments were reduced to D values by converting pressure to pressure altitude and subtracting the latter from the surveyed altitude of the station. Temperature was reduced to potential temperature by the formula $\theta = T (1000/p)^{2/7}$. Because of their relevance to vertical cross sections of the wave flow and for the reason that they generally vary more slowly with height than p and T, D and θ were used to represent the surface pressure and temperature fields, respectively. Since the

---

*Besides corrections for temperature and scale errors, a correction of minus 0.027 inch was applied for local gravity as explained in Appendix B.

measurements were made during a period of several hours and since important synoptic and diurnal changes in the fields were occurring during that time, it was found most convenient and meaningful to plot θ, D, and winds on two-dimensional (t, x') charts. On these diagrams the time, t, ranged from 0700 to 1900 PST and x' from the Sierra crest to the west slope of the Inyo Mountains. In these analyses the D field is the most complete since the continuous barograms from several stations could be used, whereas θ and wind analyses depended solely on the mobile measurements and continuous data from only one station, Manzanar. As can be seen from a horizontal flight section and from the map in Fig. 1.2, all of the stations except Manzanar (M) fall closely along x'.

Upper air observations. Meteorograph flights were made in the morning which, with a few exceptions, was before the lee waves had reached their maximum development. Lack of a sufficient number of flight personnel and the limitation of the tracking systems prvented dual exploration in the afternoon by both sailplane and power plane. Consequently the meteorograms could not be used in the same cross section as the sailplane flight data but had to be treated separately.

On the power plane flights the meteorograph was suspended in a frame under the left wing of the aircraft; temperature and pressure traces and time marks were made by three pens on the blackened chart attached to the hand-wound revolving drum. The traces were made permanent by dipping the chart in a solution of shellac and alcohol after removal from the instrument at the end of the flight. In reducing these data, the time marks were identified from the observer's notes and the distances from the flange of the contemporary pressure and temperature traces were measured by dividers. From the calibration curves of the instrument these distances were converted to pressure and temperature readings which were in turn corrected for air speed (dynamic effects) by the following formulas and table:

V_I	Δp	
80 mph	+3.2 mb	$\Delta T = 0.85\ (V_T/100)^2$
85	+2.8	
90	+2.4 where	$V_T = V_I\ (\rho/\rho_o)^{1/2}$
95	+2.0	
100	+2.0	

and V_I = indicated airspeed

V_T = true air speed

ρ = actual air density

ρ_o = density of standard conditions of p_o, T_o

The flight path was plotted both on a (Z_p,T) section and on a transparent overlay of the topographic map (scale 1:62,500); projected on the x' axis; and plotted in the (x', Z)-plane. Critical points, including the time

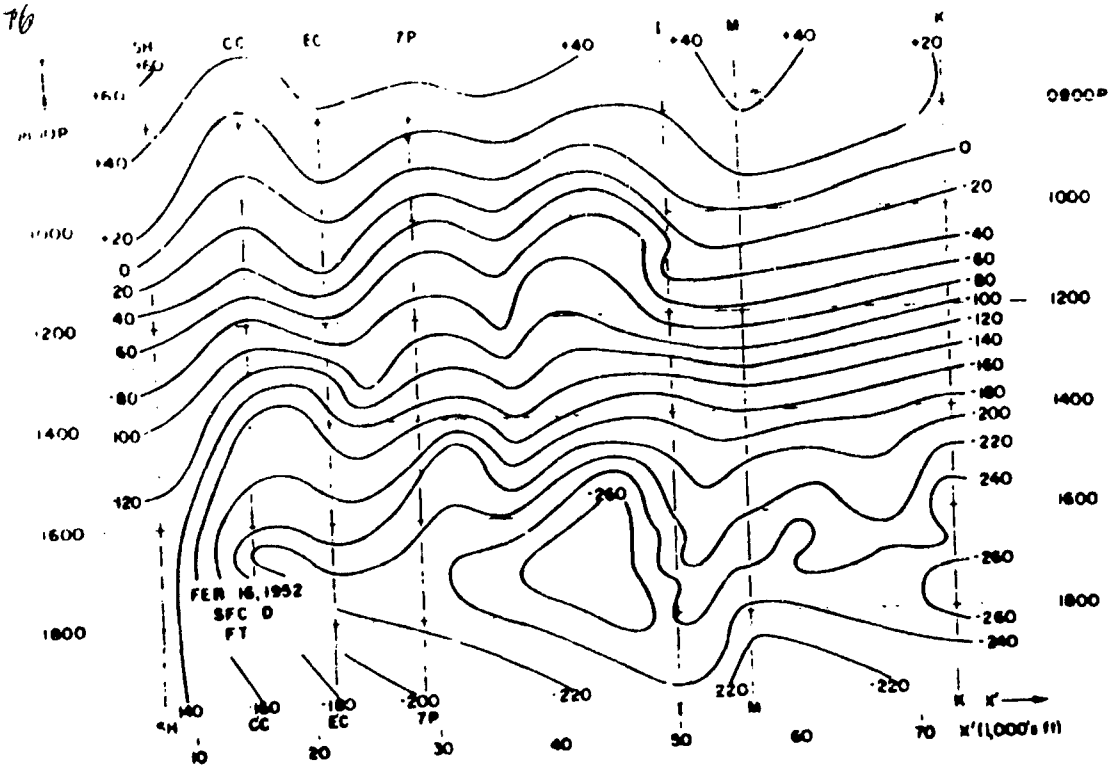

Fig. 4.1

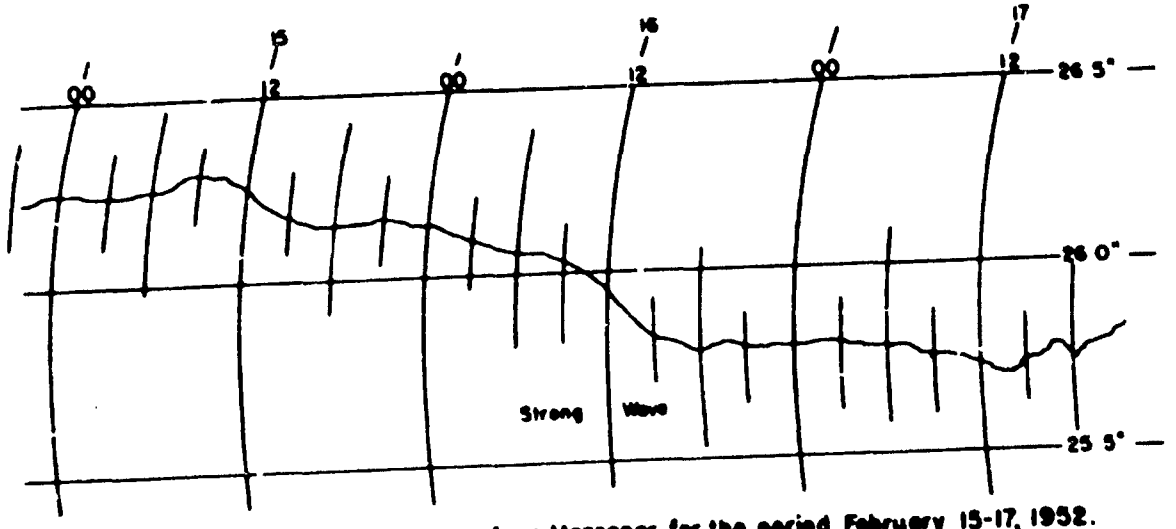

Fig. 4.2 Barograph trace from Manzanar for the period February 15-17, 1952.

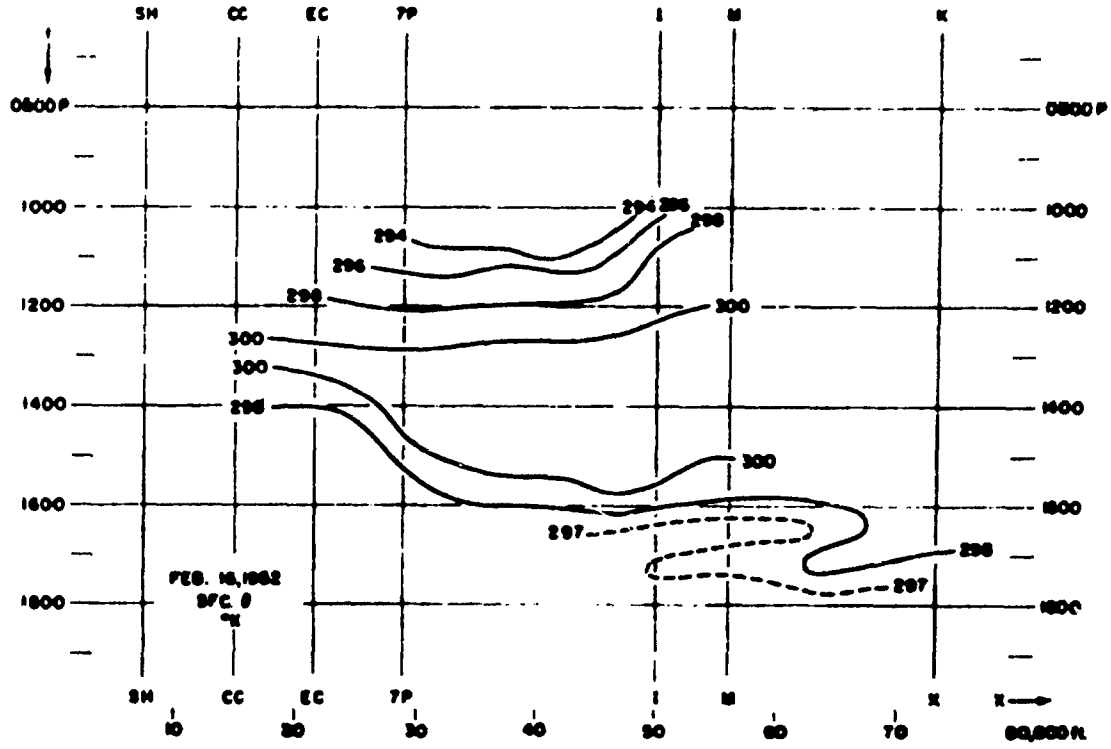
SH
CC
EC
7P
I
M
K
0600 P
1000
1200
1400
1600
1800
294
296
298
300
297
FEB. 16, 1962
SFC. θ
10
20
30
40
50
60
70
80,000 ft.

Fig. 4.3

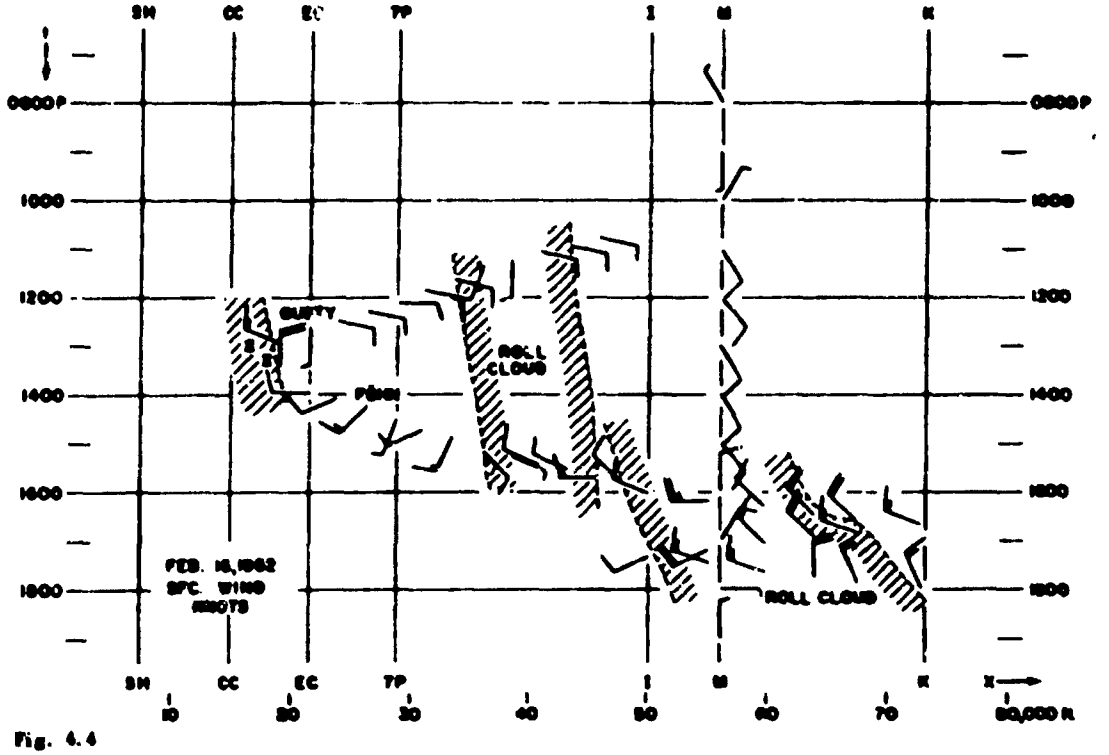
SH
CC
EC
7P
I
M
K
0600 P
1000
1200
1400
1600
1800
GUSTY
FÖHN
ROLL CLOUD
ROLL CLOUD
FEB. 16, 1962
SFC. WIND
KNOTS
10
20
30
40
50
60
70
80,000 ft.

Fig. 4.4

marks, were added where the values of θ computed as described above were plotted. This field was the only one analyzed in the vertical, there being no direct measurement made of either wind or of D value. Cloud and terrain photographs were very useful in helping to reconstruct the flight path and to synthesize the structure of the lee wave in the vertical.

Other upper air measurements used were Lodgepole (LP) soundings which were used as guides in the analysis of the G field over the Sierra and Bishop double-theodolite pilot balloon computations which were examined for effects of vertical motion.

Case I, 16 February 1952: a strong lee wave.

A review of the other observations from this date presented in Chapter 3 (Case 6), may be made by the reader. The strong wave shown in Fig. 3.28 was in the early stages of development during the meteorograph flight as can be seen by the cloud structure (Fig. 3.26a) at that time. For this reason and the fact that this was the first meteorograph operation with consequent inexperience of techniques, the data could not be made meaningful and so have not been presented here. However, the surface measurements are shown and recourse is had presently to the Flight 2018 cross section for pertinent rotor zone measurements.

In the (t, x') distribution of D in Fig. 4.1, the large pressure fall throughout the day at all stations is pronounced and the temporal gradient of D is more striking than the spatial gradient until late afternoon, when a distinct low pressure area formed west of Independence. The barogram from Manzanar is shown in Fig. 4.2.

There was no thermogram record from Manzanar on this date but, fortunately, the trip up the Sierra slope was made near the time of maximum temperature so that some idea of the diurnal change can be had. The θ analysis (Fig. 4.3) suggests that the isolines of θ are roughly parallel to the isolines of t but there are not enough data for certainty.

In Fig. 4.4 are shown the wind measurements and various observations of weather and roll cloud positions. The mobile measurements were made in a region of laterally overlapping roll cloud lines during much of the day. The southernmost band lay closer to the mountain crest than the larger band extending northward. This effect was probably due in part to stronger wind velocities aloft in the north and rather more of the upward jog in the Sierra crest in that area. It will be recalled that the same problem had to be dealt with in the analysis of the sailplane flight data on this date. In general, the winds across the Valley have large E or SE components during the morning and early afternoon, shifting to SW and then NW in the late afternoon. There is no apparent correlation with the roll cloud positions. The most abrupt change in the diurnal wind pattern occurs between 1515 and 1530 PST, when the shift between southerly and northerly winds takes place. This is clearly not a lee wave effect but appears to be of synoptic origin, perhaps a shallow frontal passage or simply the reversal of the y' pressure gradient in the Owens Valley as the lee trough becomes more intense in the Lone Pine area than in the Bishop area. The following time section at the Bishop Weather Bureau station (BIH) illustrates the changes in the various surface fields during the day:

Time (PST)	D (ft)	T (°F)	T_D (°F)	Dir.	Wind Speed & Gusts (mph)
0730	0	31	26	WNW	3
0830	- 5	37	27	SSE	5
0930	- 35	44	24	SSE	4
1030	- 45	47	21		C
1130	- 80	51	21	SSW	8
1230	-120	54	23	S	11
1330	-150	56	21	S	8
1430	-190	56	20	SSW	6
1530	-200	53	23	WNW	15 + 29
1630	-210	56	17	N	15 + 31
1730	-230	53	18	N	16
1830	-225	50	19	N	12 + 20
1930	-245	48	24	N	19

In order to ascertain quantitative values of the various synoptic fields in the vertical plane through this strong lee wave with a well-developed rotor cloud, one can review the measurements at critical points along the path of Flight 2018 on this date (Fig. 3.28), which data are summarized in Table 3.1. As mentioned in Chapter 3, the maximum w along a vertical through the inflection point upwind of the wave crest occurred at 15,250 ft altitude near the leading edge of the roll cloud. A maximum of U along the same vertical was found at 15,750 ft. The streamline of maximum amplitude passes through the center of the roll cloud but its mean altitude--that at the inflection points of the flow--is 13,500 ft. That the streamline of maximum amplitude should occur at a lower mean altitude than the altitude of the maximum updraft is a result of the dependence of the former on the maximum slope of the streamlines $\epsilon = wU^{-1}$ rather than on w alone. A large positive vertical shear in the U profile through the roll cloud gives a rotor-like character to the relative circulation in and about the stationary roll cloud. Negative values of U are found under the roll cloud between the ground and about 8,000 ft--well below the base of the cloud.

Case II, 3 March 1952: a moderate lee wave.

In this lee wave example four distinct wave crests formed across Owens Valley in the morning and, as the day progressed, the wave length increased

Fig. 4.5a - 1015 PST, 3 March 1952. Westward from 12,000 ft. High cloud deck over windward slope of Sierra with leading edge of wave cloud over Owens Valley. Mt. Whitney at center of crest.

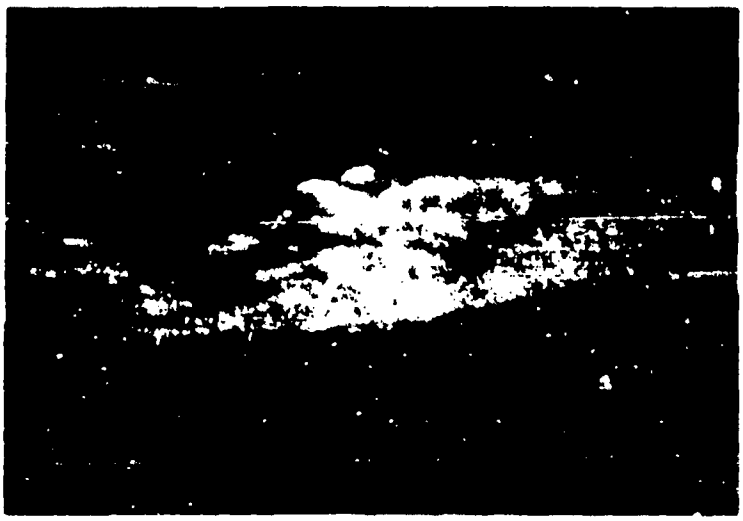

Fig. 4.5b - 1400 PST, 3 March 1952. Southward from Bishop Airport. Roll clouds and föhnwall. Two wave crests are indicated, the second lying over the western slope of the Inyo Mountains. Photo by C. Patterson, U.S. Weather Bureau.

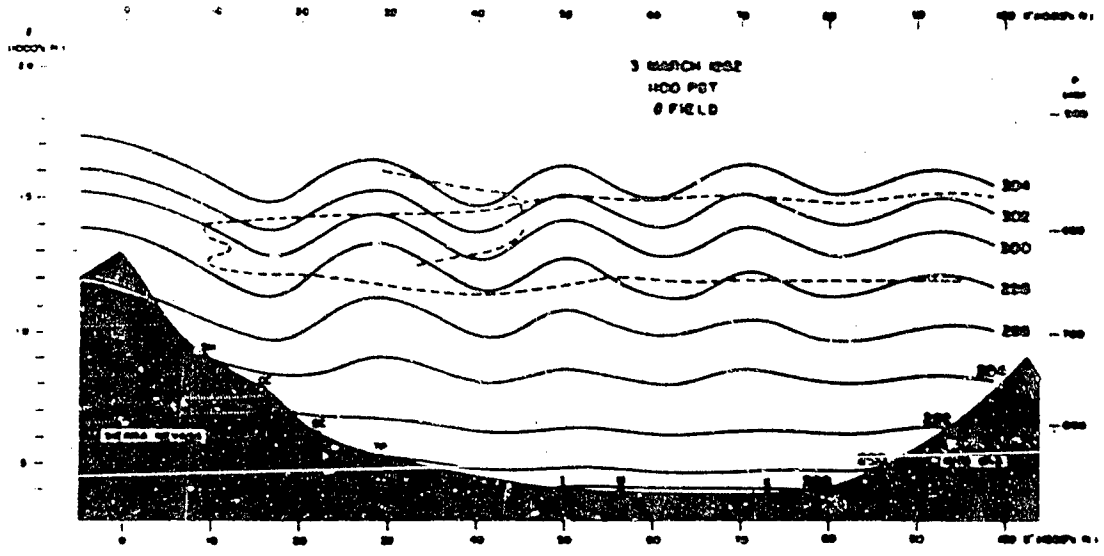

Fig. 4.6

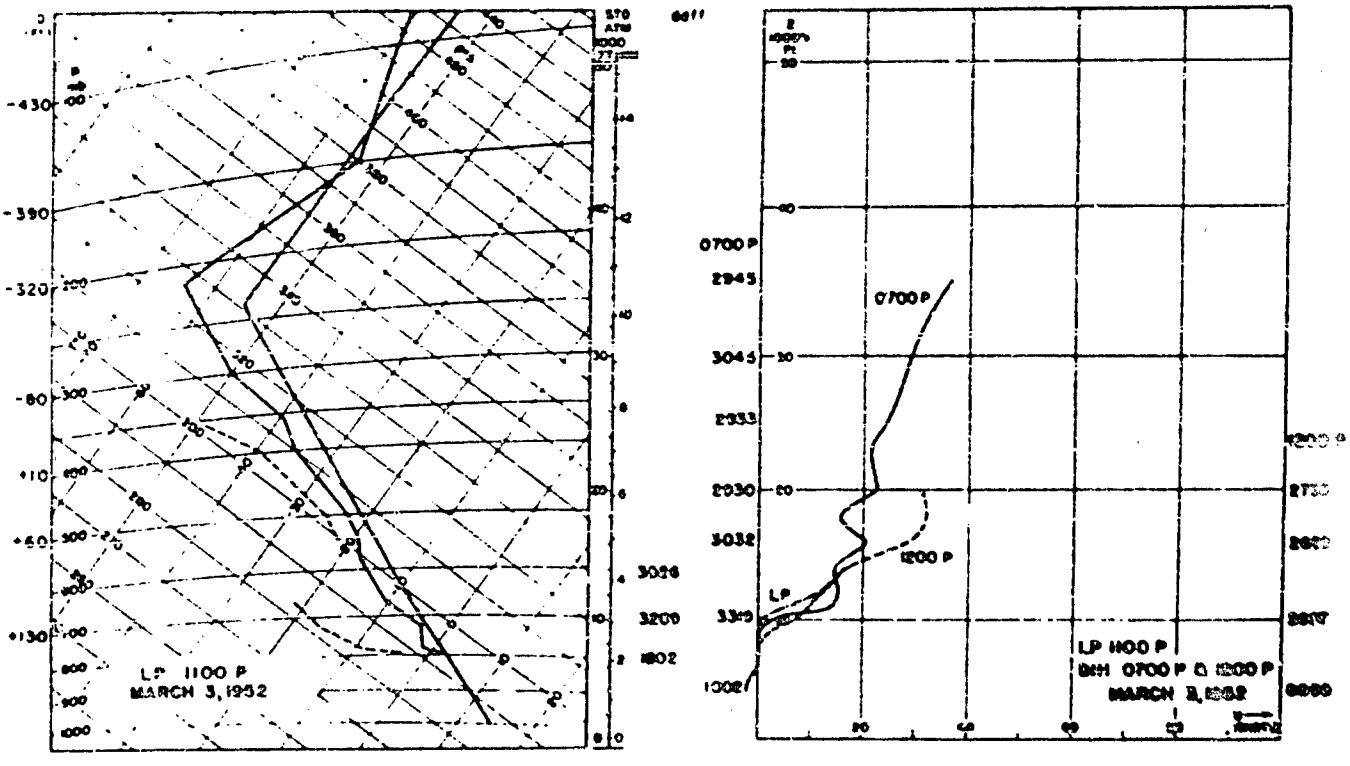

Fig. 4.7

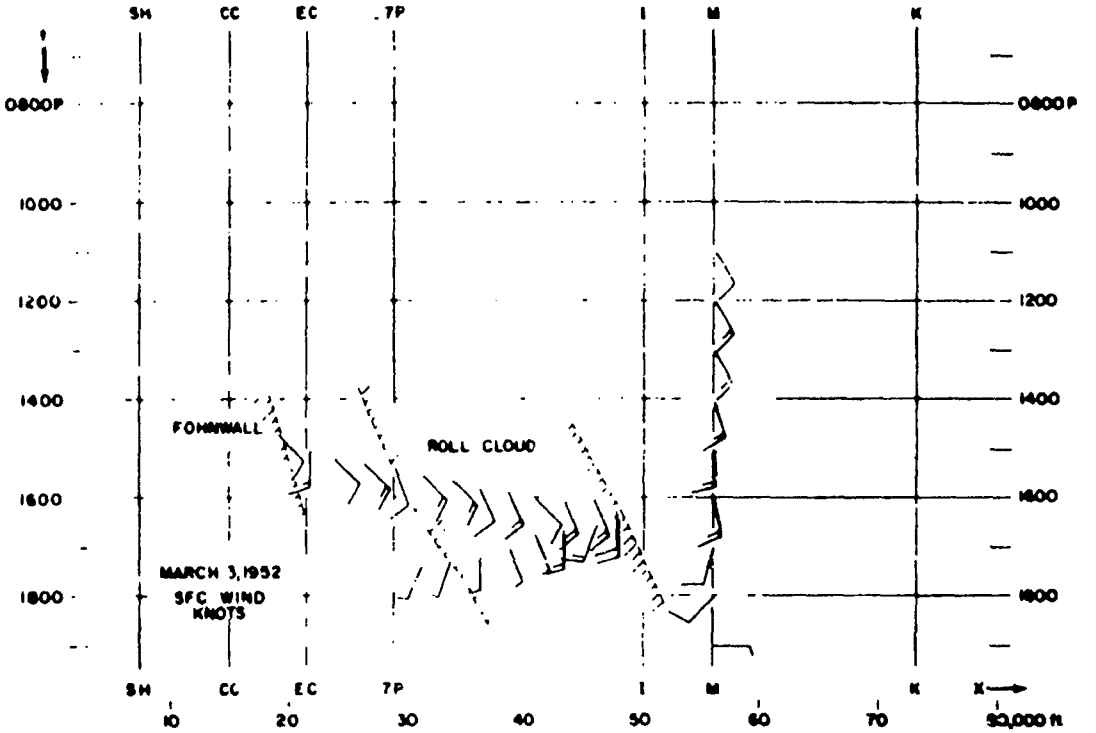
SH
CC
EC
7P
I
M
K
0800P
1000
1200
1400
1600
1800
FOHNWALL
ROLL CLOUD
MARCH 3,1952
SFC WIND
KNOTS
10
20
30
40
50
60
70
X
80,000 ft

Fig. 4.8

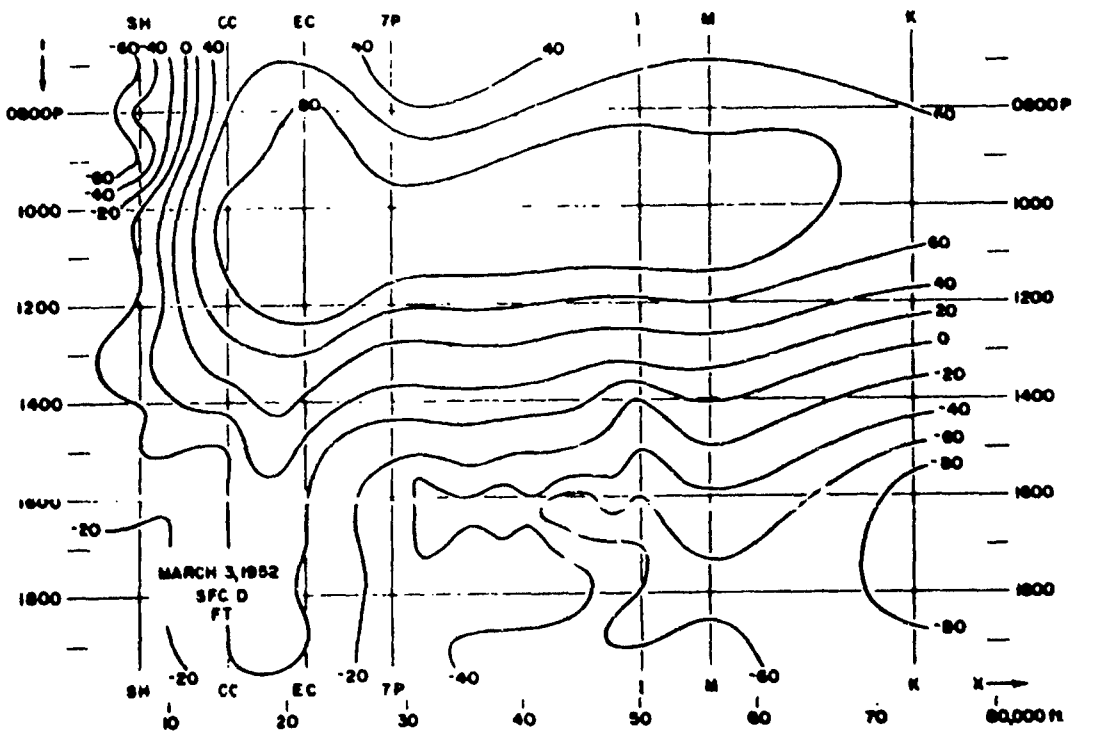
SH
CC
EC
7P
I
M
K
0800P
1000
1200
1400
1600
1800
-60
-40
0
40
80
-80
-40
-20
60
20
-20
-80
MARCH 3,1952
SFC D
FT
10
20
30
40
50
60
70
X
80,000 ft

Fig. 4.9

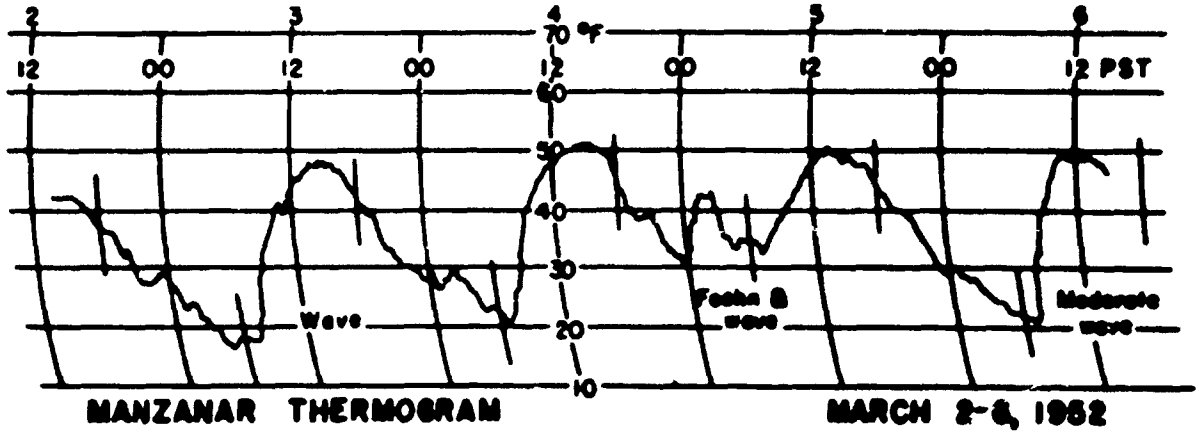

Fig. 4.10

Fig. 4.11a - 0735 PST, 18 March 1952. Northward from 14,000 ft. High wave clouds and swelling roll clouds marking two wave crests.

until two wave crests lay over the Valley and a third over the crest of the Inyo Mountains. At sunrise the sky was nearly clear, but soon after that time wave clouds formed rapidly (Fig. 4.5a). A cumulus wall built up over the Sierra at 15,000 ft, at which level roll clouds developed over the eastern slope. The wave phenomena reached their maximum intensity about 1100 PST, when both the wave and roll clouds were rather well developed south of Bishop. By early afternoon the higher cloud layers had all but disappeared and the rotor circulation was marked by detached cloud puffs instead of a solid band (Fig. 4.5b). The föhnwall swept down to about 10,000 ft at noon and strong downslope winds with blowing snow were encountered in Onion Valley. Later the wind there abated and the cap cloud became tenuous. In the evening the sky over the Owens Valley was clear but the föhnwall--probably composed of falling snow--remained for some hours. The front passed that night and by the next morning the sky was cloudless.

The analysis of the meteorogram data is shown in Fig. 4.6. The Lodgepole sounding made about one hour after the flight is shown in Fig. 4.7, together with Bishop winds at 0700 and 1200 PST. These radiosonde data were used as guides in drawing the potential temperature field over the Sierra.

Mobile observations covered only the latter part of the afternoon. In the wind field of Fig. 4.8 southerly components predominate. The föhngap was rather narrow and the second roll cloud line then lay over the east side of the Valley. The Θ field was not of sufficient coverage to permit analysis. At M the minimum value was 277° at 0700 PST, the maximum 294° at 1400 PST; a value of 295° was recorded in the föhnwall at CC near 1400 PST. In the D field (Fig. 4.9) diurnal changes predominate; the maxima were centered near 1000 PST and the diurnal minima at about 1600 PST.

The thermogram from M for the period March 2-6, 1952 is reproduced in Fig. 4.10. Three lee waves occurred at 13 hour intervals during that period. Of particular interest is the pronounced föhn effect near 0200 PST on the morning of the 5th. The CC and EC barograms show large dips near midnight of that date, similar to those of a station near a tornado passage.

Case III, 18 March 1952: a strong lee wave.

Had sailplane Flight 2022 of this date been successful in gathering continuous data along its path, the coverage would have been as great as that of Flight 2018 on February 18. Unfortunately, there exist only airborne measurements from the beginning of the flight and only tracking data from the end, and either by itself is insufficient for the meteorological analysis. However, the observations of that flight and other measurements made on this date have provided much information on this strong lee wave with rotor clouds.

Clouds and weather observations. The 17th of March was a calm transition period between the most severe storm of the winter and the great lee waves of March 18 and 19. On the afternoon of the 14th it began to snow and continued until the morning of the 16th. The Bishop Airport was isolated as deep drifts blocked the roads and heavy avalanches occurred in the nearby mountains. The morning of the 17th dawned calm and completely clear, but at sunset two orange-colored lenticular cloud stacks lay to the north and southwest of Bishop.

Dawn on the morning of the 18th revealed a nearly mature wave. There were broken cirrus and altocumulus clouds, the latter composed mostly of smooth, stationary forms. To the south was a massive cumulus roll cloud while other detached rotors were seen in the lee of the Sierra in the northern end of Owens Valley as well as over the Mono Lake basin. The Bishop barograph trace showed remarkable undulations starting at 0400 PST. The early meteorograph flight (M-19 from 0700 to 0840 PST) found strong up-and downdrafts of the order of 1,000 ft/min as low as 6,000 ft (2,000 ft above the Valley floor). Three passes were made across the Valley near Independence at 13,000, 18,000 and 9,000 ft between, over, and under the roll clouds, encountering a maximum lift of 3,500 ft min^{-1} just west of Independence at 13,000 ft altitude. The leading edge of the roll cloud was about 3 miles west of the Independence-Manzanar line, while the trailing edge was over the extreme eastern side of the Valley above the fault line at the base of the Inyo Mountains.

Since the föhnwall extended rather far eastward it was not prudent to measure the maximum downdraft in that area. The greatest rate of fall (-1,800 ft min^{-1}) occurred about over Kearsarge Station. One mile east of the Inyo Mountain crest the aircraft rose 1,000 ft min^{-1}; below, stratocumulus clouds whirled at 9,000 ft in the lee of the crest. To the north, in the latitude of Old Camp Independence, where a ridge of the Sierra meets the Valley and the Inyo Mountains bulge farthest westward, the roll cloud swept upward abruptly to form a tall, smoothly-capped tower. Above this dark gray mass was a clear gap of blue sky on either side of which was a white, stationary wave cloud; one was over the center of the Valley, the other over the lee of the Inyo Mountains (Fig. 4.11a). On the return flight it was noticed that the ripples on ponds on the east side of the Valley indicated a moderately strong east wind at the surface. While attempting to land at Bishop the aircraft continued rising 600 ft min^{-1} at 5,000 ft with the control stick thrust forward. In order to descend it was necessary to use flaps and to approach the runway in a sideslip.

The sailplane took off at 1045 PST, released in severe turbulence at 12,000 ft over Red Mountain, found an initial lift of 3,000 ft min^{-1} up which gradually decreased as it ascended. While flying in the gap between the rotors and the arch cloud, the sailplane suddenly became enveloped in a cloud. Upon breaking into the clear once more it was seen that in the same area where the roll cloud tower had been observed earlier in the morning, there was now a dark pillar of cloud connecting the rotor cloud with the upper wave deck.

From 31,000 ft at 1210 PST one could see the föhnwall, heretofore quite thick and obscuring the Sierra, becoming less dense; by 1240 it had almost completely evaporated. Shortly thereafter the roll cloud had also dissipated markedly and at 1310 the rotors were not continuous in a solid band as before but in separate patches. To the west was a high white wall but the snowy Sierra crest was clearly visible with only small Sc patches here and there becoming a continuous mass over the western slope and above the San Joaquin Valley.

Near 1400 PST a high wave cloud was observed over the Sierra crest, a band of blue beyond it, and, far to the west, another stationary band. Overhead the upper cloud, a thick altocumulus lenticularis, had reformed above a growing, nicely arched roll cloud. At 1700 PST a solid stratocumulus deck covered the Sierra at about 15,000 ft, and at sundown a towering cloud deck

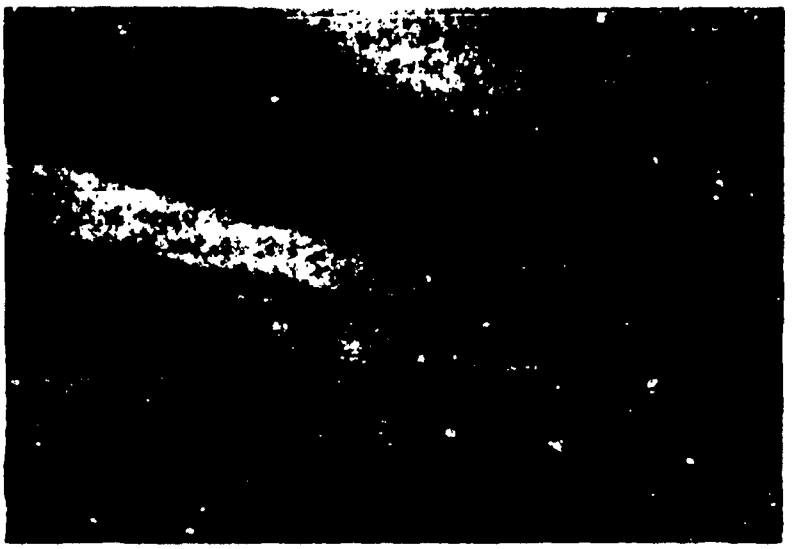

Fig. 4.11b - 0802 PST, 18 March 1952. Northwest from 14,000 ft. Roll cloud and high wave cloud of first crest (left), and leading edge of second wave cloud line (upper right). Note break in upper wave cloud upwind of Bishop where Sierra crest jogs westward.

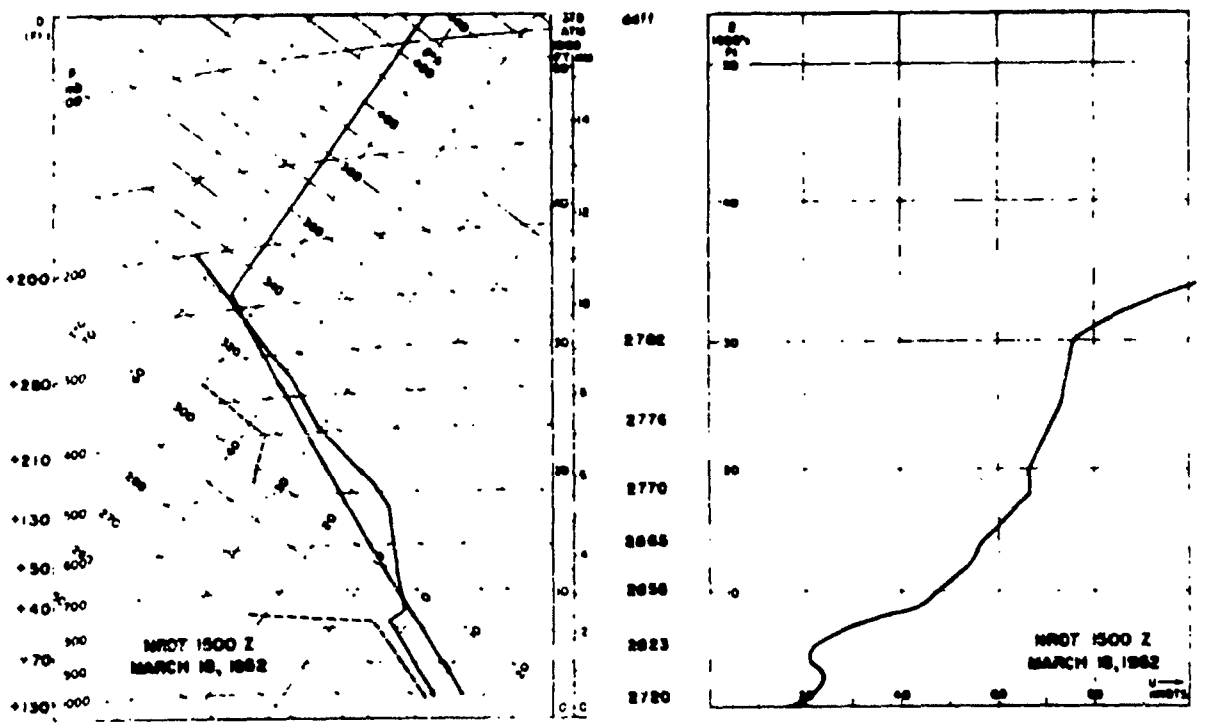

Fig. 4.12

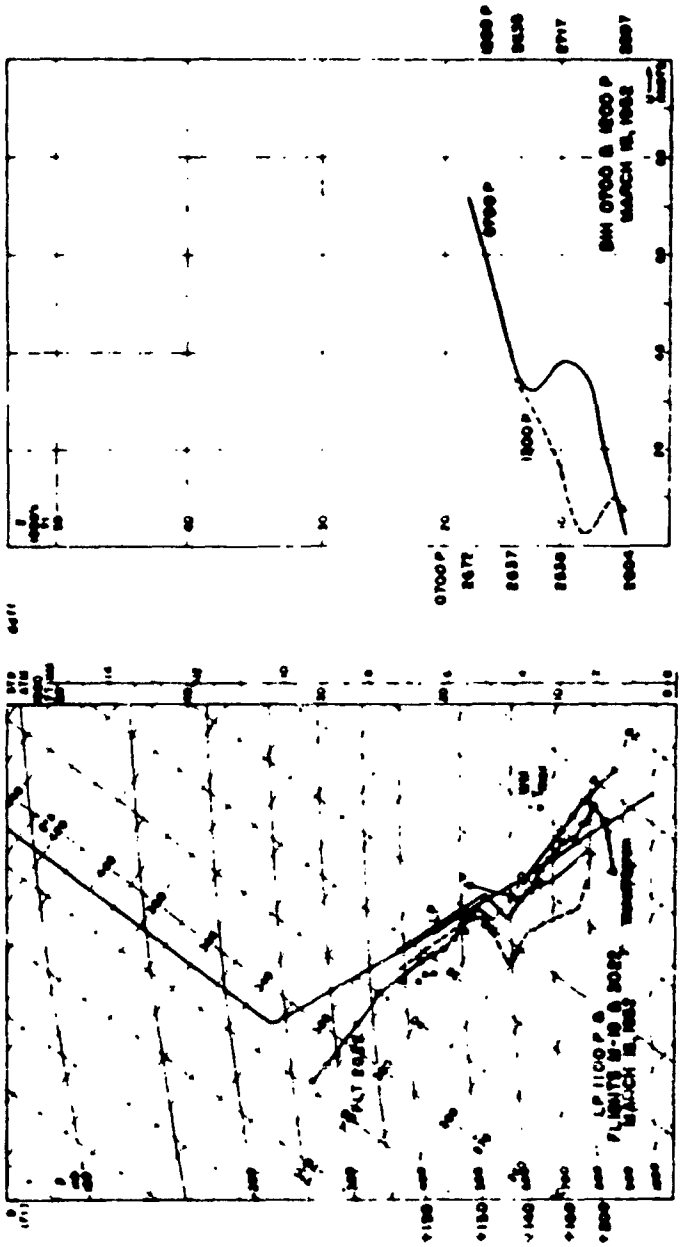

Fig. 4.13

was seen to the northwest. That night, however, the sky overhead remained clear and the strong lee wave showed no sign of diminishing.

Below is a summary of the Bishop Weather Bureau observations for the period:

Date	Time (PST)	D (ft)	T (°F)	T_D (°F)	Wind Dir.	Wind Speed (mph)	
17	1330		46	22	NNW	10	
	1630		44	30	SSE	6	
	1930		35	29	NW	6	
18	0430		27	21	NW	8	
	0730	- 65	31	23	SSE	10	
	1030	- 50	47	29	WSW	12 + 22	
	1130		52	18	S	12 + 30	
	1230		52	22	S	6	
	1330	-120	52	20	N	16 + 28	VRBL & GUSTY
	1430		54	13	N	14 + 26	
	1530		55	16	N	9	
	1630	-130	52	18	N	10	
	1930	-110	44	19	NW	4	
19	0430		43	4	S	4	

Upper air soundings. Although there were no wind soundings at levels above 10,000 ft from Oakland, Merced, or Santa Maria on this date, by a fortunate circumstance a weather ship returning to port made a sounding off the California coast, exactly upwind of the High Sierra region.* These radiosonde and rawin measurements are shown in Fig. 4.12. The Oakland sounding (not shown) has a very stable layer between 640 and 440 mb and moist air to 350 mb. The Santa Maria sounding (not shown) is similar to that of the weather ship with moist air to 800 mb and, an inversion top near 740 mb but with greater moisture between 640 and 340 mb; its tropopause is at 170 mb with a temperature of -7.°C.

In Fig. 4.13 are shown the Lodgepole (LP) sounding at 1100 PST, the flight soundings made over Owens Valley, and the two Bishop double-theodolite wind soundings. In the Lodgepole sounding can be seen the pronounced inversion

*See Fig. 5.44 in Chapter 5.

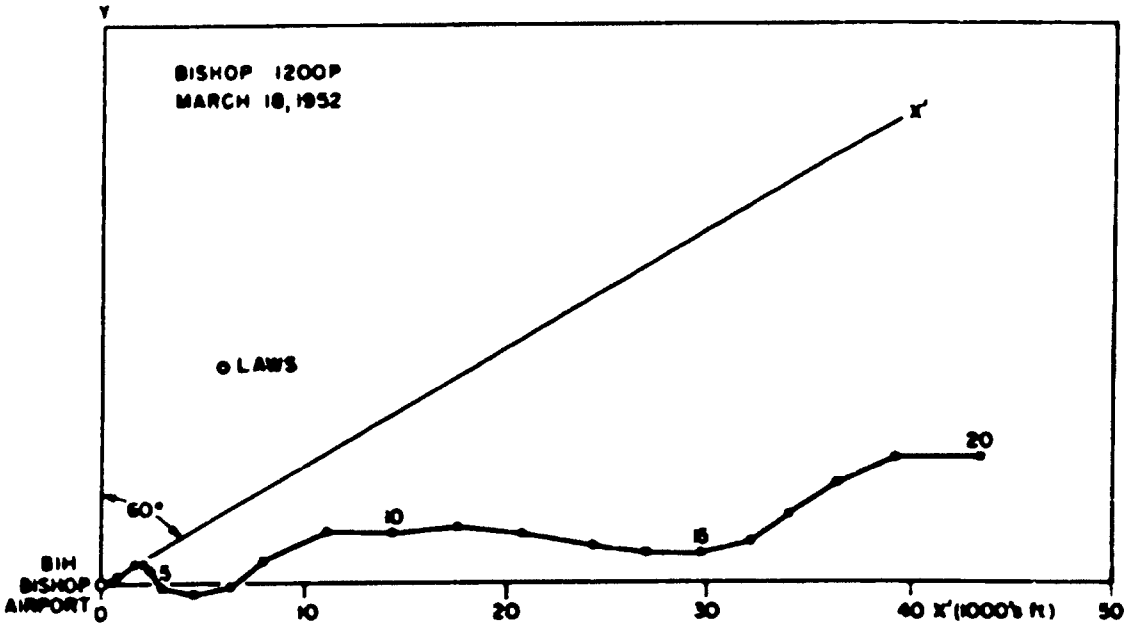
Y
BISHOP 1200P
MARCH 18, 1952
X'
o LAWS
20
60°
10
15
5
BIH
BISHOP
AIRPORT
0
10
20
30
40 X'(1000's ft.)
50

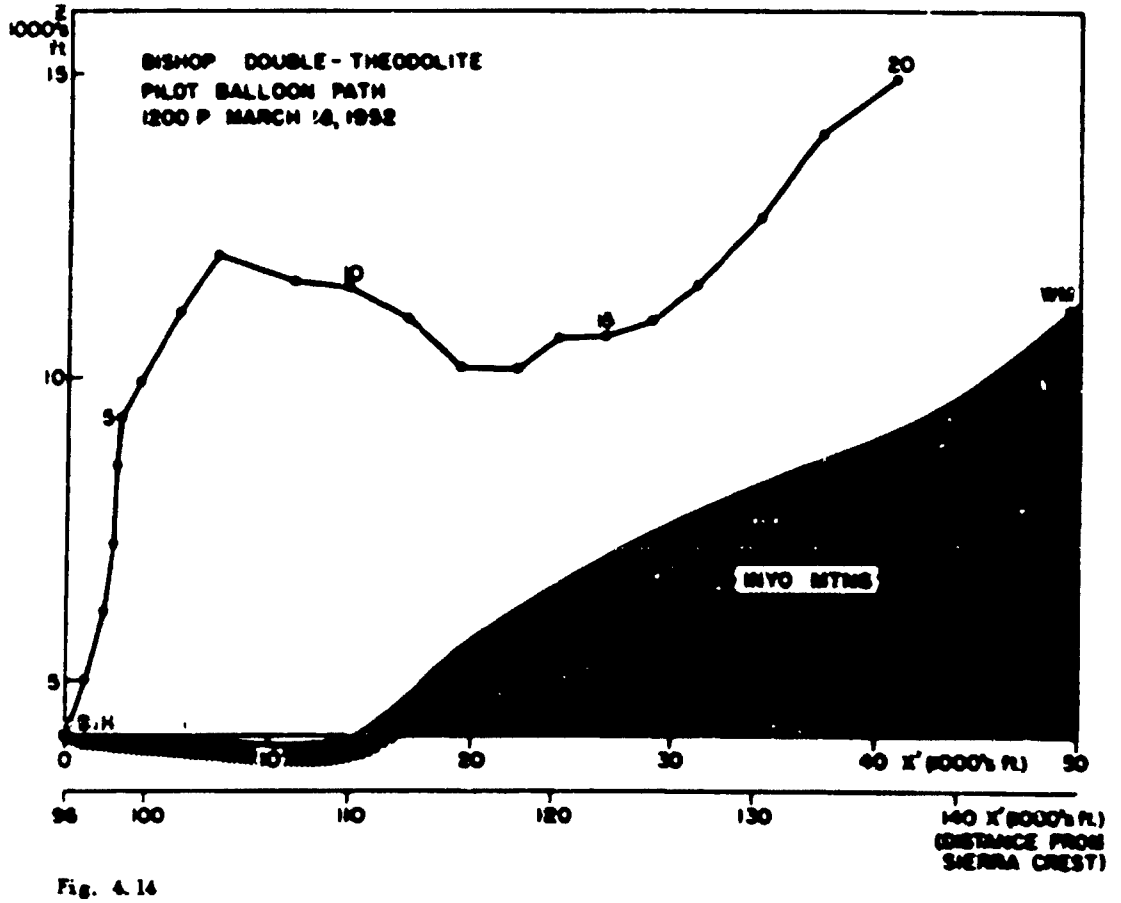
Z
1000's ft
15
BISHOP DOUBLE-THEODOLITE
PILOT BALLOON PATH
1200 P MARCH 18, 1952
20
10
5
10
15
WSW
INYO MTNS
B.H
0
10
20
30
40 X' (1000's ft.)
50
90
100
110
120
130
140 X'(1000's ft.)
(DISTANCE FROM
SIERRA CREST)

Fig. 4.14

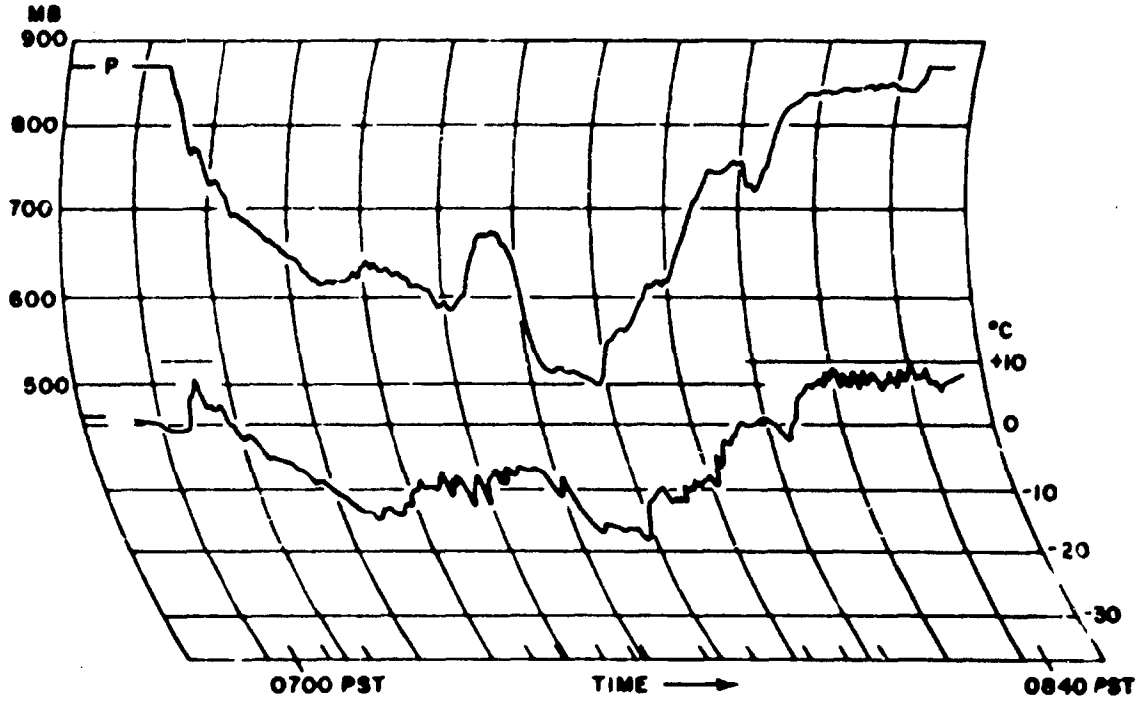

FLIGHT M-19 18 MARCH 1952

Fig. 4.15

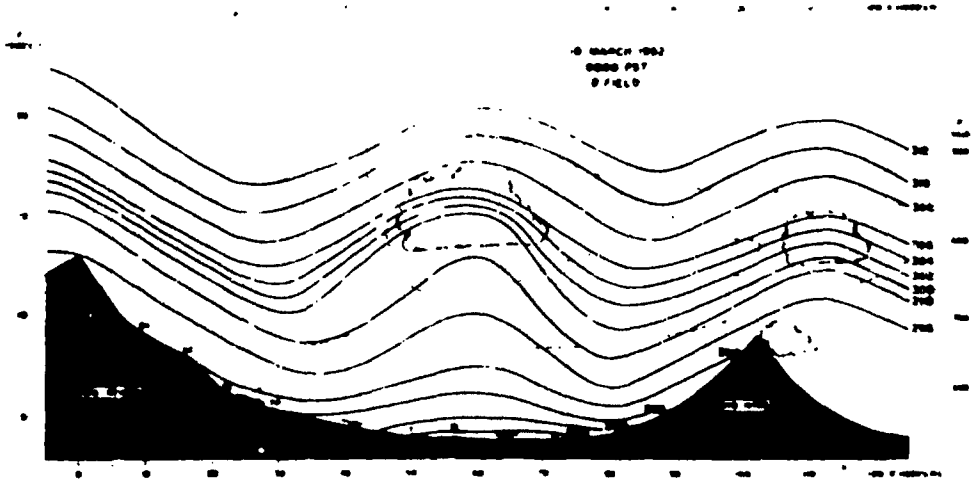

Fig. 4.16

and moisture distribution associated with the flow over the Sierra. No winds were measured at Lodgepole where light snow was falling. The flight soundings indicate the high inversion and also the greater lapse rate in the lee.

A rather remarkable pilot balloon flight from the Bishop Weather Bureau station at 1200 PST on the 18th is illustrated in Fig. 4.14. Colson (1952) has made a detailed study of the Bishop double-theodolite ascents during the spring of 1951 and has found important differences in the ascension rates of the 100 gram balloon for different months and for different altitudes. In order to obtain a rough estimate of the vertical motion of the air along the path of the balloon, the mean (February to May 1951) ascension rate for each level as determined by Colson was subtracted from the observed ascension rate at those levels. Exact values are indeterminate because turbulence tends to increase the ascension rate of the balloon. However, between the 8th and 16th minutes the balloon encountered a broad region of downdraft with vertical speeds greater than 10 ft s^{-1} and with a maximum sustained value of about - 30 ft s^{-1} between the 11th and 12th minutes. The trough in the vertical plane was near the 17th minute; for the remaining three minutes the balloon was in a region of updraft. Termination was due to obscuration of the balloon by a lenticular cloud. This example serves to illustrate the errors inherent in single-theodolite measurements based on an assumed ascent rate; in downdrafts the computed horizontal wind speed exceeds the actual speed and in updrafts the computed horizontal speed is less than the true speed. It is probable that lee waves are responsible for many sinuous wind speed curves from single-theodolite stations in mountainous terrain.

Along with the pibal data, observations from the White Mountain Research Laboratory (WM) at 10,150 ft on the crest of the mountains northeast of Bishop provide some interesting supplementary information about the circulation of the roll cloud zone. At 0800 PST they recorded a steady east wind of 23 knots. It appears from photographs and the 12,000 ft (m.s.l.) broken "Sc" reported at WM that the second wave roll cloud lay over the White Mountains at that time. The temperature there at that time was 16°F (-9°C), but the maximum temperature for the day--unfortunately the time was not given--was 34°F (+1°C). These values are plotted on the tephigram in Fig. 4.13. Since WM temperatures are representative of upper air temperatures at that level, and since the overall synoptic development led to cooling aloft during the day, it is probable that the 10°C warming was caused by the adiabatic heating in the lee wave. The implied increase in wave length and consequent approach of the second trough to the crest of the White Mountain is confirmed by the cloud observations from Bishop and from the aircraft; at noon the first roll cloud line lay over Bishop and the second in the lee of the White Mountains. The pilot balloon path in Fig. 4.14 crossed the White Mountain crest about 6½ miles south of WM.

A meteorogram from 0800 PST on 18 March is reproduced in Fig. 4.15 and a vertical θ cross section of the rotor zone based on these data and supplementary observations is shown in Fig. 4.16. The analyzed field is that of potential temperature based on data measured along the flight path (dashed line) and on the assumption of adiabatic flow. The clouds have been carefully sketched from several photographs made during the flight (e.g., Fig. 4.11). The small cloud in the lee of the Inyo Mountains appeared to form in a vertical eddy there. It is interesting to note that this was the same time at which the strong east wind at WM was recorded. This phenomenon does not occur in the lee of the Sierra where the downward speed is great and the high cloudfall is composed principally of falling snow. Although the flight preceded the Lodgepole sounding by about 3 hours, the latter data have

been used to guide the drawing of θ lines over the Sierra crest. It is quite possible that the generally higher altitude at which the θ lines occur over Lodgepole are indicative of cooling during the 3 hour interval after the meteorogram flight. The arrows near the surface represent the x' component of the surface wind at 0800 PST. The indicated wave length of the flow at the 600 mb level is 58,000 ft (17.7 km) from trough to trough and 54,000 ft (16.5 km) from crest to crest, or an average of about 17 km.

Surface measurements. A very active day of field work in which continual readings were taken across the Valley between 0800 and 1700 PST resulted in quite complete coverage of ground observations. The D field is shown in Fig. 4.17. A rather flat field in the early morning gives way to rapid pressure falls near noon after which a "lee wave field" is manifest. The latter reaches its greatest development at about 1330 PST and is shown in vertical profile in Fig. 4.18.* The rate of eastward drift of the belt of lowest pressure coincides with the rate of increase in wave length of the flow as shown by the changing roll cloud positions in Fig. 4.19. Comparing the wind field with that of D, it is seen that the air generally accelerates toward regions of low D value and decelerates toward regions of high D value. A general convergence of surface winds under the leading edge of the roll cloud is evident. In the θ field, shown in Fig. 4.20, the analysis suggests the predominance of the diurnal change. With reference to the vertical cross section of θ in Fig. 4.16, it is obvious that the observed occurrence of highest values of θ in the early afternoon and the presumed cooling aloft during the day tend toward a decrease of stability in the lapse rate and, from the point of view of observational techniques, impose greater difficulty in detecting the structure of the wave by means of the θ field. It is possible that the diurnal change of lapse rate through the mechanism of heating below and cooling aloft is in part responsible for the increase in wave length of the flow.

Case IV, 19 March 1952: a strong lee wave.

With reference to the other observations of this date discussed in Chapter 3 (Case 8) and to the synoptic charts shown in Figs. 5.45 to 5.48 of Chapter 5, the surface observations made on 19 March are treated here. In continuity with the Bishop Weather Bureau observations for March 17 and 18, the summary for the 19th and 20th is given below.

The barogram and thermogram from Manzanar during the period 14-20 March 1952 are shown in Fig. 4.21 and illustrate the diverse weather events of that week.

While a meteorogram flight was made on the 19th, there was no observer and the complications resulting from uncertainties in location of the aircraft defeated attempts at analysis. Consequently only the surface measurements are shown here. In Fig. 4.22 the extremely long wave length of the vertical flow pattern is indicated; the leading edge of the roll cloud continued to move eastward until it lay over the west slope of the Inyo Mountains in the afternoon. The wind speeds at the surface were rather big and with large westerly components over most of the Valley except the extreme east side where there was

*The relatively large pressure ascendant from west to east under the leading edge of the roll cloud forms the "pressure jump" (discussed by Knox, 1952). This observation is in agreement with the results obtained by Palm (1955) who computed the relative pressure field due to lee waves and found that, at the ground, the lowest pressure lay under the trough and the highest pressure lay under the crest.

Date	Time (PST)	D (ft)	T (°F)	T_D (°F)	Wind Dir.	Wind Speed (mph)
19	0430		43	4	S	4
	0730	- 80	41	14	[illegible]	5
	1030	- 90	48	9	[illegible]W	11 + 23
	1330	-110	51	13	[illegible]W	12
	1630	-150	49	16	[illegible]W	12
	1930	-180	40	18	[illegible]W	12
20	0430		28	9	[illegible]W	15
	0730	+130	30	10	[illegible]	19
	1030	+200	35	10	[illegible]	14
	1330	+200	38	9	[illegible]W	17
	1630	+190	38	5	[illegible]W	15
	1930	+230	32	5	[illegible]	19

an abrupt change to southeasterly or of varying direction under the rotor zone. The θ field (Fig. 4.23) is nearly parallel to the wind. The maximum values occur near 1300 PST. The highest values over the eastern side of the Valley occurred at the wind shift line under the leading edge of the roll cloud. In the D field (Fig. 4.24) the normal diurnal changes are less pronounced than are the changes in horizontal gradient. An indicated west to east pressure gradient in the morning occurs during the usual time of maximum pressure. It appears that the principal low D center changes position during the day; in the late afternoon it is again near Manzanar. The low pressure center probably tilts eastward with height from a position at the surface of varying distance upwind of the leading edge of the roll cloud. The field of D in the vertical plane is discussed in Chapter 9.

Conclusions.

From the analyses of the data from the four cases discussed in this chapter and additional observations treated in Chapter 3, the following statements are made concerning the roll cloud zone and the surface synoptic fields associated with lee waves:

1) The roll cloud forms in the crests of the lee wave near or somewhat above the level of the mountain crest and often extends upward for several thousand feet. It is associated with a temperature inversion and a

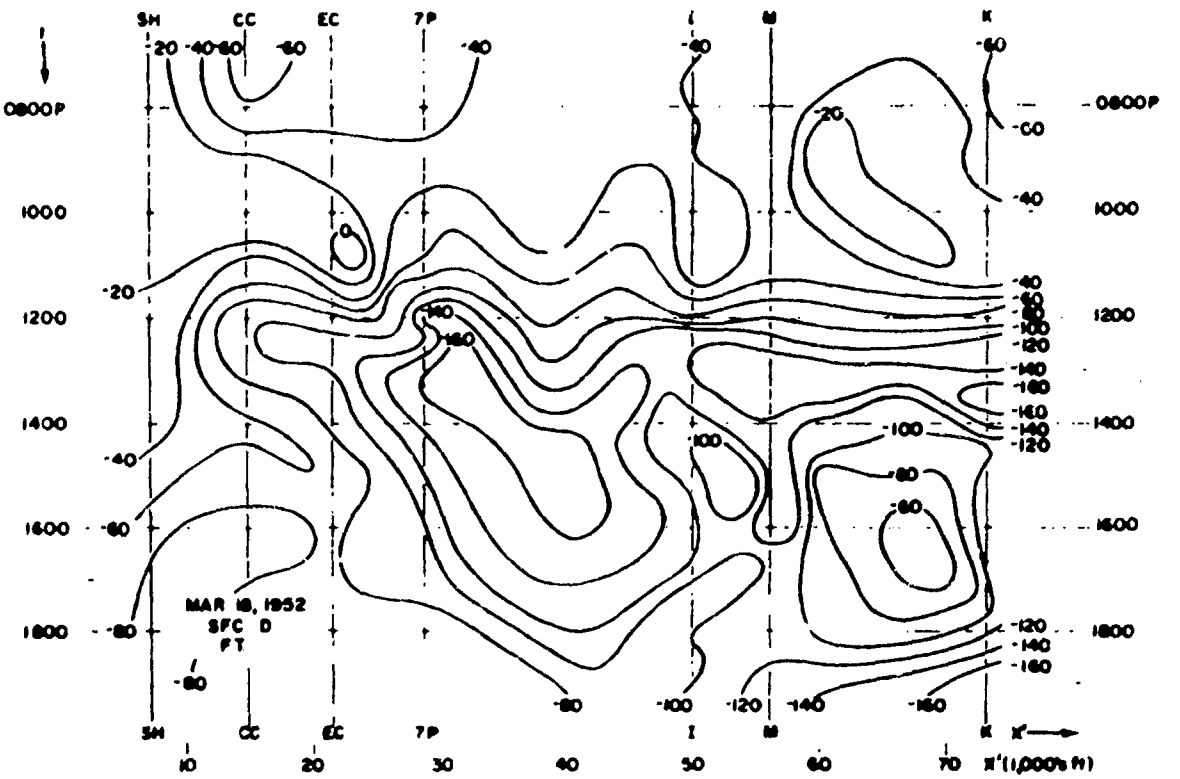

Fig. 4. 17

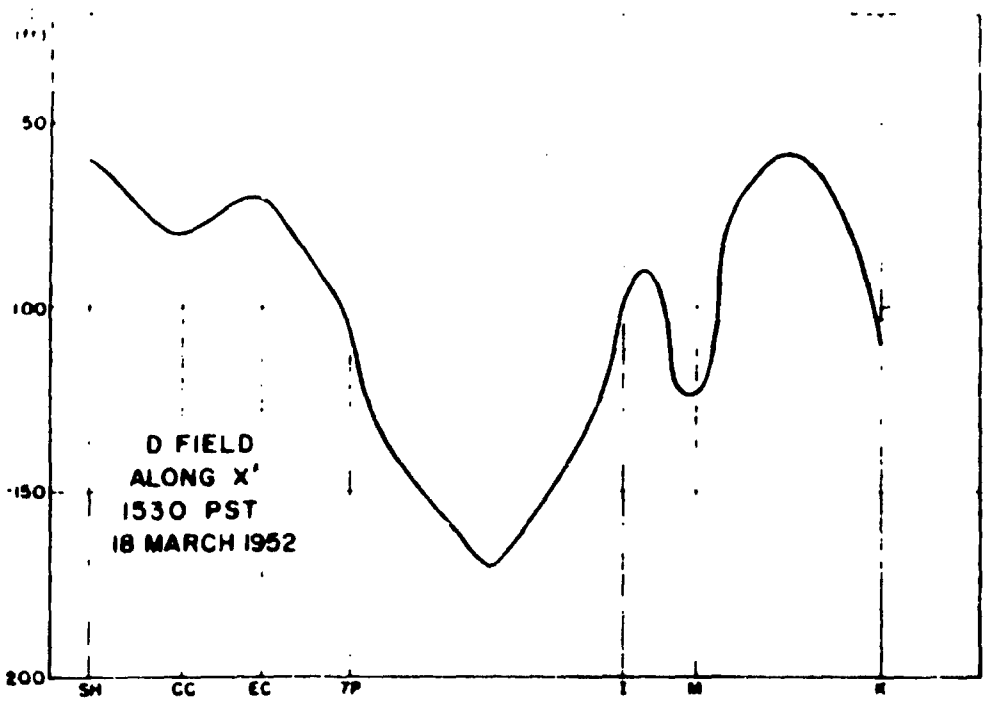

Fig. 4. 18

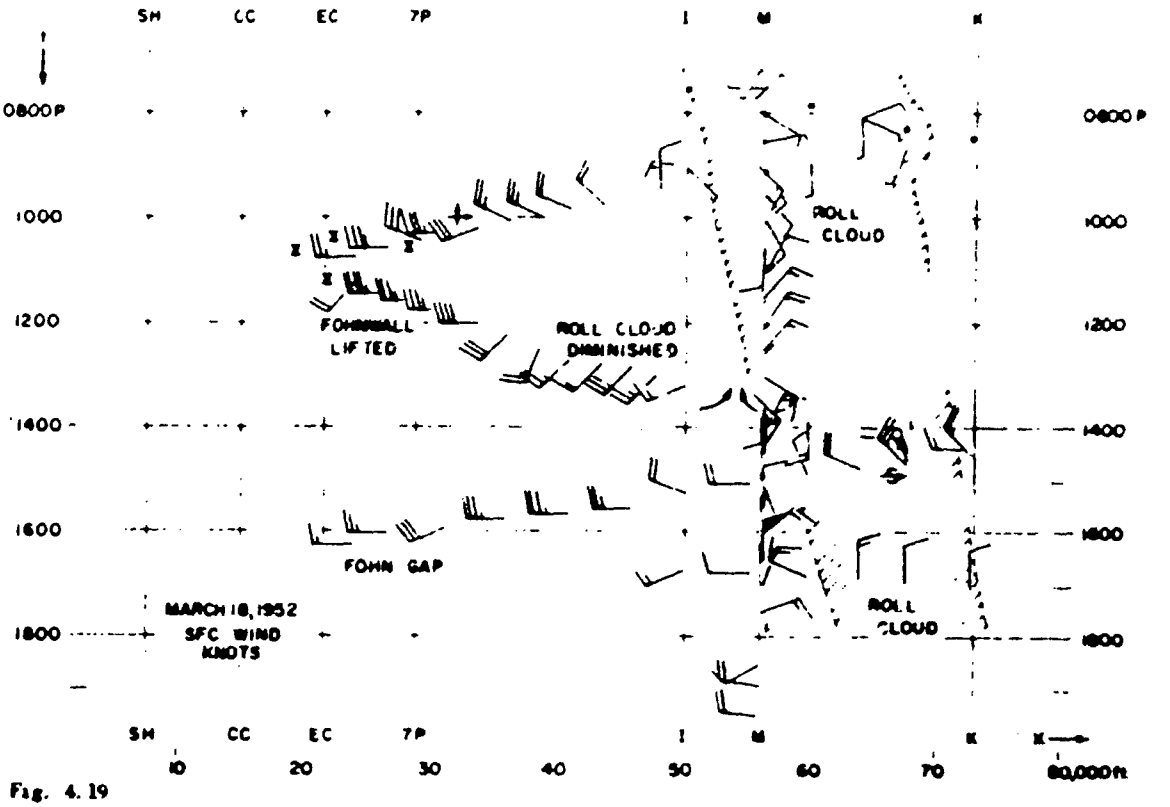

Fig. 4.19

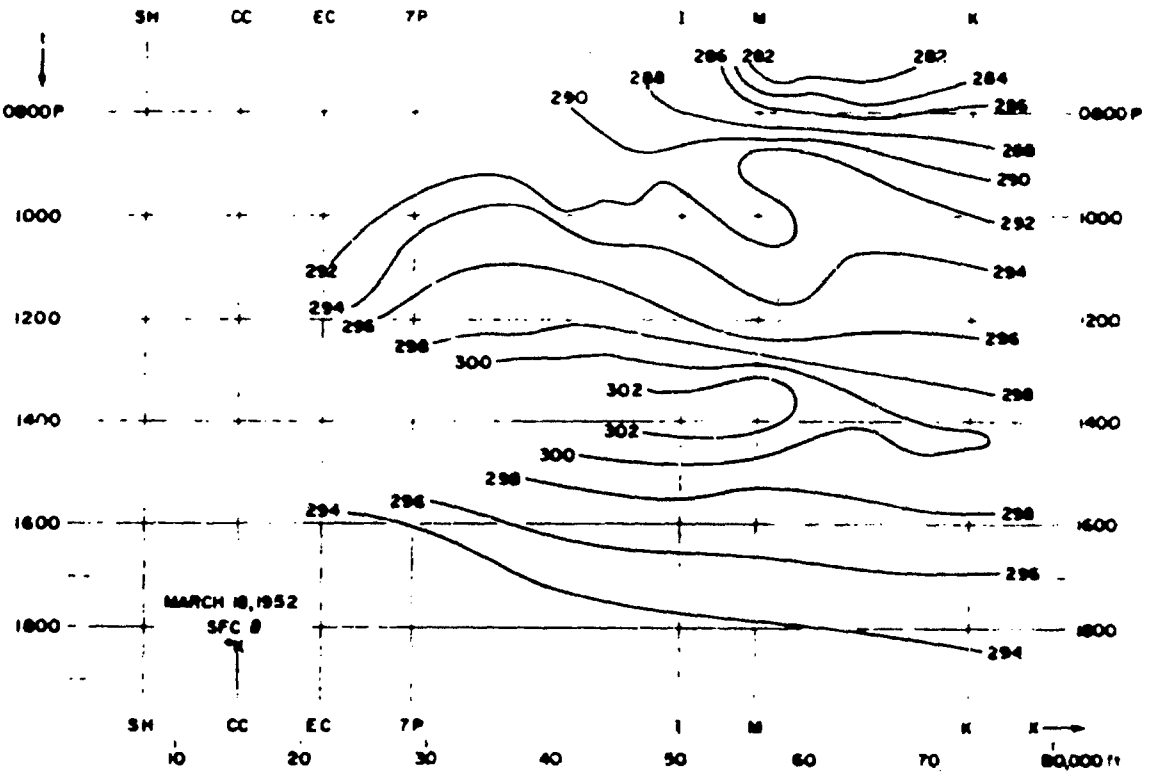

Fig. 4.20

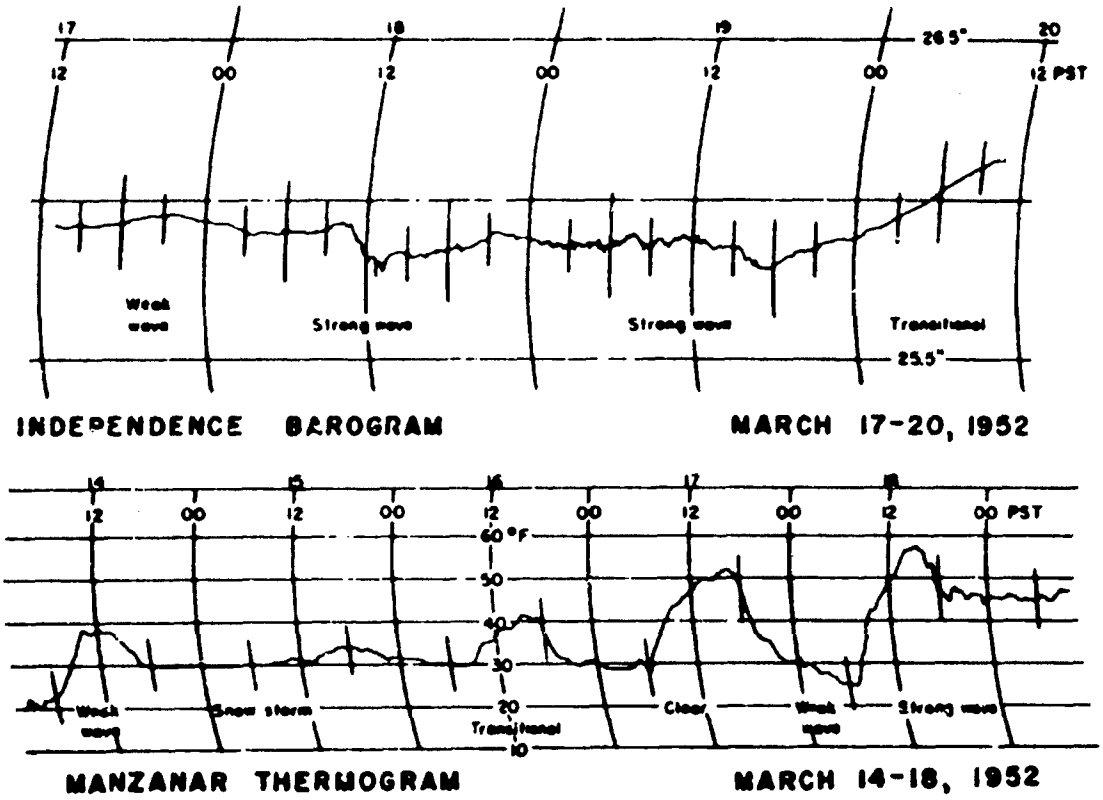

Fig. 4.21

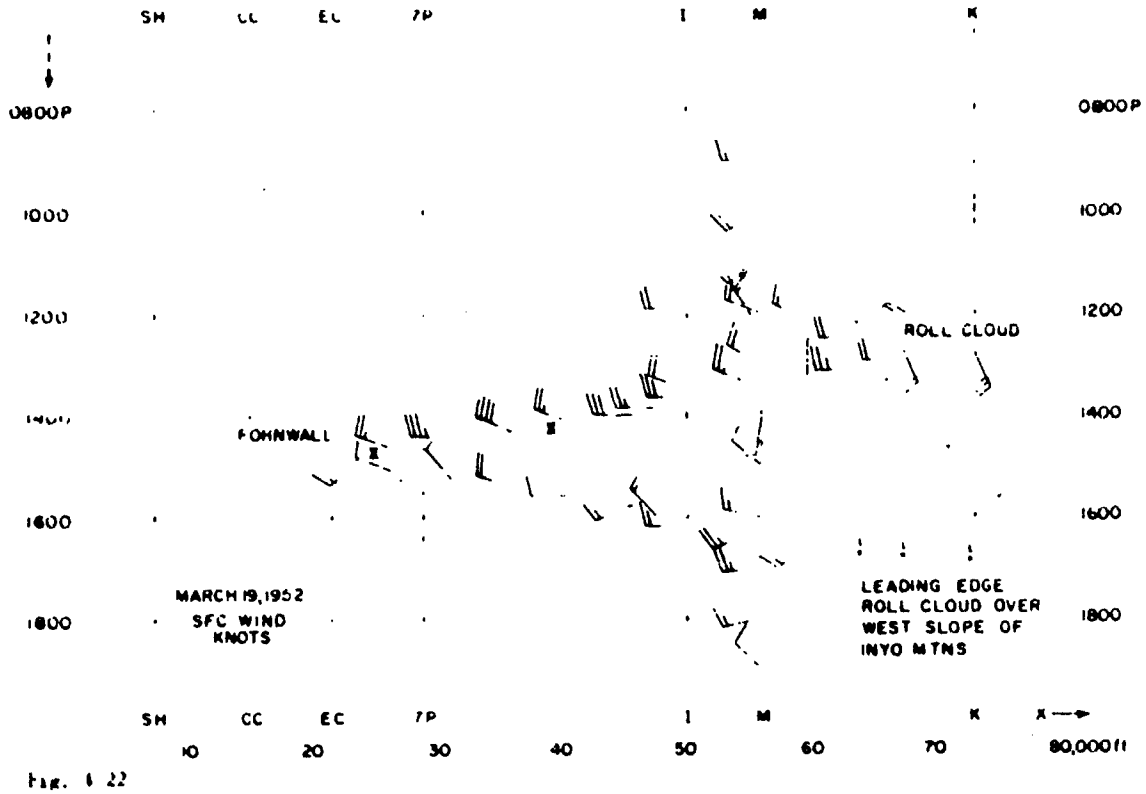

Fig. 4.22

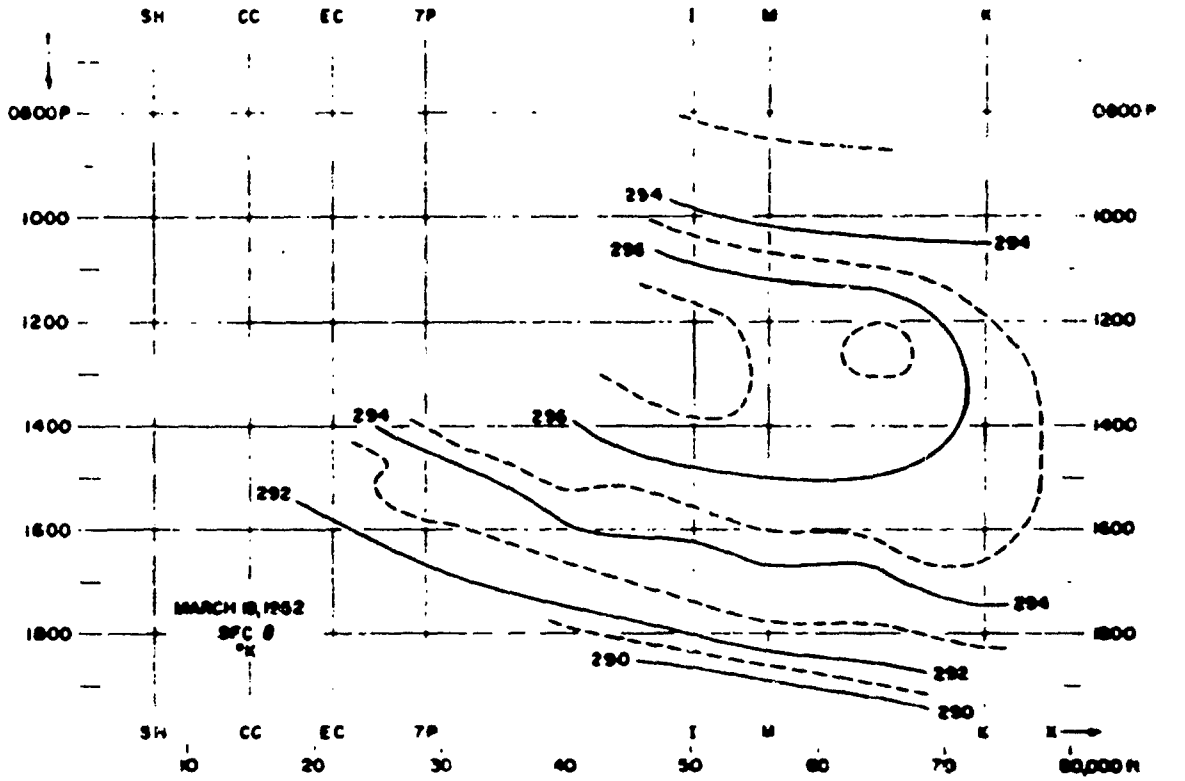

Fig. 4.23

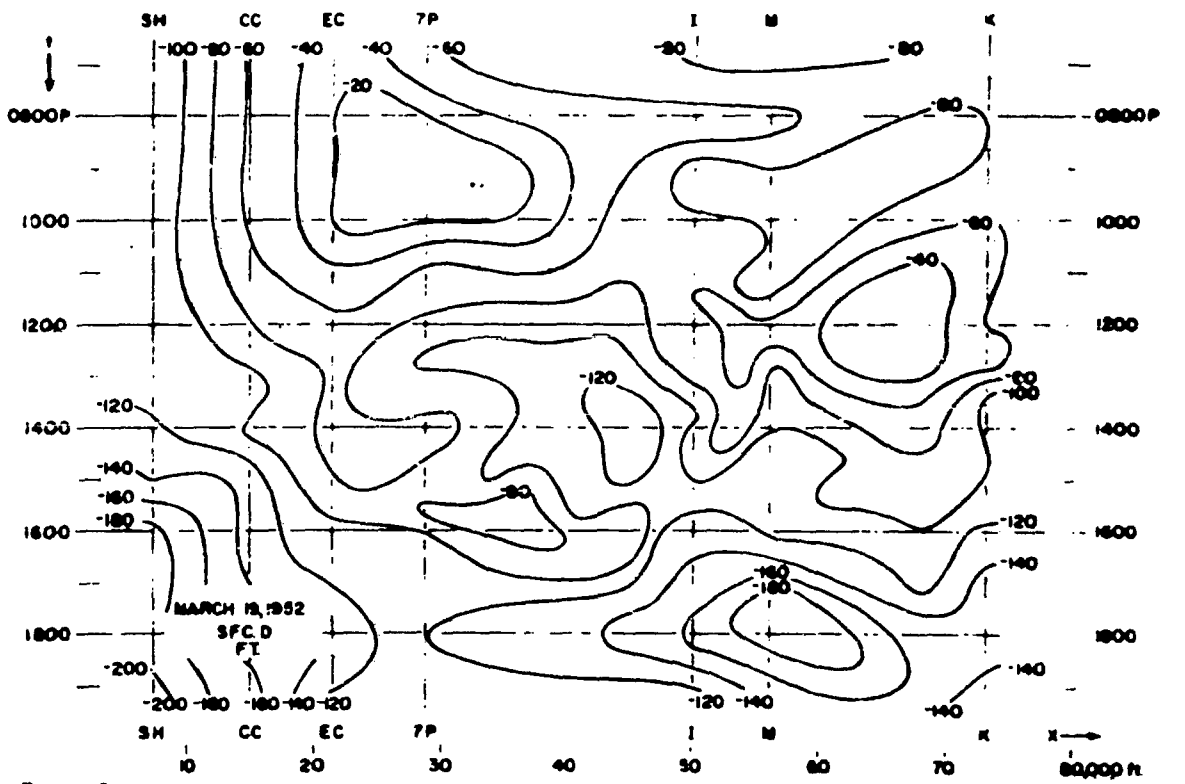

Fig. 4.24

large vertical wind shear. It is generally turbulent* in contrast to the laminar-like flow at higher levels.

2) In the best case with analyzed streamlines in the roll cloud region (16 February 1952), the mean altitude of the streamline of maximum amplitude was found at approximately mountain crest level and below the roll cloud base. The same streamline at its point of highest elevation passed through the center of the roll cloud. The maximum vertical speed in the steady state streamline pattern was found at 15,250 ft altitude, opposite the leading edge of the roll cloud.

3) A reversed flow (negative U) is not usually found in the roll cloud; it is the positive vertical shear, dU/dz, through the roll cloud that gives a rotor-like appearance to the relative movements of the particles passing through the stationary cloud. Reverse flow frequently occurs in the lower layers near the ground and below the base of the roll cloud.

4) Large vertical wind speeds lead to unrepresentative single-theodolite pilot balloon soundings. Vertical shears in double-theodolite soundings may also be exaggerated or minimized because of the change in horizontal wind speed from trough to crest.

5) The wave length of the flow may change as much as 30 per cent during a 12 hour period. In strong Sierra lee waves it is possible that a resonance effect of the Inyo Mountain range augments the wave amplitude when the distance between the Sierra and the Inyo Mountains is a multiple of the wave length.

6) Temporal changes in the surface fields of D, θ, and wind velocity are often large during the occurrence of strong lee waves. In the 12 hours between 0700 and 1900 local time the surface D change at a station may be of the order of 300 ft, θ may change by 20°K, and the surface wind velocity may change by 40 mph in speed and 180° in direction. In order to study synoptic lee wave fields a time section should be used.

7) In the 3 cases of strong lee waves studied, the largest surface pressure gradients occurred in the afternoon with low pressure under the relatively warm trough and high pressure under the relatively cold crest (roll cloud). The large pressure ascendant is analogous to a stationary hydraulic pressure jump.

References.

Knox, J. (1952): A Preliminary Report on Hydraulic Pressure Jumps as Observed with the Sierra Wave, Meteorology Department, University of California at Los Angeles, Unpublished.

Palm, E. (1955): Multiple Layer Mountain Wave Models with Constant Stability and Shear, Scientific Report No. 3, Autobarotropic Flow Project, Meteorology Department, University of California at Los Angeles, Contract No. AF 19(604)-728.

*See Chapter 10 for a discussion of turbulence observations in the roll cloud zone.

5. SYNOPTIC FIELDS

Introduction. One of the tasks of the Mountain Wave Project was to study the large-scale weather patterns in which lee waves were observed to occur. In the course of the investigation a detailed synoptic study was made of the development of the particularly strong wave which formed in the lee of the Sierra on 18 December 1951. While the wave occurred in a pre-frontal current, interest in the broader aspects concerning the nature of the storm and the manner in which it crossed the Sierra invited pursuit. Some results of that study are presented here.

The 1951-2 season was one of great storms and record precipitation in California. On 1 December gale winds forced the closing of the Golden Gate Bridge for the first time in its history. On 15 January 1952 the streamliner City of San Francisco was stalled for many hours in huge snow drifts near Donner Pass. The storm discussed here was experienced between those two dates; it crossed western United States in the period 17-20 December 1951. While each storm is certainly unique, this one can be regarded as a "typical" frontal storm of the type that approach the west coast of the United States from the northeast Pacific.

Data used in the analysis included Weather Bureau hourly (Airways) and 6-hourly surface observations and 12-hourly radiosonde and rawin soundings. Additional upper air data were obtained from Castle Air Force Base at Merced; the Naval Ordnance Test Station, Inyokern; the Lodgepole radiosonde station in Sequoia National Park; and the Bishop Weather Bureau station. Two sailplane flights on the 18th (Flights 2006 and 2007) and other observations and measurements in the lee of the Sierra provided valuable supplementary information. The analysis is presented herewith in the form of surface and isobaric charts and vertical sections. The period covered is approximately 48 hours, from the evening of the 17th to the evening of the 19th.

18 0030 GCT. The sea level pressure field is shown on the surface weather chart for 1630 PST on the 17th in Fig. 5.1. The isobars are drawn at intervals of two millibars. The base map of the western section of the United States is one on which the relief is represented by degrees of shading according to whether the elevation exceeds 1,000, 3,000, 5,000, or 10,000 feet. At the extreme northwest corner the storm which inspired this study appears as an occluding frontal wave approaching Vancouver and the Washington coast. Along the northern Rockies lay a stationary Arctic or continental polar front. The Great Basin Anticyclone centered over central Utah dominated the southern half of the region while a smaller high pressure cell was centered over the San Joaquin Valley.

Weatherwise, big pressure falls and steady rain were reported along the Washington and northern Oregon coasts. It was partly cloudy over California and Nevada with altocumulus in the north and cirrostratus in the south, and clear over Arizona. Altocumulus lenticularis clouds were observed from widely scattered stations in mountainous terrain--Bishop, Elko, Pocatello, Tucson, and Albuquerque.

18 0300 GCT. The 700 and 500 mb upper air charts for 1900 PST on the 17th, 2½ hours after the time of the preceding surface chart, are shown

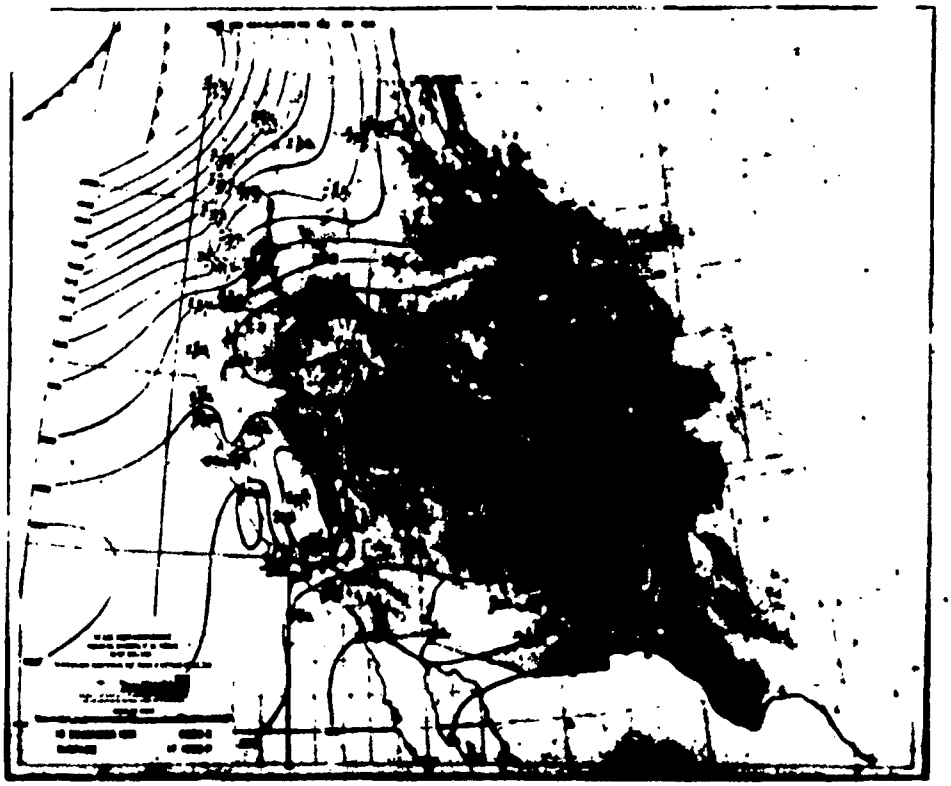

Fig. 5.1

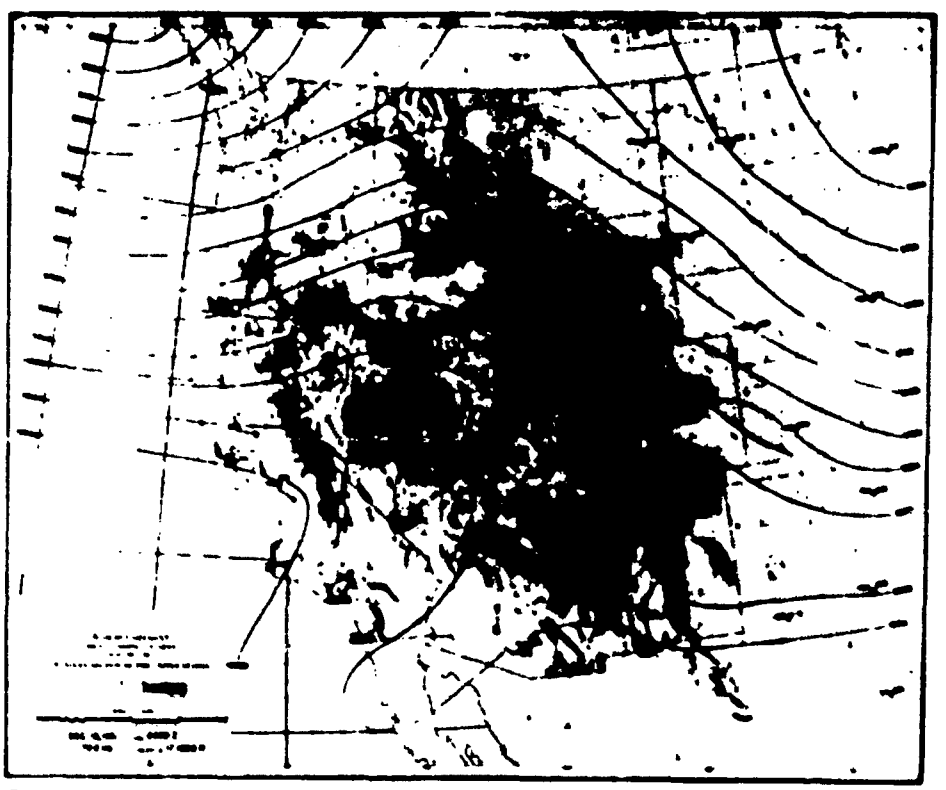

Fig. 5.2

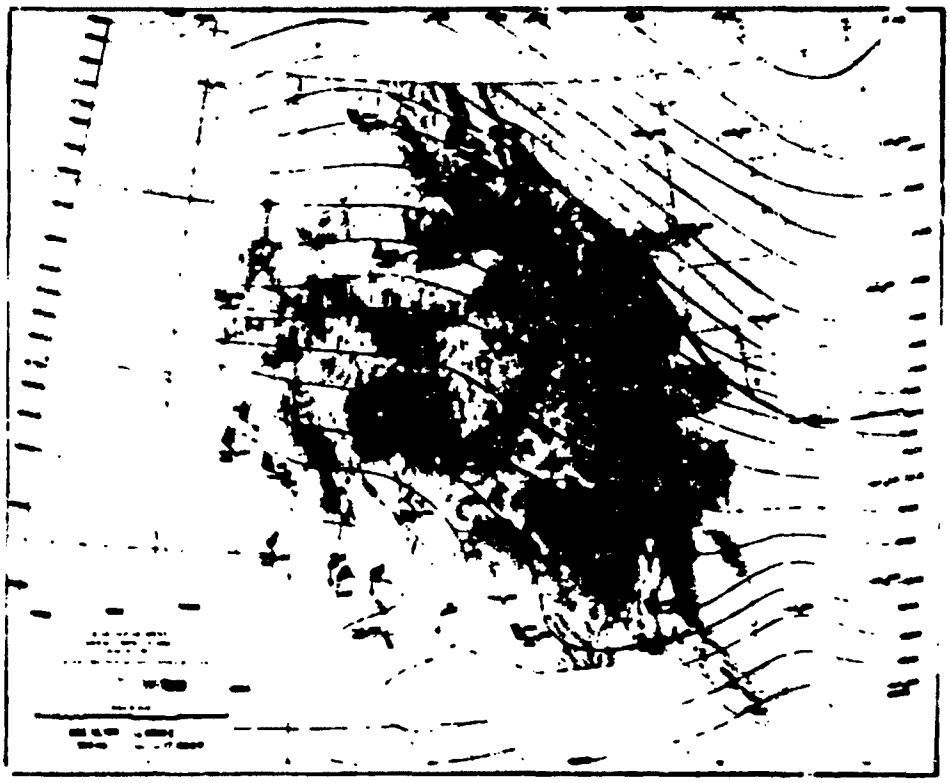

Fig. 5.3

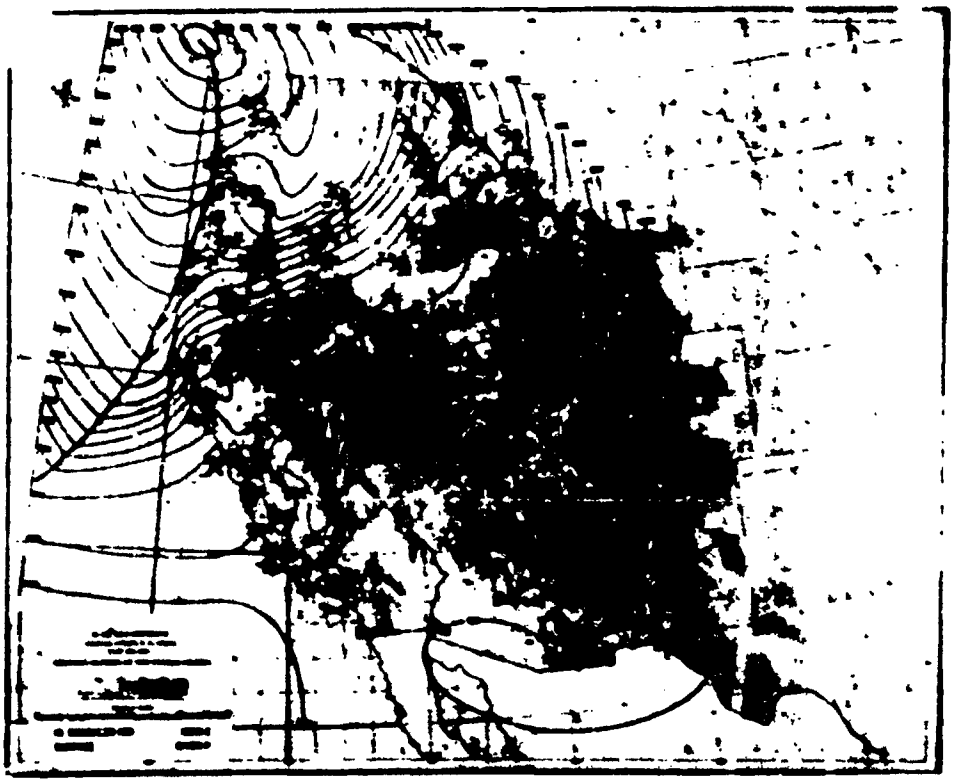

Fig. 5.4

in Figs. 5.2 and 5.3. Contours of the isobaric surfaces are drawn at 100 ft intervals. Wind directions were plotted by protractor to the nearest 10 degrees as given in the coded reports. No isotherms were drawn. At both 700 and 500 mb a portion of the Polar Front appears as a warm front east of the northern Rockies where the isobaric surface intersected the cold dome in the northeast quadrant of the chart. Over the Sierra was an anticyclonic flow of warm air with temperatures near 0°C at 700 mb and -14°C at 500 mb.

18 1230 GCT. By 0430 PST (Fig. 5.4) the occluded front lay along the Washington and Oregon coasts with steady rain extending into northern California. The Great Basin Anticyclone had diminished in size and was centered over the west side of the Colorado Rockies. Likewise, the high cell in California was then located along the western flank of the Sierra. The pressure trough in the lee of the Sierra was well developed.

18 1500 GCT. The upper air flow at 0700 PST is illustrated by the 700 and 500 mb charts in Figs. 5.5 and 5.6. The Polar Front was intersected in both the northwest and the northeast corners of the 700 mb chart. That portion associated with the surface occlusion appears as a cold front over Washington and Oregon. The Sierra lee trough is well marked in the contours at 700 mb as, to a lesser extent, are troughs in the flow over the Wind River Range in Wyoming and over the southern Rockies. A discontinuity in the contours representing a rather large pressure gradient across the Sierra is indicated where the isobaric surface intersects the mountains.*

At 500 mb the Polar Front does not appear on the chart. The lee trough is less pronounced than at 700 mb but the perturbation of the flow is augmented somewhat by an apparent trough over the San Joaquin Valley. The evidence of the latter rests almost solely on the data from Merced where it is suggested not only by the temperature--cooler by 6°C than at the same level over Oakland--and contour height, but also by the wind direction. It is especially interesting to note that at 2100 GCT (1300 PST) the 400 mb wind at Merced was 260 deg, 83 knots while that at Bishop was 300 deg, 67 knots--a 40 deg anticyclonic turning in a distance of 100 miles.

At this point the reader is referred to Fig. 3.14 showing the 1500 GCT sounding and wind profile at Merced and to the corresponding discussion of the other observations of this date (Case 3) in Chapter 3. The high inversion appearing in the Merced sounding and that of Lodgepole (Fig. 3.13) was also found in the soundings at Oakland, Santa Maria, Medford, Boise, Ely, Inyokern, and Las Vegas and can be considered to be that of a quasi-horizontal warm front. (See Fig. 1.7 for locations of stations.)

A large-scale cross section of potential temperature in a vertical plane over the Sierra from Oakland to Las Vegas is shown in Fig. 5.8. Radiosonde data from Oakland, Merced, and Las Vegas at 1500 GCT were used, together with that from Lodgepole and Flight 2006 at 1800 GCT (see Fig. 3.11). From the plotted path of the Merced balloon the approximate tilt of the radiosonde ascent curves was determined. Because of time differences in the data used

*On this and on subsequent 700 and 850 mb charts contours are dashed where they are below the surface of the terrain.

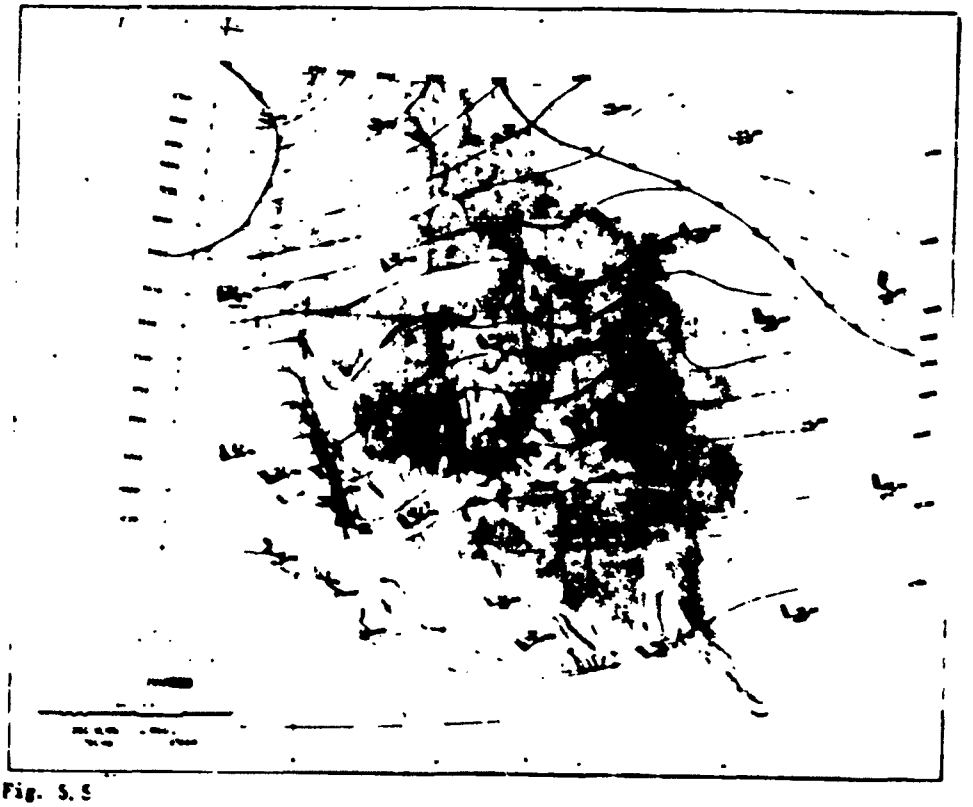

Fig. 5.5

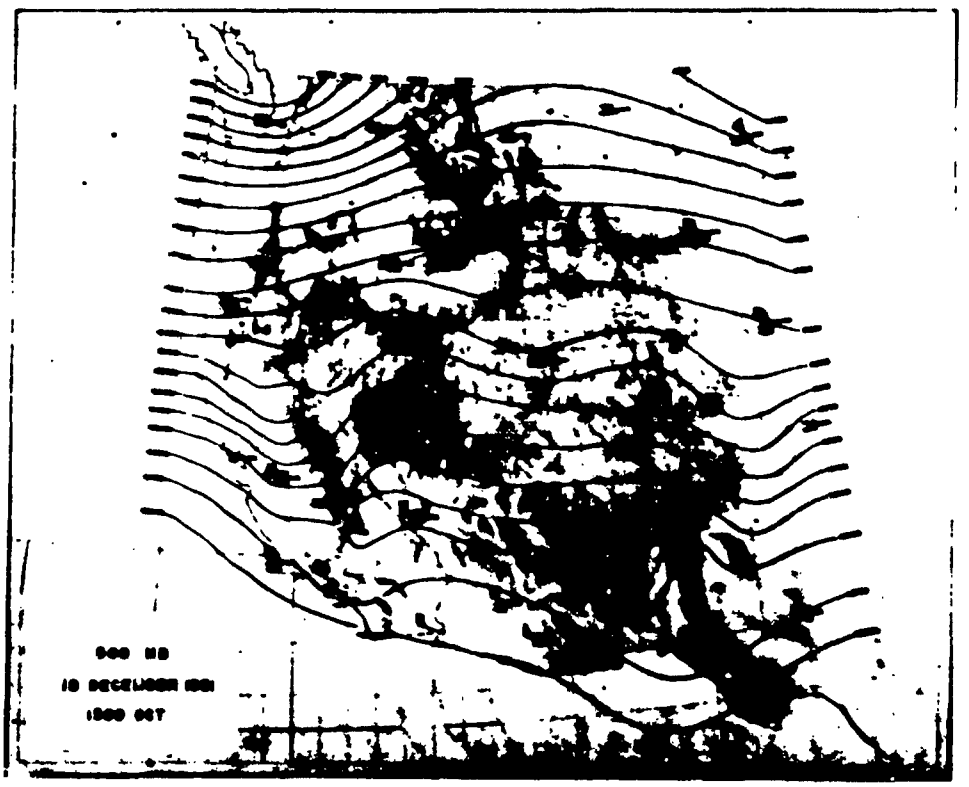

Fig. 5.6

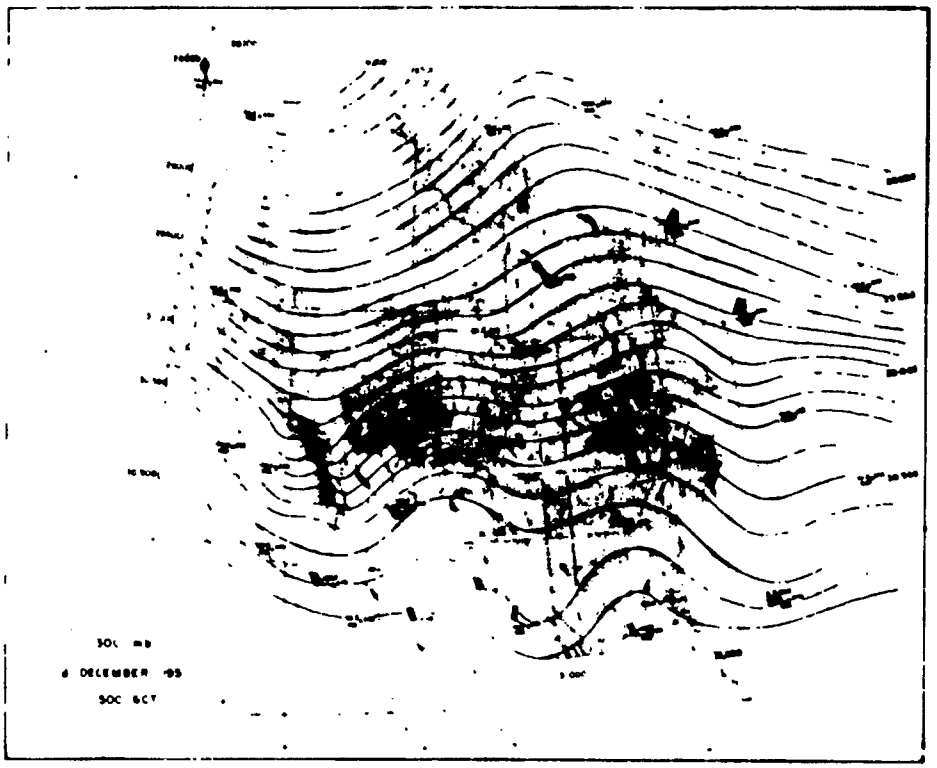

Fig. 5.7

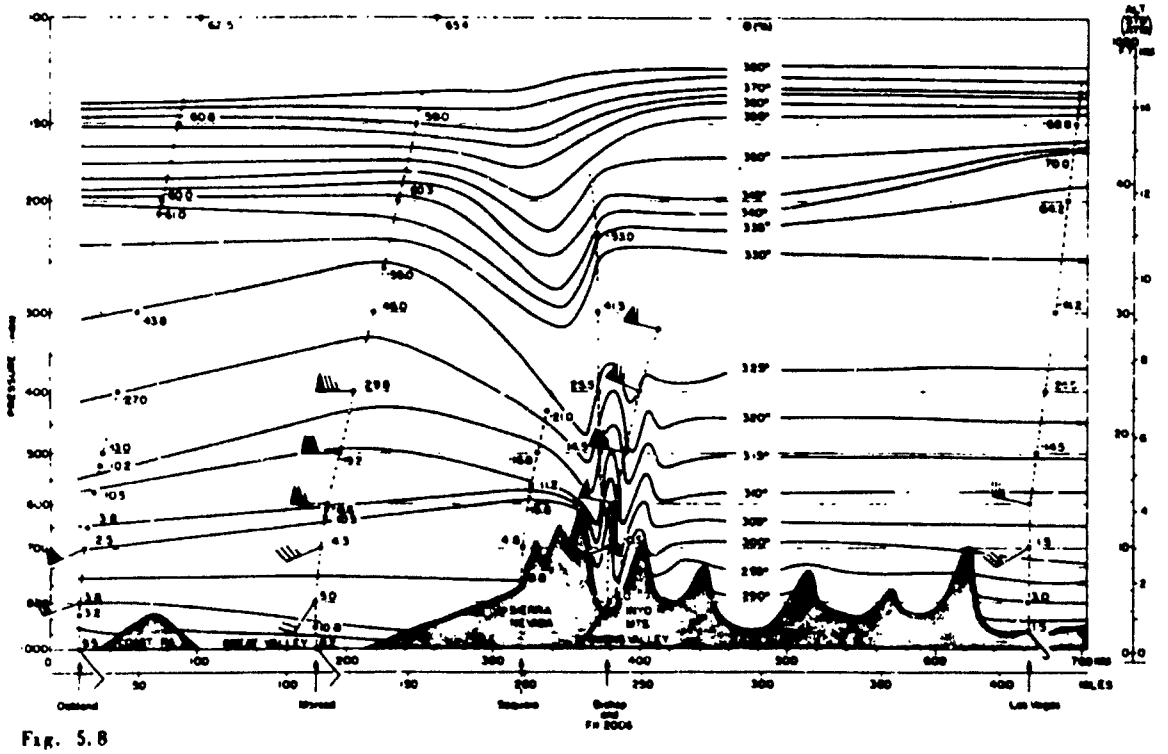

Fig. 5.8

and the fact that the section is not exactly along the direction of wind flow, caution should be had in interpreting the isentropic pattern as a literal substitute for the synoptic streamlines. The principal features, besides the small-scale lee wave, are the high level inversion or warm front which can be traced in the soundings of the three windward stations; apparent cooling over the San Joaquin Valley in the upper troposphere, perhaps indicative of ascending motion; and the large-scale warming of air through a deep layer of the atmosphere (600 to 150 mb) over the western slope of the Sierra, probably due to descending motion.

18 1830 GCT. The surface chart at 1030 PST is shown in Fig. 5.9. The front lay through central Washington and Oregon and into northeastern California with a deep low pressure center at the southern tip of Vancouver Island. Steady rain or snow fell immediately ahead of the front while showers were reported behind it. In this phase of its passage, temperatures recorded behind the front were generally warmer than those recorded ahead of it. The pressure gradient of the lee trough had intensified. A small area of high pressure appeared on the western slope of the southern (High) Sierra. The Lodgepole sounding and Flight 2006 can be considered to be synoptic with this chart.

Lee wave phenomena. Figs. 3.9 illustrate the cloud forms observed from the air over the Owens Valley between 0900 and 1500 PST. The föhn "window"--the large gap of blue sky visible between the cap cloud and the roll and wave clouds--persisted all day. It marked the downdraft area in which temperatures were considerably warmer than at comparable levels elsewhere. Maximum temperatures for the month of December 1951 occurred at Mono Lake (53°F) and Bishop (60°F) on the 18th.

Barograms of the period 17-19 December are shown in Fig. 5.10. The stations represented are Lodgepole (LP) on the western slope of the Sierra, Eckert's Cabin (EC) on the eastern slope, and Manzanar (M) in Owens Valley. The greatest pressure falls occurred between 1030 and 1330 PST and are likely the combined effect of the overall pre-frontal synoptic situation, the intensification of the lee trough, and the diurnal pressure wave. The largest horizontal pressure difference across the mountains between Lodgepole and the Independence Creek stations was 9 mb at 1530 PST. It is probable that a steeper gradient or discontinuity existed near the crest.

Vertical structure of the storm. A time section of vertical soundings at Oakland for the period 16 to 20 December 1951 is shown in Fig. 5.11. One sees in it the warm front inversion present on the 18th and its relation to the upper warm front which passed over the region on the 16th. Above the dome of cold air centered over the station at 0700 PST on the 19th, a warm tropopause dips down to 400 mb at -33°C in marked contrast to the higher (170 mb), colder (-68°C) tropopause found over the station at 1900 PST on the 17th. Between these times the temporal slope of the tropopause is indicative, if greatly exaggerated, of the spatial slope of the tropopause on the 18th, forming a stratospheric warm front over the region.

Both isotherms and isentropes are drawn at 5° intervals on the section. They show the nature of the baroclinic frontal zones and the rate and degree of cooling or warming at the different isobaric surfaces. The

Fig. 5.9

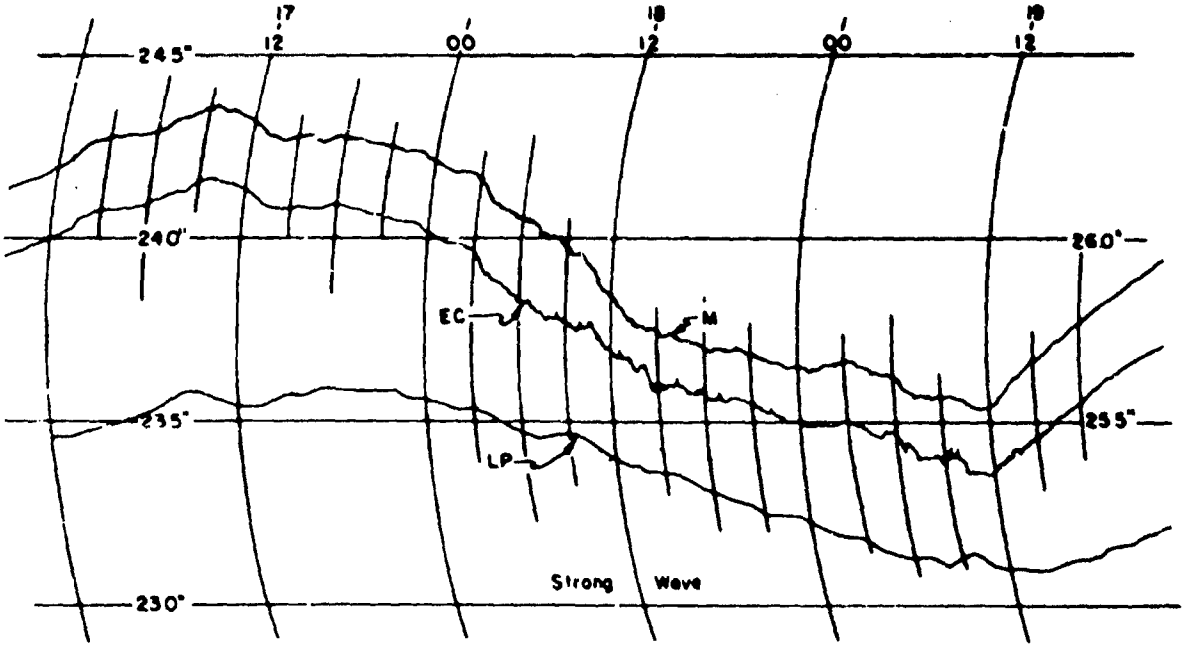

Fig. 5.10 Barograph traces from Manzanar (M) in the Owens Valley, Eckert's Cabin (EC) on the eastern Sierra slope, and Lodge Pole (LP) on the western Sierra slope for the period December 17-19, 1951. The pressure values on the left refer to EC and LP and those on the right to M.

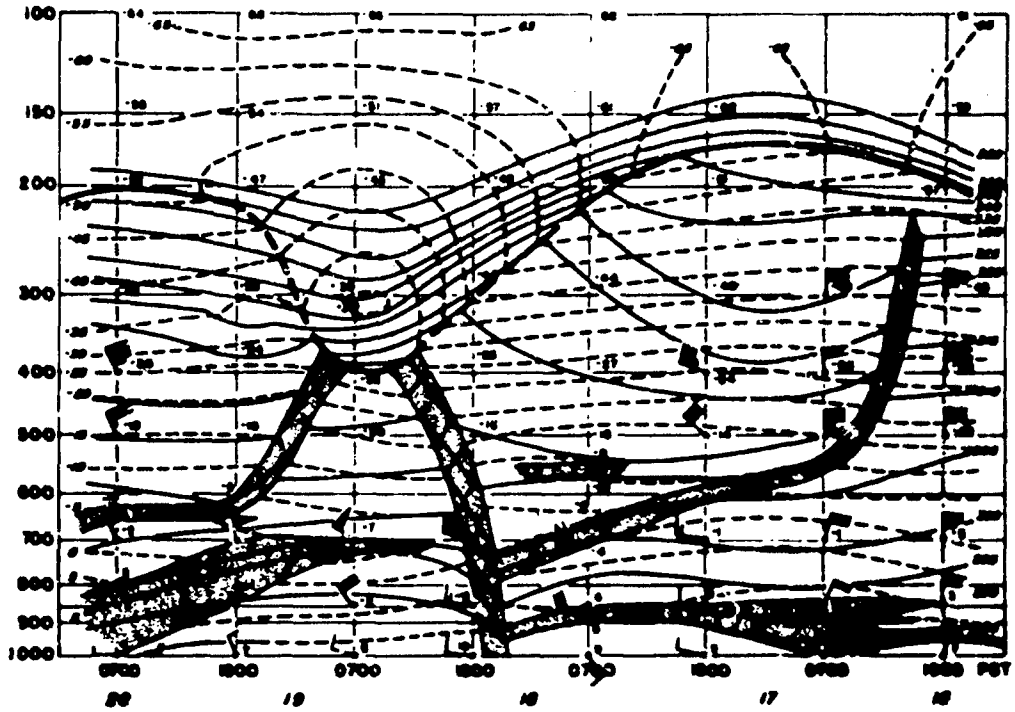

Fig. 5.11

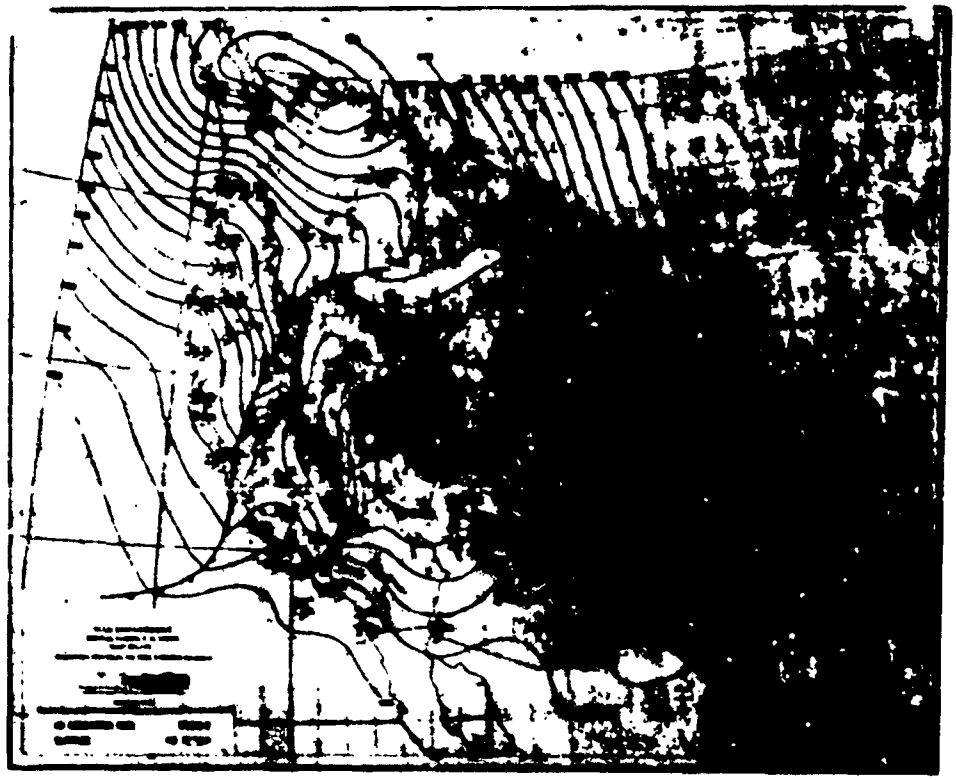

Fig. 5.12

winds are plotted according to their appearance on a level surface with north at the top. The strong westerly flow on the 18th is evident but equally noteworthy are the two examples of even stronger northerly flow associated with the western boundaries of the cold domes. Such asymmetry of wind speed is indicative of the diffluent nature of the upper troughs.

19 0030 GCT. The surface chart for 1630 PST on the 18th, near the time of maximum development of the lee wave, is shown in Fig. 5.12. By then the northern segment of the front had moved eastward rapidly into Idaho while the segment in California had moved eastward much more slowly while assuming a north-south orientation. The lee trough was strongly developed and can be clearly traced from extreme northeastern California in the lee of the Warner Mountains, along the lee of the Sierra and the Tehachapi Mountains, in an arc to its southernmost appendage in the Catalina eddy off the coast of the Los Angeles Basin. While föhn temperatures and low dew points characterized most of the leeward stations, the relatively shallow depth and cyclonic motion of the Catalina eddy tended toward a shoreward convergence of cool, moist, maritime air and thus to an increase of stratus. In such a situation the stratus often becomes so thick as to obscure the approaching altocumulus in the upper pre-frontal current. Elsewhere, diverse weather was occurring at various stations in the region. Northwest winds, pressure rises, and showers were observed at that time behind the front in northwestern California. Steady rain fell at Sacramento and steady snow at Donner Pass. Strong southwest winds and blowing sand swept across the desert in southeastern California. Lenticular clouds were reported at Bishop, Inyokern, Las Vegas, and Winslow.

Precipitation amounts for two 24 hour periods ending at 1630 PST on the 18th and 19th were plotted and analyzed. All available data were used, including those from stations reporting on the teletype circuit and the more numerous cooperative stations. Since observations at the latter sites are made at diverse times, only those stations recording between the hours of 1500 and 1800 PST were used in these studies. The pattern of precipitation for the 24 hour period ending approximately 1630 PST on the 18th (the time of the surface map in Fig. 5.12) is presented in Fig. 5.13.

The region of no precipitation on the chart includes northwestern and southern Nevada, southern California, the southern San Joaquin Valley, and the southern Sierra Nevada. Evidently no orographic precipitation occurred on the western slope of the Sierra in the southwesterly current because of the damming effect of the mountain wave or, more specifically, because of the downdraft in the layers above the altocumulus deck. Thus there was no opportunity for the vertical development of clouds over the Sierra so long as the mountain wave persisted. Areas of heavy precipitation (>1 inch) were the Trinity Alps, the Mt. Lassen area, the Feather River country, and the coast and west slope of the Coast Ranges from Fort Bragg to Monterey. It is likely that these maxima were caused not by orography alone but by the ascending motion of the warm, moist air at the frontal surface as the front stalled and steepened in those areas.

19 0300 GCT. Upper air conditions at 1900 PST on the 18th are represented by the 850 and 700 mb charts in Figs. 5.14 and 5.15. The front* and the

*On all upper level charts of this study the frontal intersections of isobaric surfaces were determined from frontal contour charts prepared from analyses of soundings of all stations in the map region.

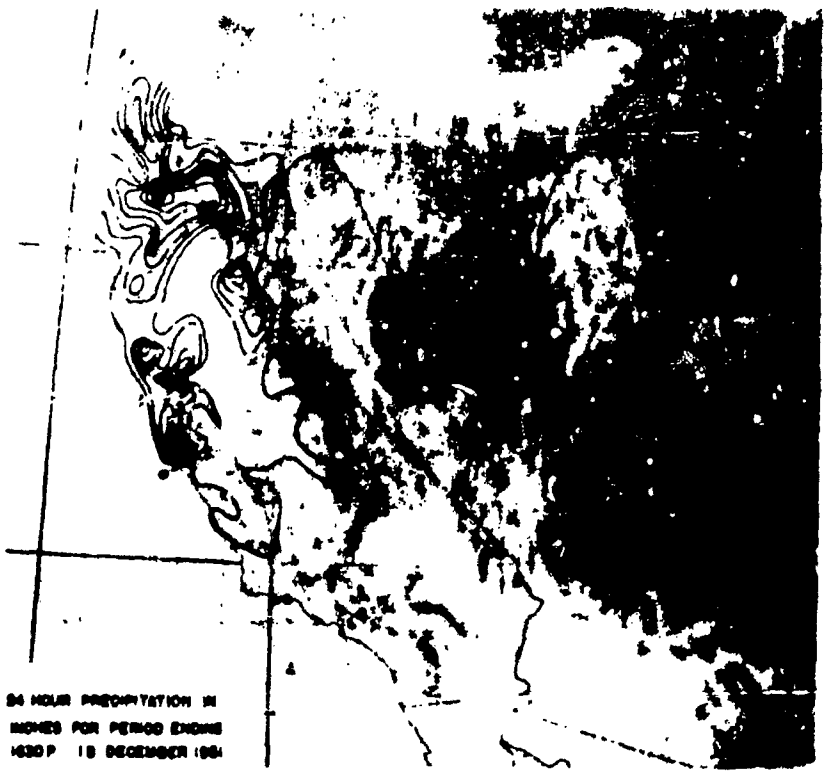

Fig. 5.13 - 24-hour precipitation amounts for period ending at 1630 PST, 18 December 1951. Isolines are drawn at intervals of 0.25 inch with only the zero line labeled.

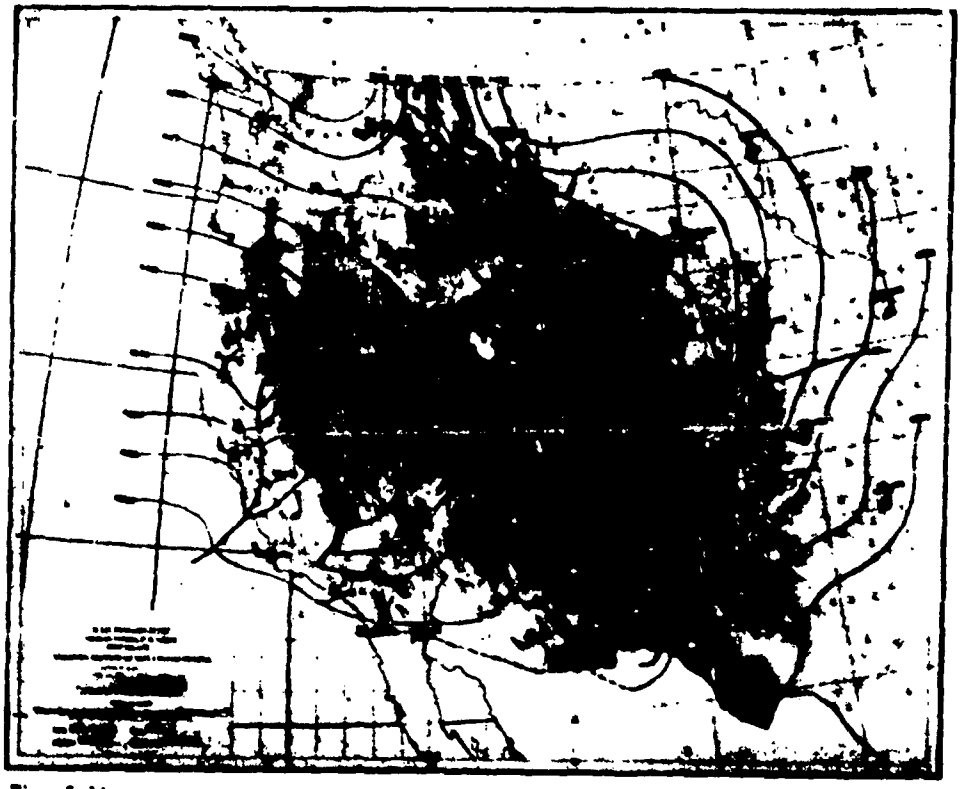

Fig. 5.14

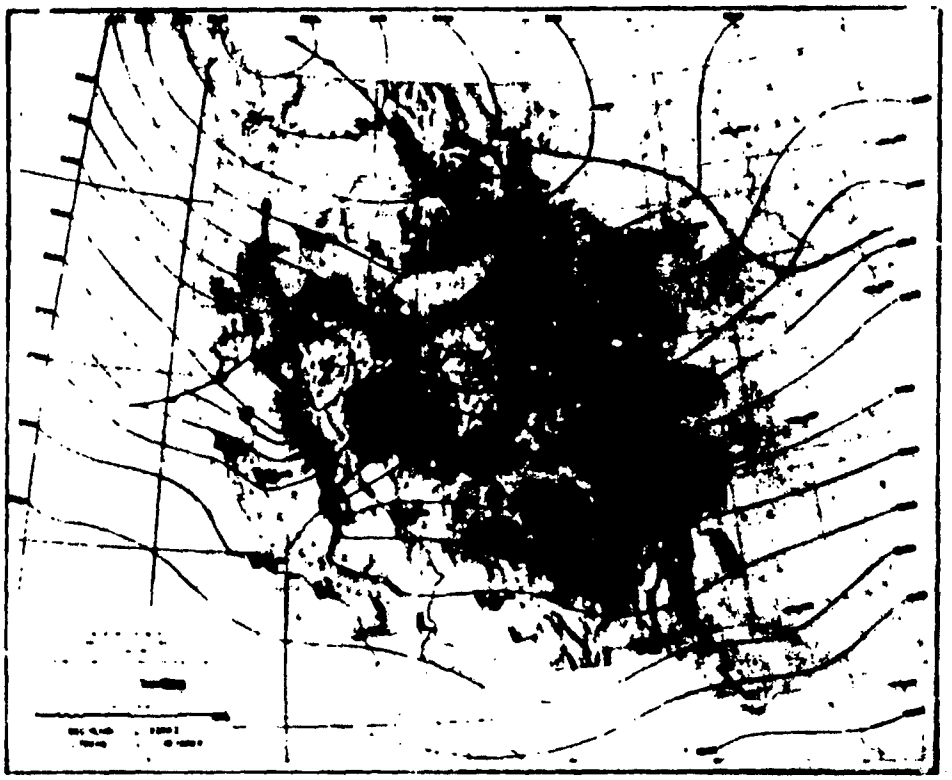

Fig. 5.15

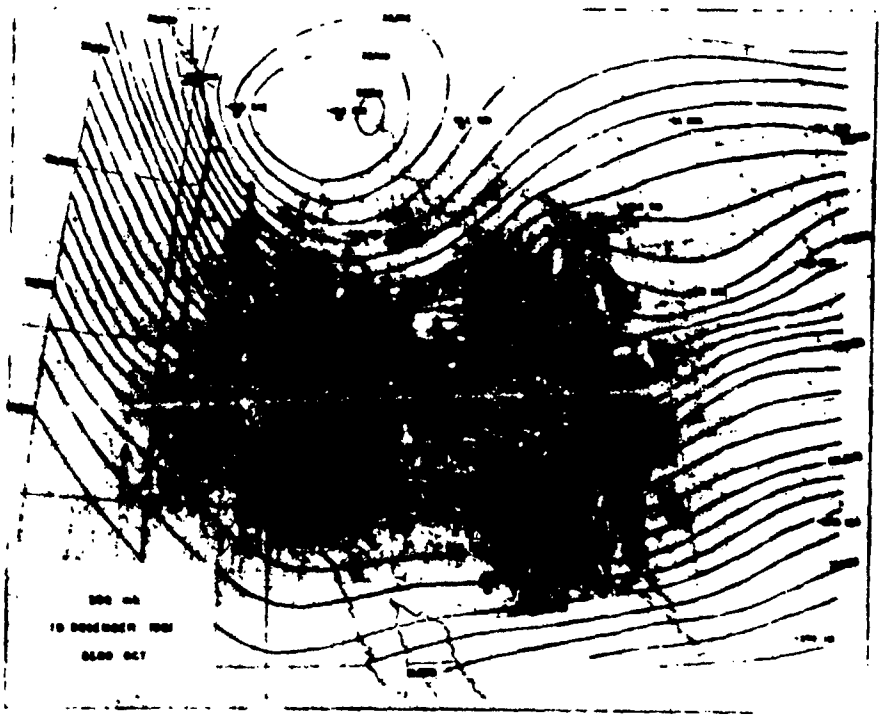

Fig. 5.16

lee trough are well marked in the wind and countour fields at both levels. Of interest is the 70 knot wind at Sacramento at 9,000 ft, above the 850 mb frontal surface there; and the relatively weak 25 knot wind at Merced at the 700 mb level directly upwind of the High Sierra. Note the trough forming in the lee of the Rockies.

19 0630 GCT. At 2230 PST (Fig. 5.17) the lee trough was still pronounced in the sea level pressure field. The front maintained its north-south orientation through California while its northern extension moved rapidly southward to lie nearly west-east across northern Nevada and Utah. The center of lowest pressure was near Salt Lake. Rain was then reported at Merced, Fresno, and Santa Barbara.

19 1230 GCT. Six hours later, at 0430 PST on the morning of the 19th, the front had passed Salt Lake City, Tonopah, Reno, Fresno, and Santa Maria and appeared to converge on the Sierra nutcracker-fashion from both west and east (Fig. 5.18). The principal low pressure center was then over south central Nevada. Snow was falling at Elko and Salt Lake City and steady rain in the cyclonic eddy over the Los Angeles Basin. Strong southwest winds continued to sweep across the desert.

19 1500 GCT. The three-dimensional structure of the front at 0700 PST on the 19th is shown in Figs. 5.19, 5.20, and 5.21. At the 850 mb level the Sierra and Rocky Mountain lee troughs are pronounced. The front lay through two low centers, one over northeastern Colorado and the other over southeastern Nevada. A shallow anticyclone appears in the north as a result of the high density of the arctic air mass. At 700 mb, 50 knot winds were reported in the cold air at Oakland and Merced. At 500 mb a single closed low center appears over southern Idaho and the cold front lies in an arc over Salt Lake City, Ely, Reno, Medford, and Tatoosh. The strongest winds occurred in two bands, one in the northwesterly flow over Red Bluff (100 knots) and the other in the westerly current over Long Beach (95 knots) and Tucson (85 knots).

19 1830 GCT. At 1030 PST on the 19th the front at the surface (Fig. 5.22) had just passed Bishop, Sandburg, Los Angeles, and San Diego. The northern segment of the front had moved into the low pressure center of southern Nevada and extreme eastern California; the lowest pressures were reported at Bishop and Las Vegas. The difference in temperature between the cold air west of the front in California and that north of the front in Nevada was by then rather large; the former was relatively mild maritime polar air from a more southerly trajectory over the Pacific while the latter was relatively cold transitional polar air of more northerly origin and longer continental trajectory. As the cold front folded back on itself about the southern Sierra, it formed a small occlusion along that portion of its length and, for a brief time, a seclusion of the "warm" air along the crest; i.e., for a time the High Sierra appeared as an island in a sea of cold air. It is interesting to note that cold air reached Owens Valley not from a spillover from the west but from the north and east. Specifically, the cold air reached Bishop from due north through Montgomery Pass in the White Mountains. As evidence in support of this, the times of pressure minima on the barograms of the Owens Valley stations, Lodgepole (LP), Inyokern (IND), and Tonopah (TPH),

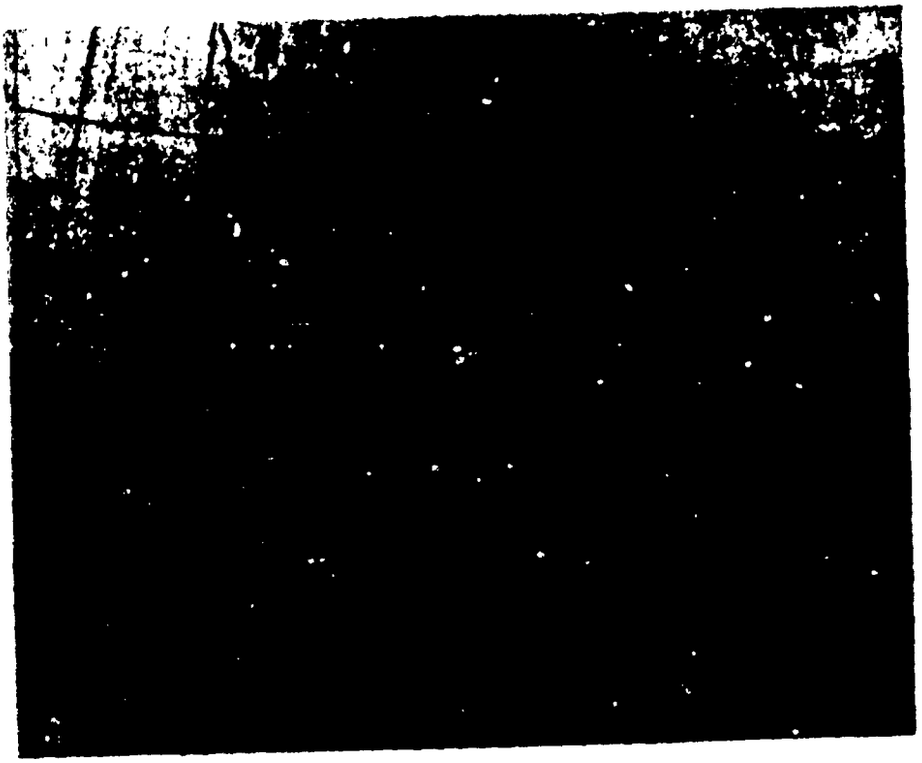

Fig. 5.17

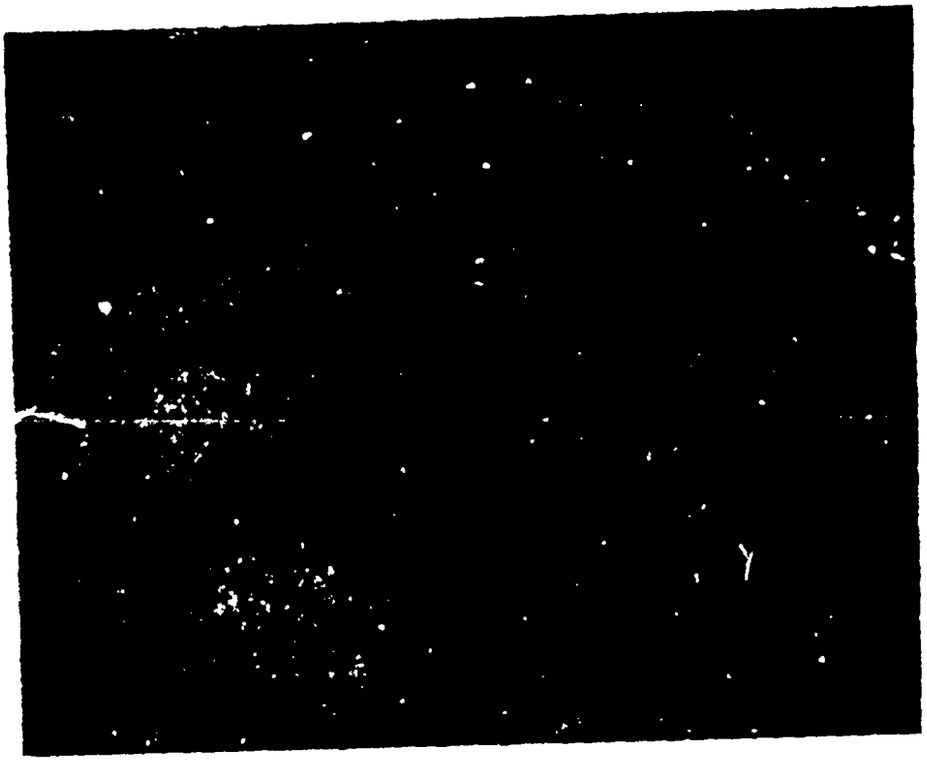

Fig. 5.18

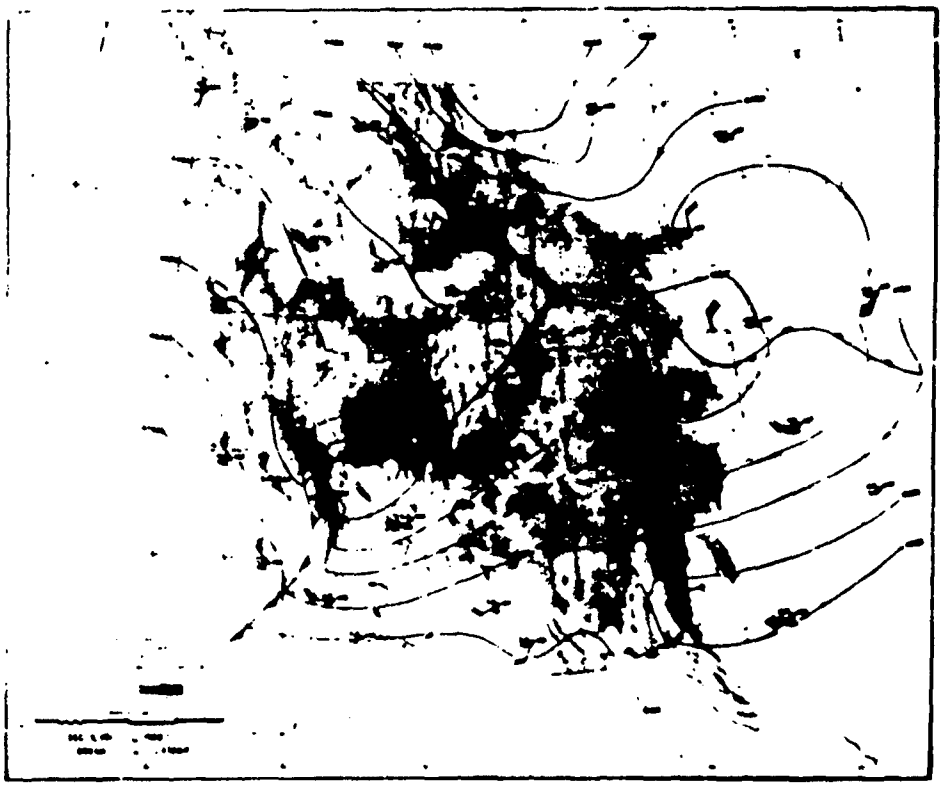

Fig. 5.19

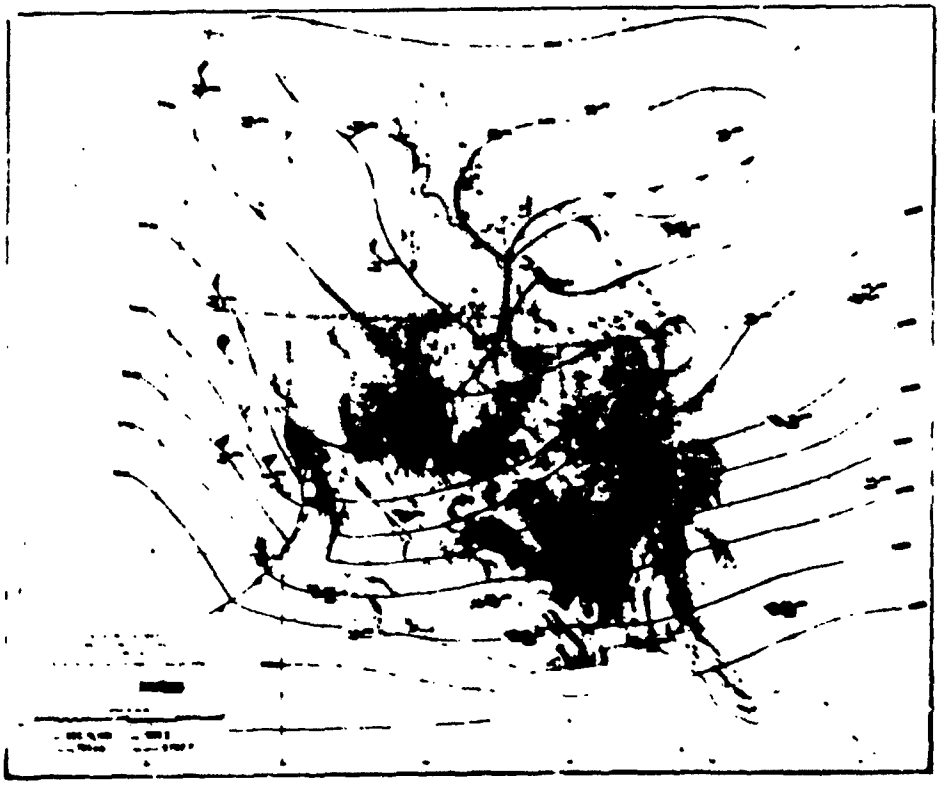

Fig. 5.20

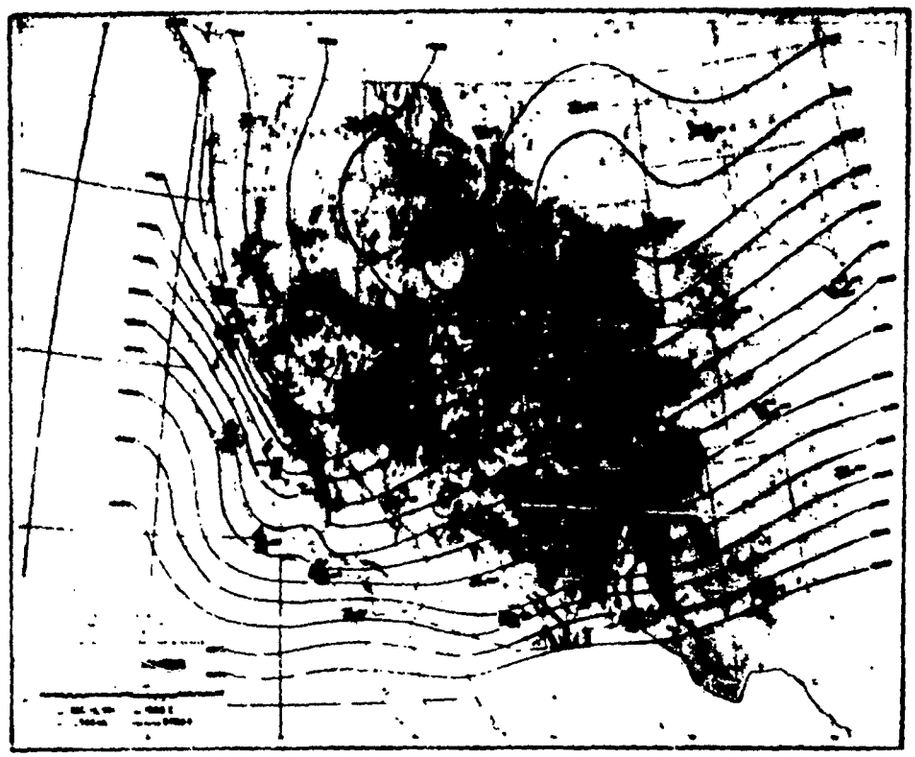

Fig. 5.21

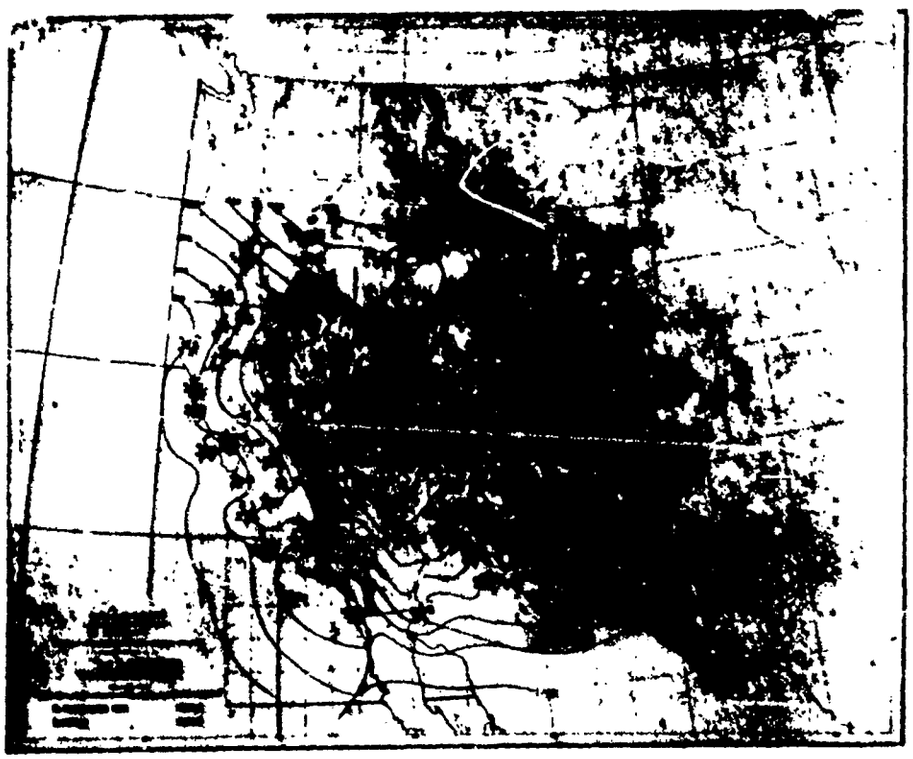

Fig. 5.22

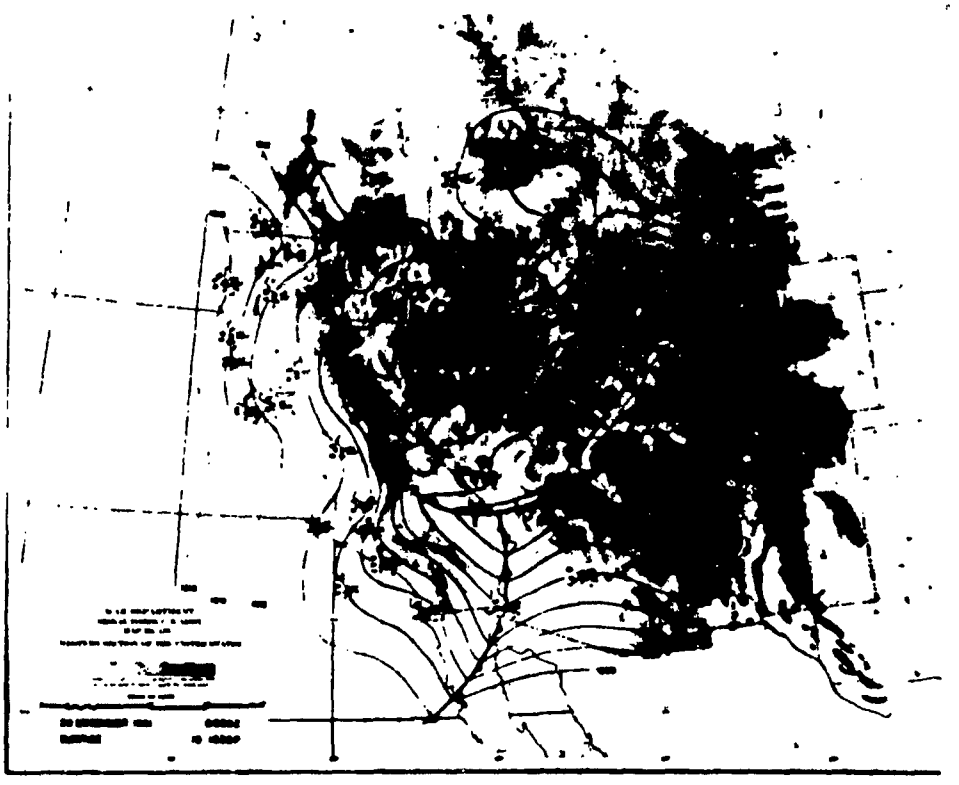

Fig. 5.23

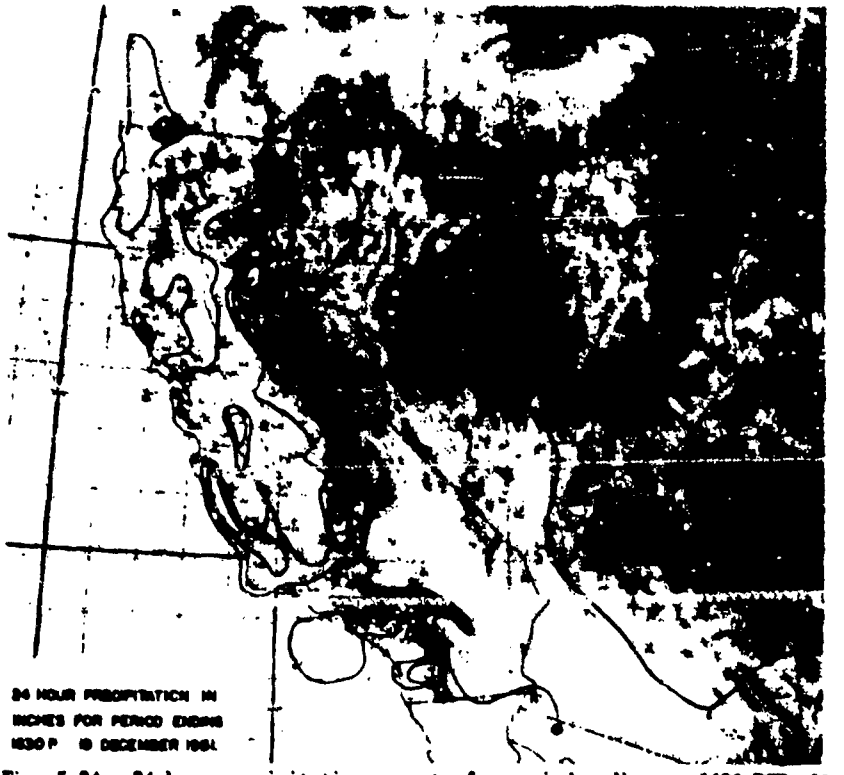

Fig. 5.24 - 24-hour precipitation amounts for period ending at 1630 PST, 19 December 1951. Isolines are drawn at intervals of 0.25 inch with only the zero line labeled.

were, in chronological order:

TPH	0500 PST	EC	1150 PST	LP	1345 PST
PLH	1000	CC	1300	NID	1500
M	1140	SH	1330		

Thus the cold air, arriving in greater depth on the eastern side of the Sierra, reached Onion Valley (SH) at 9,200 feet earlier than the cold air from the west reached Lodgepole at 6,760 ft on the western slope.

20 0030 GCT. By 1630 PST on the afternoon of the 19th the aforementioned occlusion is shown in Fig. 5.23 at what is perhaps the peak of development in its rather short-lived existence. A triple-point had formed near Needles and the tri-state intersection with strong winds in the region. The temperatures recorded in the descending air immediately behind the cold front from the north were relatively warm and dry but the temporal transition to cold temperatures was rapid. At 1030 PST, just after frontal passage, the temperature at Bishop was 46°F while at 1630 PST it was 36°F. Similarly, at Las Vegas the pre-frontal southwest current at 1030 PST was 56°F, the post-frontal northwesterly current at 1630 PST 41°F. Before frontal passage at Independence in the central Owens Valley at about 1120 PST, a maximum temperature of 71°F was reached in a föhn current. Towering cumuli were observed at Santa Maria, Fresno, Las Vegas, Tonopah, and Prescott; cumulonimbi were observed at Fresno at 1330 PST. Precipitation was occurring in the "warm" air over Arizona.

The pattern of 24 hour precipitation amounts for the period ending about 1630 PST on the 19th is shown in Fig. 5.24. The zero line then follows the east slope of the southern California mountains, the Tehachapis, and the Sierra Nevada as far north as Mono Lake; it encloses southern California and southern Nevada. It is possible that some rain or snow fell on some of the higher summits within that region; at the University of California Laboratory at 10,150 ft on the crest of the White Mountains only a trace was reported. Other regions where no precipitation was recorded are extreme northwestern Nevada and the Sacramento Valley. The heaviest precipitation fell along the western slopes of the Sierra and the southern California mountains.

20 0300 GCT. The final maps in this study are those of Figs. 5.25 and 5.26. At 850 mb the triple-point and its low pressure center are most clearly shown in the contour and velocity fields. Also on that chart the thermal properties of the air masses are best revealed. The shallowness of the southernmost cold front is evident from a comparison of 850 and 700 mb temperatures and dew points. At 850 mb the air was cooler and the temperature-dew point difference least in the northwest current over southern California; the lowest dew point in the region was that at Las Vegas in the subsiding cold air from the Plateau. At 700 mb very cold air was reported north of the front over Nevada and Utah, while south of the front the west-east temperature and moisture differences had been reversed; warmer and extremely dry, presumably subsiding, air was found over California at that level while cooler, nearly saturated, presumably rising, air was found over Arizona.

From there the storm moved eastward across New Mexico to form a rather

intense low pressure center over the Oklahoma-Texas Panhandle on the 20th, having brought general precipitation to all of the states west of the Rocky Mountains.

Conclusions. It is apparent that, while the "northwest type" of cyclonic storm is the matrix in which the greatest Sierra lee waves occur, the lee wave phenomena are not the greatest of those resulting from the influence of the mountain barrier on the pattern of air flow. The effects of the Sierra Nevada on surface winds, the distribution of precipitation, and on the course and development of the storm itself extend over a much larger region than that of the lee wave. In the pre-frontal southwesterly current the damming effect of the Sierra Wave slows the eastward movement of cold air, delays arrival of the storm to southern California, and allows the cold air to reach the trans-Sierra region from the north and east. These effects lead to a circulation pattern and air mass contrasts which favor cyclogenesis and the development of a relatively shallow but intense low pressure center over southern Nevada with subsequent movement eastward across Arizona and New Mexico. In many cases during the spring months it has been observed that this new low is responsible for the development of widespread tornado activity in the southern Great Plains. The striking resemblance of the precipitation pattern for the storm to that of the average annual rainfall for California suggests that the principal features of that pattern are due to the predominance of such cyclonic storms.

Synoptic charts of other lee wave cases.

In the second portion of this chapter are presented surface and upper air charts of the other 1951-2 lee wave examples discussed in Chapters 3 and 4. For all cases a 500 mb chart and either a surface or 850 mb chart are shown. The 500 mb charts were chosen for presentation because they are most representative of mid-tropospheric flow and the position of the frontal zone at that level gives an approximation to the location of the polar front jet stream at higher levels. For two cases of strong lee waves (16 February and 19 March 1952) 700 and 300 mb charts are also shown.

The time of the upper air charts is 1500 GCT, so chosen to include data from Lodgepole, Bishop, and Inyokern not available at the later 0300 GCT time. Surface charts shown are at 1830 GCT, which time is rather near the actual flight time and allows the charts to be roughly compared to the 1500 GCT upper air charts. The reader is invited to use his imagination to depict the inferred changes and developments in the synoptic fields during the day.

27 November 1951. (Figs. 5.27 and 5.28) A cold front approached the Northwest with cloudy skies, light to locally heavy rain in that region, and gale winds along the Washington coast. In the isobar pattern the Plateau anticyclone was strong and a weak pressure gradient existed about the Sierra. At 500 mb no frontal zone appeared. A diffluent flow pattern* was above the

*The diffluent trough (Bjerknes, 1954) is one with greater wind speeds in the air flow upwind of the trough and with lesser wind speeds in the air flow downwind of the trough where the current often diverges.

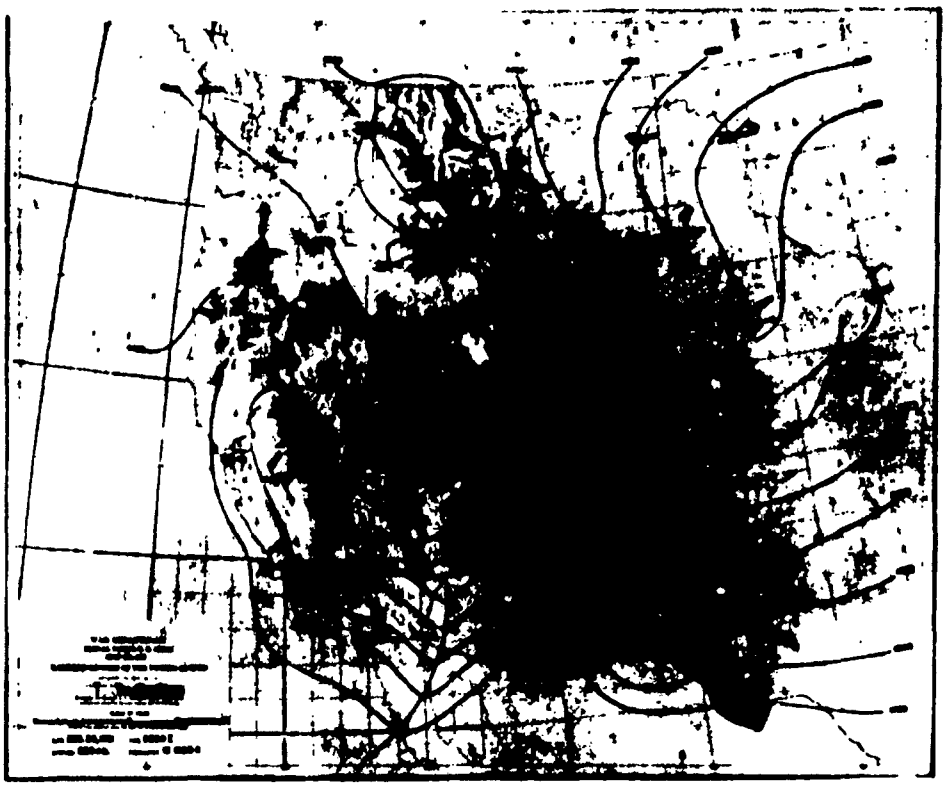

Fig. 5.25

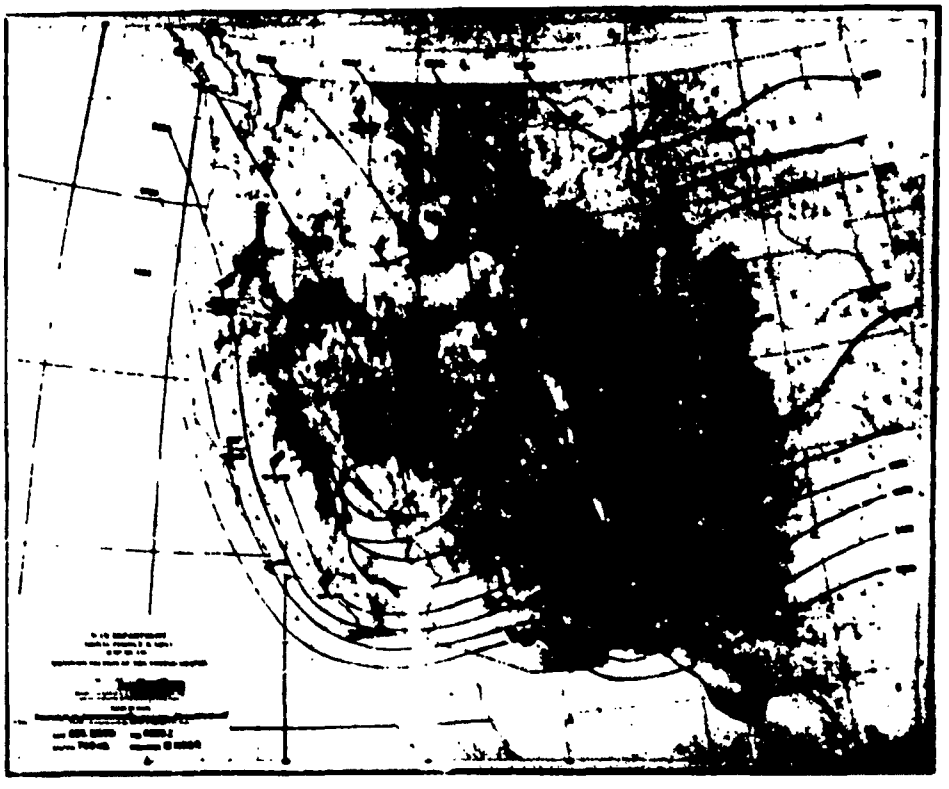

Fig. 5.26

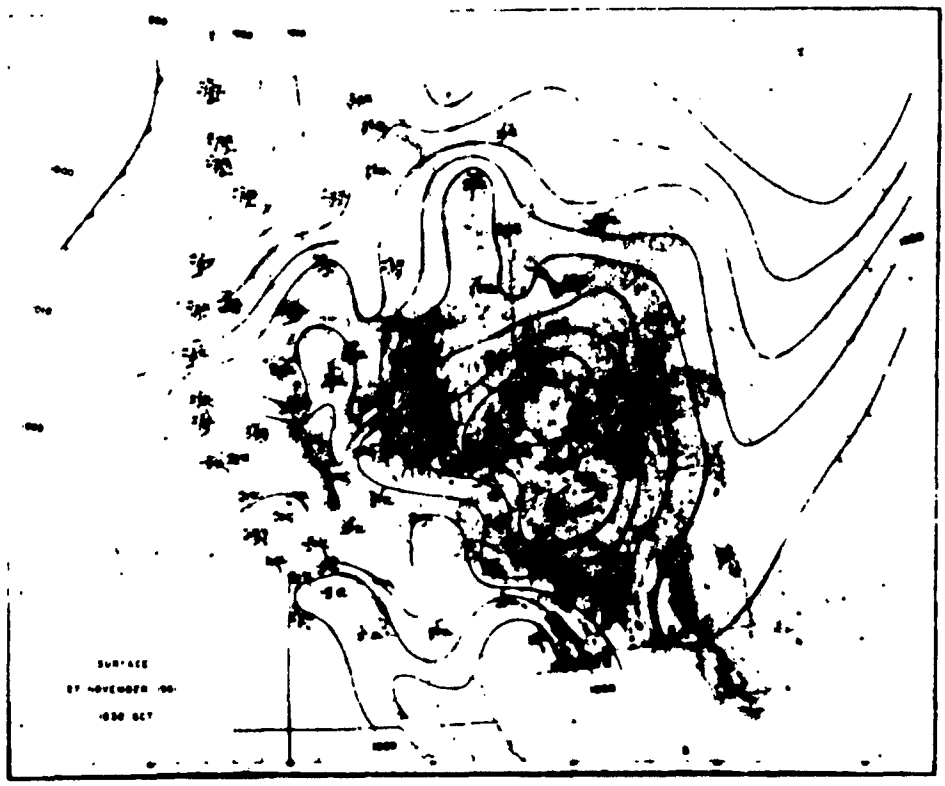

Fig. 5.27

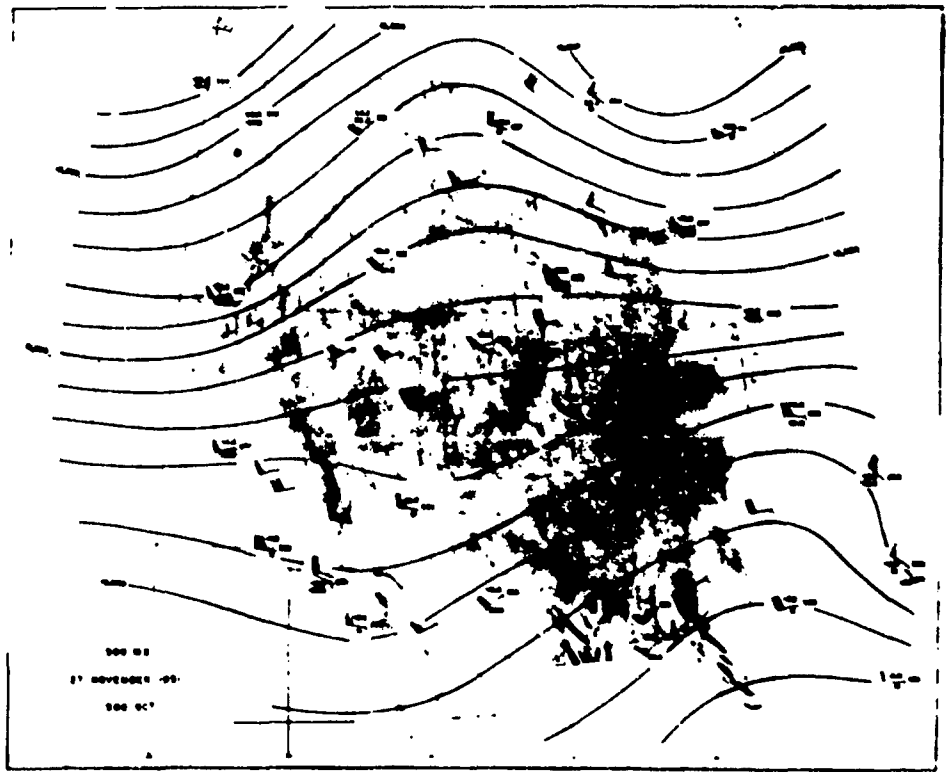

Fig. 5.28

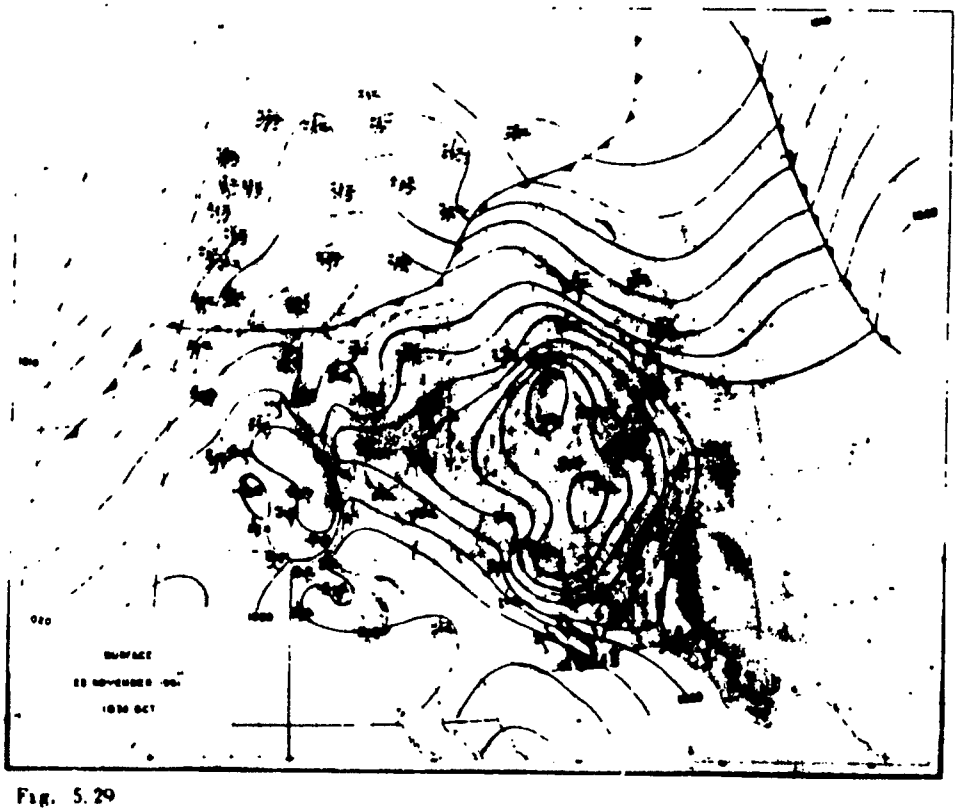

Fig. 5.29

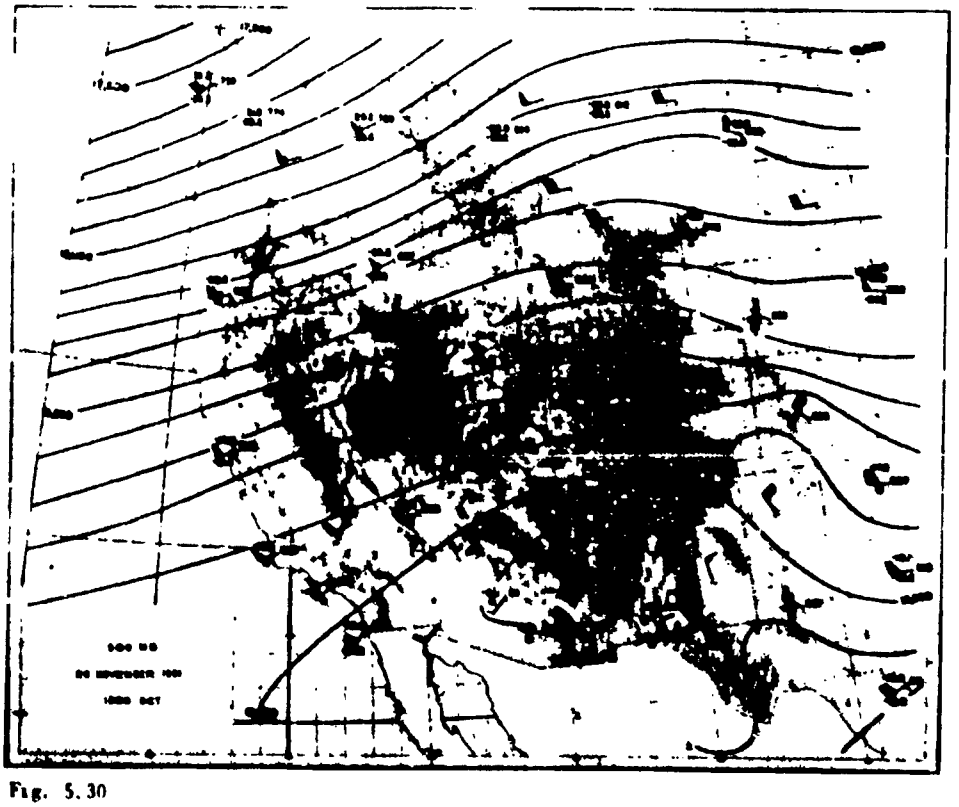

Fig. 5.30

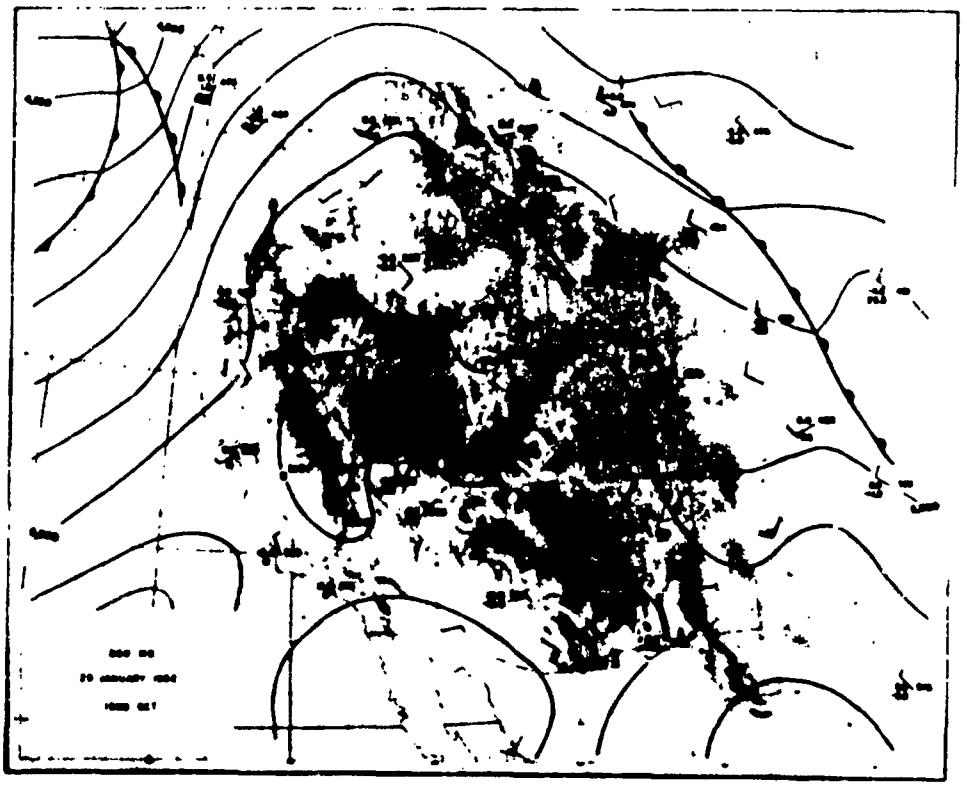

Fig. 5.31

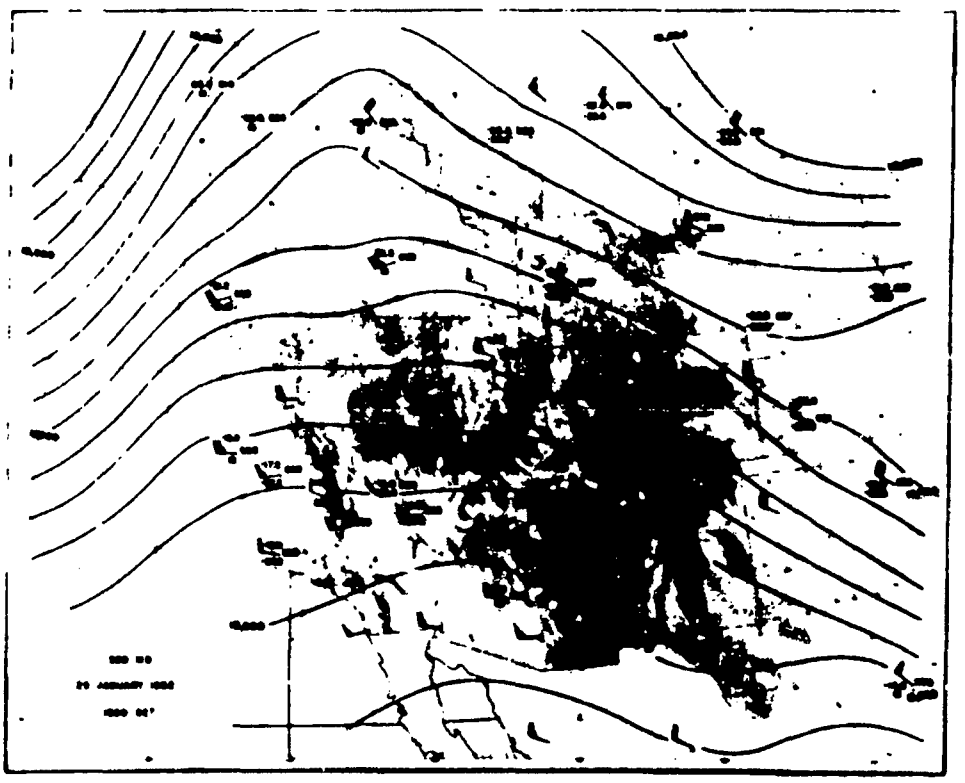

Fig. 5.32

Sierra but the wind speed evidently increased throughout the day.

28 November 1951. (Figs. 5.29 and 5.30) At the surface a slight lee trough existed between a strong Plateau anticyclone and another high pressure cell over central California. Rather weak, fast moving, frontal waves passed north of the Sierra with rain confined to extreme northern California. At the 500 mb level the front lay across the Columbia River with southwesterly flow over the Sierra.

29 January 1952. (Figs. 5.31 and 5.32) On the 850 mb chart the Plateau anticyclone enveloped the Sierra. The flow over the Sierra at 500 mb was relatively weak. A classic example of the analyst's problems in utilizing non-synoptic and inconsistent data is afforded by the contour height discrepancies at Lodgepole, Merced, Inyokern, Santa Maria, and Long Beach.

30 January 1952. (Figs. 5.33 and 5.34) The 850 mb contours show slight troughs in the lee of the Sierra and the Rockies. The Plateau anticyclone is strongly developed over Utah while a cold front moved inland from the northwest bringing rain to San Francisco and Reno. Anticyclonic flow prevailed over the Sierra at 500 mb. Merced heights are low at both isobaric levels.

16 February 1952. (Figs. 5.35, 5.36, 5.37, and 5.38) A cold front, the frontal trough, and the lee trough are pronounced features of the 850 and 700 mb contour patterns. Also of interest are the troughs in the lee of the Colorado Rockies and the Wind River Range in Wyoming. At 500 mb the flow over the Sierra was westerly with the frontal zone apparently over northern California and Idaho. The jet stream at 300 mb was north of the Sierra at 1500 GCT, but moved somewhat southward in the westerly current during the course of the day. It is to be noted that in this case of a strong lee wave the Merced data fit well the contour pattern.

21 February 1952. (Figs. 5.39 and 5.40) At the surface the front had passed the Sierra but a lee low pressure belt remained. The flow at 500 mb was WNW with relatively cold temperatures over the Sierra at that level but with no strong frontal zone. Merced data fit the pattern; Inyokern and Lodgepole data are from 1300 and 1800 GCT respectively.

3 March 1952. (Figs. 5.41 and 5.42) A cold front approached the coast as a trough developed in the lee of the Sierra. The large-scale flow pattern of troughs and ridges at 500 mb was of rather short wave length. Although the flow was northwesterly at 1500 GCT, the upper wind direction shifted rapidly to southwesterly by afternoon. In this series of fast-moving upper troughs, lee waves occurred on the 3rd, midnight of the 4th-5th, and on the morning of the 6th.

18 March 1952. (Figs. 5.43 and 5.44) By 1830 GCT the cold front lay through northern California and great lee troughs had formed east of the Sierra and Rocky Mountains. The Sierra lee trough extended into the Catalina eddy.* At 500 mb the low from the great March 14-15 storm was over the Plains.

---

*A shallow cyclonic circulation frequently observed off the southern California coast and named for Catalina Island.

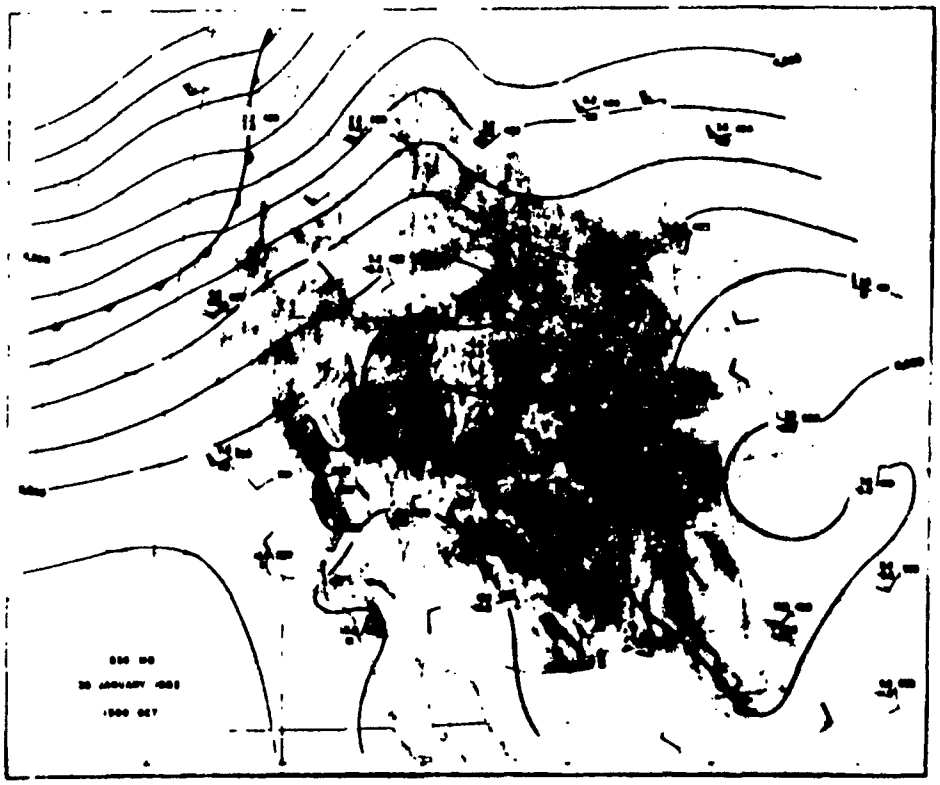

Fig. 5.33

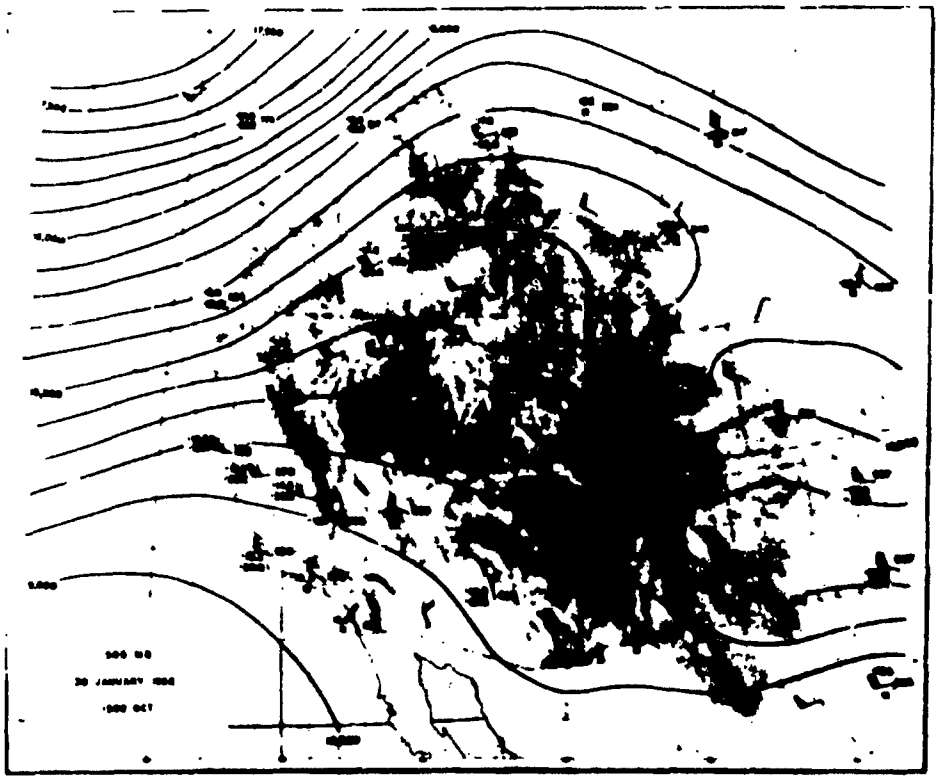

Fig. 5.34

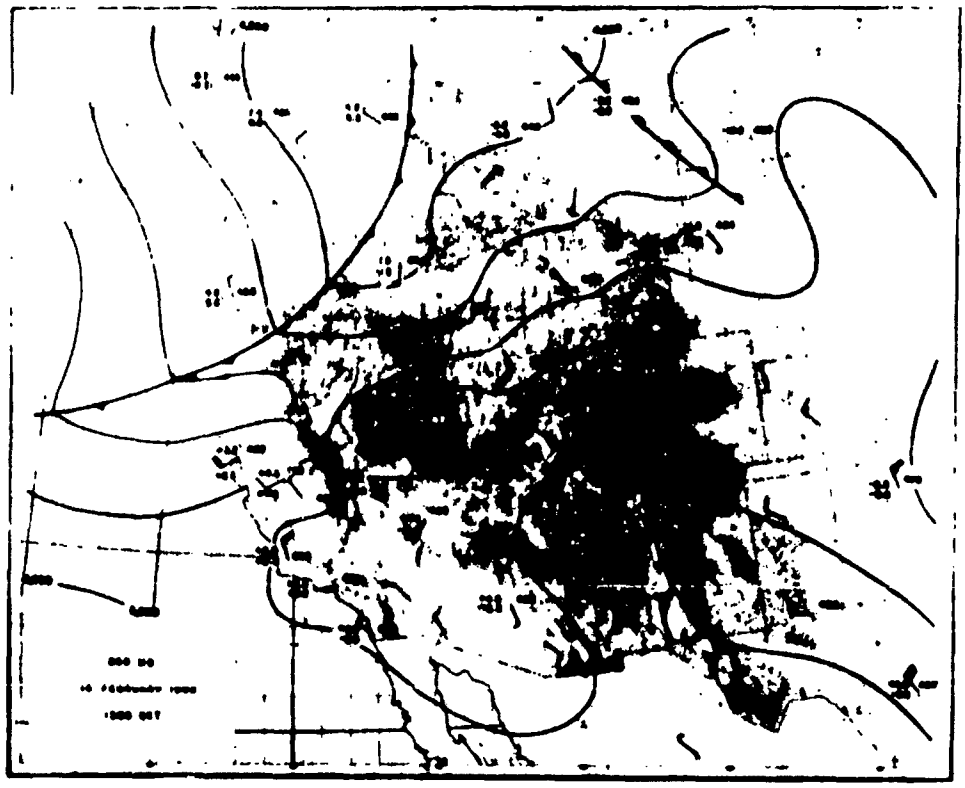

Fig. 5.35

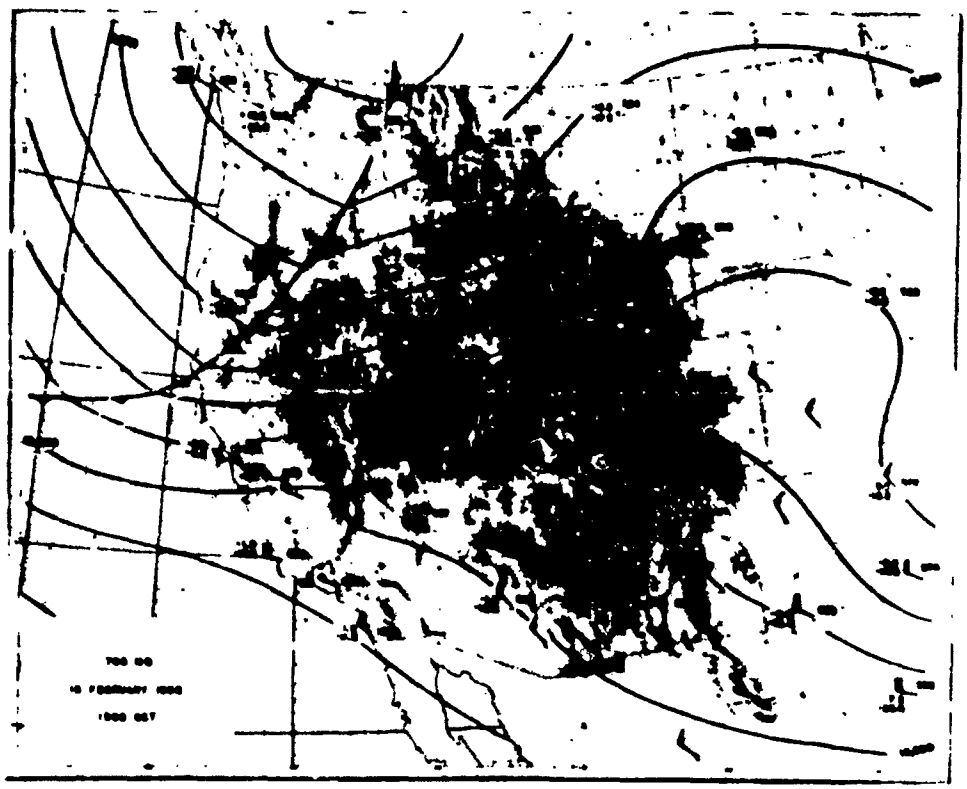

Fig. 5.36

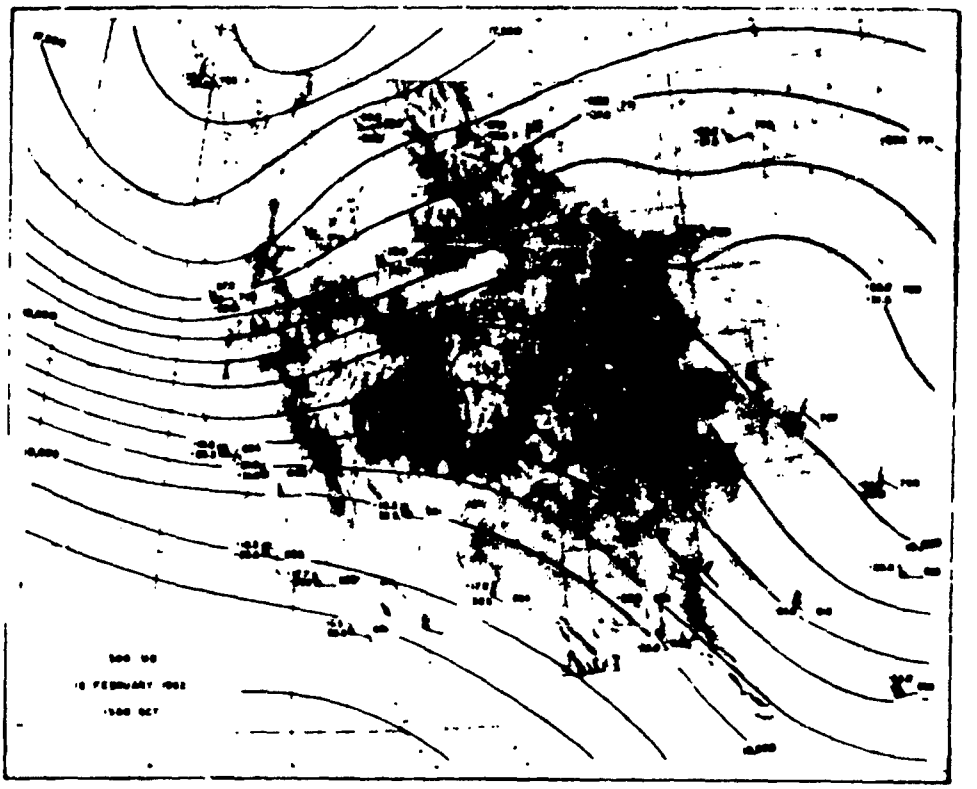

Fig. 5.37

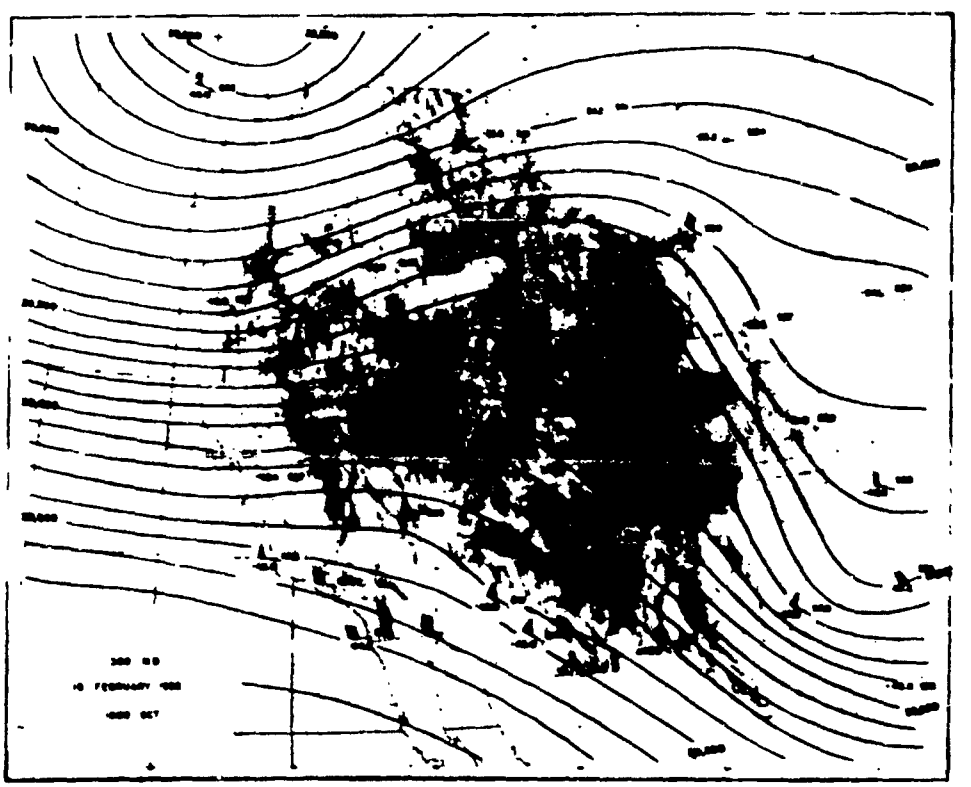

Fig. 5.38

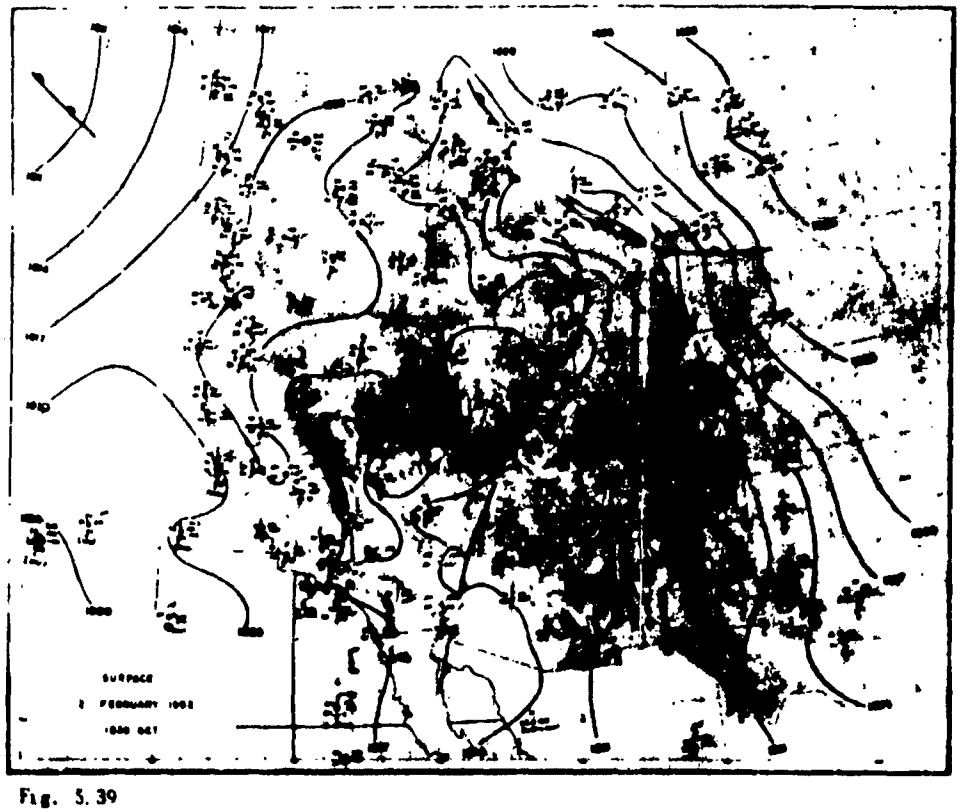

Fig. 5.39

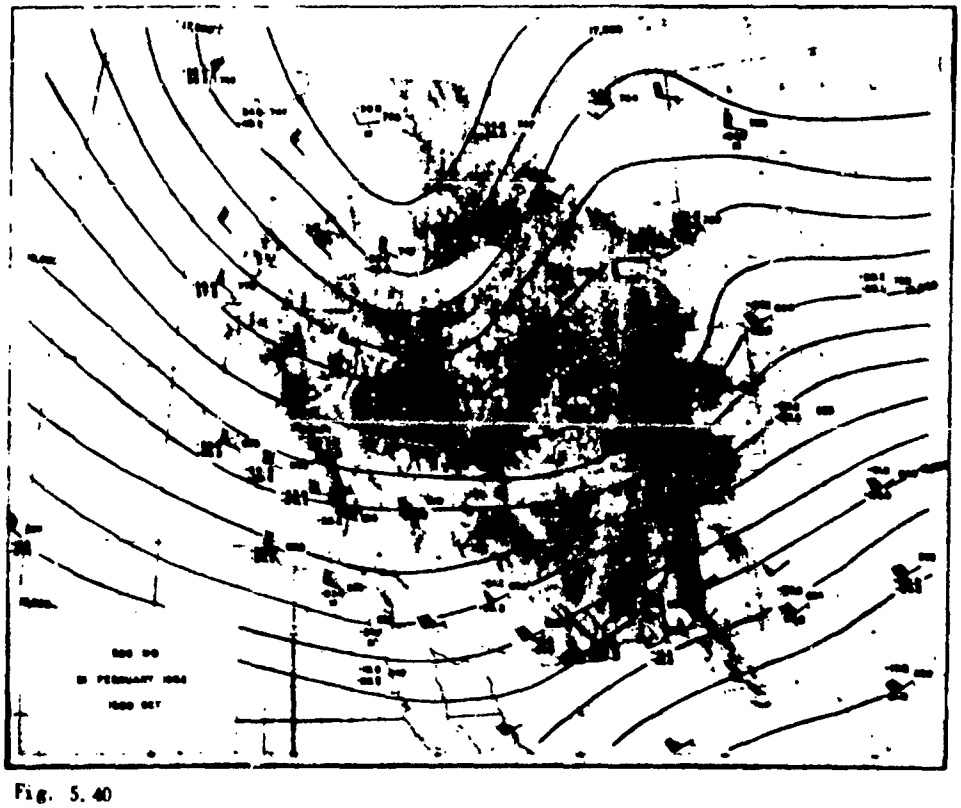

Fig. 5.40

There was strong WSW flow over the Sierra with very cold temperatures over Washington and Oregon, making for a strong frontal zone. The westerly jet stream at high levels was over central California.

19 March, 1952. (Figs. 5.45, 5.46, 5.47, and 5.48) On the surface chart the cold front had passed the Sierra region, but a trough remained off the coast and a strong pressure gradient continued to exist across the Sierra. At 700 mb the front, distorted by the lee trough, was passing the Sierra from the north. Both Sierra and Rocky Mountain lee troughs were pronounced. At Inyokern, leeward of the southern end of the Sierra, the wind speed was 100 knots at the 700 mb level. Strong surface winds on the Mojave Desert in such synoptic situations appear to result from the local jetlet of air around the southern end of the High Sierra and over the lower Tehachapi Mountains. At 500 mb there was strong zonal flow of long wave length. The front lay across the northern Sierra, warped by the lee wave of the southern Sierra and forming the föhnwall and roll cloud inversion. The zonal flow was of great strength at 300 mb, with a contour height (D value) difference between Medford and Phoenix of over 2,000 ft. During the day both the 500 mb front and the jet stream passed over the Sierra.

30 March 1952. (Figs. 5.49 and 5.50) A diffuse and shallow cold front had passed the Sierra, but the lee trough and Catalina eddy remained in the WNW flow aloft. The front at 500 mb lay across northern California and Nevada.

General conclusions.

The analyzed charts presented in this chapter show the large-scale synoptic fields associated with each lee wave occurrence of 1951-2 treated in Chapters 3 and 4. Considered as a whole, the principal results of these studies are:

1) Strong lee waves are associated with: i) an upper trough along the Pacific Coast with strong westerly flow across the Sierra (large T and D gradients parallel to the Coast); and ii) a cold front or an occluded front approaching California from the northwest.

2) The soundings and wind profiles, which are the connecting links between the large-scale synoptic fields and the small-scale lee wave cross sections, are essentially pre-frontal in character. The high level inversion that forms the fohnwall and the roll clouds may be identified as a quasi-horizontal warm front.

3) The wave length of the upper flow pattern affects the intensity of the lee wave and, in its effect upon the speed of the trough, it affects the duration of the lee wave phenomena. When the flow is strong and the wave length rather long, the strongest lee waves occur and persist for the longest period. When the wave length is comparatively short, the lee wave is usually less intense and is of a more transitory nature. In all cases, with the passage of the principal upper trough, and of the cold air throughout the greater depth of the troposphere, there is no longer a large wind speed component across the mountain range and the lee wave phenomena cease or become weak.

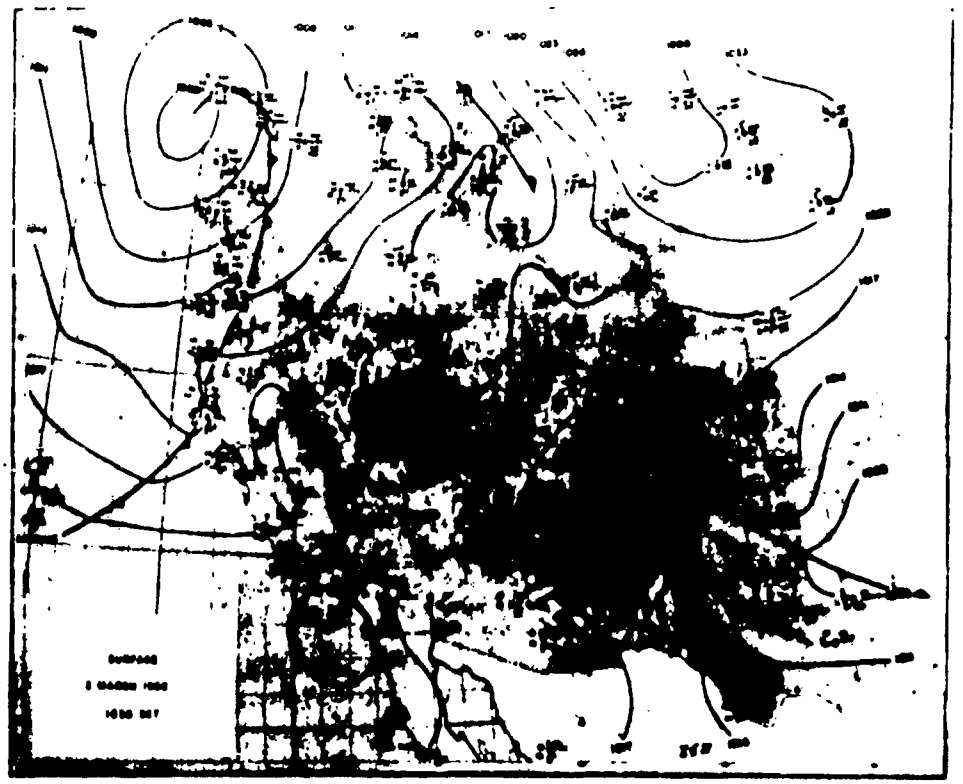

Fig. 5.41

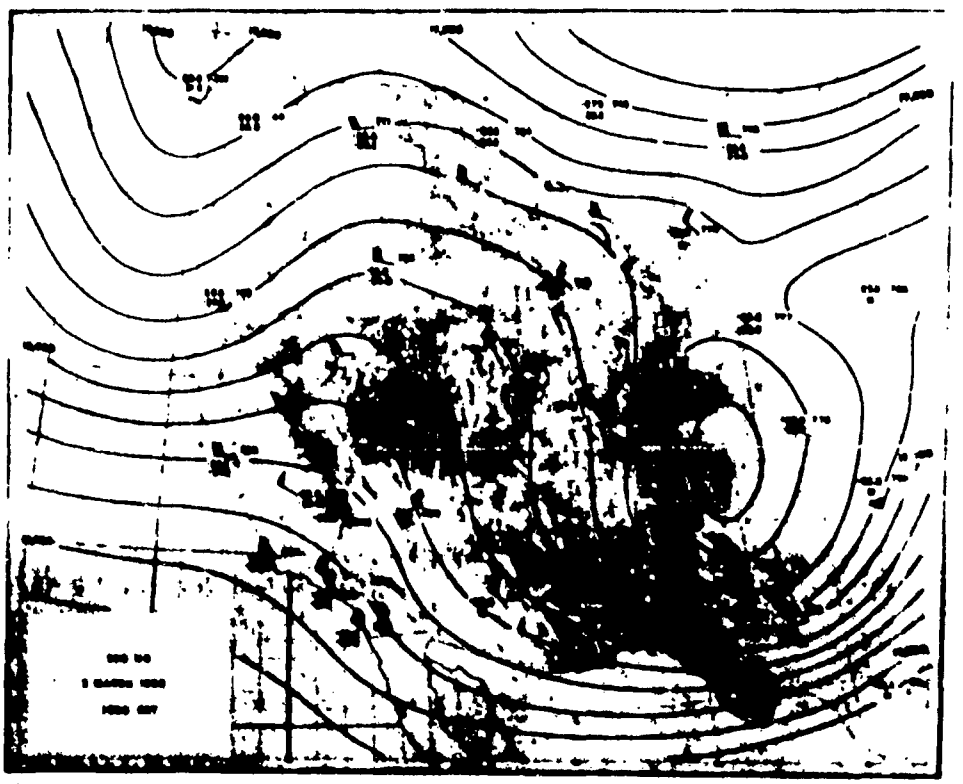

Fig. 5.42

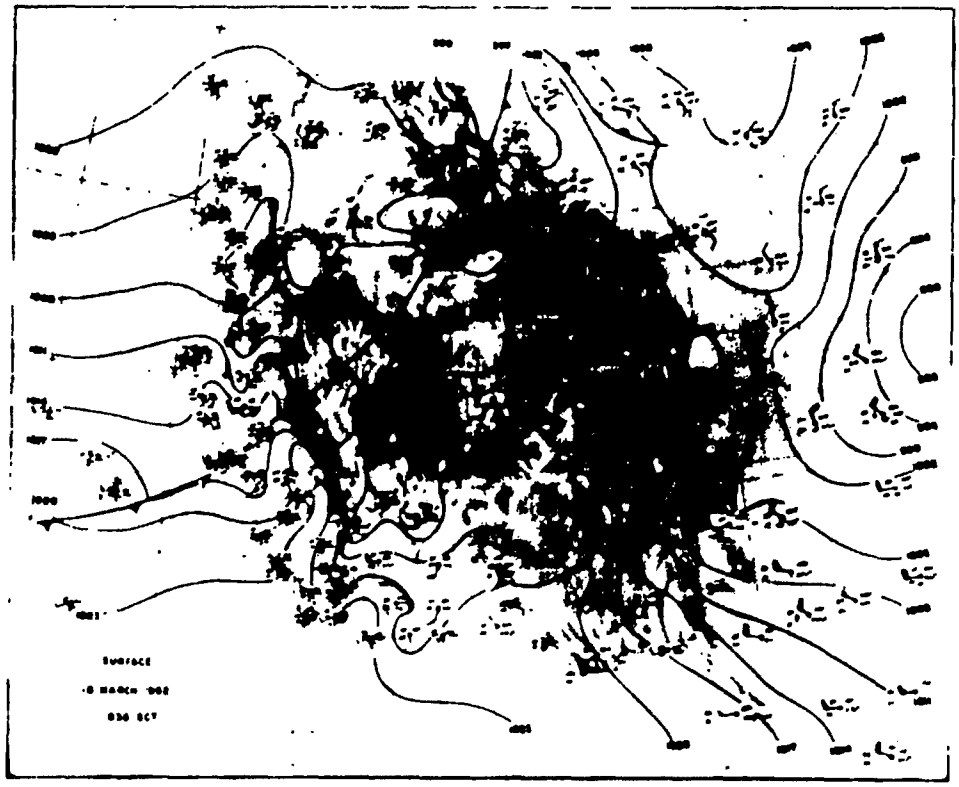

Fig. 5.43

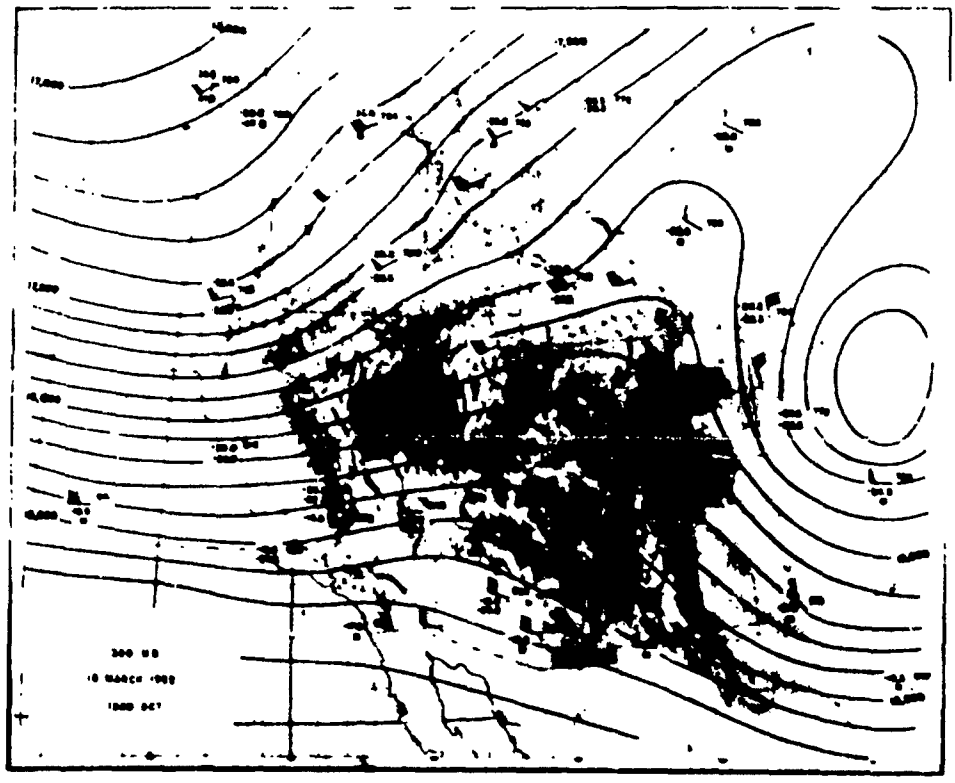

Fig. 5.44

4) The Polar Front jet stream generally crosses Oregon or northern California during the development of strong Sierra Nevada lee waves but on some occasions, e.g., 13 December 1951 and 19 March 1952, strong lee waves are associated with a westerly jet stream across the Sierra. As will be discussed in Chapter 8, strong lee waves often form rapidly during the passage or development of "jetlets" in the relatively warm air south of the principal Polar Front jet stream.

5) In some cases there is apparently a real upwind (damming) effect of the Sierra as evidenced by relatively cold temperatures and a greater southerly component of the wind in the lower troposphere over Merced in comparison with observations from surrounding stations. In other cases cold temperatures and low contour heights at Merced appear to be a result of a difference in radiosonde equipment errors between those of Castle Air Force Base, Merced, and those of surrounding Weather Bureau stations.

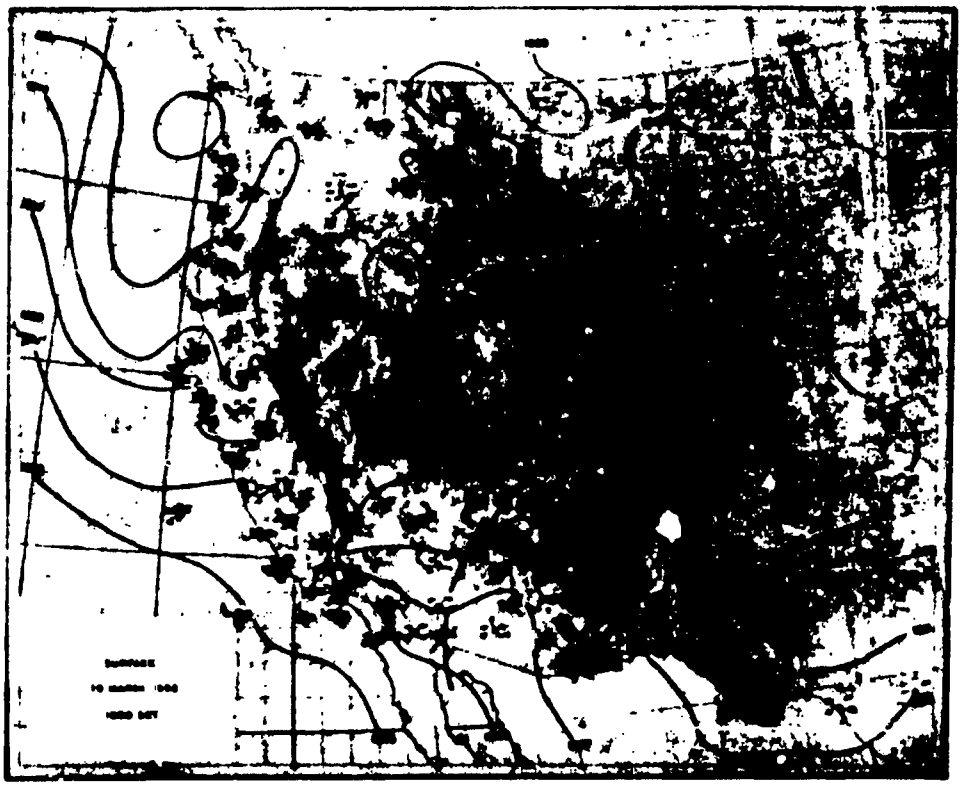

Fig. 5.45

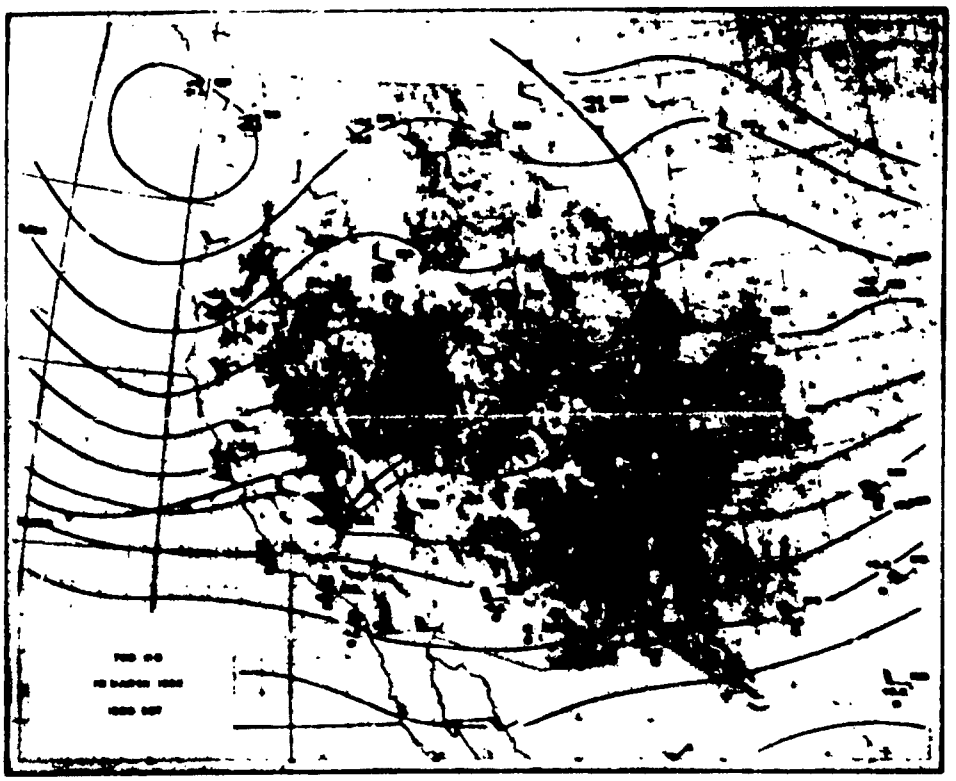

Fig. 5.46

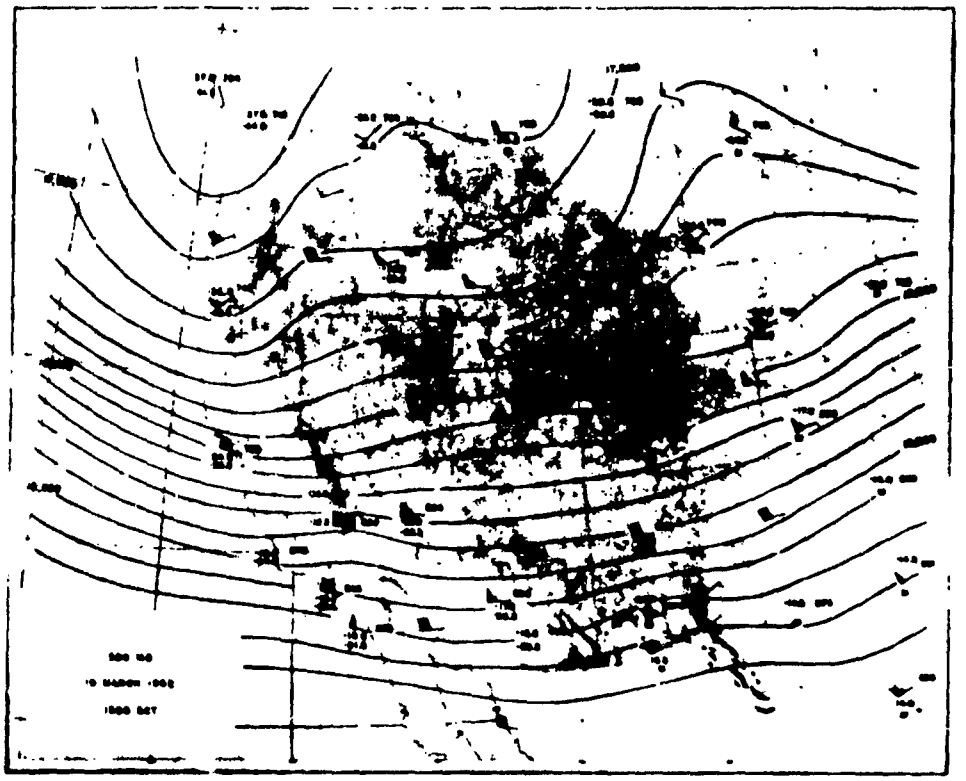

Fig. 5.47

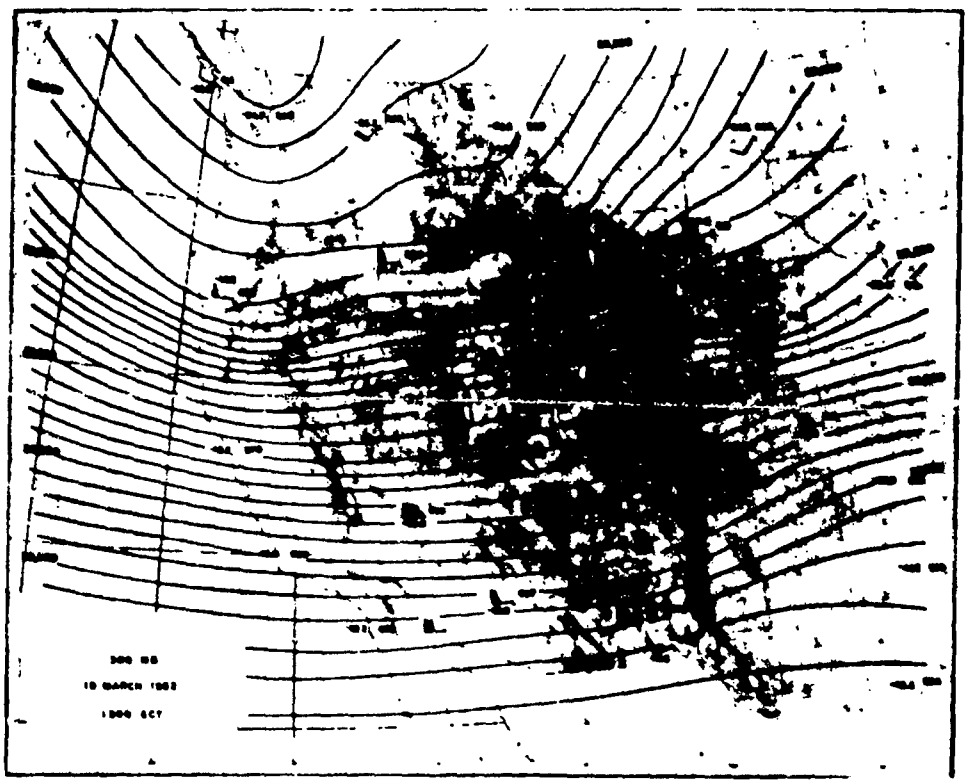

Fig. 5.48

Fig. 5.49

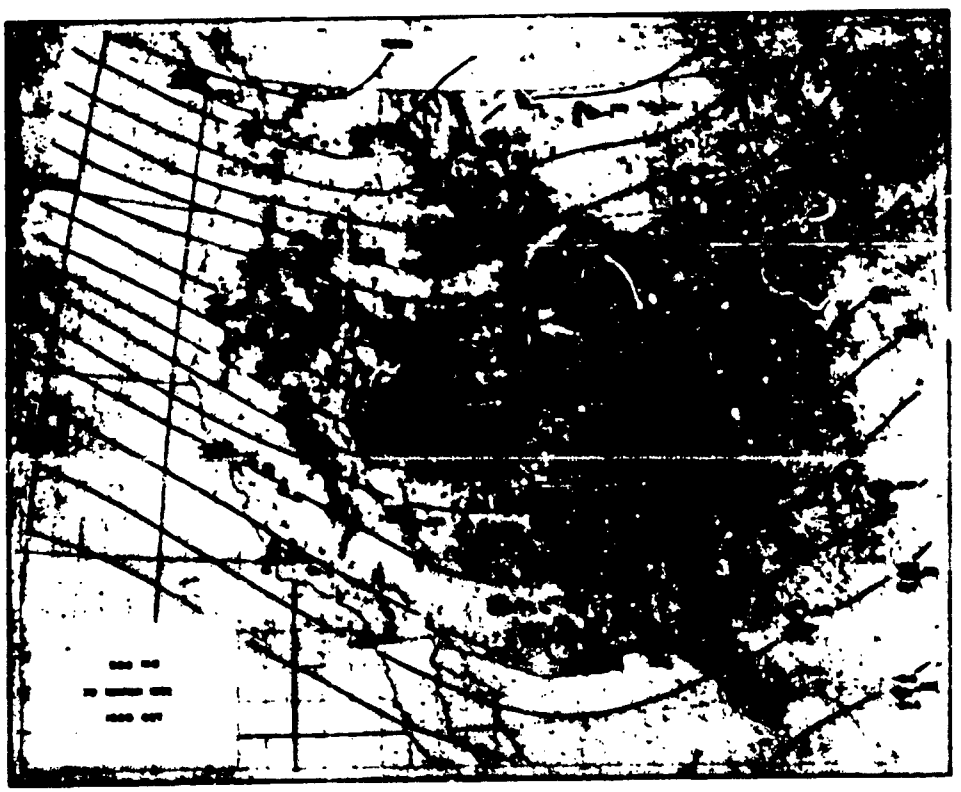

Fig. 5.50

The synoptic weather situation at 1500 GCT, 1 April 1955. The first map of this series (Fig. 6.1) is that of the surface pressure distribution and observed weather at 0730 PST (1530 GCT) on the morning of 1 April. Data plotted are those of the three-hourly observations giving sea level pressure, temperature, dew point, pressure tendency, clouds, and weather. A cold front--well marked, especially in the wind, pressure, and pressure tendency fields--lay through eastern Washington, Oregon, and northwestern California. The Great Basin Anticyclone was centered in western Colorado. Blowing sand on the Texas Plains continued in the wake of the previous northwest storm of 29 March. Ahead of the front were observed altocumulus clouds, farther out cirrus, and at Bishop and Reno, in the lee of the Sierra, altocumulus lenticularis. Clear skies were over the Southwest while steady rain or showers were observed behind the front. A slight lee trough between two anticyclones is evident in the pressure field about the Sierra; in the southern part it is possibly mostly an insolation effect but in the northern part it is the effect of the mountain lee wave in the southwesterly upper current.

Cloud developments. In Figs. 6.2a and b are shown two views from Bishop at the time of the 0730 PST surface map. In the north-northwest, cirrus bands, their leading edges in the lee of the Sierra, trailed beyond the horizon along the direction of the wind. Significantly, these forms were reported at the same time over Fallon, Battle Mountain, and Elko, Nevada.* The second photograph, looking west-southwest, is of the first-appearing lenticular cloud forms and roll cloud fragments. The former was above and somewhat upwind of the latter but of the same first wave crest in the leeward flow.

Isobaric charts. Upper air conditions at the time are shown in the isobaric charts for 500 and 300 mb (Figs. 6.3 and 6.4). At the 500 mb level the cold front was located on plotted soundings and frontal contour charts. Evident is the greater number of observations compared with that of the 1951-2 charts. Winds were plotted by a template-compass to the 10-degree accuracy of the coded reports. From the location of the reporting stations with respect to the Sierra Nevada and the direction of the upper flow, two cross sections were suggested, one parallel to the Sierra from Medford through Tonopah to Phoenix, and the other perpendicular to the range from Fresno through Bishop and Tonopah to Lander. From Reno to Phoenix the winds at the 500 mb level decrease from 40 to 15 knots; the temperature difference is 4.6°C. From Fresno to Lander the winds decrease from 45 to 25 knots; the temperature and height differences are small. At 700 mb (not shown) the Sierra lee trough was quite evident in the resultant analysis of Oakland, Reno, Fresno, Tonopah, and Las Vegas data.

At the 300 mb level (Fig. 6.4) the jet stream lay between Portland and Medford. As in the 500 mb chart it is seen that the Medford-Phoenix cross section is nearly perpendicular to the upper flow. Also, in the Fresno-Lander section, the wind speed varies from 50 to 35 knots and the temperature and height differences are small. Note the 40 knot winds at

*See Fig. 1.7 for locations of stations mentioned in this chapter.

Fig 6 1

Fig. 6.2a - 0730 PST, 1 April 1955. NNW from Bishop Airport. Cirrus bands.

Fig. 6.2b - 0730 PST, 1 April 1955. WSW from Bishop Airport. Roll cloud fragments and lenticular-form altocumulus.

Beatty and Caliente in spite of rather small isobaric slope in that region. North and south of there--at Fresno, Tonopah, and Ely, and Edwards and Las Vegas, respectively--the winds are all consistent.

Vertical cross sections. In Fig. 6.5 the potential temperature field in the Medford-Phoenix cross section at 1500 GCT is shown. The θ field is drawn at 5°K intervals from sounding data. In the horizontal scale, the distance from Medford to Phoenix is about 850 miles. The terrain profile is shown in the vertical scale which is exaggerated by about 50:1 over the horizontal scale. At the bottom are plotted the surface observations from stations along the section. The front, tropopause, temperature gradients, stability and barotropic and baroclinic regions can be easily discerned and need no further comment.

A contemporary D analysis of the same cross section is shown in Fig. 6.6. The values of $D = Z-Z_p$ were drawn at 100 ft intervals from sounding data and from intersection of the analyzed contours at all standard isobaric levels up to 100 mb. Since the winds were nearly perpendicular to this section, the spacing of the D lines can be considered to be inversely related to the strength of the total geostrophic wind. The strongest winds are evidently at 200 mb over Reno.

Similar analyses of the θ and D fields in the other, along-the-wind, cross section at 1500 GCT are shown in Figs. 6.7 and 6.8 respectively. The terrain profile is seen to be of high relief as the section crosses, besides the Sierra, several other high mountain ranges. In the surface observations along the section can be seen the observed wind, pressure, temperature, and clouds. East of the Sierra at Bishop are falling pressure and a few roll and wave clouds (Fig. 6.2a); the slight perturbation in the θ field over Owens Valley is drawn on this information. The tropopause, inversion, stable and less stable layers can be seen in the analysis.

The D field (Fig. 6.8) confirms the assertion that the section lay nearly along the upper contours at that time. All values were positive except at 100 mb over Hill Field (HIF) and Lander (LND); over Lander there was a cooler stratosphere and, consequently, a component of the geostrophic wind out from the section there. All of the soundings appear to cross the Standard Atmosphere between 300 and 350 mb from warmer below to cooler above.

Note: Since radiosonde data were available from the A.E.C. stations and most of the Weather Bureau and military stations surrounding the Sierra at 2100 GCT, the isobaric charts and cross sections for that time were also analyzed and used in the study. However, they are not essential to the discussion and so have been deleted.

Flight observations. By 1400 PST (2200 GCT) the skyscape from Bishop appeared as in Figs. 6.9a and b. Roll clouds and high wave clouds were well developed north of the station and were beginning to develop rapidly to the south. By that time the B-29 had been flying across the Sierra for 4 hours and the B-47 was gaining altitude above Fresno. The horizontal paths of the two aircraft crossed the Sierra near Big Pine. The B-29 flew at 30, 25, and 20,000 ft and the B-47 at 30, 35, and 40,000 ft. A mile north of these paths the sailplane made its flight in the period 1420 to 1700 PST.

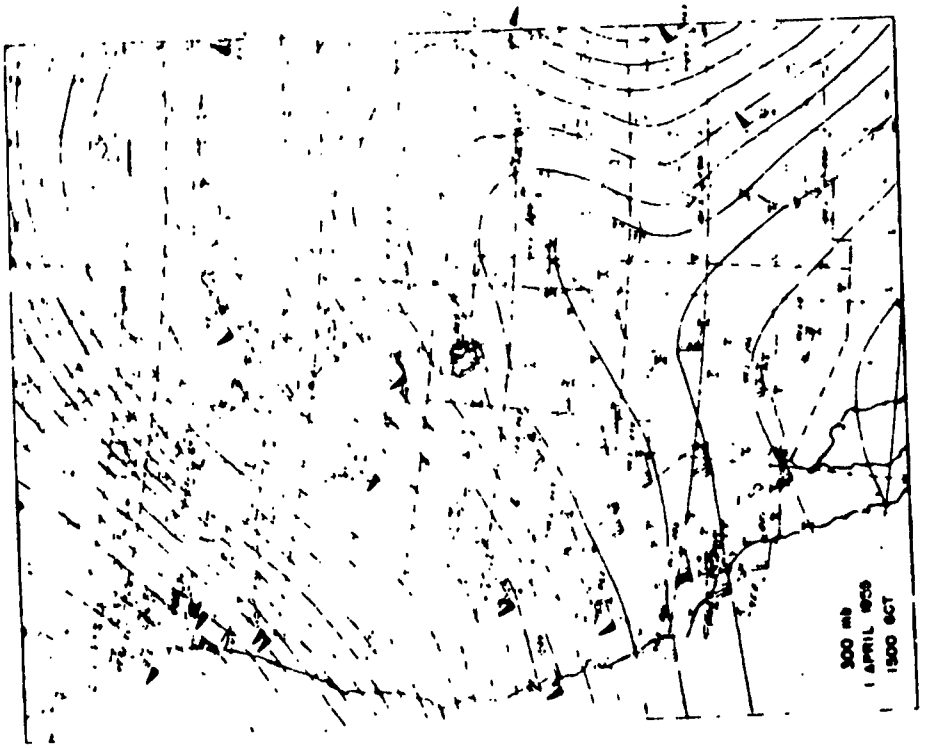

Fig. 6.4

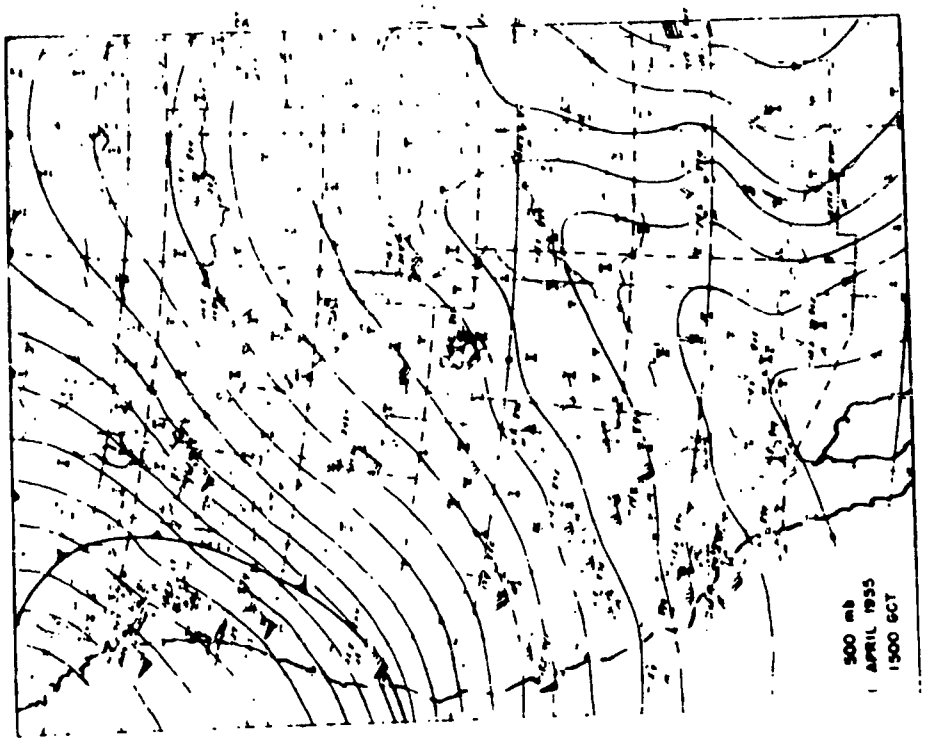

Fig. 6.3

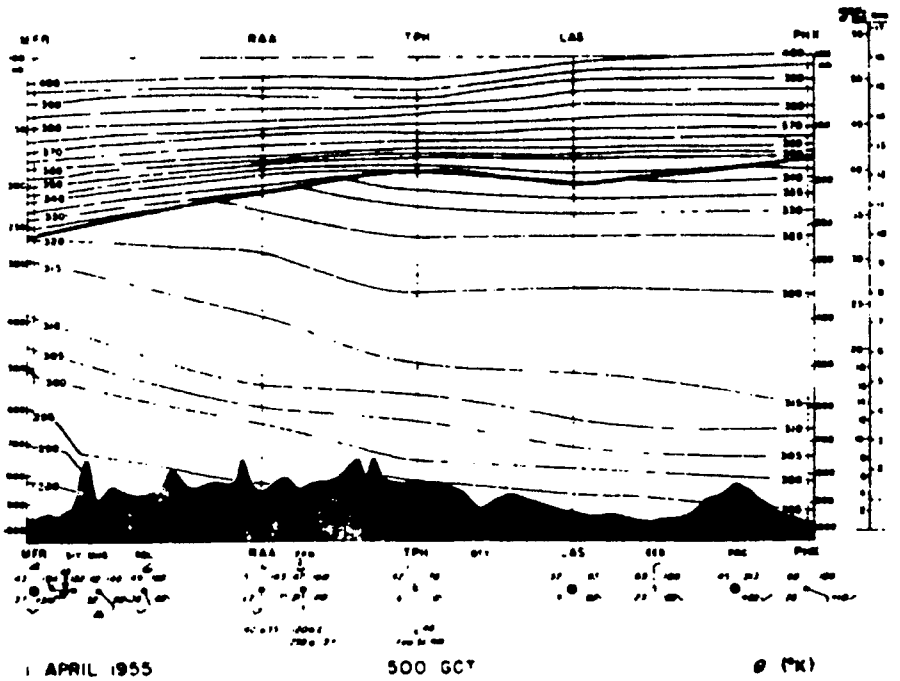
1 APRIL 1955
500 GCT
θ (°K)

Fig. 6.5

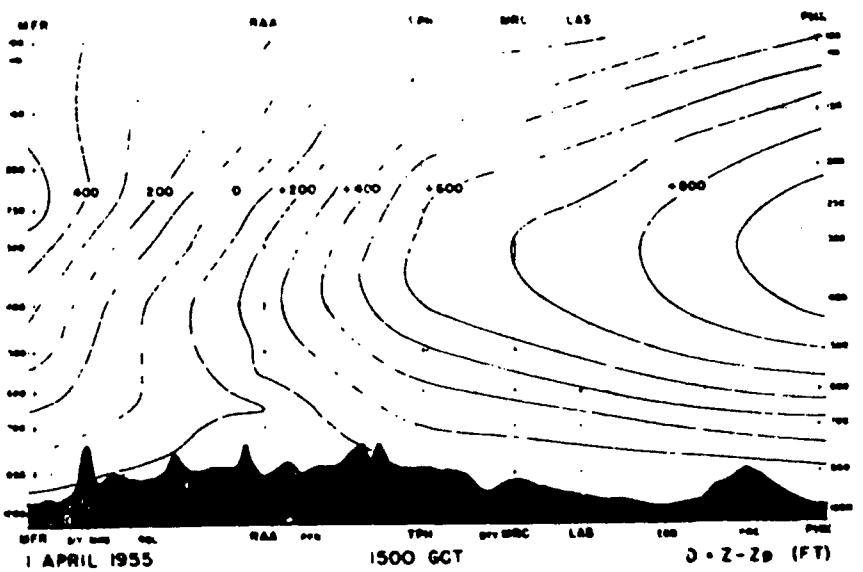
-600
-200
0
+200
+400
+600
+800
1 APRIL 1955
1500 GCT
D - Z - Zp (FT)

Fig. 6.6

From the sailplane in flight the clouds appeared as in Fig. 6.10. Toward NNW from 30,500 ft (Figs. 6.10a and b) wave clouds in at least three levels and at least two bands could be seen. The fohnwall appeared over the Sierra to the west, a cirrus band in the north. In a panorama from west to south at 38,000 ft, one could see the altocumulus deck over the San Joaquin Valley becoming the cumulus fohnwall over the Sierra; the break in the cumulus over the Kings River Canyon, and the incipient development of the fohnwall over the Sierra crest to the south. Noting that the sailplane is apparently over the crest of the Sierra at that altitude while still ascending, evidence is had of the upwind tilt of the lee wave updraft zone with altitude. Finally, the view south over the Owens Valley as seen from 30,000 ft is shown in Fig. 6.11. The path of the sailplane with respect to the wave clouds was a rise to 40,000 ft just upwind of them, a downwind run over and through the highest lenticular, a descent in the ensuing downdraft, and a return flight upwind over the White Mountains (Fig. 6.12a) and through the second-wave roll cloud zone to Bishop (Fig. 6.12b). A gentle rocking motion fore and aft was experienced by the sailplane at 40,000 ft while headed into the wind, and rather severe turbulence was encountered in the second roll cloud zone at 16,000 ft.

The roll cloud zone. Data from the B-29 upwind run at 20,000 ft are presented in Figs. 6.13, 6.14, and 6.15. It was attempted to maintain constant pressure altitude by altitude-controlled auto-pilot and constant power setting. The indicated air speed in the "undisturbed" air at the beginning of the run was 195 mph. As seen in Fig. 6.13 the indicated air speed varied by a total of approximately 90 mph; the lowest value of 145 mph was very close to the stalling speed of the aircraft and occurred in the downdraft area behind the roll clouds.

In Fig. 6.14 are shown the actual wind velocities measured* by the B-29. It can be seen that the wind velocity at the level of the top of the roll cloud varied by 50 knots and by 45 degrees. The wind was cyclonic and at minimum speed in the troughs of the vertical flow pattern, and anticyclonic and at maximum speed in the crests--immediately above the roll clouds-- of the vertical perturbation. The approximate vertical displacement of a streamline (Fig. 6.15) at this level was derived from measured temperatures, upwind soundings (Fig. 6.16), and the assumption of adiabatic flow. It is noteworthy that the first wave, with a maximum total displacement of about 7,000 ft, is predominant.

These data show quite clearly that the principal hazards of mountain waves to aircraft are the strong downdraft immediately in the lee coupled with the dangers of turbulence, of reaching stalling speed, and of icing in the roll cloud or cap cloud.

The stratospheric mountain wave. In Fig. 6.16 are shown the 1500 and 2300 GCT soundings at Fresno and the temperatures measured by the B-47 in the upper levels over Fresno while the aircraft was ascending to and descending from 40,000 ft. Between 1648 and 1736 PST the B-47 made a downwind run and an upwind run at 40,000 ft. The temperatures encountered enroute and the

*The technique of measurement, which is considered to be quite accurate, is based upon a new application of the Doppler principle for radar.

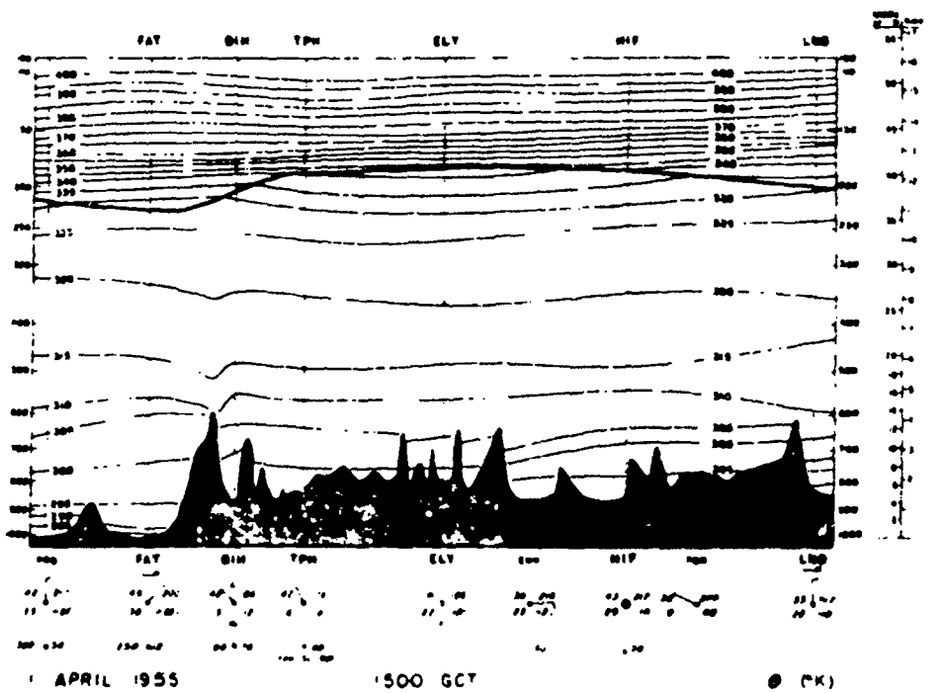
FAT
BIH
TPH
ELY
MIF
LND
1 APRIL 1955
1500 GCT
θ (°K)

Fig. 6.7

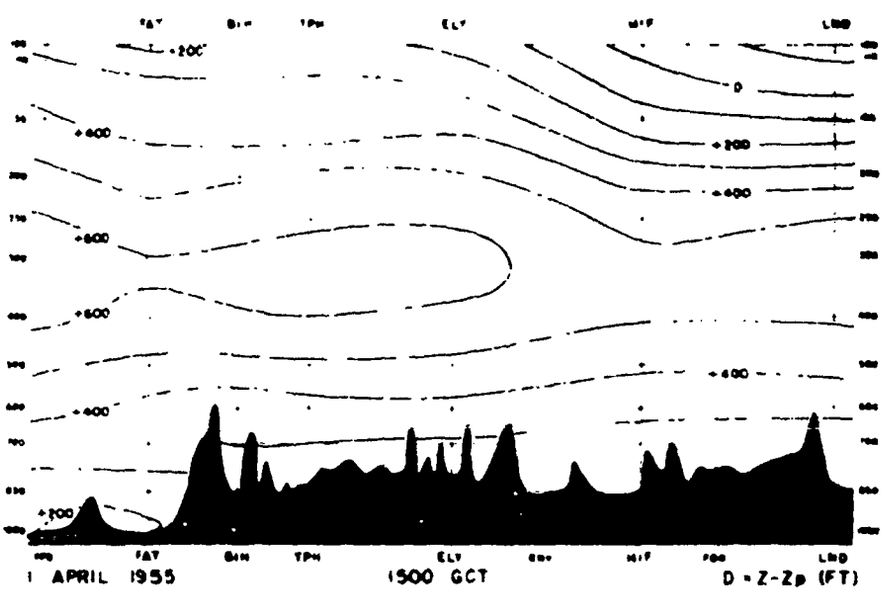
FAT
BIH
TPH
ELY
MIF
LND
+200'
0
+200
+400
+600
+800
+1000
1 APRIL 1955
1500 GCT
D = Z-Zp (FT)

Fig. 6.8

Fig. 6.9a - 1350 PST, 1 April 1955. Northwest from Bishop Airport. Roll clouds and lenticular wave clouds. P-8 sailplane ready for flight.

Fig. 6.9b - 1350 PST, 1 April 1955. South from Bishop Airport. Developing roll clouds.

Fig. 6.10a - 1515 PST, 1 April 1955. North from 32,000 ft. Lenticular cloud forms of the first wave crest (left) and the second wave crest (center), the latter upwind of the White Mountains.

Fig. 6.10b - 1550 PST, 1 April 1955. WNW from 38,000 ft. The fohnwall with altocumulus becoming cumulus near the Sierra crest. East slope of Sierra appears at lower right.

Fig. 6.10c - 1552 PST, 1 April 1955. SW from 38,000 ft. Developing föhnwall with break in cumulus clouds over the Kings River Canyon. Altocumulus (right) and haze over the San Joaquin Valley.

Fig. 6.10d - 1552 PST, 1 April 1955. South from 38,000 ft. Developing cumulus föhnwall over the southern High Sierra.

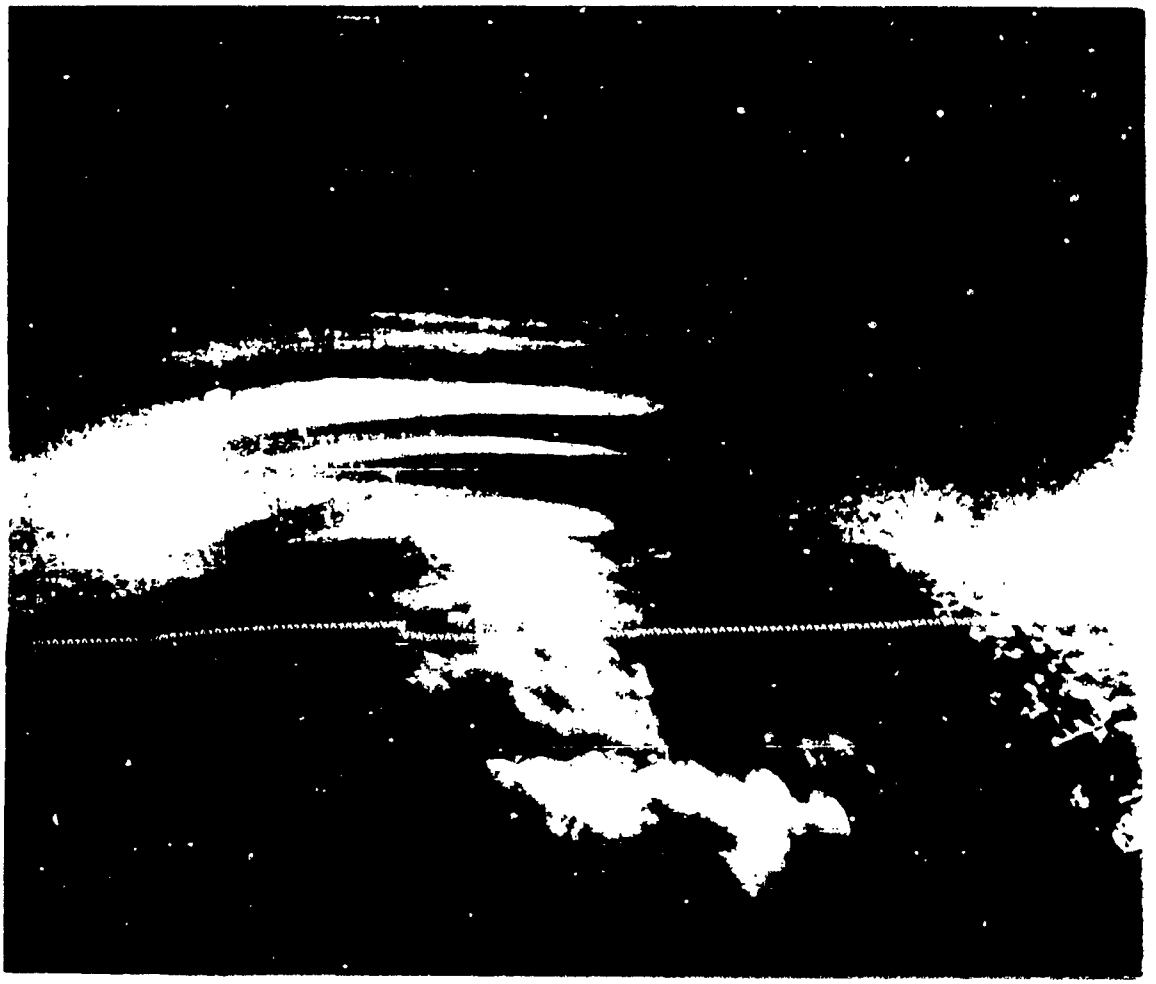

Fig. 6-11. View southward over Owens Valley from 30,000 ft on 1 April 1955. Cloud decks at 5 different levels are shown. The roll clouds are at about 15,000 ft while the highest wave cloud is near 39,000 ft. On the right the föhnwall is developing over the Sierra. This photograph, taken by Hydrographer Tom Henderson, is printed by courtesy of the California Electric Power Company.

Fig. 6.12a - 1037 PST, 1 April 1955. North from 21,000 ft. Cloud decks of the second wave crest over the White Mountains.

Fig. 6.12b - 1715 PST, 1 April 1955. SSE from Bishop Airport High lenticular deck and roll clouds of the first wave crest.

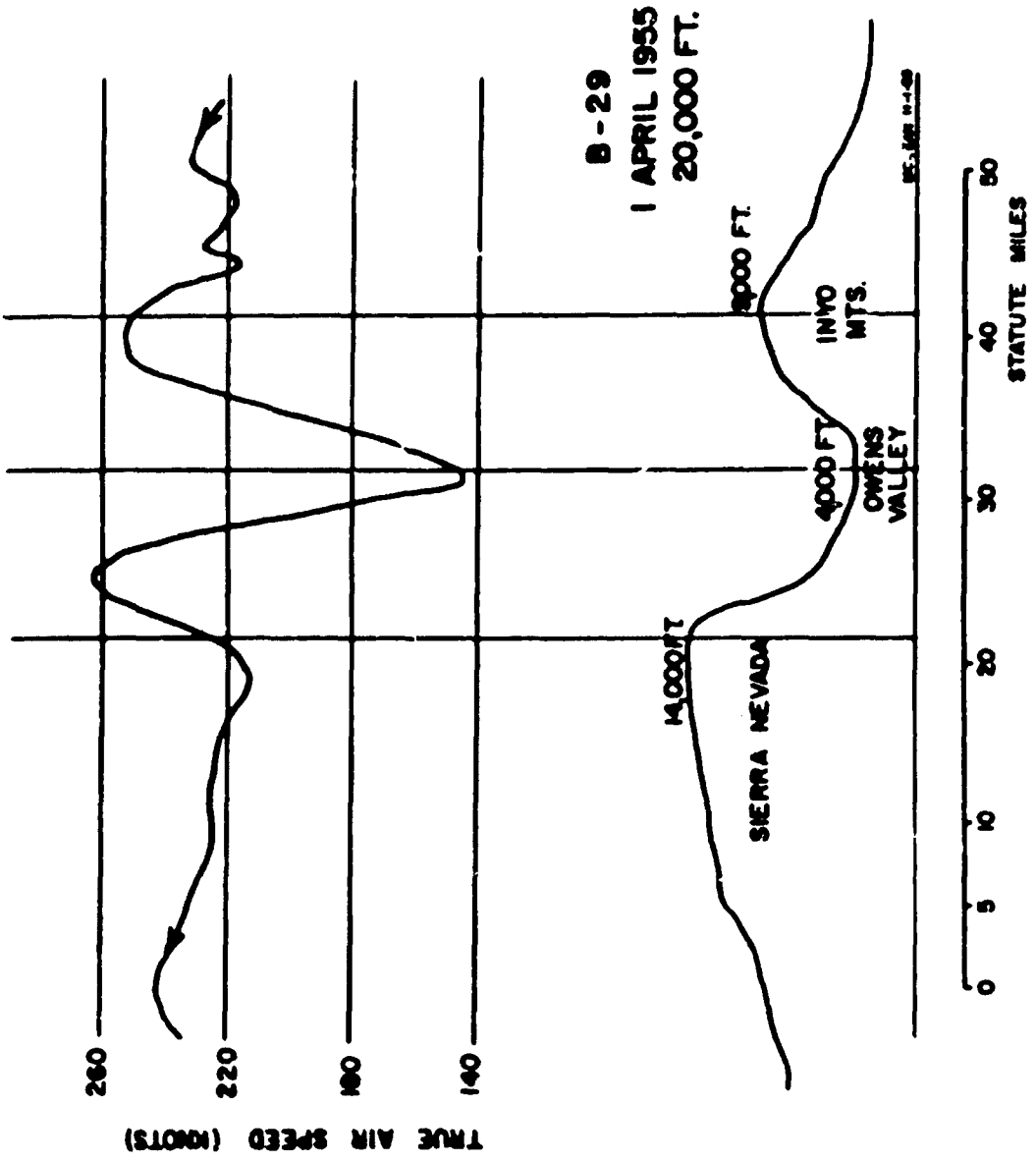

Fig. 6.13 - (Prepared by the Air Force Cambridge Research Center)

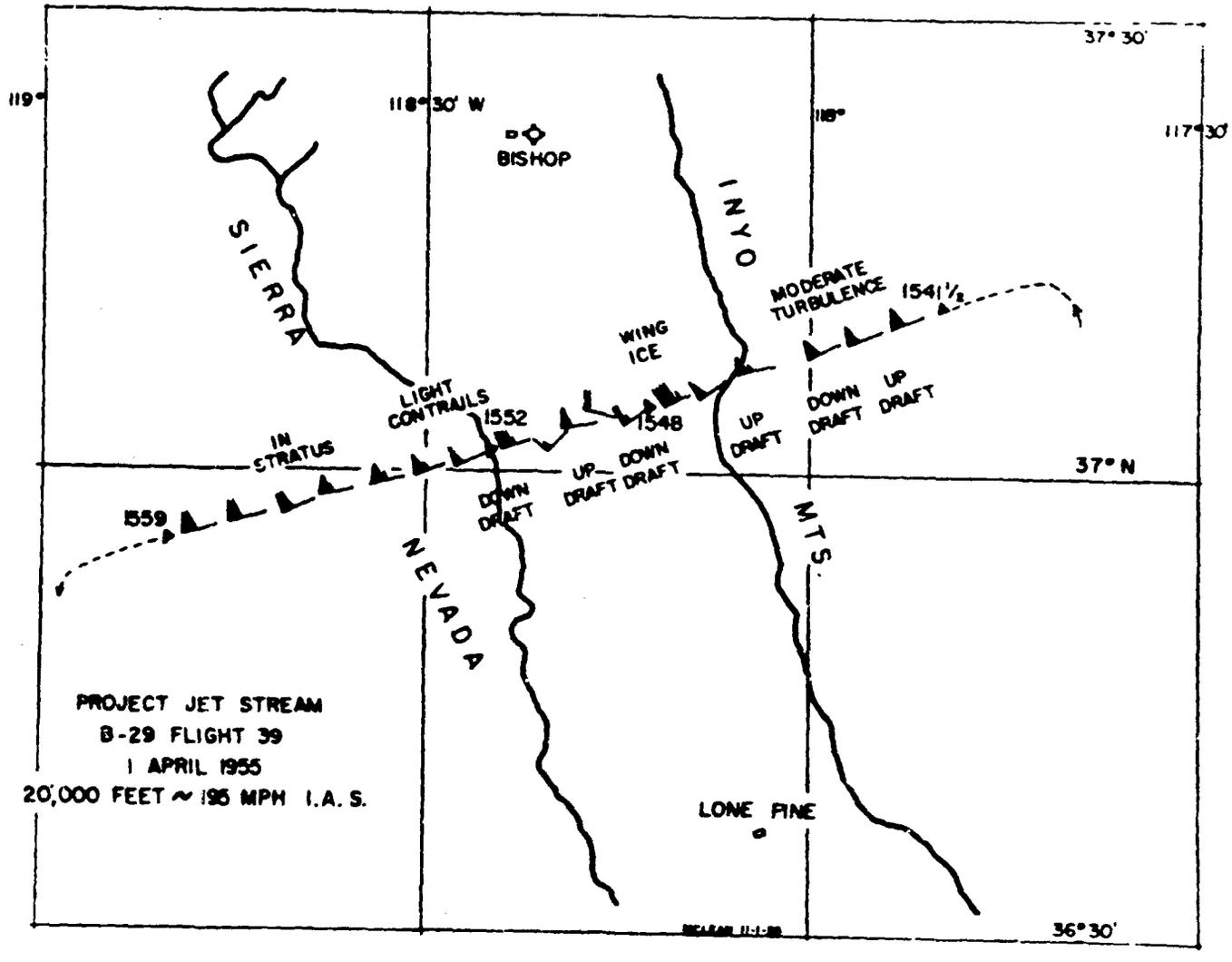

Fig. 6.14 - (Prepared by the Air Force Cambridge Research Center)

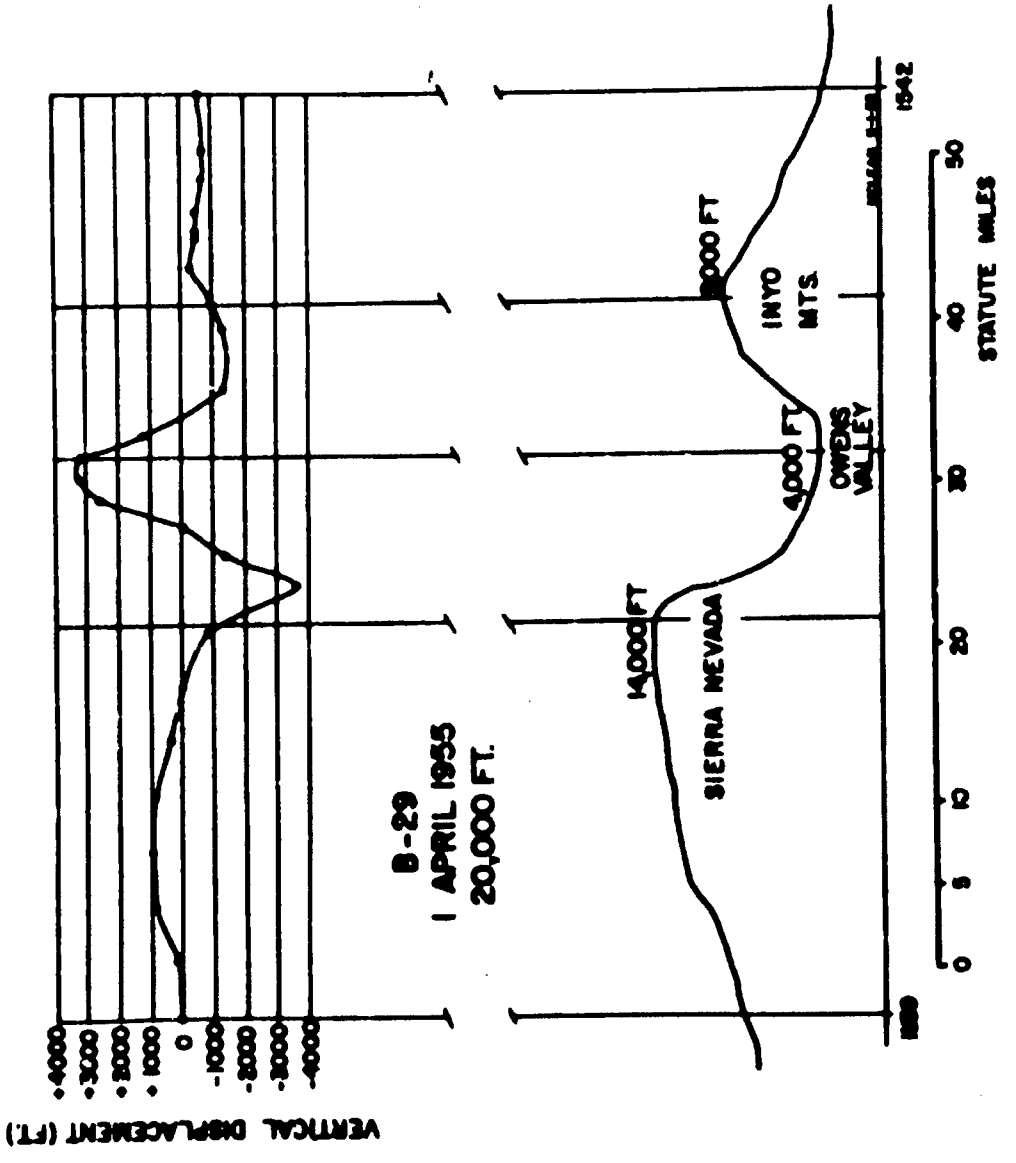

Fig. 6.15 - (Prepared by the Air Force Cambridge Research Center)

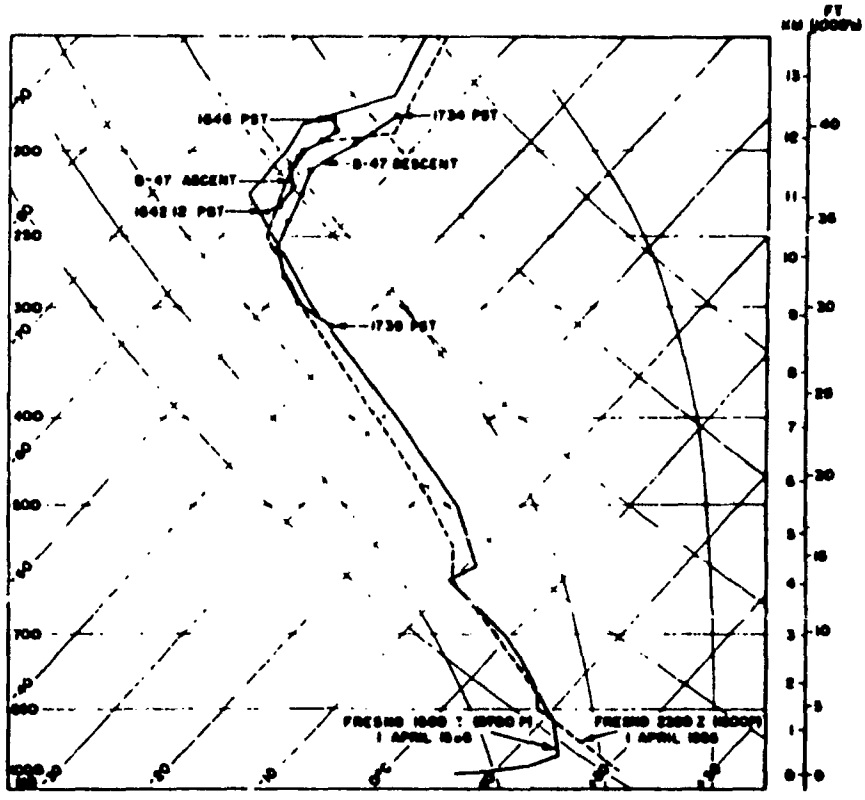

Fig. 6.16 - (Prepared by the Air Force Cambridge Research Center)

resulting computed displacement of a streamline are shown in Fig. 6.17. As startling as the measurements of the B-29 at 20,000 ft is the 15°C temperature difference measured by the B-47 within the distance of 12 miles at 40,000 ft. The close agreement of the results from the two runs suggests that this perturbation is a stationary phenomenon rather than a traveling one. Contrails observed in the area of the wave crest are absent in the trough. Noteworthy are the striking "mirror image" of the flow pattern in the stratosphere to that of the underlying terrain profile, and the fact that only one great descent and rise of the air is indicated, all other lee waves apperently damped out at that level. If this be a lee wave at 40,000 ft, the wave length is many times that of the flow pattern at 20,000 ft.

Other charts--from the 25,000, 30,000, and 35,000 ft runs--not shown here, gave results which were transitional between the pattern of flow at 20,000 ft and 40,000 ft. That at 25,000 ft was similar to the roll cloud region with the lee wave pattern of crests and troughs evident but with less amplitude and less change of horizontal wind velocity (40 knots, 30 deg.) at that level. At 35,000 ft the pattern was that of lee waves, but since the two pairs of runs of the B-47 were more than 2 hours apart, the discrepancies between the two sets of data--first a cooling in time followed by a warming in time at the same level-- and the apparently chaotic temperature pattern of the second run, at first unsolvable, were at last resolved into a satisfactory explanation: During the course of the flights the tropopause "descended" through the 35,000 ft level. Data on successive runs at the other levels and the soundings (Fig. 6.16) verified this development; the stratosphere was warming, the troposphere cooling. Temperature and height changes over the region were indeed big during the course of the flights, especially in the period 2100-0300 GCT. It was impossible to integrate all of these airborne observations into a synoptic picture using the absolute values of these data. However, what could be derived was the pattern and amplitude of the isotherms and isentropes at each level and these were amenable to integration as guides in the construction of the trans-Sierra cross section at 02 0300 GCT (01 1900 PST).

In Fig. 6.18 a composite picture of the air flow over the Sierra is shown by the temperature pattern determined from the B-47 runs at 40,000 ft, two of the B-47 runs at 35,000 ft, and the B-29 run at 20,000 ft. It appears that there is a pronounced upwind tilt with height of the lee waves as the indicated position of troughs and crests at 20,000 ft are reversed at 35,000 ft.

The synoptic situation at 0300 GCT, 2 April 1955.

A series of 4 isobaric charts, the 700, 500, 300, and 200 mb surfaces (Figs. 6.19 to 6.22) represent the upper air flow pattern at different levels at 1900 PST on 1 April near the time of maximum lee wave development. At 700 mb (Fig. 6.19) the front is well-marked in the temperature, wind, and pressure fields. The low pressure center is over Burns, Oregon. Lee troughs of the Sierra and the Rockies are pronounced. Contour heights not drawn for on this chart are Mercury (observations at 0200 GCT), Rapid City, and Long Beach (both improbable).

On the 500 mb chart (Fig. 6.20) the coldest air and lowest pressure

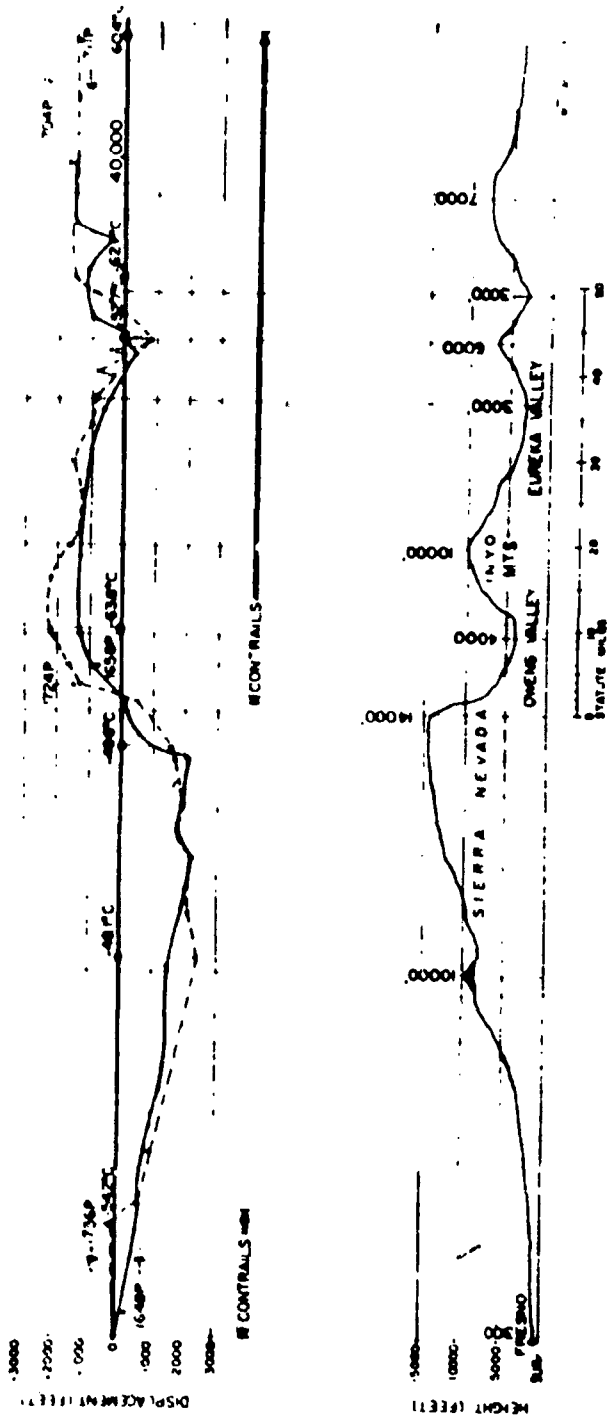

Fig. 6 17 - (Prepared by the Air Force Cambridge Research Center)

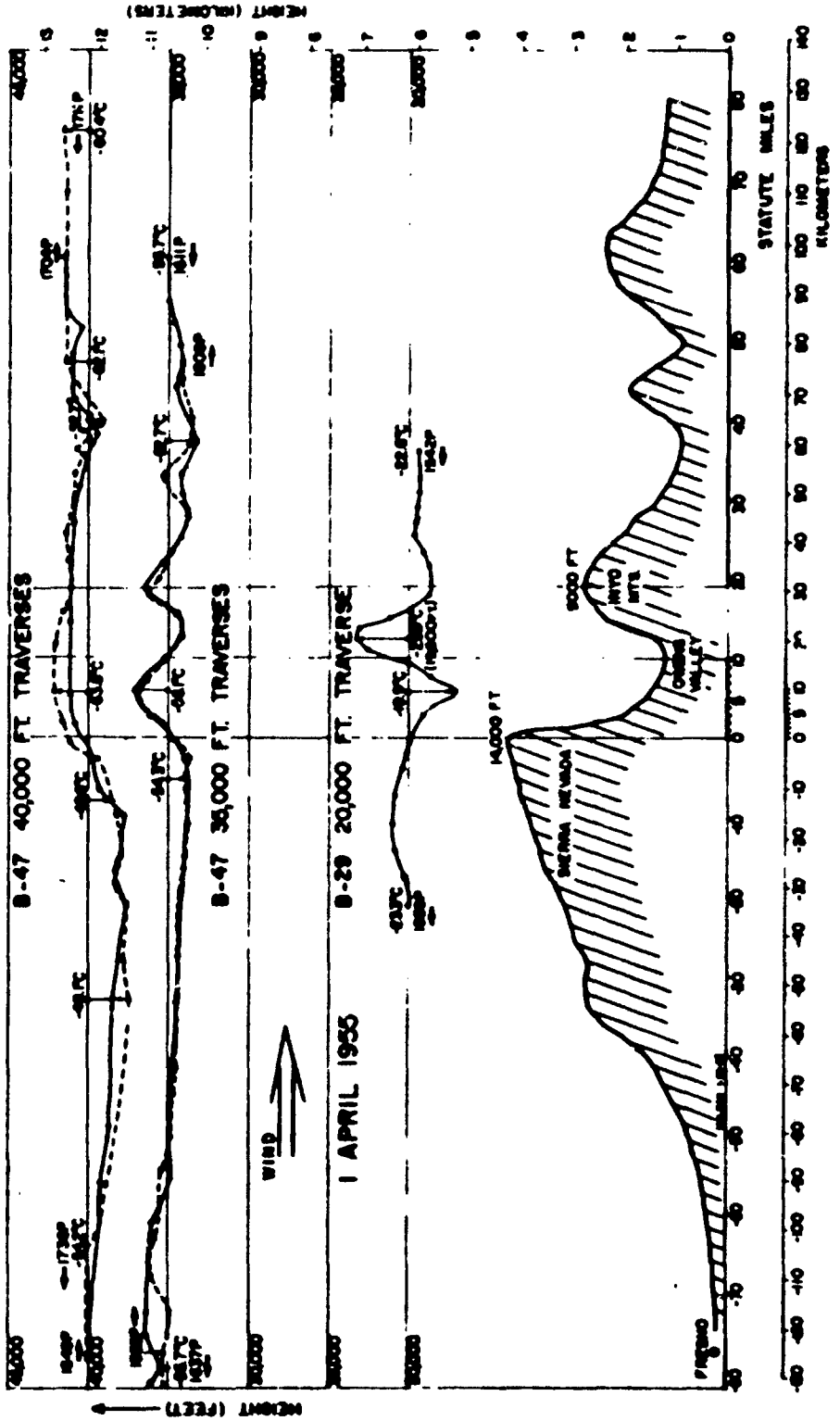

Fig. 4.10 - (Prepared by the Air Force Cambridge Research Center)

are over Medford, the warmest air and highest pressure over Tucson. In comparison with the previous 12 hourly chart the Reno-Phoenix temperature difference is now quite large. Also, a reversal from the previous time are the wind speed and temperature increase from Fresno to Lander. A 5°C cooling in 12 hours occurred over Fresno while the air over Lander warmed 0.3°C; this relative cooling and warming along that section is reflected in the contours and consequently in the wind flow which has become more southwesterly. Note the relatively light wind at Fresno and the secondary, nonfrontal, band of wind speeds over 50 knots. Data not drawn for are the heights at Long Beach, San Diego, Rapid City, Tucson, and Mercury (the last obtained at 0200 GCT).

At 300 mb (Fig. 6.21) the weak wind at Fresno in contrast to the much stronger winds to the north and south is striking. The polar front jet stream had moved in 12 hours from over Portland to over Reno. The strongest observed wind speed, 80 knots at Beatty, is apparently super-geostrophic.

A double jet stream is most clearly evident at the 200 mb level (Fig. 6.22). Contour heights on either side of the mountains are consistent, but again the Beatty wind of 90 knots is super-geostrophic. Of equal interest on this chart is the verification of the stratospheric temperature pattern measured by the B-47; the 200 mb temperature at Fresno is -48°C while that at Tonopah is -60°C. It is quite possible that the maximum difference was even greater along some distance between the two stations where the trough and crest of the tropopause probably lay.

Cross sections of θ and D between Medford (MFR) and Phoenix (PHX) for this time are shown in Figs. 6.23 and 6.24. Locations of the front and the tropopause on these sections were derived from carefully constructed frontal and tropopause contour charts. The front and associated inversions and baroclinic zones are well defined in the vertical. Surface observations also demonstrate the contrasting post- and pre-frontal phenomena, at Reno (RAA), near 4,000 ft, the temperature is 38°F while at Tonopah (TPH), near 6,000 ft, the temperature is 54°F.

In the D field (Fig. 6.24) the cooling in time is reflected in the southward movement of the D = 0 line. The height difference between Medford and Phoenix has increased by 400 ft in 12 hours as a result of greater cooling in the north than in the south. The greatest $\partial D/\partial t$ was at 300 mb over Reno (-740 ft per 12 hours). The maximum gradient along the section ($\partial D/\partial y'$) was then between Reno and Tonopah. From the 2100 GCT data referred to earlier but not shown, it was found that $(\partial D/\partial t)_p$ was not linear for the 12 hour period between 1500 and 0300 GCT. For the first 6-hour period the maximum rate in the cross section was -50 ft per hr over Medford at 300 mb while in the second 6-hour period the maximum rate was over -100 ft per hr at 300 mb over Reno.

For the analysis of the θ field in the trans Sierra cross section (Fig. 6.25), the airborne data were used as guides in the section between Fresno (FAT) and Tonopah (TPH). As a first approximation, the isentropes can be considered as representative of the actual streamlines of the flow in this plane. Note the front, the displacement of the tropopause, surface observations, and the locations of inversions and near-adiabatic layers. The predominance of a single updraft in the upper levels suggests, along with the physics of ice crystal formation, the explanation for the high cirrus bands

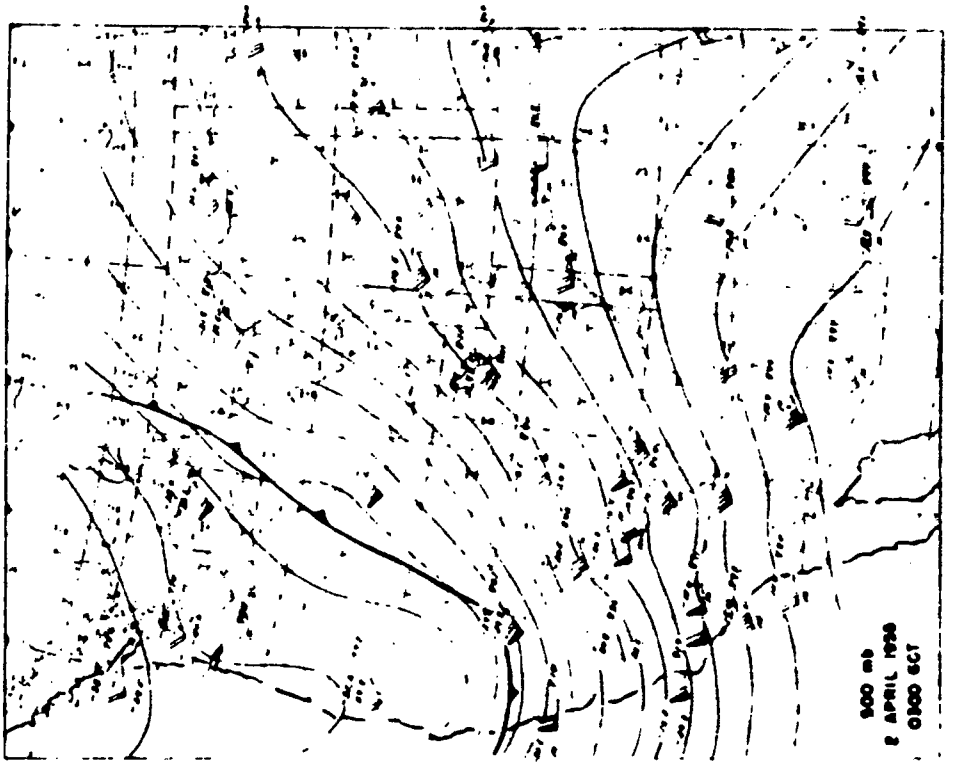

Fig. 4.20

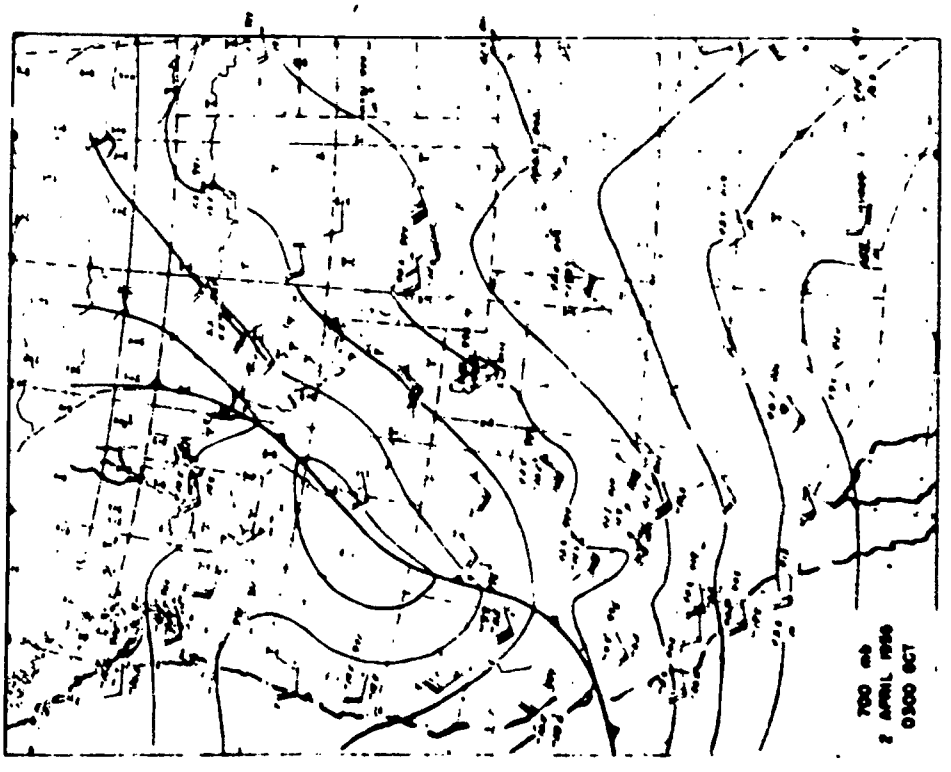

Fig. 4.19

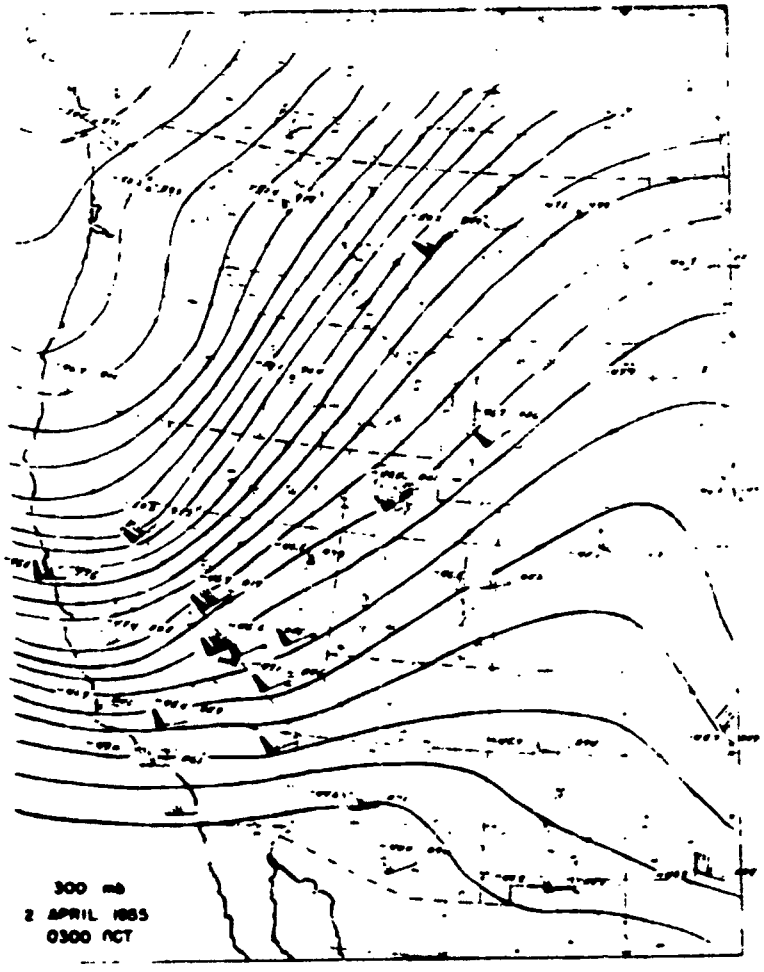

Fig. 6.21

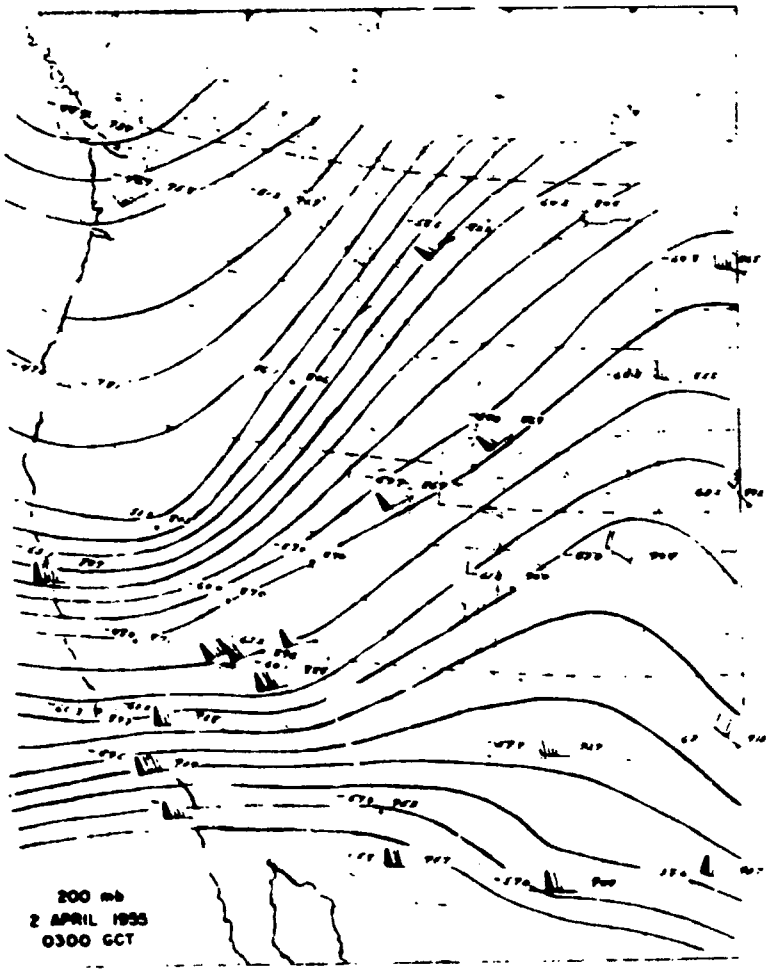

Fig. 6.22

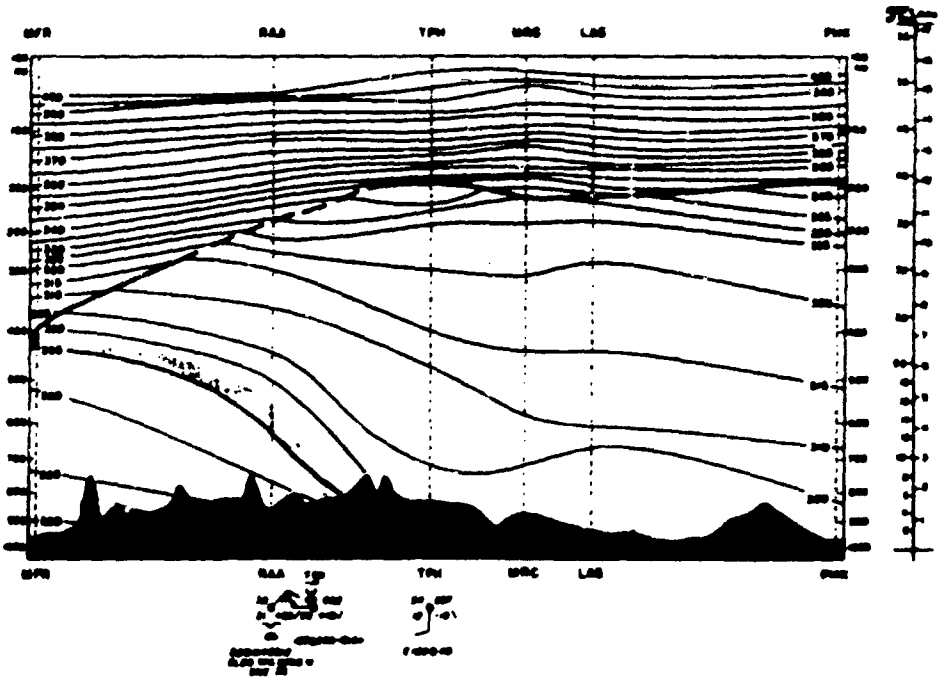

2 APRIL 1955 0300 GCT θ (°K)

Fig 6.23

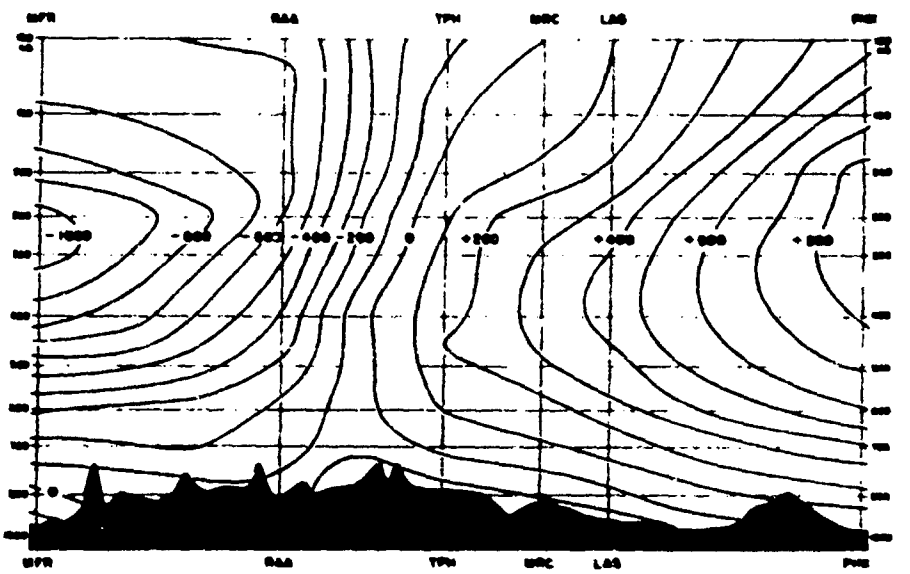

2 APRIL 1955 0300 GCT D = Z − Zp (FT)

Fig. 6.24

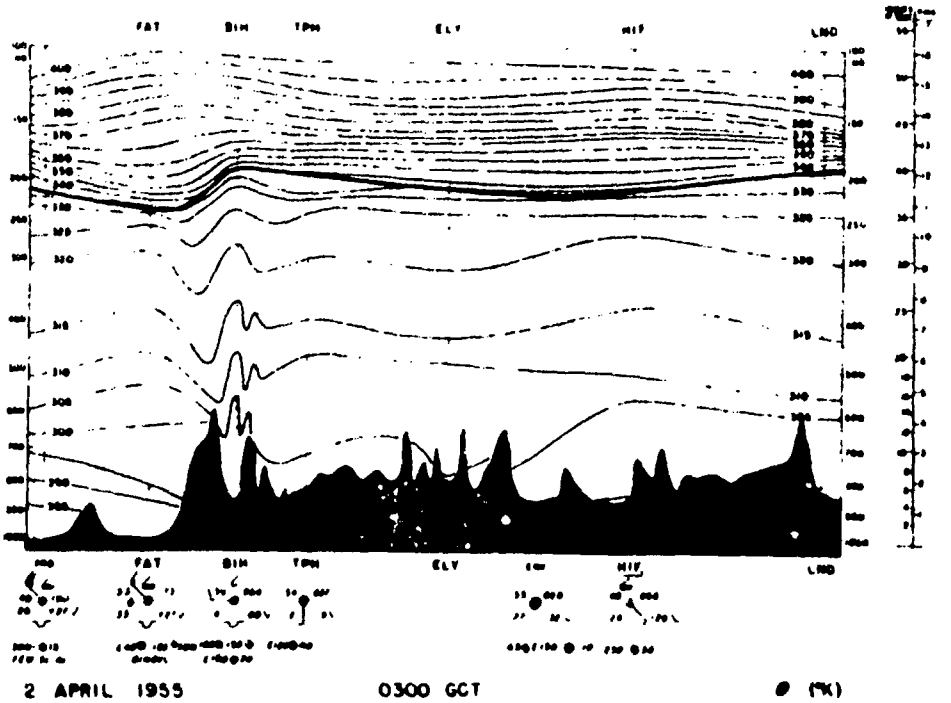

Fig. 6.25

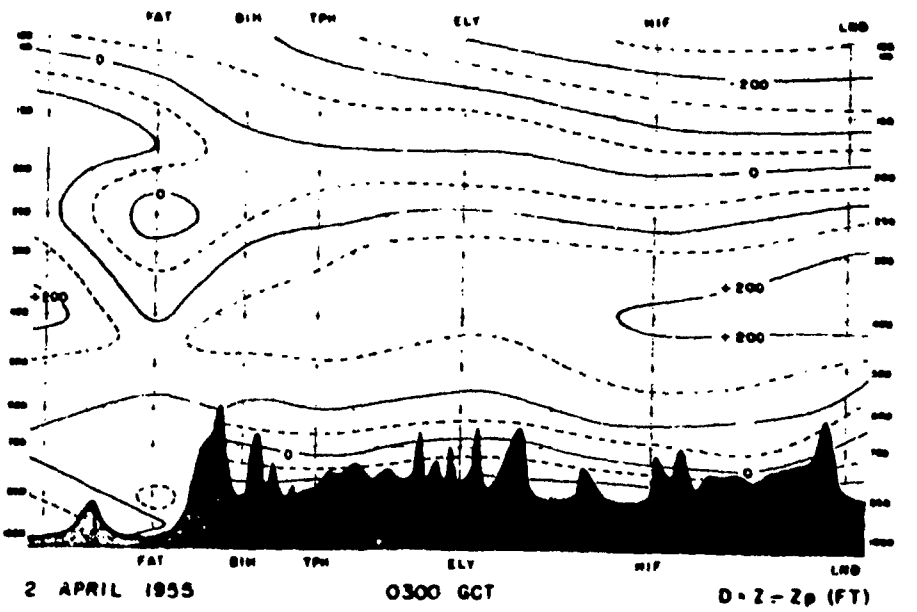

Fig. 6.26

(Fig. 6.2a) often observed to form in the lee of the Sierra and to trail, sometimes for hundreds of miles, downwind. Forming in the initial updraft at temperatures near -50°C, they suffer no attrition from slight adiabatic warming and continue to grow slowly while moving downstream. Because of their relatively slow growth and subsequent slow evaporation or fall-out, and the high speed of the current necessary for the formation of a high lee wave, they can extend for many miles downstream while their leading edges remain, like lower lenticular forms, stationary for many hours in the lee of the Sierra. The lateral separation of these bands is still unexplained.

The contemporary D analysis (Fig. 6.26) shows a belt of maximum values between 400 and 300 mb with lowest values over Fresno at each level from 700 to 250 mb. The minimum is located at 250 mb above which the sounding becomes warmer than Standard Atmosphere in the great downdraft upwind of the Sierra. The lee trough in the lower levels is shown by discontinuities of the D lines at the mountains. Intermediate 50-ft intervals are indicated by dashed lines. The warm stratosphere over the Great Valley makes the flow there more nearly westerly and, consequently, with a component out from the plane of the cross section. The maximum $(\partial D/\partial t)_p$ for the preceding 12 hour period was -500 ft per 12 hrs at 250 mb over Fresno, but again the rate was not linear. From 1500 to 2100 GCT the maximum $(\partial D/\partial t)_p$ was at 300 mb over Tonopah, while from 2100 to 0300 GCT the maximum change was -490 ft at 300 mb over Fresno.

Post-wave. The synoptic situation at 0730 PST (1530 GCT) on the morning of 2 April is shown in Fig. 6.27. The front lay through low centers in northern Utah and northern Arizona. Warm, cold, and modified maritime polar air masses lay adjacent to each other at various portions of the frontal boundary. Surface winds were strongest about the front. Precipitation in the form of snow fell about the northern sector of the front while blowing sand was experienced along its southern extension. Stratus clouds were observed at many stations behind the front while altocumulus forms were reported at several stations ahead of it. Wave clouds were observed at Prescott, Roswell, and Alamosa and cirrus bands at Grant Junction and Casper. Pressure rises were general behind the front and rises ahead. The Catalina eddy persisted due to the strong northwest flow aloft over the west-east oriented southern California mountains. On the previous evening destructive winds of over 50 knots, with gusts to 80 knots, had swept across the San Joaquin Valley and caused a severe dust storm at Bakersfield between 1830 and 2000 PST. Gale winds hit the San Fernando Valley and 55 knot winds with blowing sand closed roads over the desert.

Upper air observations for this period are shown in the 850, 700, 400, and 200 mb charts in Figs. 6.27 to 6.31. At 850 mb there is a double cold front structure over southern California, the polar air from the Pacific being warmer and moister than that from due north. In both the cold and warm air masses the temperature field is nearly uniform. A lee-low near Sheridan influences the Lander wind. The shallowness of the Catalina eddy is evident from its apparent non-existence at this level.

At 700 mb (Fig. 6.29) the front is well marked in temperature, contours, and wind velocities. There is some evidence of a second transition zone--perhaps the top of the shallow secondary front--and this has been shown by a dashed line. The strongest winds at this level were those ahead of the front. A trough in the lee of the Rockies was well formed.

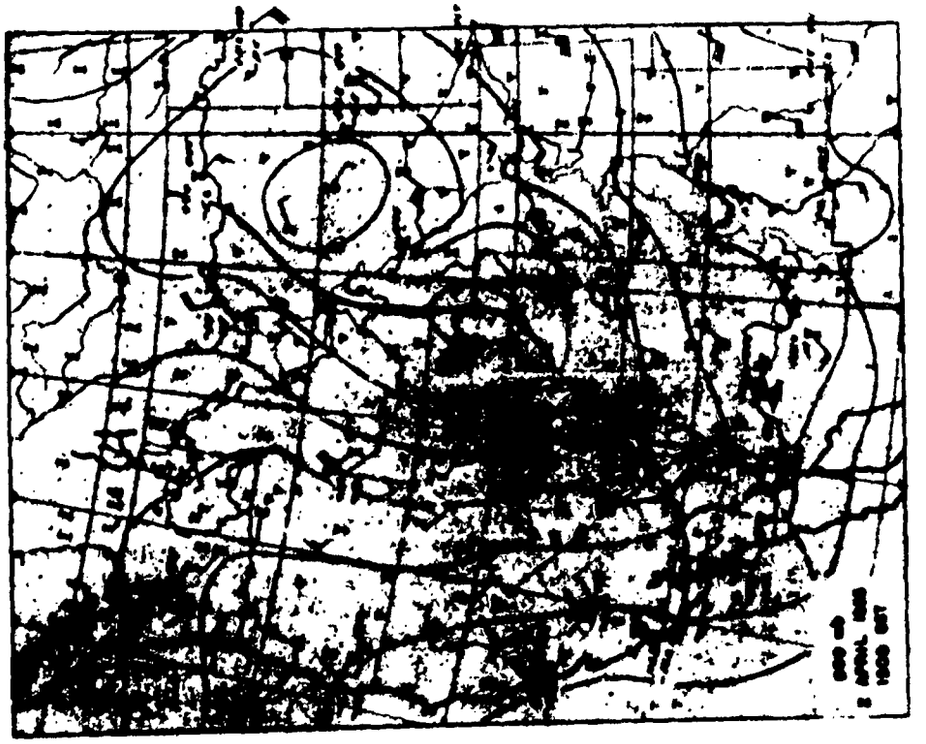

Fig. 6.26

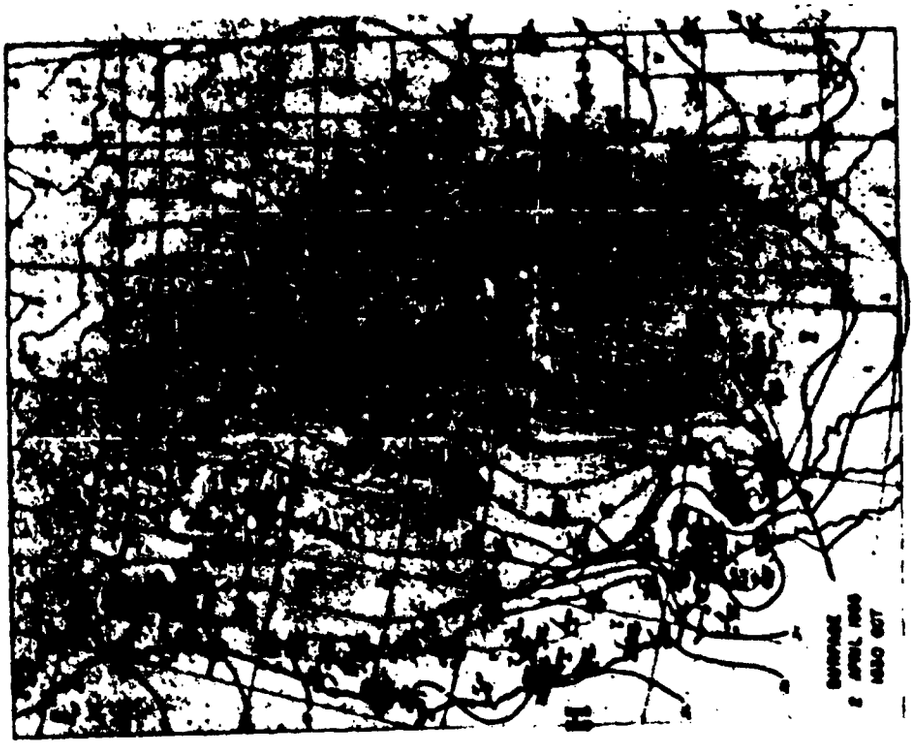

Fig. 6.27

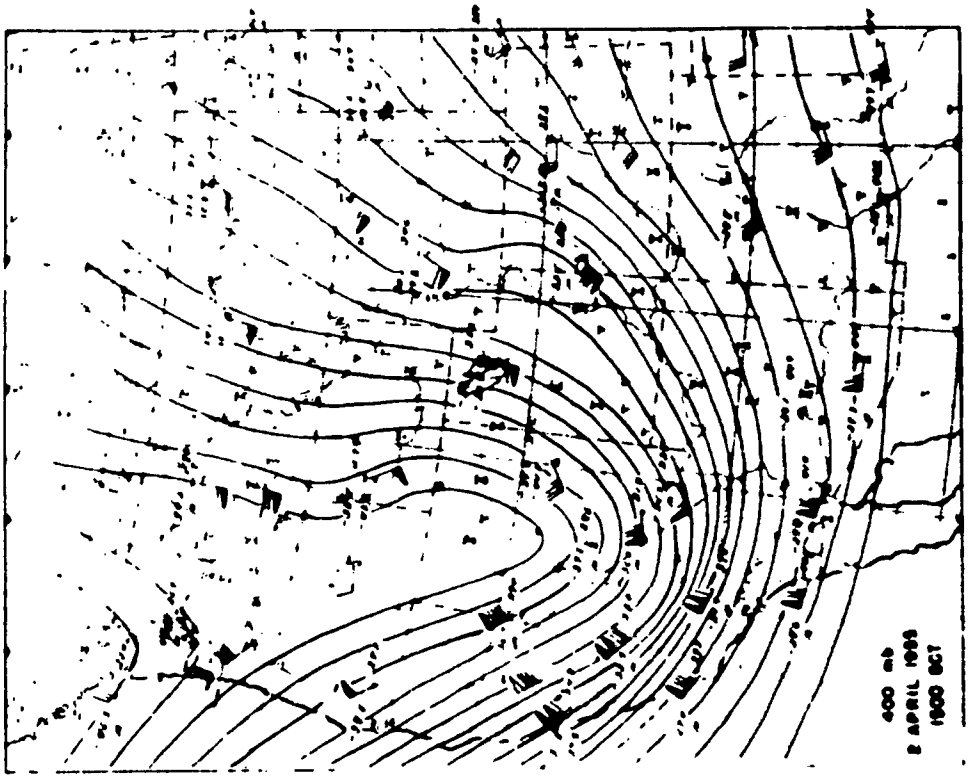

Fig. 6.30

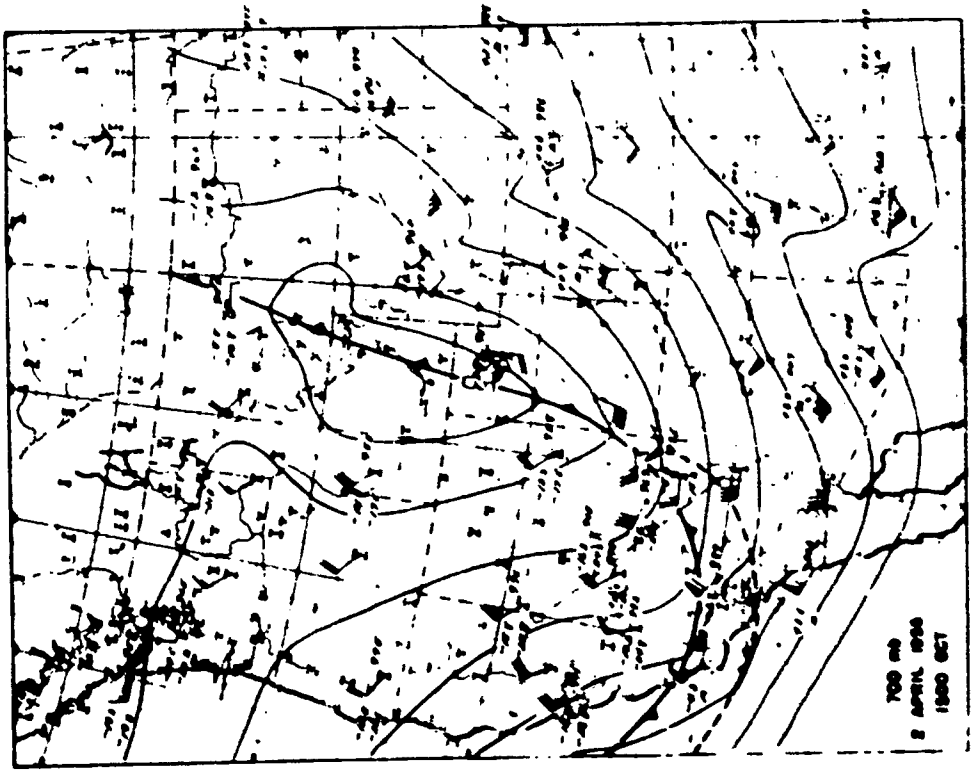

Fig. 6.29

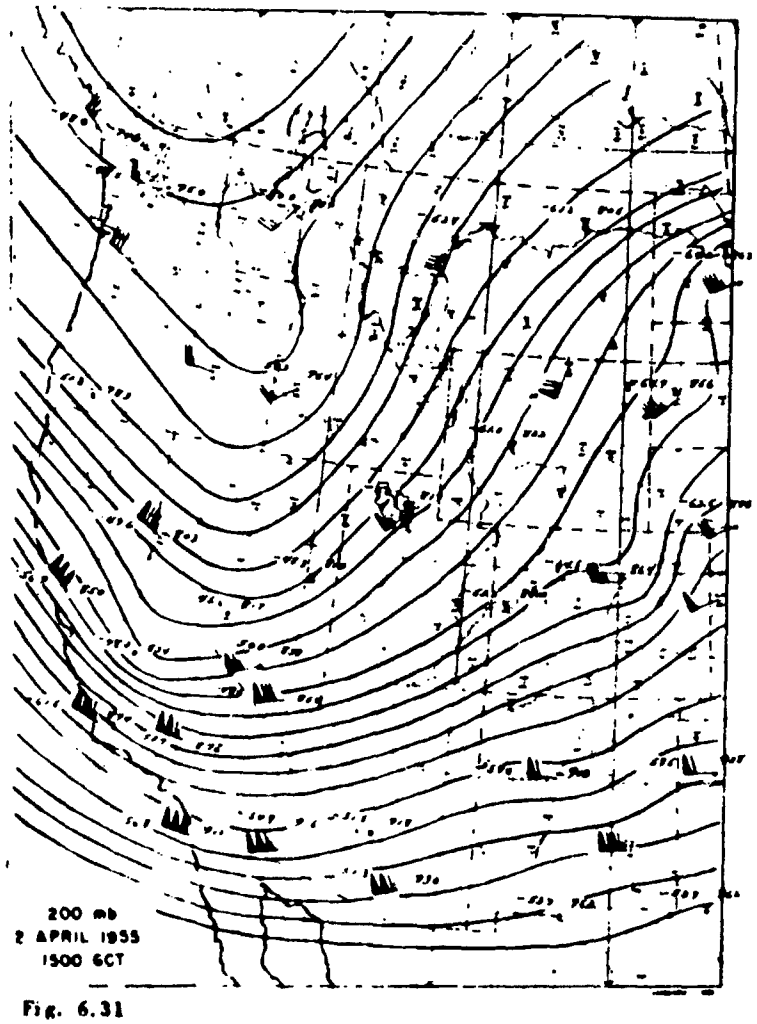

Fig. 6.31

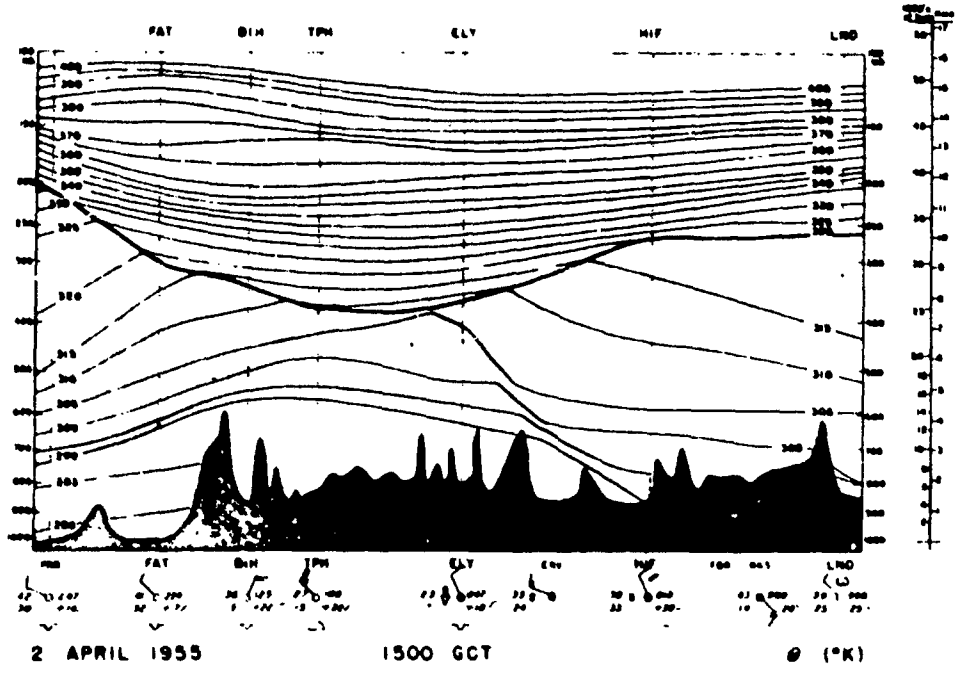

Fig. 6.32

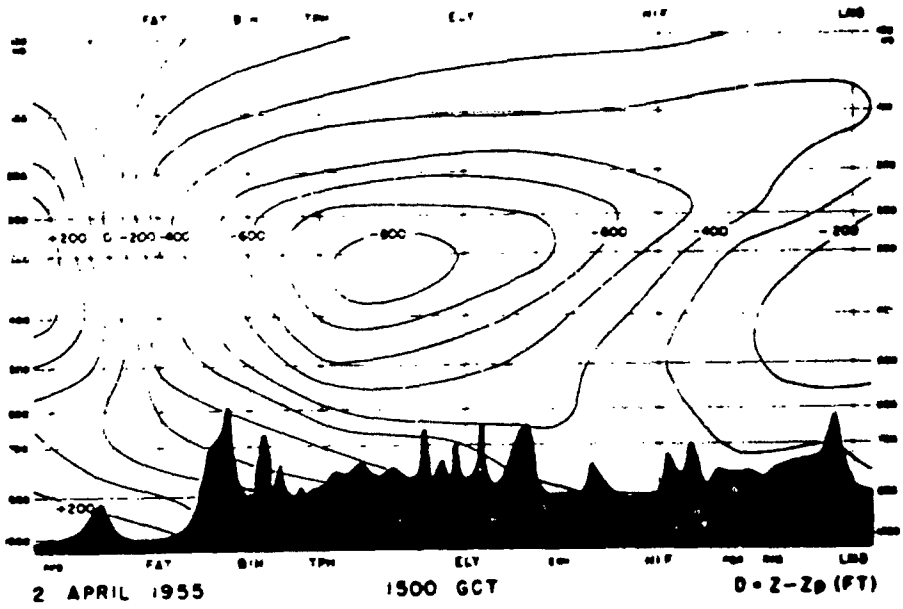

Fig. 6.33

Fig. 6.34 - 1200 PST, 2 April 1955. Northwest from Bishop Airport. Stationary wave cloud in northwest wind.

Noteworthy is the usefulness of interpolated data from the White Mountain stations near Bishop.

Winds in excess of 100 knots were measured at Oakland, Fresno, and Edwards Air Force Base in northwesterly flow at the 400 mb level (Fig. 6.30). The diffluent nature of the trough is best seen at this level. Ultimately, this is a result of the asymmetry of the cold dome; the warm front at its western boundary has a greater temperature gradient than that of the cold front at its eastern boundary. The low center tilts westward with height.

Strong winds occurred also at the 200 mb level (Fig. 6.31) where 150 knot speeds were reported over Oakland and San Diego. The warmest temperature at this level (-45.6°C) was over Tonopah; the coldest temperatures (<-60°C) were over Rapid City, Denver, Bismarck, Lander, and Santa Maria.

The Fresno-Lander cross sections of θ and D are shown in Figs. 6.32 and 6.33. In the θ field the tropopause is seen to be lowest over Tonopah and Ely. The warm and cold fronts are indicated but it is obvious that all the baroclinity is not concentrated in the frontal zones. Note that the horizontal gradient is greatest in the warm air to the west of the cold dome and that the air is most stable in the warm air to the west. Surface observations of winds, clouds, precipitation, and pressure tendency are of interest for comparison and correlation with the upper air structure.

In the D field one sees a pattern in marked contrast to that of the last 12-hourly section. The minimum D value is at 300 mb in the cold air between Tonopah and Ely. The asymmetry of the cold dome and the diffluent structure--particularly at 500 and 400 mb--are evident. The maximum 12 hourly $(\partial D/\partial t)_p$ was -970 ft at 300 mb over Ely.

As a final observational note to this study, a stationary wave cloud observed in the jet-like northwest flow over Bishop at 1200 PST (2000 GCT) on 2 April is shown in Fig. 6.34. It appeared that the cloud formed in a lee wave induced by the Sierra in the Mono Lake area north of Bishop.

Other observations of the 1955 field season.

Airborne data from 10 and 13 April were limited by the failure of the wind measuring equipment and the fact that upwind soundings were nearly adiabatic through great depths making difficult the analysis of wave length and amplitude from small temperature differences. The only resulting flight sections from these dates are shown and discussed below. In addition, the upwind soundings and cloud phenomena for 3 other dates of strong wave occurrence are illustrated. These data were chosen to represent specific types of strong lee waves which are further discussed in later chapters. The limited observations from these 5 days are treated briefly below in chronological order. No synoptic charts for these dates are shown.

29 March 1955. An aerial photograph illustrating the rather unusual phenomena of this date is reproduced in Fig. 6.35. Both project sailplanes attained 40,000 ft altitude in the updraft zone which lay exceptionally far east of the Sierra crest. The wave length was approximately 20 miles

Fig. 6.35 - 1405 P, 29 March 1955. SSE from 18,000 ft. Wave cloud and cirrus bands. Note smoke from grass fire (lower) and dust from Owens "Lake" (horizon) describing surface wind flow.

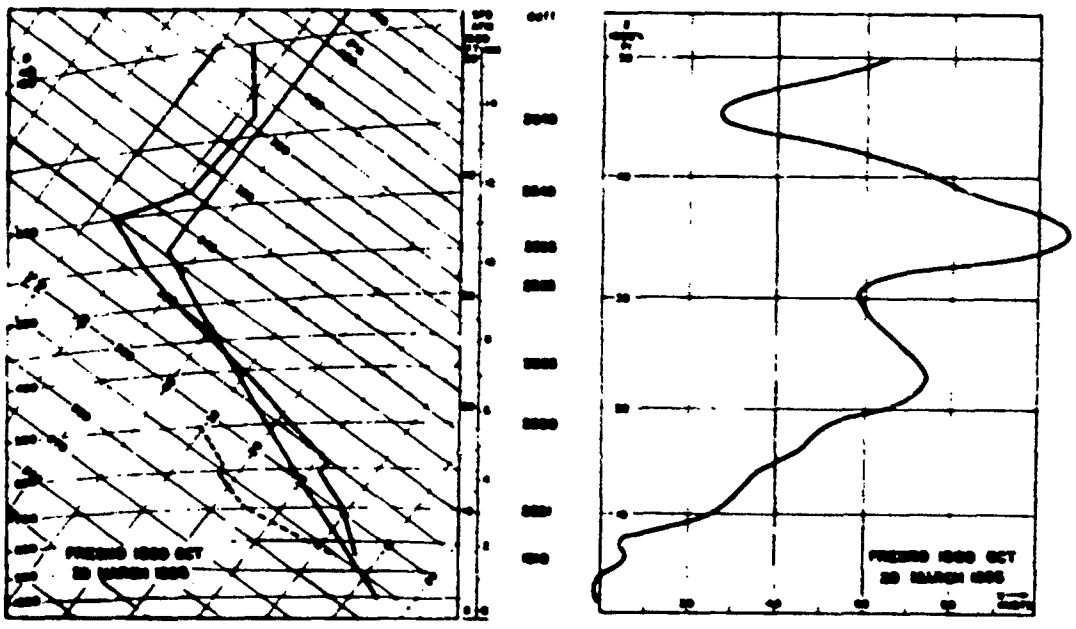

Fig. 6.36

(32 km).* The 1500 GCT sounding and U-profile at Fresno are shown in Fig. 6.36. An inversion appears near mountain crest level but the dew points are low which probably accounts for the absence of lower wave or roll clouds. A maximum wind speed of 107 knots occurs just below a sharply marked tropopause.

10 April 1955. On this date a cold front had passed Bishop and the winds over the mountain crest were northwesterly while those at higher levels were from the west-southwest. Both sailplanes soared in the strong wave with the Pratt-Read reaching 31,000 ft and the 2-25 reaching 40,000 ft. The B-47 flew over the Sierra at the 25,000 and 30,000 ft levels; data from the 25,000 ft runs are shown in Fig. 6.37. No lee waves are observed but a single crest is found over the center of the Owens Valley. No roll or wave clouds were visible at the time of the flight. The temperatures indicate a general descent over the western Sierra slope but with the lowest temperature above the Inyo Mountains just downwind of the single bump over the Valley. The maximum altitude variation of a streamline is about 3,000 ft. Data from both runs suggest lee waves upwind of Fresno, perhaps induced by the Coast Ranges.

13 April 1955. Updrafts in a developing moderate lee wave were explored by the Pratt-Read sailplane to 36,000 ft, while the B-29 traversed the Sierra and Owens Valley at 25,000 ft and the B-47 flew across at 30, 35, and 40,000 ft. Temperature measurements from the 40,000 ft, east to west, run of the B-47 are shown in Fig. 6.38. This lee wave occurred in the "warm" air south of a frontal zone and the tropopause was above 40,000 ft. In contrast to the 40,000 ft stratospheric pattern found on 1 April (Fig. 6.17), true lee waves appear in the displacement curve. These waves in the upper troposphere are of relatively small amplitude and of insufficient vertical speed to support a sailplane. The flow upwind of the Sierra appears disturbed but without the general descent over the west slope as observed on 1 or 10 April.

14 April 1955. This case represents the more nearly "normal" type of strong wave as illustrated by the cloud phenomena in Fig. 6.39. Dr. Kuettner reached an altitude of 43,000 ft in the 2-25 sailplane while Miss Betsy Woodward soared to 40,000 ft in the P-R sailplane. In Fig. 6.40 are shown a composite 2100 GCT sounding from Oakland and Santa Maria together with the U-profile from the 2100 GCT Merced rawin. The lee wave developed to greater intensity as the wind speed increased from that of the previous day.

25 April 1955. The cloud phenomena of this date (Fig. 6.41) illustrate a rather uncommon and dangerous type of strong lee wave. The leading edge of the roll cloud deck, instead of following the jog of the Sierra crest near Bishop, continued in an unbroken line northward over Bishop. To the west the föhnwall towered to 20,000 ft and swept far down the eastern Sierra slope. The massive roll cloud extended eastward over the White and Inyo Mountains with an indistinct trailing edge and with no visible gap in the clouds in that direction. For this reason it was necessary for the two sailplanes, which had both reached 40,000 ft, to descend in the gap of clear sky between the föhnwall and the roll cloud. Near 14,000 ft they encountered extremely severe turbulence in which the P-R broke apart. The pilot, Larry Edgar, was saved by his parachute. Accounts of these flights and a discussion of the turbulence are given in Chapter 10. The 1500 GCT Merced sounding and wind profile are shown in Fig. 6.42. An

*The most outstanding feature of this lee wave was the complete lack of a rotor zone and its associated turbulence. The smooth lee wave existed as low as 4,000 ft over the ground and increased in intensity to 30,000 ft.

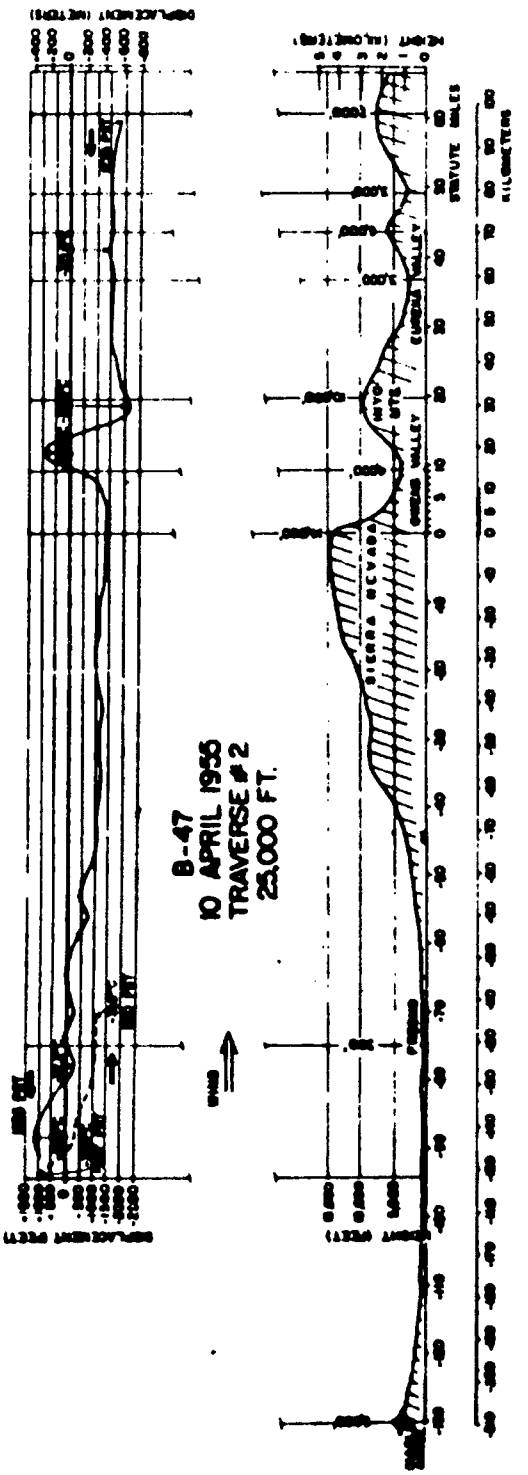

Fig. 6.37 - (Prepared by the Air Force Cambridge Research Center)

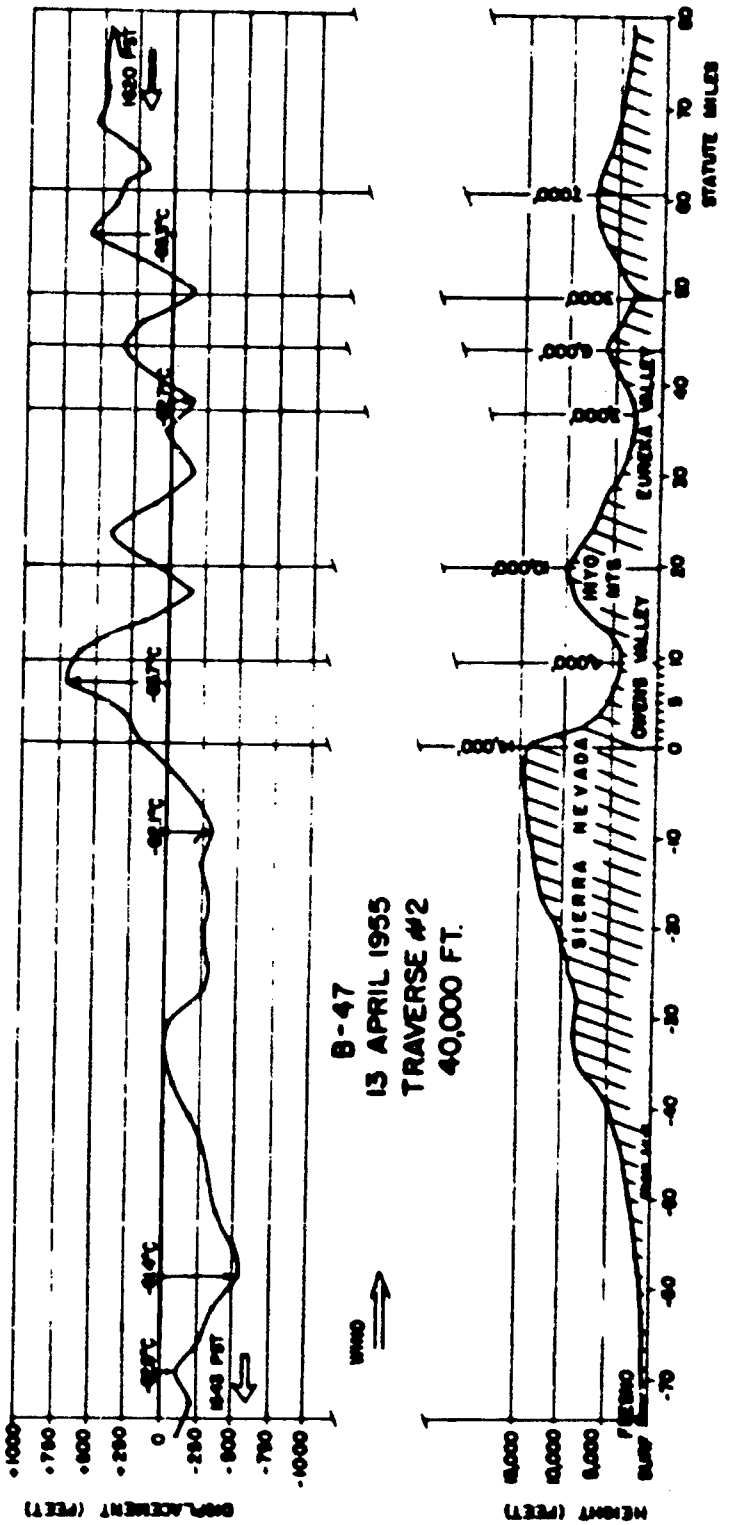

Fig. 6.38 - (Prepared by the Air Force Cambridge Research Center)

Fig. 4 39 - 0630 PST, 14 April 1955. South from Bishop Airport. High wave cloud, roll clouds, and cirrus bands.

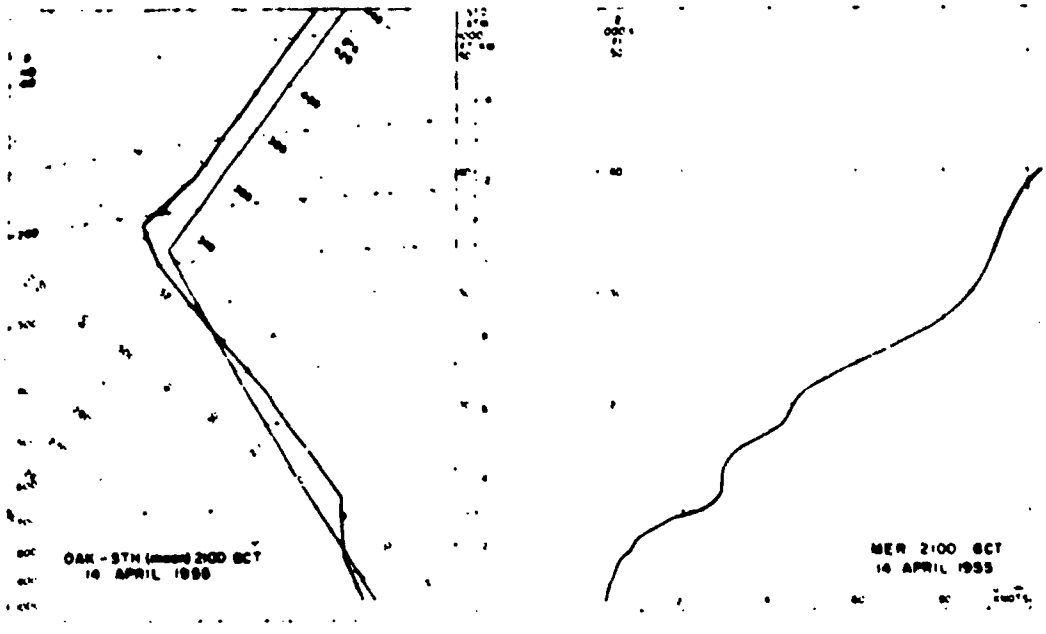

Fig. 4

Fig. 6.41 - 0945 PST, 25 April 1955. South from Bishop Airport. Föhnwall and base of dense rotor cloud.

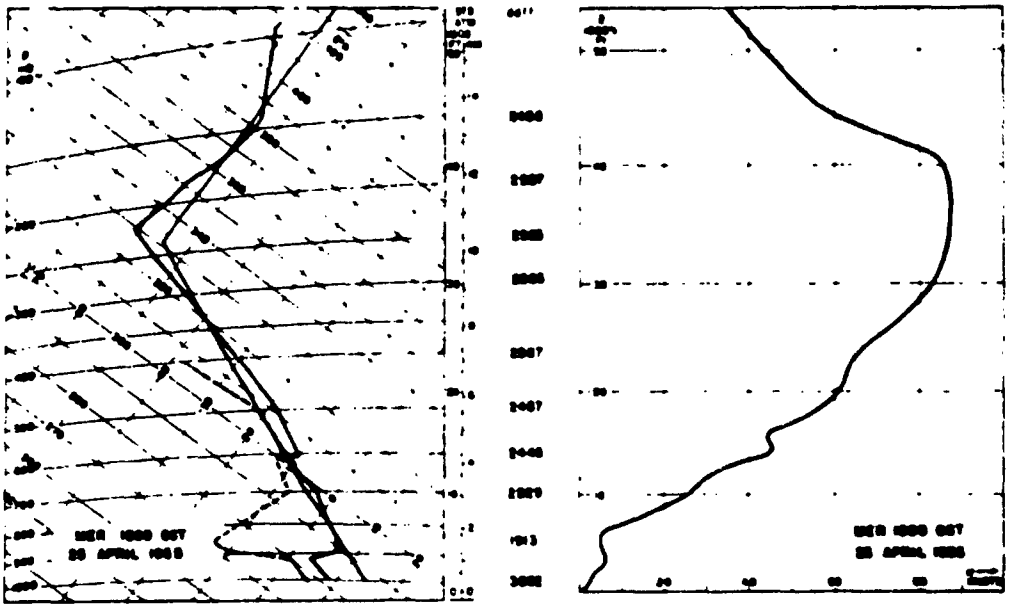

Fig. 6.42

inversion appears at 600 mb with moist air to 400 mb. Later in the day the high-level inversion became greater and wind speeds of over 130 knots were measured in the upper troposphere at Oakland and Merced.

Results.

The Mountain Wave-Jet Stream Project of 1955 provides the most complete upper air synoptic data for the study of the air flow over the Sierra Nevada, and the first flight measurements of the mountain wave at constant levels including the flow both upwind and downwind of the range. Rather complete results for one selected case study and limited results from 5 other specific cases are cited in this chapter. Observations from these dates provide examples for the topics of the remaining 6 chapters of this report.

Acknowledgements.

The enormous tasks of reduction, analysis, and interpretation of the B-29 and B-47 flight data were carried out by the team of Dr. Joachim Kuettner, Roy Endlich, and Robert Rados of the Geophysics Research Directorate, Air Force Cambridge Research Center. These results have been made available to the Project by Dr. Kuettner in order that they could be integrated with the corresponding synoptic studies. A forthcoming G. R. D. report will treat in detail the instrumentation of the aircraft and both the meteorological and aerodynamical implications of the airborne data.

References.

Bjerknes, J. (1954): The Diffluent Upper Trough, Archiv für Meteorologie, Geophysik. und Bioklimatologie, Band 7.

Knox, J. (1956): A synoptic study of the intensification mechanism of a diffluent trough. Final Report Synoptic Processes Research Project, Contract AF 19(604)-1236. University of California at Los Angeles.

.. CLASSIFICATION OF FLOW TYPES

Introduction.

This chapter describes the principal types of waves observed in the lee of the High Sierra and discusses some of the more important variations of these. A more objective approach based on the upwind soundings and wind profiles is presented in Chapter 12, where it follows the relevant theory. Some examples are given there comparing observed wave lengths with those computed from upwind flow characteristics.

Lee wave types.

From a descriptive point of view, the lee waves observed over the Owens Valley may be divided into 3 types based on their wave length and the intensity of their vertical wind speeds. There is, in fact, a whole spectrum of wave forms observed but, in the interest of simplicity, Table 7.1 provides a convenient grouping. The values given are for order of magnitude only and vary considerably from one case to another. Further characteristics and examples of each of the 3 types, and subdivision of the strong wave type to include certain rather rare but extremely interesting cases, follow below.

Table 7.1

Wave type	L	$2\ell_{max}$	w
Strong	8 - 20 miles (13 - 32 km)	4,000 - 8,000 ft	±30 to ±60 ft s^{-1}
Moderate	5 - 8 " (8 - 13 ")	2,000 - 4,000 "	±15 to ±30 " "
Weak	2.5- 5 " (4 - 8 ")	500 - 2,000 "	± 5 to ±15 " "

Note: L = wave length, $2\ell_{max}$ = maximum altitude variation of a streamline, and w = vertical wind speed.

Strong waves. The near-legendary reputation of the Sierra Wave derives from the spectacular phenomena associated with the lee waves of strong intensity. All of the dozen or so sailplane flights to altitudes over 40,000 ft* have been made in waves of this type. From these flights we can conclude that there are vertical updrafts of several meters per second at these altitudes; whether vertical speeds of this order can be found at altitudes up to 50,000 or even 60,000 ft is not known at present.

---

*The maximum altitude attainable by a sailplane is that at which the vertical speed of the air is equal and opposite to the sinking speed of the sailplane. The latter is a function of the sailplane design, the air-density, and the forward speed of the sailplane which in turn is made equal and opposite to the horizontal wind speed in hovering flight. In several of the flights over 40,000 ft, higher altitude could have been achieved but was not attempted because it approached the critical limit of non-pressurized sailplanes or because of the adverse effects on both sailplane and crew of prolonged exposure to extreme cold. The updrafts required to keep the Pratt-Read sailplane above 40,000 ft exceed 7 ft/sec.

The diverse features of strong lee waves can be seen in the illustrations to the several examples treated in this report. These cases and the corresponding figures are listed here:

Date	Figures (inclusive)
18 December 1951	3.9 - 3.14, 5.1 - 5.16
16 February 1952	3.26 - 3.30, 5.35 - 5.38
18 March 1952	4.11 - 4.20, 5.43 - 5.44, 9.2
19 March 1952	3.36 - 3.40, 5.45 - 5.48
29 March 1955	6.35 - 6.36
1 April 1955	6.1 - 6.26
10 April 1955	6.37
14 April 1955	6.39 - 6.40
25 April 1955	6.41 - 6.42

Of these and all the other strong waves observed during the past five years of intermittent project observations, there are three interesting subtypes one of which is most common and two of which are comparatively rare, but are each illustrated by one example in the above list.

1) The normal case. In these the wave length varies from 13 to 20 km so that the first wave crest lies over the Owens Valley and the second over or just in the lee of the Inyo Mountains. Typical examples of the cloud phenomena are seen in Figs. 3.26, 6.11, and 6.39. These phenomena usually include at the mature stage of development the cap-cloud (föhnwall), high lenticular cloud decks, and rotor (roll) clouds which last may at times appear rather small as in Fig. 6.39.

2) The rotorless wave of long wave length. This type of leeward flow pattern is illustrated in Fig. 6.35. On that date, 29 March 1955, two sailplanes found a smooth updraft zone over the west slope of the Inyo Mountains and soared to 40,000 ft before making a forced descent. The first wave crest was marked by high arch clouds and cirrus bands, but no trace of a rotor cloud was seen nor was there any turbulence encountered to suggest the presence of a rotor zone. In the illustration cited, the smoke from a brush fire in the center of the Owens Valley nicely traces a streamline over the crest of the Inyo Mountains. The photograph also shows the eastward drift of the fine dust from Owens dry Lake. (On "normal" wave days the dust is often carried northward by southerly surface winds along the eastern side of the Valley.) The indicated wave length was of the order of 30 to 32 km (20 miles)--roughly the same as the distance between the crests of the Sierra and the Inyo Mountains. These observations of 29 March 1955 being the first and only record of the occurrence of such a lee wave, it remains for future observations to determine the degree of rareness of this phenomenon. Certainly it lies at the extreme end of the spectrum of observed wave lengths; the next in order is that of 19 March 1952 with an indicated wave length of about 28 km.

3) The dense rotor cloud without visible downdraft. In certain cases with extremely strong wind shears and high moisture content in the lower troposphere, a massive roll cloud forms with its leading edge extending in a nearly straight line over the Owens Valley (in contrast to the usual manner in which the cloud line curves with the mountain crest) and with no apparent trailing edge, the cloud extending eastward over the White and Inyo Mountains. As pointed out by Dr. Kuettner, this form resembles a nonperiodic pressure jump and is the subtype associated with the most severe turbulence in the rotor zone (see Chapter 10). The scale of this turbulence--of which, understandably, no quantitative measurements have been made--may be such as to produce sufficient mixing to significantly alter the existing stability stratification and thus to prevent the formation of a visible train of lee waves. In the few cases reported, the rotor cloud was several thousand feet thick in the vertical and its top appeared to be several thousand feet higher than the top of the föhnwall. An example of this type is the wave observed on 25 April 1955 in the above list.

Moderate waves. Of this second type there are the following examples in this report:

Date	Figures (inclusive)
27 November 1951	3.1 - 3.4, 5.27 - 5.28
28 November 1951	3.5 - 3.8, 5.29 - 5.30
30 January 1952	3.20 - 3.25, 5.33 - 5.34
3 March 1952	4.5 - 4.9, 5.41 - 5.42
30 March 1952	3.41 - 3.44, 5.49 - 5.50
13 April 1955	6.38

In these waves the highest altitude attained by sailplanes was about 30,000 ft; in the average it was nearer 25,000 ft. These cases are often "dry waves in which there may appear only a few cloud fragments. In most cases the wave is indicated either by roll cloud lines or a high lenticular arch cloud; the latter is almost always a single cloud sheet in which there is no indication of the shorter wave length encountered in the lower layers by sailplanes or marked by roll cloud lines. In some cases, when the flow is from the southwest and the front is quite near, the air is very moist and a moderate wave persists though there appears to be a complete overcast from the ground; this is known as an "obscured wave." In such a wave on 29 March 1954 the sailplane reached 25,000 ft in a narrow "grand canyon" between a dense roll cloud and a towering föhnwall. As the canyon, or föhn-gap, filled rapidly with cloud, the flight was terminated in time to allow a descent through the last remaining hole in the undercast.

Weak waves. This type occurs much more frequently than the number of examples would indicate. It is simply less productive of sufficiently strong updrafts to allow a sailplane to explore in a single flight a worthwhile cross section of the flow pattern. Maximum altitudes attainable in these waves

seldom exceed 18,000 ft. Also, the two-dimensional picture is often blurred by the effects of position and orientation of individual ridges of the mountain range. There are usually no roll clouds with these, but there are often scattered lenticular forms or a high arch cloud, with their leading edges just in the lee of the Sierra crest. The two examples treated in this report are:

Date	Figures (inclusive)
29 January 1952	3.15 - 3.19, 5.31 - 5.32
21 February 1952	3.31 - 3.35, 5.39 - 5.40

Time changes and the effect of terrain. A gradual increase in wave length occurs when the speed of the air flow over the Sierra increases. Usually, once a wave has formed and is visible in the clouds, the observed wave length does not change by more than 30% in one 12-hour period. If the flow remains westerly, the change from one day to the next may be of the order of 50%. One of the most remarkable series of this kind was observed in late December 1955 when over a span of three consecutive days the wave length of the roll clouds changed successively from 8 to 11 to 16 km--the last just prior to a complete overcast and the heavy rains which brought great floods throughout northern California.

Occasionally, when the upper wind speeds are increasing rather rapidly, the change in wave length appears to take place discontinuously. For a period of an hour or two the wave will be indistinctly marked by the clouds after which it will again be clearly visible with a significantly longer wave length. This suggests resonance effects caused by the shape of the underlying terrain. The average slope of the east flank of the Sierra from the crest, at an average height of 13,000 ft, to the break in slope at the top of the alluvial fans, at an average height of 6,000 ft, is 30%. The distance from the crest of the Sierra to the crest of the Inyo Mountains averages 32 km (20 miles) in the Independence-Lone Pine area, while it is about 26 km (16 miles) in the cross section through Taboose Pass just south of Big Pine. Strong waves often reach their greatest development in the latter area where the highest altitude is most often attained in a sailplane. To what degree the form of the Owens Valley influences the shape of the lee wave is a matter for further study. The observations suggest that the eastern Sierra slope is the most important terrain feature in the creation of the lee wave but that the best developed waves are those that are roughly in phase with the mountain ranges and valleys downstream from the Sierra.

8. MOUNTAIN WAVES AND JET STREAMS

Introduction.

The inter-relationship of mountain waves and jet streams is a subject on the frontier of current meteorological research. Awareness of jet streams, the comparatively narrow bands of maximum wind speeds in the upper troposphere, as important features of the complicated air flow patterns over the earth has come about only within the past decade. The phenomenon itself being at present incompletely described and understood, there remains much exploration to determine the manner of formation and evolution of jet streams and their relationship to both large- and small-scale weather developments. Although no formal definition is possible, it is tacitly understood by most writers that a jet stream in the winter season has wind speeds of 100 knots or more in a band 300 miles or less wide and extends along a distance of at least 1,000 miles. Wind maxima of similar speeds but of lesser width and length may be termed "jetlets."

The principal jet stream found by wind measurements and delineated by contour analysis of upper air isobaric charts is that associated with the polar front and which, according to Palmén (1948) is generally situated directly above the 500 mb isotherm concentration. The 500 mb front is found between the isotherms of -20° and -30°C and usually near -25°C. Also, as pointed out by Riehl et al (1954), a pronounced temperature gradient at 200 mb lies directly above the jet stream axis, indicating a break in the tropopause. The position of the jet stream core with respect to this break--which amounts to a difference in height of the tropopause on either side of the jet core of the order of 10,000 ft--has tended to discredit the earlier concept of the "advection" of "polar" and "tropical" tropopauses and suggests instead a dynamic development in which, looking downstream, the air to the left of the jet stream core is subsiding and warming, and that to the right is rising and cooling. Below these indicated vertical motions the reverse is believed to occur, that is, ascending motion in the cold air mass and descending motion in the lower troposphere of the warm air mass.

Other significant jet streams are frequently observed both to the north and south of the polar front jet stream. The speeds of these are often quite high although they are associated with temperature gradients considerably less than those of the polar front. Of these, only the more southerly one has an influence on the formation of Sierra lee waves.

Over the Pacific the polar front jet stream is found, on the average, to be about 20° of latitude farther south than over the Atlantic (Riehl et al, 1954). This eccentricity of the "jet pole" is undoubtedly related to the uneven distribution of large land masses as well as to the paths of certain ocean currents such as the Gulf Stream. When the jet stream crosses the west coast of the United States it usually appears as a wide, relatively slow speed, stream of air. Speeds over 100 knots are strong and speeds of 150 knots or greater are rather uncommon. In addition to the polar front jet stream whose position is much more variable over the west coast than over the east coast of the United States, there is found in winter a nearly constant jet stream at latitude 30° N across the southern United States. The presence of this latter jet stream and the development of a southward-moving westerly or southwesterly polar front jet stream somewhat farther north tend

to maintain for a period of several hours over the Sierra a very broad, relatively fast, current with small lateral gradients but with a gradual increase in speed with time. From the above considerations it can be seen that the association of a jet stream with the development of mountain lee waves is largely dependent on the latitude and orientation of the mountain range. For this reason the remarks made in this chapter refer only to the Sierra Nevada although some may be applicable to other ranges.

In the discussion which follows, the subject has been divided among five principal topics. These are:

1) The location of the polar front jet stream and the steady increase of wind speeds over the Sierra during lee wave occurrence.

2) Longitudinal variations of wind speeds associated with the flow pattern of the lee wave at the jet stream level.

3) Local periodic variations of wind speed associated with travelling waves in or near the jet stream.

4) Rapid, non-periodic, local increase of wind speed that may be due to travelling wind speed maxima (gusts) and/or to the local topography, e.g., deep transverse canyons and passes in the mountain range.

5) The vertical and horizontal wind profiles of typical Pacific Coast jet streams.

These topics are discussed in that order below.

Relationship of Sierra Nevada lee waves to the polar front jet stream

One may begin a discussion of the position and lateral movement of the jet stream during the occurrence of Sierra lee waves by examing the contour patterns on pertinent isobaric charts. Since the radiosonde observations on which the smoothed analyses are based are often rather sparse--and uncertainty is often aggravated by the difficulty of reconciling Weather Bureau and military observations as pointed out by Riehl (1954)--the geostrophic "jet stream" probably exaggerates the width of the band of exceedingly strong winds and minimizes the maximum speed in comparison with what might have been measured by aircraft flights made perpendicular to the current. Nevertheless, it is doubtful if the position of the true jet stream varies appreciably from the region of the maximum contour gradient on carefully drawn charts. Some examples of upper air charts on 3 days of strong lee waves during the 1951-52 season are shown in Figs. 5.7 and 5.10 (18 December 1951), Fig. 5.38 (16 February 1952), and Fig. 5.48 (19 March 1952). On these charts the geostrophic "jet stream" appears to be very broad over the Pacific Coast. For the other lee wave cases discussed in Chapters 3 and 4 and for which the upper tropospheric flow patterns are not shown, the positions of the principal jet streams can be approximately determined by the position of the polar front or the maximum isotherm gradient on the 500 mb charts. Mean charts for the 18 strongest lee waves in the period 1949-52 are shown by Colson (1954).

During the 1955 season the network of radiosonde, rawin and pibal observations was much more dense, enabling more accurate determination of the jet stream position by both contours and measured winds. The case study of 1 April

1955 given in Chapter . affords a typical and more detailed example of the position of the jet stream with respect to both the front and the Sierra during the development of a strong mountain wave. Relevant illustrations in this series are the 300 and 200 mb charts shown in Figs. 6.4, 6.21, and 6.22, and, particularly, the vertical cross sections of D-values shown in Figs. 6.6 and 6.24. From these charts and cross sections of 1 April 1955 and the unpublished analyses of all the notable cases of both the 1951-52 and the 1955 seasons, it appears that strong lee waves usually occur in the relatively warm, easterly or southwesterly current ahead of an approaching cold front and south of the polar front jet stream. In the cases of 18 December 1951, 19 March 1952, and 25 April 1955, the synoptic data and the flight measurements suggest that the principal jet stream lay over the High Sierra during the time of the sailplane flights.

There are a number of variations to the 'typical' case, a few of which may be briefly mentioned. In certain cases, when a cyclonically curved jet stream corsses the Sierra from the west or southwest, there is no visible evidence of a lee wave because of obscuration by dense clouds and precipitation. On two such occasions, 14 January 1952 and 14 March 1952, strong winds were encountered at 14,000 ft by the sailplane on tow but no wave motion was found over the Owens Valley. In either case it was imprudent to penetrate the cloud ceiling for further exploration and whether or not a lee wave existed at high altitudes is a matter for conjecture. In the cases where a westerly polar front jet stream crossed southern California--a situation that brings heavy rains in that region--south of the High Sierra, no lee waves were observed, probably because of the presence of a low tropopause, the lack of a stable stratification in the cold air mass, and weaker wind speeds aloft.*

In the case of 30 January 1952 the flow at 500 mb (Fig. 5.34) was relatively slow but at altitudes near the 200 mb level wind speeds of over 100 knots were reported at several stations in the region. In fact, during the week comprising the end of January and the beginning of February 1952, the zonal index was the highest of that winter season, and during that week moderate Sierra lee waves were observed on 6 consecutive days. The strong winds at levels near 40,000 ft during that period appeared, from perusal of the upper contour charts, to have been due to a strengthening and northward movement of the more southerly, non-frontal, jet stream.

Northwesterly jet streams over the Sierra are usually associated with frontal passages and post-frontal flow at the surface but sometimes, if the cold air mass is relatively shallow, may be associated with lee waves. One of the most memorable cases of this type occurred on 12 November 1951. Riehl and Tewles (1952) have treated the large-scale synoptic developments of this period and report a jet stream of 200 knots--an extremely high speed--over northern California on the 12th. At Bishop the double-theodolite pibal measurements showed a wind speed of 80 knots at mountain top level (14,000 ft). A sailplane flight to 34,000 ft was made over Bishop before landing in a 40 mph northerly wind and sandstorm accompanying the frontal passage. Shortly after, the large timber and sheet-metal roof the Airport hangar was blown off in a 60 mph gust. Frontal passages in the lee of the Sierra are rarely so violent, but marked passages from the north accompanied by strong winds presage severe weather on the Great Plains in the lee of the Rockies in 24 to 36 hours. When

---

*The effects of static stability and wind profile are discussed in Chapter 12.

the air is relatively dry and few clouds appear, later development over the Plains usually brings strong, dry northerlies and dust storms. But when the northerly frontal passages at Bishop are accompanied by dense cloud formation and some rain, the aftermath often leads to thunderstorms and tornados over the Plains. An example of the latter are the observations made at Bishop on 24 May 1955--a moderate lee wave with roll clouds followed by overcast, rain, and northerly sandstorm--which preceded by one day the severe tornado destruction at Udall, Kansas.

Jet streams from other directions have little to do with Sierra lee waves. Northerly jet streams above the post-frontal flow (see Figs. 6.30, 6.31, and 6.33) are often more intense and in a narrower band than those downwind of upper air troughs, but of course are nearly parallel to the range as well as having considerably different, and less favorable, wind and stability profiles. Southerly jet streams are almost always associated with very moist air, dense clouds, and widespread precipitation. The extremely rare easterly jetlet--so called because it seldom extends for more than a few hundred miles--may cause a short-lived "reverse" wave over the Owens Valley which is then in the lee of the White and Inyo Mountains. Such a case occurred on 13 December 1951 when a cyclonic circulation ("cut-off low") over southern California brought strong easterly flow over the White Mountains and enabled the towplane to be soared to 20,000 ft.

Stationary wind speed maxima associated with the mountain wave

As discussed in Chapter 3 (Table 3.1) and in Chapter 6 (Fig. 6.14), there are in strong lee waves large longitudinal variations in wind speed which remain nearly stationary with respect to the underlying terrain. Obviously, when a strong lee wave occurs with a jet stream overhead, the wind of the fastest current will be speeded up in some portions of the wave flow and slowed down in other portions. Where the disturbed flow in the higher levels has the form observed from the B-47 flights of 1 April 1955 (Fig. 6.17), extremely strong jetlets have been found to exist for many miles downstream. These observations were first made by Robert Symons of Bishop who also was the first to point out that the cirrus bands associated with such strong winds originated in the lee of the Sierra and extended for a few hundred miles or more downstream. Symons explored these phenomena with a sailplane and on several occasions encountered wind speeds considerably in excess of 100 knots while flying above 30,000 ft and downwind of the principal lee wave clouds. A cross country sailplane flight to Ely by Symons was made in about 1½ hours with the help of the strong tailwinds encountered after reaching a high altitude in a strong lee wave. The strong wind speeds at Beatty on 1 April 1955 (Figs. 6.21 and 6.22) may be related to the large-scale effect of the Sierra on the upper air flow pattern.

Periodic variations in wind speed

There is no regular means of measuring local pulsations of wind speed in the upper air. However, the most convenient and sensitive tool at present is a sailplane which, by attempting to hover in the updraft zone of a strong lee wave, can measure rather accurately the variations in horizontal wind speed. Such observations were made by Dr. Kuettner (1952) on the afternoon of 25 February 1951 while attempting to remain motionless over the terrain at 30,000

ft in a Sierra lee wave. At first a true speed of approximately 70 mph (42 mph indicated) was necessary to equal the wind speed, but within a few minutes the sailplane began to drift slowly backward and the forward speed had to be increased. The wind continued to increase in speed until finally a true speed of 110 mph (65 mph indicated) was necessary to compensate for the wind. Due to the high forward speed with respect to the air, the sinking speed of the sailplane increased and altitude was lost in the effort to prevent drifting back into the downdraft area. This rather difficult situation lasted for about 8 minutes, after which the wind speed decreased continuously until a true speed of 70 mph (42 mph indicated) was again sufficient for hovering flight. The entire cycle was repeated once again before the flight was terminated because of the late time of day. These observations suggest that the period of such travelling pulsations is of the order of 20 minutes. Variations of surface pressure of similar periods have been recorded by sensitive barographs or pressure variographs at times when a jet stream or jetlet was overhead.

Non-periodic increase of wind speed associated with jetlets

One of the most fascinating occurrences in trans-Sierra weather is the rapid build-up of a strong lee wave within a few hours after the appearance of the first lenticular clouds. Such short-lived waves are associated with the development of local jetlets which may in turn be connected with relatively fast-moving troughs in the main upper air flow. Time-lapse motion pictures and sequences of still photographs have recorded the rapid development of such waves on several occasions. An outstanding example of this phenomenon occurred on 4 April 1954 when a sailplane piloted by Dr. Kuettner released from tow just south of Bishop where the roll and lenticular cloud decks were building most rapidly. A maximum altitude of 35,000 ft was reached within 17 minutes as the lee wave phenomena reached their most impressive stage of development. At 32,000 ft it was observed by Kuettner that the wind speed at the center of the jetlet was about 120 knots while on either side within a total band of about 50 miles the speed dropped to 70 knots. Staying near the center of this wind speed maximum as it moved southward, and utilizing updrafts in lee waves of other mountain ranges, Kuettner completed a cross-country flight to Las Vegas.

These jetlets occur most frequently in the relatively warm air several hundred miles south of the principal polar front jet stream. It is a curious fact, and a vexing one from the standpoint of research flight planning, that all of the many cases of this kind observed during the last 4 years have occurred in the afternoon with the lee wave phenomena reaching their greatest development shortly before sunset. This is one of the interesting facets of the mountain wave-jet stream relationship that needs further exploration. It suggests a diurnal solar effect closely related to the 24-hour component of the atmospheric tide. Some memorable examples of such rapid developments of strong waves occurred on 28 March 1954, and 16, 24, and 28 April 1955. Each of these 4 cases signaled the approach of the polar front and preceded frontal passage by about 36 hours. Two of the cases (28 March 1954 and 28 April 1955) preceded moderate lee waves on the following day and the other two (16 and 24 April 1955) were succeeded by strong waves occurring in closer proximity to the polar front jet stream. On the afternoon of 24 April, preceding the strong wave of 25 April mentioned above and discussed in Chapter 6 (Figs. 6.41 and 6.42), high, ribbed, cloud bands of the types described by Schaefer (1953) and Frost (1953 and 1954) were seen passing overhead at speeds of the order of 100 knots.

It should be mentioned further that, while the jetlets are meso-scale features of the upper air flow which generally travel or develop in the large-scale upper currents, certain topographical forms augment the maximum speed of the jet stream or may themselves cause local jetlets in a fast current of broad lateral extent. The most pronounced effect of this type has been observed on many occasions in the area just south of Big Pine in the Owens Valley and just downwind of Taboose Pass in the Sierra. On either side of this broad cleft in the Sierra crest are transverse canyons, that on the western slope being the deep canyon of the South Fork of the Kings River (see Fig. 6.10c). Strong west-southwest winds are channeled along the canyon and through the pass making the wind speeds along that vertical cross section stronger than those on either side. As related in the last chapter, this is also the cross section along which the distance between the crest of the Sierra and the crest of the Inyo Mountains is a minimum; when wind speeds aloft increase with time a resonance wave of wavelength near 13 km will develop first and best in this area. For these reasons, sailplanes are often released from tow just south of Big Pine where the strongest updrafts are found and the highest altitude can be attained.

Vertical and horizontal velocity profiles

In comparison with the structure of many jet streams found over the east coast as reported by Endlich (1954), Riehl et al (1954), and others, the structure of many Pacific Coast jet streams in both vertical and lateral profiles is one lacking in a sharp peak of maximum wind speed. Examples of this blunter profile in the vertical can be seen in Figs. 3.30, 3.40, 6.40, and 6.42. The reasons for this--lesser temperature gradients defining the polar front over the West Coast and the proximity of a higher, more southerly jet stream--have been suggested above. The lack of a pronounced wind speed maximum in the lateral direction and, instead, a quite broad band of strong wind speeds is responsible for rather long-lived lee waves that may persist for one or two days before their dissipation. Westerly wind profiles with sharp maxima are most often found in the jetlets and the strong waves associated with these are consequently rather short-lived.

The principal effect of the structure of a westerly jet stream over the Pacific Coast on mountain lee wave formation is in creating a favorable velocity profile for the development of "resonance waves." As discussed by Professor Holmboe in Chapter 12, strong waves in the lee of the Sierra are favored by a high tropopause and a rather strong positive vertical wind shear in the troposphere. In the period October through May such a profile is common in a prefrontal westerly or southwesterly current over the Sierra when the polar front jet stream crosses southern Oregon or northern California, and it is augmented by the intensification of another jet stream at high altitudes over southern California and Arizona.

Further outlook

More observations and research on the mountain wave-jet stream relationship are needed to supply important details presently lacking from our knowledge of the subject. To date there have been no aerological studies of jet streams over the western United States of the type conducted by Project Arowa and Project Jet Stream over the eastern United States. Aircraft traverses of strong

westerly currents over the Pacific Coast and downwind of the Sierra Nevada will shed much light on the structure of jet streams in that region. Some of the relevant problems to be solved by this or other observational techniques, e.g., sailplanes, strategically placed rawinsonde stations, etc., are noted here:

1) What temperature changes aloft are associated with the formation and movement of jet streams and what are the mechanisms of the temperature and wind speed changes?

2) What is the effect of the mountain wave temperature field at the tropopause level on the wind flow pattern? What effect has this large temperature difference across the Sierra on the speed and direction of the large-scale jet stream?

3) In strong westerly flow, is there frequently a double jet stream structure with one jet core to the north of and the other to the south of the High Sierra? If so, is this a large-scale effect of the mountain wave?

4) What is the ozone distribution at high levels (30,000 to 40,000 ft) over the Sierra during the occurrence of a strong lee wave? Has ozone an effect on the differential heating of the air and the creation of local jet-lets?

5) How high does the mountain wave extend? What happens at the level in the stratosphere where the wind speed drops to zero?

It is hoped that all of these questions will be answered during the next decade.

References

Colson, D., 1954: Meteorological Problems in Forecasting Mountain Waves, Bull. Amer. Met. Soc., Vol. 35, pp. 363-371.

Endlich, R., et al., 1954: "Project Jet Stream," Bull. Amer. Met. Soc., Vol. 35, pp. 143-153.

Frost, B., 1953: Flying in Jet Stream Winds, Shell Aviation News, No. 186.

Frost, B., 1954: More About the Jet Stream, Shell Aviation News, No. 195.

Kuettner, J., 1952: On the Possibility of Soaring on Traveling Waves in the Jet Stream, Aeronautical Engineering Review, Vol. 11, No. 12.

Kuettner, J., 1955: The Exploration of the Jet Stream by Sailplanes, Soaring, Vol. 19.

Palmén, E., 1948: On the Distribution of Temperature and Wind in the Upper Westerlies, J. Meteor., Vol. 5, pp. 20-27.

Riehl, H., and Tewles, 1952: Cyclogenesis of November 12-13, 1951 (to be published)

Riehl, H., 1954: Jet Stream Flight, March 23, 1953, Archiv für Meteorologie, Geophysik, und Bioklimatologie, Vol. 7, pp. 56-66.

Riehl, et al., 1954: The Jet Stream, Meteorological Monographs, Vol. 2, No. 7, Amer. Met. Soc.

Schaefer, V., 1953: Cloud Forms of the Jet Stream, Tellus, Vol. 5, pp. 27-31.

9. PRESSURE FIELDS AND ALTIMETER ERRORS

Introduction.

A discussion of the field of pressure in lee waves and of its implications to altimeter readings of aircraft would soon require a review of the principles of pressure measurement and of the techniques of determining heights of aircraft. For this reason these subjects are treated in Appendix B, together with a discussion of radiosonde pressure-heights. It was deemed pertinent to begin this chapter with a section on altimeters and the errors involved in both instruments and methods, irrespective of "errors" caused by extraordinary atmospheric phenomena such as thunderstorms and mountain waves. Upon these foundations the spatial variation of pressure in lee waves are examined and their meteorological and operational significance discussed. In treating this subject the problems of both meteorologists and pilots have been considered and, wherever possible, appropriate examples have been chosen for illustration.

The pressure altimeter.

The measurement of pressure in upper air soundings and the most generally used method for determination of the heights of aircraft both make use of the aneroid barometer. In the case of aircraft, the instrument is known as an altimeter and the readings are "indicated altitude" in accordance with the pressure-altitude relationship defined by the U.S. Standard Atmosphere. The most commonly used pressure altimeter is one in which one revolution of the principal pointer corresponds to 1,000 ft and in which a second pointer indicates thousands of feet, and a third the tens of thousands of feet. The instruments are calibrated for gross mechanical errors and usually there is some estimate of the corrections to be applied for dynamic pressure effects dependent on the speed and design of the various types of aircraft. An adjustable knob allows the pilot to change the "altimeter setting" and consequently the dial pointers in order that they may indicate the known geometric altitude of the airfield from which he is taking off. Similarly,

before landing, the altimeter setting is radioed to the pilot in order that he will know the (nearly) exact indicated altitude at which the wheels of his aircraft will touch the ground. Most pilots have cognizance of the fact that the appropriate altimeter setting for indicating true altitude changes much more with altitude than from one altimeter-setting station to the next, but, in general, this correction is not applied in routine flights; the problem of terrain clearance, to which this effect has particular relevance, is ostensibly solved by specifying a minimum flight altitude over mountains. In a rather definitive study of altimeters, the Operations and Engineering Group of the International Air Transport Association has issued a report (1953) on the various errors involved in pressure-altitude measurement. The following material has been extracted from that report.

There are three basic types of errors that can be distinguished in the pressure altimeter, namely:

1. Mechanical [or instrumental] errors, which depend upon inperfections in the mechanical system.

   a) Diaphragm error. Due to material imperfection and the construction of the aneroids, the diaphragm deflection will not be linear but will differ for the same given change of atmospheric pressure at different heights.

   b) Hysteresis error. Due to imperfection of the elastic properties of the aneroid material, a certain time will elapse after a pressure change before the aneroids have completely assumed the shape corresponding to the new pressure. ("Lag" is the process that occurs at a certain height when the aneroid is gradually taking the shape corresponding to the pressure at that height.)

   c) Friction error. Due to friction in the transmission mechanism between the aneroids and the pointers, the pressure change must reach a certain value, or the instrument must be exposed to vibrations of a certain magnitude to move the pointers. Moreover, there exists friction located at the temperature compensator pins, which could not be overcome by vibrations.

   d) Temperature error. Due to the instrument being normally tested at a fixed temperature (generally 20°C), any variation of the temperature of the instrument during actual operations will introduce an error, as the construction of the instrument only partly compensates for the temperature deviation.

   e) Backlash error. Due to play in the gear transmission between the pressure scale and the height scale and in the idler gear of the instrument errors may arise.

   f) Balance error. Due to the impossibility to coordinate the state of balance of all moving parts of the altimeter to such a degree that the instrument will be entirely independent of its position in relation to its calibration position (1013.2 mb, 29.92in), an error will occur.

   g) Coordination error. Due to incompletion in the coordination between the pressure scale and the height scale of the altimeter, an error may arise.

h) Instability error. Due to different reaction of the instrument during two consecutive climbs or descents, an error may arise in the indication. (Instability error, being additional to the foregoing, has been found to take effect at any time after the original calibration has been made, and is consequently outside the limits laid down by the tolerance curves for the diaphragm and hysteresis corrections. It can be a combination of one or more of the above stated errors.)

2. Operational [or installation] errors, which depend upon the way that the pressure altimeter is operated, and the possibility of reading and setting the altimeter.

a) Static system error. Due to difficulties to find a location for the static intakes that is undisturbed under all flight conditions, an error in the indication will occur.

b) Zero-setting error. Due to the shape of the tolerance curve generally decreasing with height, the tolerance at certain heights is different if a zero-setting other than 1013.2 mb (29.92 in.) is used.

c) Readability errors.
   i) Due to the height scale of the altimeter being graduated in intervals, it is impossible to obtain a greater accuracy in the reading than approximately half the graduation.
   ii) Due to the pressure scale of the altimeter being graduated in intervals, it is impossible to set the pressure scale with a greater accuracy than approximately half the graduation.

3. Principle [or inherent] errors, which depend upon the method used to convert pressure into height indications, i.e., the use of the standard atmosphere.

a) Density error. As the density of the real atmosphere generally differs from the density of the standard atmosphere, the indicated height over the pressure datum on the pressure scale will deviate from the true height.

b) Pressure datum error. Due to the change of pressure, in time and space, the setting of the pressure scale will not correspond entirely to the atmospheric pressure at the reference datum.

In connection with the foregoing, the following terms are applicable:

a) The tolerance curve is the curve that indicates the maximum acceptable corrections.

b) The calibration curve is the curve that indicates the results obtained from any particular instrument during the course of test caused by diaphragm and hysteresis inaccuracies.

The magnitudes of these various errors have been carefully estimated for different altitudes and for different specific uses of altimeters--terrain clearance enroute, approach and landing, vertical separation of aircraft, and

measurement of D value.* These estimated maximum errors for two of these uses are given in the two tables below.

Table 9.1. Terrain Clearance Enroute

Height (1,000's ft)	1,	3,	6,	10,	15,	22,	30
Mechanical errors:							
a) Diaphragm and b) Hysteresis	50	50	65	100	150	220	300
c) Friction	20	25	30	30	45	55	75
d) Temperature	5	5	10	10	10	10	10
e) Backlash	10	10	10	10	10	10	10
f) Balance	20	20	20	20	20	20	20
g) Coordination	25	25	25	25	25	25	25
h) Instability	30	30	35	40	45	55	75
Operational errors							
a) Static system**	0	0	0	0	0	0	0
b) Zero setting	8	8	15	15	15	15	15
c) Readability							
i Height scale	10	10	10	10	10	10	10
ii Pressure scale	15	15	15	15	15	15	15
Principle errors							
a) Density (3%)	30	90	180	300	450	660	900
b) Pressure datum	200	200	200	200	200	200	200
Maximum correction	±415	488	615	775	995	1295	1655 ft

Note: If the cruising level has been maintained for at least half an hour, the diaphragm and hysteresis correction could be reduced by 30 ft above 10,000 ft.

---

*In measuring D value by aircraft it is, of course, necessary to measure both Z_p and Z. The latter is either determined by a radio altimeter as by reconnaissance aircraft over the ocean or level ground, or by some other means of absolute altitude tracking such as of sailplanes in the Mountain Wave Project.

**Correction should be applied for this error.

Table 9.2. Measurement of D - value

Height (1,000's ft)	1,	3,	6,	10,	15,	22,	30,
Mechanical errors:							
a) Diaphragm and							
b) Hysteresis		50	65	100	150	220	300
c) Friction		25	30	30	45	55	75
d) Temperature		5	10	10	10	10	10
e) Backlash		10	10	10	10	10	10
f) Balance		0	0	0	0	0	0
g) Coordination		0	0	0	0	0	0
h) Instability		30	35	40	45	55	75
Operational errors							
a) Static system*		0	0	0	0	0	0
b) Zero setting		0	0	0	0	0	0
c) Readability							
i Height scale		10	10	10	10	10	10
ii Pressure scale		15	15	15	15	15	15
Principle errors							
a) Density (3%)		0	0	0	0	0	0
b) Pressure datum		0	0	0	0	0	0
Maximum correction		±145	175	215	285	375	495 ft
Reduced max. corr:**		± 70	85	90	110	130	170

Note: If the cruising level has been maintained for at least half an hour, the diaphragm and hysteresis correction could be reduced by 30 ft above 10,000 ft.

---

*Correction should be applied for this error.

**If a calibration curve is used and correction applied (as for the static system error), the diaphragm and hysteresis errors can be reduced to zero. If the instrument is locked in the 1013.2 mb (29.92 in) position, backlash and readability (pressure scale) will also disappear. The "reduced max. corr." is then obtained.

From the above tables it is seen that the most serious errors are: the combined diaphragm and hysteresis errors, density errors, and pressure datum (altimeter setting) errors. One example of each of these is given below.

Example 1. Hysteresis and diaphragm errors. In Fig. 9.1 the calibration curves for two 50,000 foot altimeters are shown. One set--that of lesser amplitude--is of a somewhat better instrument of the type used in current military aircraft. The other is probably typical of most altimeters currently used in commercial and private aircraft. In the latter, corrections

of over 300 feet are indicated with a maximum difference between the ascent and descent curves of about 400 feet. In reality, in an undulating flight, jumps in the readings do not occur because of lag and it is then that accurate determinations of Z_p are most difficult to ascertain.

Example 2. Altimeter setting error. At the Bishop Airport Weather Bureau station (Z = 4,110 ft) a barometric pressure* of 25.735 in. corresponds to Z_p = 4,110 ft and D = 0. (See Fig. B.1.) In this case the altimeter setting, A, would be 29.92 in. Now, when the Bishop pressure is 25.26 in., Z_p = 4,610 ft, D = - 500 ft, and A = 29.38 in. (which is about as close as one can read the altimeter setting dial). Checking the formula for obtaining Z_p from the altimeter and supposing the instrument to be perfect, i.e., no instrumental errors, we have:

$$Z_p = Z_I + 925\ (29.92 - A)$$

$$= 4{,}110 + 925\ (29.92 - 29.38)$$

$$= 4{,}110 + 500 = 4{,}610 \text{ ft}$$

This is the same result as obtained from the nomogram of Fig. B.1 or from Bellamy's tables of p vs Z_p when p = 25.26 in. was known. It can be seen that the term 925 (29.92 - A) is equal in magnitude to the D value but of opposite sign and, therefore, that the local altimeter setting is merely the correction for the local, surface D value. Had the altimeter setting been 29.92 in., again assuming a perfect instrument, the indicated altitude would have been 4,610 ft.

Example 3. Density error. In the vertical cross section from Medford to Phoenix at 0300 GCT on 2 April 1955 (Fig. 6.24), the D values at 300 mb for Medford and Phoenix are, respectively, -1,050 ft and +860 ft. Now suppose that the surface D values at each station were both zero; this is very nearly so as D decreases with height in the cold air over Medford and increases with height in the warm air over Phoenix. (Here "cold" and "warm" are relative to the Standard Atmosphere sounding.) Then at each station, if an aircraft were flying from one to the other, the altimeter setting would be the same, namely 29.92 in., and, if the instrument and operational errors and time changes of D are neglected, it would correctly indicate the true heights of the fields at both Medford and Phoenix. But if the aircraft flew at 300 mb, the altimeter would read 1,050 ft too high over Medford and 860 ft too low over Phoenix while always showing the same indicated altitude of about 30,050 ft. The total deviation is close to 2,000 ft.

The lee wave pressure field.

Non-hydrostatic effects. It has been recognized for many years that mountain waves, like thunderstorms, are among the phenomena excepted from the general assumption that pressures measured in the atmosphere reflect only

*Corrected for scale, temperature, and gravity error but not for elevation (4,145 ft) of the former station site in the town of Bishop.

hydrostatic conditions. In these exceptions to hydrostatic conditions the deviations of true pressures from pressures resulting solely from the "weight" of the air are caused by vertical accelerations in the air flow. The principal difference between the non-hydrostatic pressures in lee waves and those in thunderstorms and related phenomena is that in the latter the vertical motion and its pattern of accelerations are rather unsystematic and non-steady whereas in the former they are systematic and approximate a steady state. Therefore, if the synoptic streamline pattern of a lee wave is known, it is possible to calculate the effect of the vertical velocity accelerations on the pressures measured by aircraft. The derivation of the formula is as follows.

The equation of motion for steady flow ($\partial/\partial t = 0$) in the vertical plane, with the Coriolis and viscosity terms ignored, can be written:

$$\underset{\sim}{V}\cdot\nabla\underset{\sim}{V} = (V^2/R)\,\underset{\sim}{n} + V\,\partial V/\partial s\,\underset{\sim}{t} = -\alpha\nabla p + \underset{\sim}{g}$$

where $\underset{\sim}{V} = V\underset{\sim}{t}$, $\underset{\sim}{n}$ is the lefthand normal, $1/R$ is the curvature, and s is along the streamline. For points on trough and crest lines $\underset{\sim}{t} = \underset{\sim}{i}$, $\underset{\sim}{n} = \underset{\sim}{k}$, $s = x$, $V = U$, and $w = 0$, so here one gets:

$$(U^2/R)\,\underset{\sim}{k} + (U\partial U/\partial x)\,\underset{\sim}{i} = -\alpha\nabla p - g\underset{\sim}{k}$$

Multiplying by ρ and rearranging terms,

$$-\nabla p = \rho(g + U^2/R)\,\underset{\sim}{k} + \rho(U\partial U/\partial x)\,\underset{\sim}{i} \qquad (1)$$

Integrating along a tilting trough or crest line one gets:

$$p_0 - p_1 = \int_{z_0}^{z_1} \rho(g + U^2/R)dz + \int_{x_0}^{x_1} \rho(U\partial U/\partial x)dx \qquad (2)$$

At the trough line R is positive and at the crest line R is negative. In an upwind-tilting lee wave, $\partial U/\partial x < 0$ at the trough line and $\partial U/\partial x > 0$ at the crest line since that configuration requires greater wind speed in the downdraft areas than in the updraft areas. For a non-tilting lee wave, equation (1) reduces to:

$$\therefore\quad p_0 - p_1 = \int_{z_0}^{z_1} \rho(g + U^2/R)dz \qquad (3)$$

If a streamline in the lee wave is defined by $y = y(x)$, its slope is $y' = w/U$ and its curvature at a trough or crest is

$$1/R = y'' = (w/U)' = U^{-1}\,\partial w/\partial x - wU^{-2}\,\partial U/\partial x$$

But $w = 0$ at trough and crest lines so that $U^2/R = U\,\partial w/\partial x$. For periodic flow, $w = w_{max}\cos 2\pi x L^{-1}$ and

$$\partial w/\partial x = w_{max}\,2\pi L^{-1}(-\sin 2\pi x L^{-1})$$

At crests and troughs $x = L/4$ and $3L/4$, respectively. Then at the trough lines, $(\partial w/\partial x) = +\,w_{max}\,2\pi L^{-1}$ and at the crest lines,

$$(\partial w/\partial x) = -\,w_{max}\,2\pi L^{-1}.$$

A convenient form of equation (3) is:

$$(4) \qquad p_0 - p_1 = \int_{z_0}^{z_1} \rho g \, dz \pm \overline{\rho U w_{max}} \, 2\pi L^{-1} \Delta Z$$

where the plus sign applies at troughs and the minus sign at crests. This equation states that the difference in atmospheric pressure measured along a vertical between level z_0 and a higher level z_1 is equal to the hydrostatic pressure, i.e., the weight of air in the column of unit cross section, plus the integrated effect of the vertical centrifugal accelerations. It is apparent that the critical regions where both terms on the right side reach maximum values at any level are the troughs and crests of the vertical streamline pattern. Considering first the hydrostatic term, wherever the lapse rate is less than the adiabatic lapse rate, and assuming that the only temperature changes of air parcels in the wave flow are adiabatic, temperatures in the crest will be coldest and those in the troughs warmest at any level. This difference leads to a horizontal pressure gradient from trough to crest which in a non-tilting wave would increase with height. In the extreme case of an adiabatic lapse rate there would, of course, be no temperature difference and hence no hydrostatic pressure gradient from trough to crest. Near an inversion, on the other hand, such as is generally found in the roll cloud zone, the temperature difference from trough to crest is often of the order of 10°C. At the inflection points in the flow the hydrostatic pressures, temperatures, and D values should be representative of the mean or undisturbed flow.

Examining next the vertical acceleration term of equation (4), it is seen that the vertical accelerations in steady flow are greatest in the troughs and crests. The vertical centrifugal accelerations which are positive at the trough and negative at the crest, tend to make the air "heavier" at the trough and "lighter" at the crest and thus act to reduce the horizontal hydrostatic pressure gradients in lee waves.*

Integrating equation (1) along a constant level, one gets an equation relating the horizontal variation of pressure to the corresponding horizontal wind speed variation:

$$(5) \qquad p_{x_0} - p_{x_1} = \int_{x_0}^{x_1} \rho U \, \partial U/\partial x \, dx \approx \overline{\rho U} \, (U_{x_1} - U_{x_0})$$

which states that the horizontal wind speed increases in the direction of the horizontal pressure gradient and by an amount proportional to the magnitude of the pressure difference.

The following four examples taken from the 1951-2 cross sections illustrated the pressure fields in lee waves.

Example 1, D values and horizontal wind speed variations. At the 300 mb level in the lee wave cross section of 16 February 1952 (Fig. 3.28 and Table 3.1), the measured D values were lowest in the crest and highest in the troughs. This relationship is in general agreement with the observed acceleration of the wind from trough to crest and invites a computational check. Since the U field is more accurately measured, we can compute from equation (5) above the horizontal pressure gradient required for the

*This is not surprising, since it is the balance between hydrostatic and hydrodynamic forces which determines the flow characteristics.

observed acceleration of U. With reference to Table 3.1:

$\bar{\rho} = 0.47\ (10^{-3})$ ton m^{-3},

$\bar{U} = 26$ m s^{-1},

$\Delta U = +10$ m s^{-1} from 1st trough to 1st crest and -10 m s^{-1} from 1st crest to 2nd trough.

Then: $$p_{x_1} - p_{x_0} = -\bar{\rho}\,\bar{U}\,\Delta U = -(0.47)\ (10^{-3})\ (26)\ (\pm 10)$$

$$= \mp 0.12 \text{ cb} = \mp 1.2 \text{ mb}$$

At the 300 mb level a difference in pressure of 1.2 mb is equivalent to a difference in D of about 90 ft which, considering the degree of accuracy obtainable in measuring Z and Z_p, is in rather close agreement to the observed ΔD's of - 120 ft from 1st trough to 1st crest and + 80 ft from 1st crest to 2nd trough.

Example 2, comparison between observed and hydrostatic D values. If one considers the first run under the roll cloud on Flight 2018, 16 February 1952 (Fig. 3.28) and, for the points cited in Table 3.1 and the contemporary surface data from the (t,x')-sections (Figs. 4.1 and 4.3), computes their altitudes hydrostatically, the following results are obtained (there are no measurements from the troughs):

Time PST	Position	Z ft	D ft	D (hydrostatic) ft
1217	Downdraft	12,580	- 55	(+ 100)
1220	Crest	10,850	0	(+ 20)
1223	Updraft	11,180	- 110	(0)
1224	Updraft	13,330	- 40	(+ 60)

The absolute differences should not be compared because of possible absolute errors in T, Z_p, and Z measurements; rather, it is the relative differences within the two sets of D values that pertain to this discussion. In the hydrostatic D field, the value of + 20 ft at the crest is a near minimum with respect to points on either side. Since we are computing from the ground upward, this result is in agreement with the expectation of coldest mean temperatures and lowest hydrostatic heights of pressure surfaces in a non-tilting crest. In contrast to the hydrostatic D field, the D values measured directly from Z and Z_p show a relative maximum at the crest line. The conclusion suggested is that, in this case, the effect of the mean centrifugal acceleration at the crest line, within the layer between the ground and the points cited, acted in opposition to the hydrostatic effect and thereby reversed the pressure gradient between warm trough and cold crest.

Example 3, the D field in the vertical plane. In order to assess the magnitude of the hydrostatic and non-hydrostatic contributions to the pressure field in a strong lee wave, computations were performed on the data from the case of 18 March 1952 treated earlier in Chapter 4. Using the θ field analyzed from the meteorogram at 0800 PST (Fig. 4.16) and the surface pressures at the same time (Fig. 4.17), several soundings along x' were plotted and the D values in the vertical plane were computed; the resultant analysis is shown in Fig. 9.2. Comparing this D pattern with the θ pattern of Fig. 4.16, one sees that the maximum hydrostatic pressure (D value) at levels between 700 and 500 mb is found in the trough and the minimum hydrostatic pressure (D value) is found at the crest as expected. At the 500 mb level the hydrostatic D gradient from the trough (where D = + 60 ft), to the crest (where D = - 210 ft) is equivalent to -270 ft (-5.8 mb) in 30,000 ft (9 km) horizontal distance.

Although no winds were measured on the meteorogram flight of 18 March, it is possible to estimate the values of U from the Bishop pibal (Fig. 4.13) and the values of w from the up-and downdrafts encountered by both the powered aircraft and the sailplane. The wave length and density distribution are known from the analyzed θ field. Considering now just the vertical acceleration (centrifugal) term in equation (4), the following conservative values apply to the layer between 700 and 500 mb:

$\bar{\rho}$ = 0.785 (10^{-3}) ton m^{-3} at the trough and

0.814 (10^{-3}) ton m^{-3} at the crest

$\bar{U}$ = 30 m s^{-1}

$\overline{w_{max}}$ = ± 3,000 ft min^{-1} ≅ 16 m s^{-1} at inflection points

L = 16 km

Δz = 2,606 m at the trough and 2,521 m at the crest

Letting $\Delta p = \int_{z_{70}}^{z_{50}} \rho \, U \, w_{max} \, 2\pi L^{-1} \, \Delta z$, we get

at the trough Δp = + (0.785) (10^{-3}) (30) (16) (2π) (1/16) (10^{-3})(2,606)

= + 0.39 cb = + 3.9 mb

at the crest Δp = - (0.814) (10^{-3}) (30) (16)(2π)(1/16)(10^{-3})(2,521)

= - 0.39 cb = - 3.9 mb

At the middle of this layer, near 600 mb, Δp of 3.9 mb corresponds to approximately 150 ft in ΔZ_p. Thus the thickness of the 700 to 500 mb layer increases from trough to crest by about 300 ft (ΔD = + 300 ft) due to centrifugal forces only.* Now, in the hydrostatic D field (Fig. 9.2),

*One could now recompute Δp using corrected values of Δz but this refinement would still result in a relative correction of 300 ft.

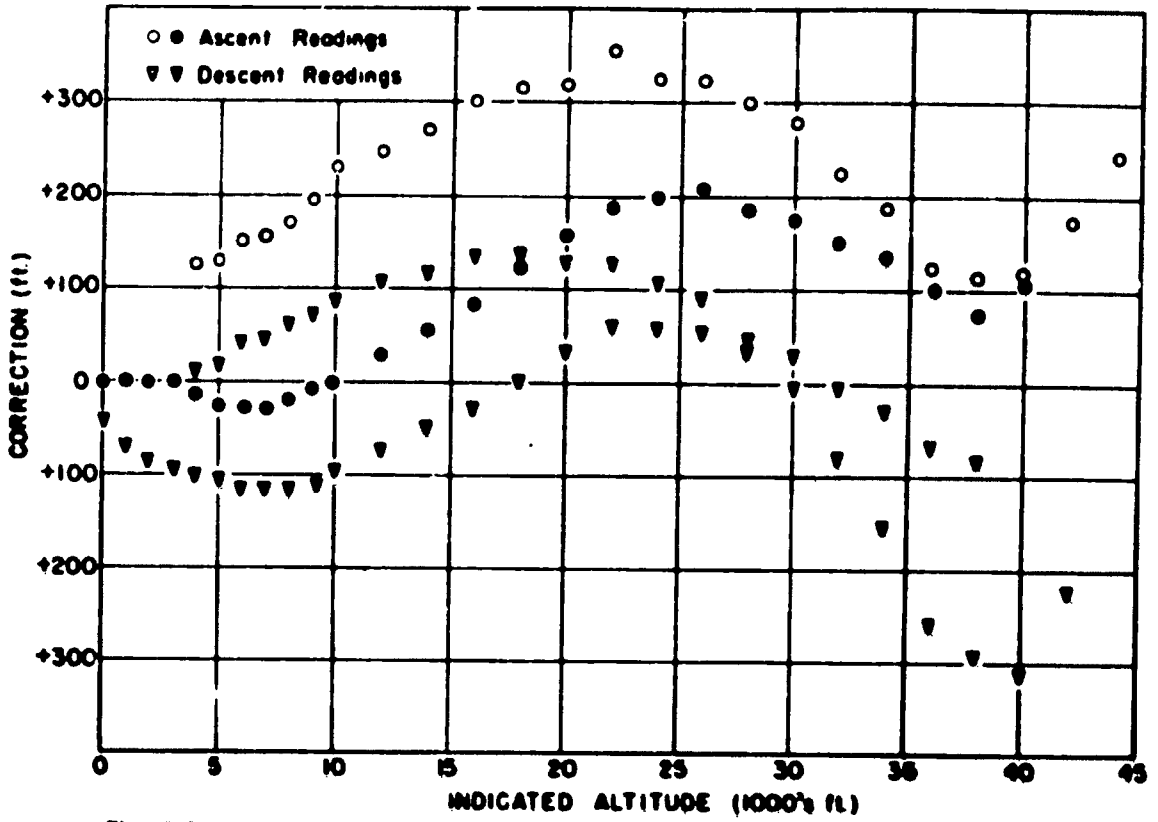
Ascent Readings
Descent Readings
+300
+200
+100
0
+100
+200
+300
CORRECTION (ft.)
0
5
10
15
20
25
30
35
40
45
INDICATED ALTITUDE (1000's ft.)

Fig. 9.1

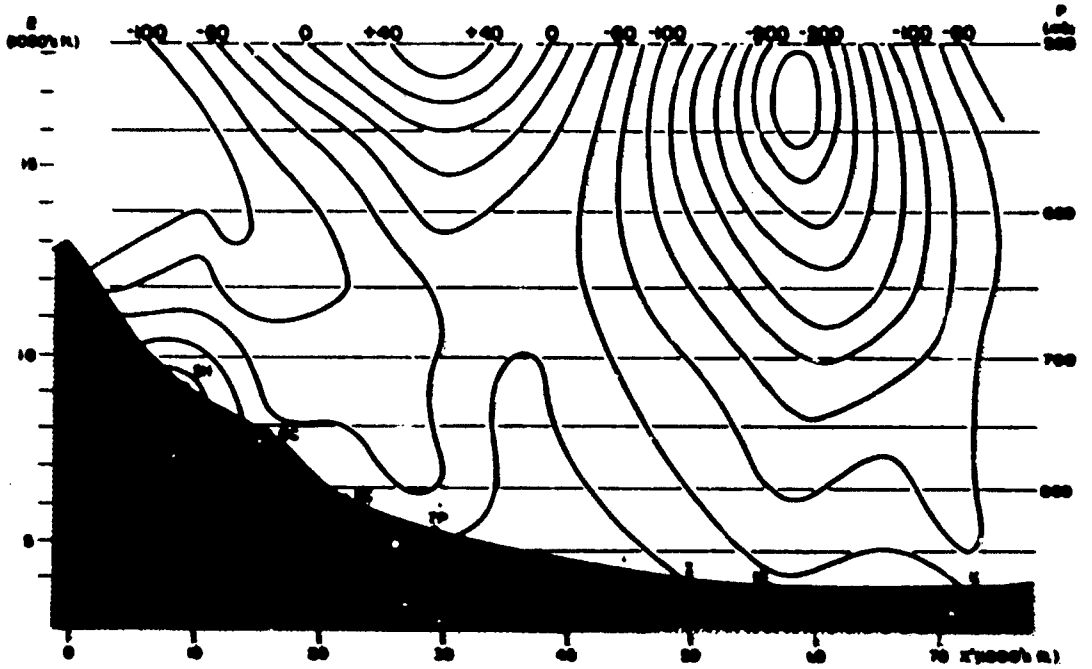

Fig. 9.2

in the trough $D_{50} - D_{70} = + 60 - (-50) = + 110$ ft and in the crest $D_{50} - D_{70} = - 210 - (-120) = - 90$ ft. Thus the thickness of the layer decreases from trough to crest by 200 ft due to hydrostatic effects only ($\Delta D = - 200$ ft) and appears to be overcompensated by the hydrodynamical effects ($\Delta D = + 300$ ft). This result is in agreement with the pattern of wind speeds and actual D values measured in the lower troposphere of the strong lee wave of 16 February 1952 as shown in Table 3.1, and in Example 2 above.

Example 4, the pressure field across the Sierra. If one considers the potential temperature cross section over the Sierra at 1000 PST on 18 December 1951 (Fig. 3.11) and computes hydrostatic pressure-height values along the verticals above BC (through the trough) and M (through the crest), the following results are obtained for comparison with the radiosonde data at LP:

p	Hydrostatic D (ft)		
(mb)	LP (6,760 ft)	BC (6,166 ft)	M (3,830 ft)
	(Windward slope)	(Lee trough)	(Lee crest)
Sfc	+ 210	- 80	- 40
800	+ 240	- 80	- 70
700	+ 220	- 40	- 110
600	+ 230	+ 80	- 150
500	+ 270	+ 250	- 170
400	+ 360	+ 470	- 100
300	-----	+ 660	0

From this table it can be seen that the hydrostatic pressure gradient (difference in D value) across the Sierra is greatest at the surface and decreases with height, apparently reversing itself slightly above 500 mb. On the other hand, the difference in D value from trough to crest is least near the surface and the hydrostatic gradient of D from trough to crest increases with height.

To obtain a rough estimate of the total effect of the vertical accelerations of the streamline field in the layer from 800 to 300 mb, and recalling the large vertical speeds encountered by aircraft on that day, the following calculation is made:

$$\Delta p = \pm \bar{\rho}\, \bar{U}\, \overline{w_{max}}\, 2\pi L^{-1}\, \Delta z$$

$$= \pm (0.75)(10^{-3})(30)(10)(2\pi)(1.15)(10^{-3})(7{,}200)$$

$$= \pm 0.64 \text{ cb} = \pm 6.4 \text{ mb}$$

At 300 mb, 6.4 mb corresponds to 475 ft in D but in applying this Δp to the entire layer one must use the average height difference or that for about 500 mb which is 320 ft. Subtracting 320 ft from the hydrostatic height of the 300 mb surface over EC (trough) and adding 320 ft to the hydrostatic height of the 300 mb surface over M (crest), it can be seen that the total difference of 640 ft nearly equals the fictitious hydrostatic gradient of 660 ft from trough to crest at the 300 mb level. The same argument holds for any other layer and isobaric surface in the lee wave. Again we find the compensation between hydrostatic and hydrodynamic pressures.

Palm (1955) computed the pressure field due to resonance waves and found a nodal surface near the level of maximum streamline amplitude; above that level there was a pressure gradient from trough to crest but at the surface the lowest pressure was under the trough and the highest pressure was under the crest. The observations of 16 February 1952 (Examples 1. and 2. above) and 18 March 1952 (Example 3. above and Fig. 4.18) are in agreement with Palm's theoretical model.

Altimeter errors and aircraft flights over mountains.

One of the most dramatic myths about the Sierra Wave is that concerning large altimeter errors of the order of 1,000 or even 2,000 feet associated with the disturbed air flow near the mountains. The alleged facts, widely circulated and widely believed, are based upon the stories of pilots who have flown in strong mountain waves and who have indeed noted significant differences between their altimeter reading and their apparent altitude. Without doubting the honesty of these men--but with, perhaps, a wink at their enviable ability to spin a good yarn before a credulous audience--project experience suggests that these "errors" are either real instrumental or principle errors or, in some cases, discrepancies caused by optical illusion. Listed in order of importance, reported altimeter errors in the Sierra Wave may be due to any of the following:

1. Large principle errors, particularly in air much colder than the Standard Atmosphere and with an altimeter setting that is too high for the region. In Table 9.1 the maximum altimeter correction at an altitude of 15,000 ft, near the crest of the Sierra, is of the order of 1,000 ft, half of which is density error. Pressure datum (altimeter setting) errors, generally minimized by experienced pilots, become important where surface pressure falls rapidly during a flight. (See examples 2. and 3. at the end of the section on the pressure altimeter in this chapter.)

2. A combination of large instrument errors--particularly diaphragm and hysteresis errors--in the altimeter used and operational errors, including static system. (See Table 9.1 and example 1. of the first section of this chapter.)

3. An upwind approach to the Sierra in which the pilot glances at his altimeter when near the trough of the wave just prior to encountering a 3,000 or 4,000 ft per min downdraft, and one minute later finds the aircraft approaching the mountain side at an altitude obviously 3,000 or 4,000 feet lower than intended. (If he were not so busy at the instant of

comprehending this danger and had time to look at his altimeter, it would, in all probability, verify the unpleasant fact.)

4. An optical illusion caused by either the lack of a level horizon when flying under clouds in mountainous terrain or by a looming effect caused by refraction of light by a temperature inversion near the level of the mountain crest.

As for errors caused by the vertical accelerations in the lee wave, the computations and measurements indicate that these effects are smaller than the hysteresis errors and are therefore generally undetectable. It should be pointed out that in the non-steady flow of certain strong mountain waves, there are probably large vertical accelerations of short duration, but in such instances the associated turbulence is by far the greater hazard and concern over the slight effect on the altimeter reading is irrelevant.

The "one minute later effect" (3. above) may be the real Lorelei of the mountain wave for pilots. Often the downdraft is so smooth as to be hardly perceptible if one were not watching either instruments or terrain; the aircraft is simply pushed rapidly and steadily toward the ground. The strong downdraft coincides with strong horizontal wind speeds, which means that a lee wave with a downdraft of 4,000 ft per min may have four times the effect as one with a downdraft of 2,000 ft per min on an aircraft flying upwind, since it will require twice as much time to traverse the dangerous area. Also, the total loss of altitude will be even greater if the aircraft approaches the mountain range obliquely and will be at a maximum when flying parallel to the range along the downdraft area. The result of a minute's inattention and reliance on the automatic pilot in such conditions can be as catastrophic as falling asleep while driving an automobile.

References.

Determination of Absolute Height and Wind for Aircraft Operations (1944). Prepared by the Weather Division, Headquarters Army Air Forces, C4-7408, AF. ("Restricted")

Holmboe, J., Forsythe, G., and Gustin, W. (1945): Dynamic Meteorology, New York: John Wiley & Sons, Chapter 4, pp. 81-124.

Palm, E. (1955): Multiple Layer Mountain Wave Models with Constant Stability and Shear, Scientific Report No. 3, Autobarotropic Flow Project, Meteorology Department, University of California at Los Angeles Contract No. AF 19(604)-728.

Report of the OPS/ENG Study Group (1953), International Air Transport Association. (DOV OPS/2062).

---

*See Chapter 10, Fig. 10.4.

10. [illegible] TURBULENCE

It is well known among glider pilots that a combination of severe turbulence in certain flow sections with unusual smoothness in others is typical of the mountain wave. In general, the distribution of these flow regimes is made visible in the cloud formations; the cumulus or fracto-cumulus type roll clouds representing the lower turbulent layer, the lenticular type altocumulus or cirrus clouds depicting the smooth upper wave flow. Occasionally, but quite rarely, a high layer of slight to severe turbulence has been found in the neighborhood of the tropopause. A case of this sort of high level turbulence is described below. The more typical arrangement is as follows:

Lower turbulence zone

The smooth wave flow of the upper troposphere "rests" on a turbulent air mass originating downwind of the mountain range close to the ground and probably directly connected with the stable* air mass falling from the "cap cloud" ("föhn mauer" over the mountain crests) down the lee slope. The "cloud fall" which makes this gravitational descent impressively visible is not always present, depending on the humidity conditions. Its smooth contours are deceiving. It has been found impossible to control an aircraft venturing into this flow. In view of the hazards connected with the turbulent low level flow, very little is known on details of the flow characteristics close to and below the mountain crests. A few miles farther downwind, the so-called "rotor flow" has been better explored, and it is there where most encounters with severe turbulence have been made.

As discussed in an earlier section, the "rotor flow" owes its name to the fact that winds in its lower parts are either weak or reversed. This, however, is only an average statement. A streamline flow does not seem to exist in the rotor area. The air mass under and in the roll cloud is in a state of continuous mixing, the highest degree of turbulence being encountered at the leading edge of the roll cloud at about the level of the mountain crests.

Unfortunately, most of the glider tows have to penetrate upwind through the rotor flow in order to reach the wave updraft ahead of the roll cloud, putting an enormous strain on equipment and crews. Much involuntary experience has been collected in this way on the characteristics and magnitude of turbulence under and ahead of the main roll cloud whose base in the Sierra Nevada is generally found at crest level (4 km ± 1 km) and whose tops vary from 5 to 7 km with an observed maximum of 9 km (30,000 ft).

The type of turbulence encountered in the rotor flow differs from that

---

*The air mass is "stable" in the sense that it is generally covered by a more or less thin boundary layer of great potential stability, while internally, the air mass may be unstratified due to mixing.

of thermal convection and is best described by the following excerpt of flight report 2007 from 18 December 1951 by L. Edgar, research pilot of the Mountain Wave Project in sailplane P-R:

> The turbulence became more severe as we progressed under the roll cloud. It was not possible to keep the sailplane in level flight attitude even with full controls being applied. The magnitude of the vertical change of the position between the two aircraft was very great. The rate at which these changes occurred was amazing. Too, the distances between the two aircraft would change with no apparent change in speed or attitude. The towplane would suddenly loom larger and we would be rapidly overtaking it with the sailplane.
>
> This became quite disconcerting as on one occasion, when we had overtaken the towplane, the BT raised very suddenly and turned a little across our path. We were now looking up at the towplane at about a 25 or 30 degree angle with a large loop of slack tow line coming toward the sailplane. The rope came back across the top of the left wing, over the canopy and then the right wing.
>
> Before I could release, the rope was yanked off the top of the sailplane. The slack was then taken out of the line and there appeared to be no damage done.
>
> We released under the roll cloud when the tow plane dropped, pitched forward and disappeared from sight. The release was made before the tow rope could become tight and jerk the nose of the sailplane. The time was 14:48 and altitude 11,000 feet. The maximum accelerometer readings on tow were found under the roll cloud with a = +5 and -2 G.
>
> The towplane came along beside us. To have the towplane flying beside us off to our right, really gave us a picture as to what was going on. We would suddenly rise and the tow plane would drop out of sight. Soon the towplane would come back up and we would be on our way down. It reminded me of two elevators operating side by side.

Most characteristic for this type of turbulence are the horizontal gusts. They affect the aircraft's airspeed in a disturbing way, quite different from the well known convective turbulence. This is, however, not surprising since the rotor flow is always connected with strong horizontal winds approaching jet stream conditions. Maximal vertical accelerations during tow in the rotor zone, as read from the sailplane's accelerometer exceeded 7 G, a value not very reliable in view of possible over-shooting of the instrument needle.

A more accurate record of rotor turbulence has been obtained by the flight analyzer of the B-29 during the joint operation of the Jet Stream and Mountain Wave Projects in 1955. The case in question (1 April) was a powerful mountain wave with average turbulence in the lower levels. The aircraft was circling over Bishop about 15 miles downwind of the Sierra crest at 5.3 km high in the general area of the rotor zone. As Fig. 10.1 reveals, vertical gust velocities of 30ft/sec (or more) occurred 13 times within 50 seconds, the maximum being 69 ft/sec negative. These are derived gust velocities according to the present NACA formula which takes gust gradients (rather than sharp edge

gusts) into account.

While these surprisingly high values represent only the average conditions to be found beneath mountain waves, a certain critical arrangement of the rotor flow (which is, fortunately, rare) displays a turbulence of destructive magnitude. It can be recognized by the following characteristics:

(1) Roll cloud: Deep with tops unusually high, exceeding considerably the tops of the cap cloud over the mountains. [In the Sierra Nevada 30,000 ft (9 km) have been observed.]

(2) Leading edge of the rotor cloud system: Unusually far downwind. (In the Sierra Nevada 15 miles distance from the crests have been observed.)

(3) Hurricane force surface winds between mountain range and rotor zone carrying dust into the roll cloud.

(4) Straight leading edge of the roll cloud not following the bends of the mountain range and great lateral extension. (In the Sierra Nevada roll clouds of more than 150 mile lateral extension have been observed.)

(5) Rotor cloud extending far downwind without periodicity.

(6) Turbulence concentrated in small cloud puffs ahead of the roll cloud's leading edge.

These conditions were fulfilled, for example, on 25 April 1955 when both project gliders ran into excessive turbulence between 13,000 and 14,000 feet while penetrating the described small cloud puffs at the leading edge of the roll cloud. Over the town of Bishop horizontal gusts of about 90 ft/sec were measured while 5 miles farther south the project glider P-2 (designed for 10 1/2 G) was destroyed by gusts estimated at 120 ft/sec. Excerpts of the two flight reports may illustrate this experience:

From flight report #5015 A, J. Huettner in Schweizer 2-25 sailplane:

> After a plus 4G,- 3G acceleration I tried to take speed back to 45 mph, but in spite of the "nose up attitude" speed increased rapidly to 80 mph and turbulence became so severe that I lost control. This happened when small cloud puffs formed around my ship in front of the main roll cloud. I had no other choice than to penetrate between them while trying to descend below the base of the huge roll cloud.
>
> After encountering 1000 ft/min down and 1600 ft/min up in close succession, a second cloud puff gave me an even worse experience and the speed, due to a horizontal gust, exceeded 90 mph, nose up, with an acceleration of the order of 4G. The aircraft lost control due to a "high speed stall."

From flight report #5015 B, L. Edgar in Pratt-Read sailplane:

> The flight path went into the very top of the little cloud puff. It seemed to swell up before the nose in the last moment.

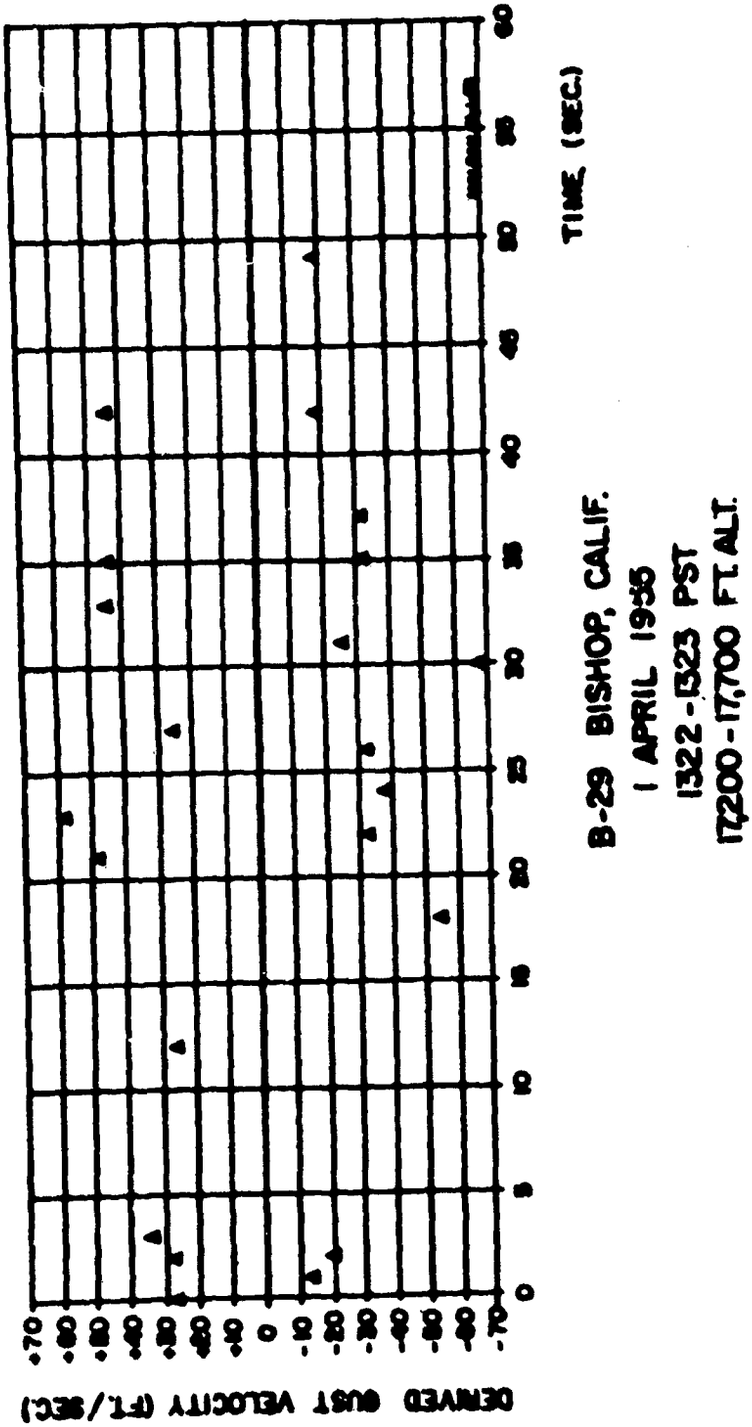

Fig. 10.1 - (Prepared by the Air Force Cambridge Research Center)

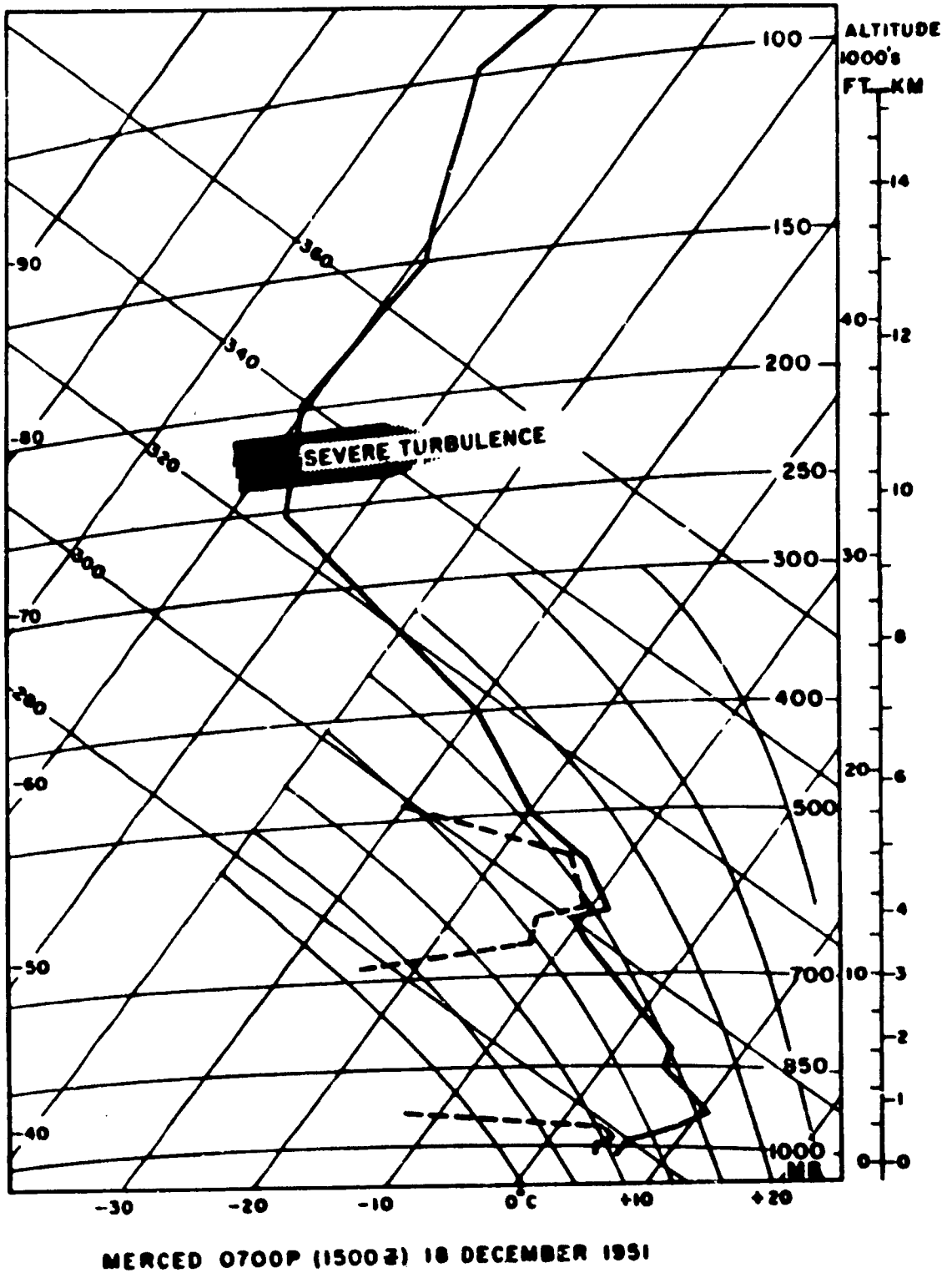

MERCED 0700P (1500Z) 18 DECEMBER 1951

Fig. 10.2 - (Prepared by the Air Force Cambridge Research Center)

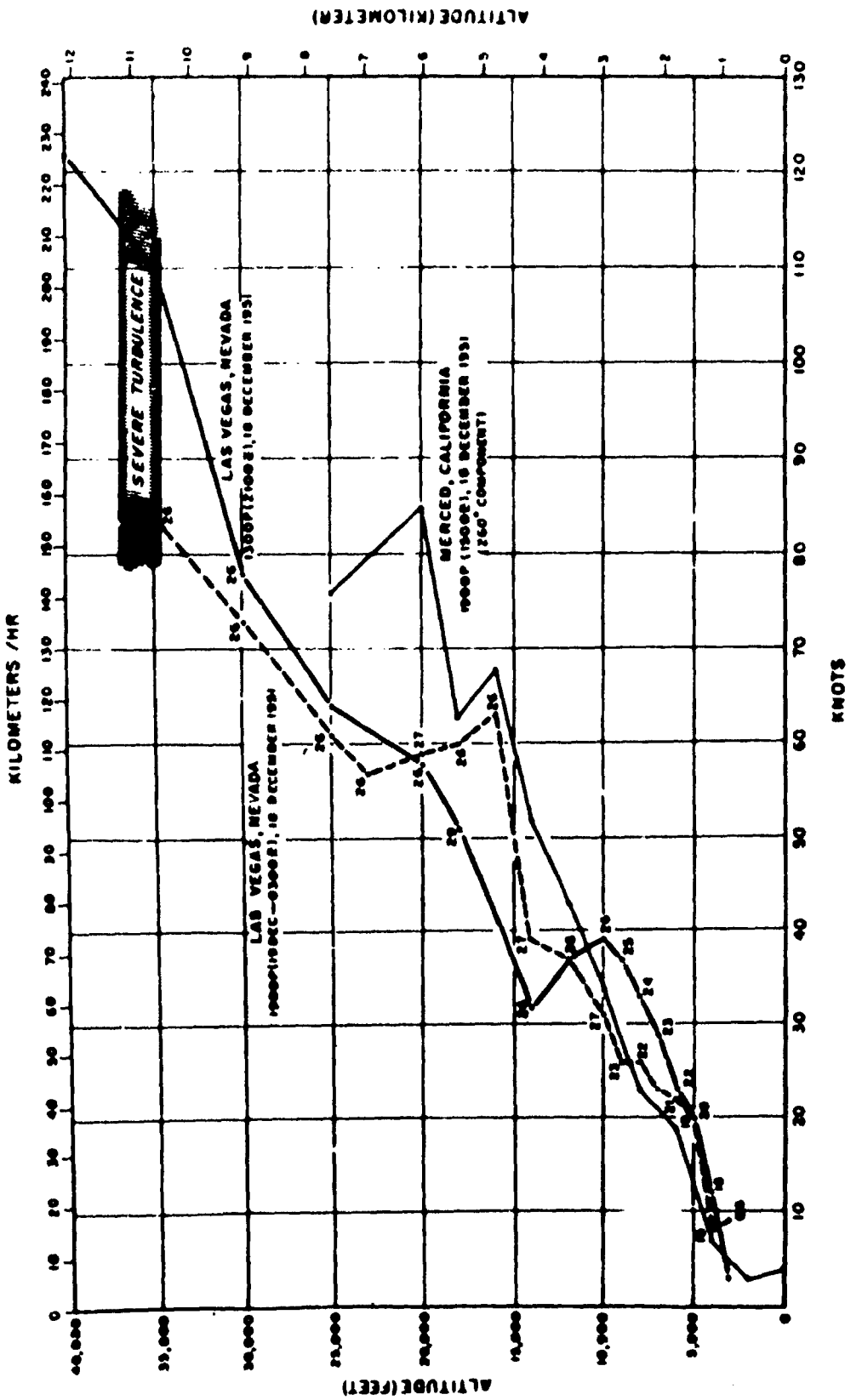

Fig. 10.3 - (Prepared by the Air Force Cambridge Research Center)

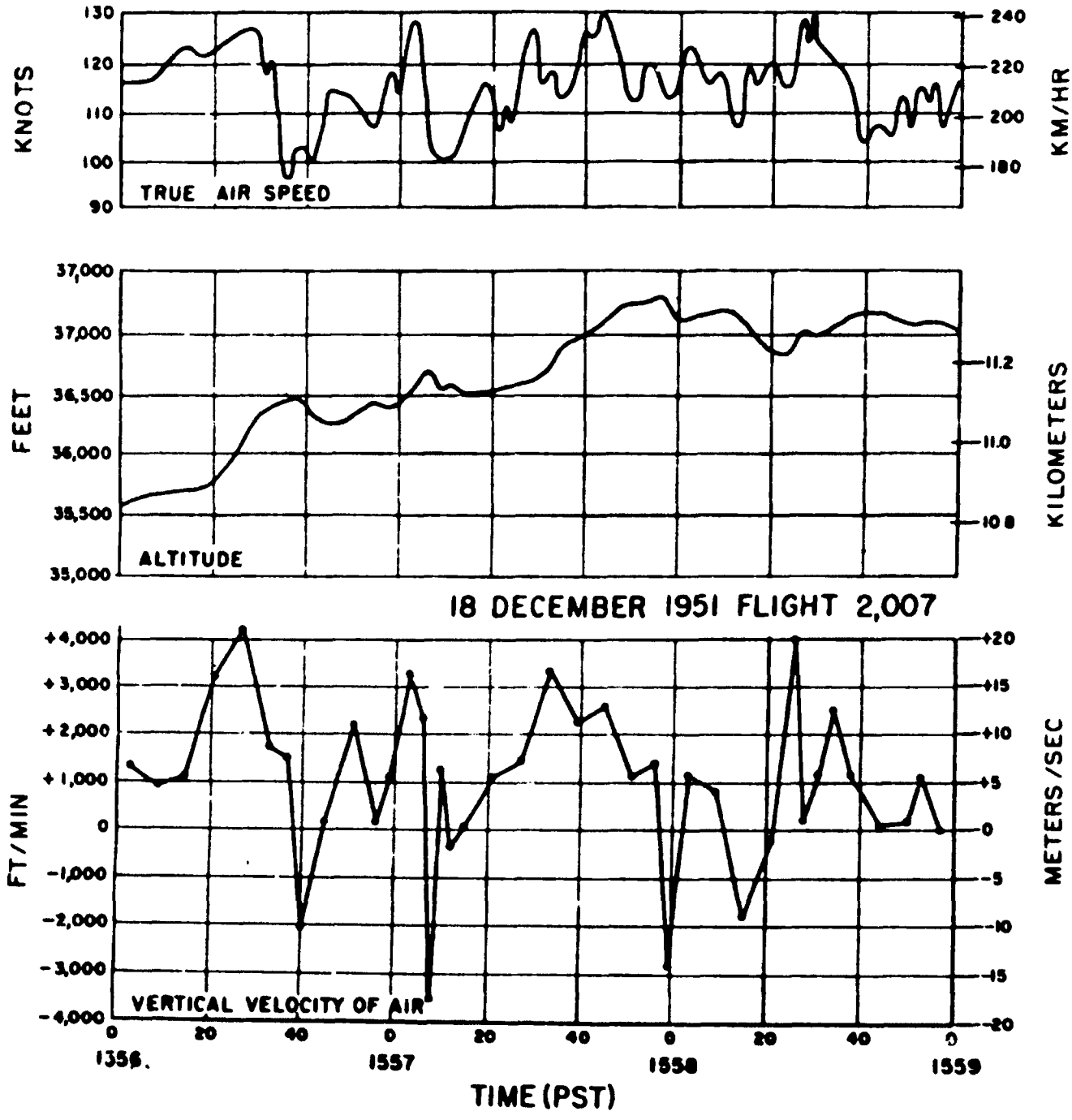

Fig. 10.4 - (Prepared by the Air Force Cambridge Research Center)

I looked at the needle and ball. Suddenly and instantaneously the needle went off center. I followed with correction but it swung violently the other way. The shearing action was terrific. I was forced sideways in my seat, first to the left, then to the right. At the same time when this shearing force shoved me to the right, a fantastic positive G load shoved me down into the seat. This positive load continued. Just as I was blacking out, it felt like a violent roll to the left with a loud explosion followed instantaneously with a violent negative G load.

I was unable to see after blacking out from the positive G load. However, I was conscious and I felt my head hit the canopy with the negative load. There was a lot of noise and I felt like I was taking quite a beating at this time. I was too stunned to make any attempt to bail out.

Just as suddenly as all of this violence started, it became quiet except for the sound of the wind whistling by. I felt I was falling free of all wreckage except something holding both feet.

It is unlikely that aircraft can be designed strong enough to withstand these excessive loads. Like boats staying away from the Niagara Falls, the remedy for aircraft is to avoid flights into the rotor zone when the critical signals are up.

Upper turbulence zone

It has been mentioned above that the air flow in the mountain wave above the rotor flow is laminar and exceptionally smooth. This is generally true for altitudes as high as the lower stratosphere. Frequently, the tropopause is perceptible by a very slight rocking motion of the sailplane resembling a boat drifting in a light summer breeze.

Occasionally, however, severe turbulence is again encountered at levels above 10 km. This is especially true if the jet stream core is close and the temperature sounding shows the typical gradual transition between tropospheric and stratospheric lapse rate (Fig. 10.2). It is not clear at the present time what the mechanism of this turbulence is and whether or not the strongly negative vertical shear gradient on top of the jet stream core is involved. An example may illustrate this phenomenon.

On 18 December 1951 a strong mountain wave allowed the sailplanes to reach 42,000 feet. The vertical temperature and wind soundings (Figs. 10.2 and 10.3) indicate the closeness of the jet stream core with winds reaching 125 knots at 40,000 ft. In the stable transition layer between troposphere and stratosphere extending roughly from 33,000 to 38,000 ft (10 to 11.5 km) turbulence of unusual features and magnitude was encountered. Fig. 10.4 shows the vertical motions of air within 3 minutes of flight time (lower diagram). Up and downcurrents of 3,000 to 4,000 ft/min alternate in close succession reaching at one point a total amplitude of 7,000 ft/min (35m/sec) within 5 seconds* of flight

*These are carefully evaluated mean values over several seconds and are not to be interpreted in terms of accelerations which, generally, cover shorter intervals and cannot be evaluated from altitude records.

time. The corresponding altitude (center curve) is close to 37,000 ft. That it is impossible to keep airspeed constant under such conditions is evident from the record of the P-R sailplane (upper curve), the variations reaching 30 knots. In agreement with the pilot's impression, the diagram seems to indicate the existence of very large eddies or turbulence elements which, if drifting in the wind, should have a characteristic size of about 2 km (or 40 seconds flight time). Maximum indicated accelerations were +4G/-2G. The corresponding (true) "derived gust velocities" again exceed 100 ft/sec. Height and structure of this type of turbulence may represent a serious hazard to modern aircraft which cross mountain ranges close to the jet stream core and the tropopause. Not enough experience has been collected so far to allow a generalization of this observation.

Note: The sailplane's flight characteristics are: Wingloading: 58 lbs/sq ft
Aspect ratio: 13

References.

Kuettner, J. (1952): A Note on High Level Turbulence Encountered by a Glider. Air Force Survey in Geophysics No. 29.

11. FLIGHT HAZARDS OF THE MOUNTAIN WAVE

It must be clear by now that the combined phenomenon of wave and rotor flow presents serious hazards to aviation. In the order of severity these hazards are:

a. Downdrafts
b. Turbulence
c. Local change of upper winds
d. Altimeter errors

While each of these flow characteristics has been discussed at some point in this report, a separate treatment from a pilot's viewpoint appears appropriate. The history of aviation is replete with disasters of aircraft in mountainous terrain. Many of these accidents have been listed as "pilot's error" for lack of better explanation. The more probable interpretation is that the relatively rare case of a very powerful mountain wave has been encountered by an experienced pilot for the first (and last) time.

The significance of the four hazards listed above will now be discussed, first separately, then in their critical combination.

a. Downdrafts

The more important locations of severe downdrafts are over the lee slope of the mountain range and on the downwind side of the rotor cloud (Fig. 3.28). They are separated by an area of strong updrafts near the leading edge of the roll cloud. The two main downdrafts are about 5 to 10 miles apart. Here, 2,000 ft/min down are rather usual variometer readings while in severe cases 3,000 to 5,000 ft/min have been observed. These high values are centered around the height of the mountain crests. Very few airplanes can match such downdrafts with full power. Any length of time spent in the wide downdraft areas will inevitably bring the aircraft down into the layer of severe turbulence (See b.) and into close proximity to the mountains. This is especially true if airspeed is kept constant.

Things are not less critical if the pilot tries to remain on the assigned flight level or if the aircraft is on altitude controlled autopilot. Fig. 6.13 shows an attempt of the Jet Stream Project's B-29 to traverse the powerful mountain wave of 1 April 1955 at 20,000 ft (=6km) against headwinds. Intentionally, the pilot, Capt. Doud, did not change throttle settings and the autopilot corrected automatically for loss of altitude by change of attitude. As a consequence, the aircraft lost speed at a dangerous rate and approached stalling. This occurred in the very smooth wave flow where such happenings may go unnoticed. Actually, the autopilot was not able to keep altitude constant and over 500 feet were lost in 2 minutes. Any further loss of altitude could have brought the slowly-flying aircraft into the turbulent rotor zone where a flight with marginal airspeed may become critical. In this particular case the total variation of true airspeed amounted to about 120 knots, part of which is, however, due to a rapid variation in horizontal wind speed (See c.).

5. Turbulence

Chapter 10 has dealt with this matter from a meteorological standpoint. From a pilot's outlook it is important to realize that this type of clear air turbulence compares with the most severe in-cloud-turbulence encountered in thunderstorms.

At the present time, the specific characteristics of air flow and synoptic weather situation causing heavy turbulence are not well enough understood to permit reliable forecasts. As a consequence, the pilot must be aware of impending danger in every strong mountain wave. He has to follow certain rules which will be discussed at the end of this chapter.

As described in the foregoing chapter there may be two distinct layers of turbulence downwind of a mountain range under wave conditions. With rare exceptions, the lower one is always present in a more or less dangerous form, reaching from the ground to above the mountain crest level. An aircraft flying (according to present safety rules) at 2,000 feet above mountain top will, in the majority of cases, run into this turbulence zone at some point since the top of the rotor flow exceeds the height of the mountain range considerably. The encounter with this turbulence is quite sudden, after smooth flight, and if passengers have not fastened seat belts in time, there may be injuries aboard.

Besides this discomfort to crew and passengers, control of the aircraft in instrument flight is quite difficult and, in severe cases, impossible. Even structural failure may result as indicated by the accident described in the foregoing chapter. Vertical and horizontal gusts may combine in such a way as to cause G loads beyond the ultimate load factor This is especially true if a high speed aircraft flies with tail wind into the roll cloud. The cases of excessive turbulence are rare and can be identified at the present time only from direct observations at the particular locality.

Some of the visible characteristics are described in the foregoing chapter. The most impressive of these is a very high top of the stationary roll cloud (cumulus, cumulus congestus or fractocumulus, in contrast to the smooth upper lenticular clouds). If this cloud cannot be cleared no attempt should be made to cross the mountain range at this specific point. Some air disasters have been definitely identified with an attempt of the pilot to continue flight through marked roll clouds at insufficient height. The safest flight level from a viewpoint of turbulence is about 25,000 feet. It should be realized that even mountain ranges of less than 5,000 ft height may cause a dangerous degree of turbulence.

A so-called "dry wave" which does not give warnings by visible cloud features may be almost as critical as the "obscured wave" which is hidden in a deep overcast possibly containing precipitation and icing.

The upper level of turbulence is in all probability connected with the existence of a jet stream over mountainous terrain. As described in the foregoing section, this type of turbulence may, in rare cases, be of destructive force, reaching vertical and horizontal gusts of 4,000 ft/ min. (See Fig. 10.4) Flights across extended mountain ranges close to the jet stream core and the tropopause (that is, between 30,000 and 45,000 ft) have a certain chance to encounter heavy clear air turbulence. The usual high level turbulence is sometimes compared to cobblestone driving; this specific

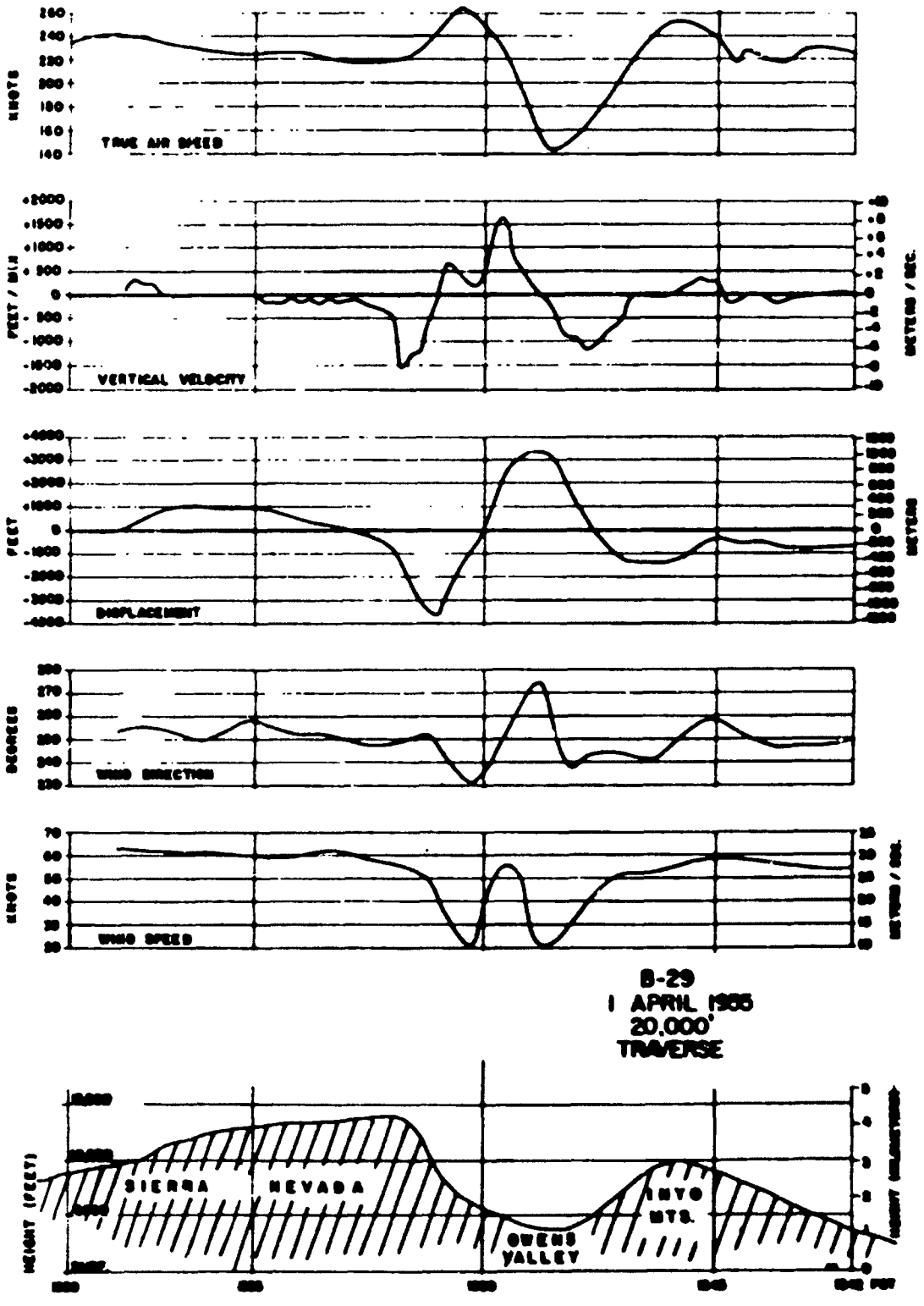

Fig. 11.1 - (Prepared by the Air Force Cambridge Research Center)

turbulence "feels" different, namely, like riding on powerful eddies of a mile in diameter. Not enough observations exist to establish reliable criteria for this phenomenon which, however, is relatively rare compared to the aforementioned low level turbulence. Again a flight level around 25,000 feet is recommended.

c. Local variations of upper level winds.

Strong, but gradual changes of wind directions and speed have been observed over horizontal distances of 10 miles or less. They may be due to a vertical variation of the wave pattern, or to lateral irregularities of the mountain range. There is also indication from glider flights that a jet-like increase of wind velocity occurs at certain levels leeward of mountain ranges. The implications for aviation are obvious:

1. Position errors may follow from the erroneous use of the last wind determination.

2. Prolonged stay in downdraft areas due to excessive head winds may cause rapid loss of altitude.

3. The airspeed may drop to undesirable values in suddenly diminishing head winds.

Position errors of the kind mentioned under (1) have been definitely responsible for let-downs into mountain peaks.

Loss of ground speed in downdraft areas, according to (2), will bring the aircraft down into close proximity to the mountain range. If the wave crests tilt upwind with height (this is the common arrangement), strong winds will coincide with downdrafts.

Loss of airspeed according to (3) may be critical* if the aircraft is already slowing down to keep altitude in downdraft areas (see a. of this chapter). The curves of Fig. 11.3 give a more detailed analysis of the airspeed variations depicted in Fig. 6.13. The aircraft approaches the Sierra Nevada from right to left (see lower cross section) at 20,000 feet against headwinds of 50 to 60 knots. On passing into the Owens Valley the winds diminish rapidly (lowest curve) to about 20 knots and turn 35 degrees towards the right (second curve from bottom). While the headwind component drops almost 40 knots in less than 2 minutes of flight time, the aircraft begins to enter downdrafts of over 1,000 ft/min (second curve from top) slowing down further through the action of the autopilot. This combined effect of wind decrease and downdrafts causes the airspeed to drop over 100 knots until stalling speed is almost reached (upper curve). When entering the updraft portion of the lee wave with over 1,500 ft/min up, winds increase in less than one minute of flight time by 35 knots and turn rapidly to the left. This combination raises the true airspeed about 100 knots in one minute. Further gain is counteracted by another rapid drop in head winds, but the total variation of true airspeed amounts to 120 knots. Although the main downdraft over the mountain slope with 1,500 ft/min vertical velocy is subsequently entered (second and third curves from top) the drop in airspeed is far less than

*The adaptation of modern aircraft to horizontal wind variations (in contrast to vertical drafts) is very slow.

before since headwinds increase again by about 40 knots. Also some altitude reserve had been gained in the updraft which is now sacrificed, thus counteracting the loss in airspeed. In this particular case total wind variations reached about 45 degrees in direction and 40 knots in speed, which is a large fraction of the undisturbed wind (60 knots) at this level. The case is probably not unusual, but it is the first time that lee winds could be recorded and reported in this detail. Since there is sometimes no warning by turbulence of the rapid changes in air flow, only the dials on the instrument panel and the slowly changing noise of the engines may indicate to a pilot that something unusual is happening. Sudden loss of control may easily follow from such a situation.

It should not go unmentioned that a pilot crossing mountainous terrain cannot put too much faith in the measured winds supplied to him by the meteorologist. It is obvious from Fig. 11.1 that a rawin or pibal released in the mountains will give entirely different wind values depending upon whether it crosses a given level 5 or 10 miles farther downwind from the mountain ranges.

d. Altimeter errors.

A more detailed discussion of altimeter errors in air flow over mountains is found in Chapter 9. As shown there, earlier claims that altimeter errors may reach 1,000 to 2,000 feet in certain sections of the mountain wave have not been confirmed by this project's flights. However, it must be realized that in the maximum updraft area where gliders spend most of their flight time, dynamic pressure deviations are expected to be at a minimum.

It should be quite clear to the pilot that the "normal" D-value (difference between true altitude and the pressure altitude which is indicated by the altimeter, based on the standard atmosphere) is not a specialty of the mountains but a temperature effect of the air mass in which he is flying and that in winterly weather his altimeter is generally indicating higher than the aircraft is flying. For lack of comparison this may not occur to him until he is faced with a mountain peak of a given altitude. This is not the type of altimeter "error" under discussion. It is common knowledge that our altimeters are measuring pressure, not altitude.

It is the local deviation from this "normal" D-value which may be termed "altimeter error" due to a mountain wave. As discussed in Chapter 9, this pressure disturbance is composed of static and dynamic components; the first being due to the complicated temperature field of the wave pattern throughout the atmosphere, the other due to inertia forces such as centrifugal forces on a curved streamline. Both components tend to compensate each other and the total altimeter error in a mountain wave does not seem to exceed the order of several hundred feet. This has to be added (or subtracted according to the sign) to the "normal" seasonal D-value and may, in extreme cases, reach a maximum total of 1,000 feet, the major part of which is probably not due to the lee wave but to the air mass temperature.

As the mountain wave is a winterly phenomenon, there is a normal tendency of the "seasonal" and the "mountain error" to coincide. This may become somewhat critical if the aircraft has been forced down in a strong downdraft. If visibility is restricted, the pilot should always allow for 1,000 feet total deviation from his altimeter reading when crossing a

mountain range in winterly weather with high winds.

Nevertheless the altimeter error over mountains appears to have been somewhat over-estimated. With vertical air motions of several thousand feet per minute present, a sudden loss of altitude in severe downdrafts will generally far outweigh the error in altimeter readings.

e. Combination of hazards in a mountain wave.

It has already been pointed out in the foregoing paragraphs that certain combinations of the listed hazards can become quite critical. A very typical combination is the following:

Due to an upwind tilt of the waves, streamlines are packed on the downwind side of the waves. This increases not only the downdraft velocity of the air, but also the flight time spent in the downdraft area during a headwind flight. The aircraft will continue to lose altitude. Attempts of the pilot to climb with full power will slow down the aircraft further and trap it in the downcurrent. In a matter of a minute or two the plane may descend into the low level rotor zone where it encounters excessive turbulence with insufficient reserve speed. Loss of control may follow precisely at the moment when it is most needed; namely, during flight at mountain crest level. The situation is aggravated by unreliable altimeter readings and a collision with the mountain may become unavoidable if visibility is restricted.

There are many other dangerous combinations conceivable which may have caused air disasters in the past, especially if the aircraft was in instrument flight.

f. Suggested rules for flying the wave.

As long as the unsatisfactory safety rules on minimum height over mountains are not changed, the responsibility rests with the meteorologist and the pilot himself. Although the present safety margin of 2,000 feet may be lost in less than one minute, a general change of minimum heights has not been adopted thus far as it would eliminate most non-pressurized aircraft from flying over the Rocky Mountains. Under these circumstances, the pilot should observe certain flight rules after having been properly briefed by the meteorologist that mountain wave conditions may be expected. Few pilots are aware of the fact that, in winter, this is the case in one out of four days.

The following ten rules are suggested as a guide:

1. If it is not feasible to fly around an area of obvious wave activity, cross the mountain range at about 25,000 feet or at a level which is at least 50% higher than the height of the mountain range above the surrounding terrain.

2. Avoid all flights in the turbulent rotor cloud (also called "roll cloud").

3. Do not enter the "cap cloud" over the mountain crest with its severe downdrafts.

4. Do not fly high-speed aircraft into the wave below 20,000 feet; particularly, do not fly downwind.

5. Do not penetrate a strong mountain wave on instrument flight.

6. If you are trapped in a severe downdraft, change course quickly to a tailwind direction.

7. Allow for 1,000 ft total error in altimeter readings near mountain peaks.

8. If flying above 30,000 ft, avoid levels with ragged edges of lenticular clouds; they may be indications of severe high level turbulence. Avoid them by changing height.

9. If flying against headwinds, use updraft areas (especially the one upwind of the rotor cloud) as an aid in gaining altitude reserve to pass through the next downdraft area.

10. Cross a powerful mountain wave at right angles to the mountain range in order to keep flight time in downdrafts to a minimum.

12. THEORY OF STATIONARY AIR FLOW OVER A MOUNTAIN

Introduction. In the final report of the Sierra Wave Project [17] a brief historical account was given of the development of the mathematical theory for the flow of an air current across a mountain range, including the contributions which were made under the sponsorship of the project. In this chapter some of the salient features of the theory will be reviewed, and the results will be compared with the observed flow patterns over the Sierras.

Most of the existing theory has been derived under the assumption that second order terms in the governing equations can be ignored so the problem can be investigated with sufficient accuracy with linearized equations. It is generally agreed that this approximation is reasonably good (except perhaps in the immediate vicinity of the mountain) if the effective width of the mountain is much larger than its height, which is usually the case in nature.

It is further assumed that non-isentropic processes (radiation, condensation, turbulent mixing, and molecular dissipation) can be ignored. The air is considered a perfect gas of uniform composition whose physical changes obey the adiabatic law. Apart from the condensation there appears to be reasonable justification for these approximations. However, the cross-mountain flow is usually accompanied by typical cloud formations. It would be very difficult to incorporate this condensation process in the theory, and it has therefore been left out of the theory so far.

In the flow over very wide continental mountain systems which it takes the air a day or more to cross, the rotation of the earth becomes one of the dominant factors in the dynamics of the flow. The streamlines have large horizontal defelctions on the lee side of the mountain range. However, if the mountain is only moderately wide like the Sierra range, the air will cross it in a few hours. The dynamic effect of the earth's rotation is then unimportant and may be ignored altogether. Within this approximation the flow is two-dimensional in vertical planes perpendicular to the mountain.

The linearized theory with the above approximations is reviewed in the first section below. The elimination process leading to the basic wave equation (13) is given in some detail. This is included since the various investigators have derived the equation with different and not altogether systematic additional approximations based on numerical estimates of atmospheric values of the physical parameters in the undisturbed flow. The complete wave equation (13) cannot be solved with present mathematical knowledge. It is therefore necessary to consider simplified atmospheric models which resemble observed conditions. The rest of the chapter reviews the theory of some of these models, and compares the flow predicted by them with observed flow patterns. It is shown that the agreement is rather good in the most recent models.

1. Stationary flow of a stratified atmospheric current over a small amplitude two-dimensional mountain profile. - In the basic undisturbed state (with the mountain absent) the air flows steadily in the fixed horizontal direction of the unit vector $\underset{\sim}{i}$ (the x-axis) with a velocity U which has an arbitrary variation along the vertical $U = U(z)$. The mass distribution in this undisturbed current is hydrostatic with arbitrary stratification, that is, the specific volume α is an arbitrary function of height, $\alpha = \alpha(z)$. The stratification is conveniently described by the relative vertical gradient of specific volume

$$s = s(z) = \frac{d}{dz} (\ln \alpha). \tag{1}$$

The physical changes of the air (in the disturbed flow) are prescribed to obey the adiabatic law, which may be written in the differential form

$$\frac{D}{Dt} (\text{density}) = b \frac{D}{Dt} (\text{pressure}). \tag{2}$$

The parameter b is the coefficient of pietzotropy. For adiabatic changes b is the inverse square of the speed of sound. Its value is obtained from the equation of state

$$\sigma = \frac{RT}{p} = \frac{R\theta}{100} \left(\frac{p}{100}\right)^{-1/\kappa}; \qquad \kappa = c_p/c_v$$

by individual time differentiation, which for adiabatic changes gives

$$\frac{1}{\alpha} \frac{D\alpha}{Dt} = -\frac{1}{\rho} \frac{D\rho}{Dt} = -\frac{1}{\kappa p} \frac{Dp}{Dt},$$

and hence, by comparison with (2)

$$b = \frac{1}{\kappa \alpha p} = \frac{1}{\kappa RT} = \frac{1}{C^2}. \tag{3}$$

The vertical stability of the current is determined by the gradient of the potential temperature θ, obtained by differentiation along the vertical of the equation of state for the undisturbed fields. Thus, using the hydrostatic equation we get

$$\frac{d}{dz} \ln \left(\frac{\alpha}{\theta}\right) = -\frac{1}{\kappa p} \frac{dp}{dz} = \frac{g}{\kappa \alpha p} = bg,$$

and hence

$$\frac{d}{dz} \ln \theta = \frac{d}{dz} \ln \alpha - bg = s - bg = \sigma. \tag{4}$$

In this system we introduce a small amplitude two-dimensional perturbation in the vertical zx-planes,

$$\underset{\sim}{v} = \underset{\sim}{v}(x,z) = u(x,z)\underset{\sim}{i} + w(x,z)\underset{\sim}{k}, \tag{5}$$

and explore under what conditions, if any, the resultant motion is steady. Let the corresponding small local departures of pressure and mass be denoted by a bar over the respective symbols, so the resultant fields are

$$p(z) + \bar{p}(x,z) \quad ; \quad \alpha(z) + \bar{\alpha}(x,z).$$

If the resultant motion is steady, the individual time derivative is the convective change

$$\frac{D}{Dt} = (U\underset{\sim}{i} + \underset{\sim}{v})\cdot\underset{\sim}{\nabla} = U\frac{\partial}{\partial x} + \underset{\sim}{v}\cdot\underset{\sim}{\nabla} ,$$

so the equation of pietzotropy (2) becomes

$$-(U\frac{\partial}{\partial x} + \underset{\sim}{v}\cdot\underset{\sim}{\nabla})(\alpha+\bar{\alpha}) = b(\alpha+\bar{\alpha})^2(U\frac{\partial}{\partial x} + \underset{\sim}{v}\cdot\underset{\sim}{\nabla})(\bar{p}+p),$$

or, when second order terms are ignored,

$$-U\frac{\partial}{\partial x}(\bar{\alpha} + b\alpha^2\bar{p}) = w(\frac{d\alpha}{dz} + b\alpha^2\frac{dp}{dz}) = \alpha w(\varepsilon - bg) = \alpha\zeta\sigma.$$

Let ζ denote the vertical displacement of the particle from its equilibrium level, write $w = U\frac{\partial\zeta}{\partial x}$, and integrate with respect to x. We then get the physical equation in its most convenient form

$$-\bar{\alpha}/\alpha = b\alpha\bar{p} + \zeta\sigma. \tag{6}$$

The dynamic equation of the resultant disturbed motion is

$$(U\frac{\partial}{\partial x} + \underset{\sim}{v}\cdot\underset{\sim}{\nabla})(U\underset{\sim}{i} + \underset{\sim}{v}) + (\alpha+\bar{\alpha})\underset{\sim}{\nabla}(p+\bar{p}) = \underset{\sim}{g}.$$

The terms $\alpha\underset{\sim}{\nabla}p = \underset{\sim}{g}$ cancel due to the hydrostatic balance of the undisturbed flow so, when second order terms are ignored, we get

$$U\underset{\sim}{v}_x + U'w\underset{\sim}{i} + (\bar{\alpha}/\alpha)\underset{\sim}{g} = -\alpha\underset{\sim}{\nabla}\bar{p} = -\underset{\sim}{\nabla}(\alpha\bar{p}) + \bar{p}\underset{\sim}{\nabla}\alpha.$$

Here partial differentiation on the perturbation velocity is denoted by subscript, and the total differentiation with <u>respect to height</u> on the parameters of the basic undisturbed flow by accent. The last term on the right may be written $\bar{p}\underset{\sim}{\nabla}\alpha = \alpha\bar{p}\underset{\sim}{\nabla}(\ln\alpha) = \alpha\bar{p}s\underset{\sim}{k}$. Substitute further for $\bar{\alpha}/\alpha$ from (6). The dynamic equation then becomes

$$U\underset{\sim}{v}_x + U'w\underset{\sim}{i} + \sigma(g\zeta - \alpha\bar{p})\underset{\sim}{k} = -\underset{\sim}{\nabla}(\alpha\bar{p}), \tag{7}$$

or, when the local pressure departure is eliminated by $\underset{\sim}{\nabla}\times$ differentiation,

$$U(\underset{\sim}{\nabla}\times\underset{\sim}{v})_x + U'\underset{\sim}{k}\times\underset{\sim}{v}_x + \underset{\sim}{\nabla}(U'w)\times\underset{\sim}{i} + \sigma(g\underset{\sim}{\nabla}\zeta + U\underset{\sim}{v}_x + U'w\underset{\sim}{i}) \times \underset{\sim}{k} = 0.$$

All the vectors here are perpendicular to the xz-plane so, taking their scalar values, we have the corresponding scalar equation

$$U(u_z - w_x)_x + U'u_x + (U'w)_z - \sigma(g\zeta_x + Uu_x + U'w) = 0$$

Divide by U, change sign, and substitute $\zeta_x = w/U$, thus

$$(8) \qquad w_{xx} - u_{xz} + (\sigma - \frac{U'}{U})u_x - \frac{U'}{U}w_z + (\frac{\sigma g}{U^2} + \frac{\sigma U'}{U} - \frac{U''}{U})w = 0.$$

From this equation u_x may be eliminated with the aid of the equation of continuity,

$$\nabla \cdot \underline{v} = -(\alpha+\bar{\alpha})\frac{D}{Dt}(\rho+\bar{\rho}),$$

which, combined with the equation of pietzotropy (2), becomes

$$u_x + w_z = -b(\alpha+\bar{\alpha})(U\frac{\partial}{\partial x} + \underline{v}\cdot\nabla)(\bar{p} + p),$$

or, when second order terms are ignored,

$$u_x + w_z = -bU\frac{\partial}{\partial x}(\alpha\bar{p}) - bw\alpha\frac{dp}{dz}.$$

The local pressure departure may be eliminated with the aid of the horizontal component of the dynamic equation (7), so we get

$$u_x + w_z = bU(Uu_x + U'w) + bgw.$$

Introduce the non-dimensional parameter

$$(9) \qquad M = 1-bU^2 = 1-(U/C)^2$$

and assemble terms, thus

$$(10) \qquad -Mu_x = w_z - b(g+UU')w.$$

Now to eliminate u_x from (8), apply the factor M, write

$$-Mu_{xz} + M(\sigma - \frac{U'}{U})u_x = -(Mu_x)_z + (\sigma - \frac{U'}{U} + \frac{M'}{M})Mu_x,$$

and then substitute for Mu_x from (10). The result is

$$Mw_{xx} + w_{zz} - b(g+UU')w_z - [b(g+UU')]'w - (\sigma - \frac{U'}{U} + \frac{M'}{M})[w_z - b(g+UU')w]$$
$$- M\frac{U'}{U}w_z + M(\frac{\sigma g}{U^2} + \frac{\sigma U'}{U} - \frac{U''}{U})w = 0.$$

After rearrangement this equation has the form

$$(11) \qquad Mw_{xx} + w_{zz} - Aw_z + Bw = 0$$

where

$$A = b(g+UU') + (\sigma - \frac{U'}{U} + \frac{M'}{M}) + M\frac{U'}{U} = s + \frac{M'}{M}.$$

$$B = M(\frac{\sigma g}{U^2} + \frac{\sigma U'}{U} - \frac{U''}{U}) + bU^2(\frac{g}{U^2} + \frac{U'}{U})(\sigma - \frac{U'}{U} + \frac{M'}{M}) - [b(g+UU')]'$$

$$= (\frac{g}{U^2} + \frac{U'}{U})(M\sigma + bU^2\sigma - bUU' + bU^2\frac{M'}{M} - b'U^2) - b(UU')' - M\frac{U''}{U},$$

or, since $M+bU^2 = 1$,

$$B = \frac{g}{U^2}\left(\sigma - 2bUU' - b'U^2 + bU^2\frac{M'}{M}\right) + bg\frac{U'}{U}$$

$$+ \frac{U'}{U}\left(\sigma - 2bUU' - b'U^2 + bU^2\frac{M'}{M}\right) - bUU'' - M\frac{U''}{U} .$$

In the parentheses substitute from (9)

$$-2bUU' - b'U^2 + bU^2\,(M'/M) = M'(1 + bU^2/M) = M'/M,$$

so B reduces to

$$B = (\sigma + M'/M)g/U^2 + (s + M'/M)U'/U - U''/U.$$

With these values of A and B substituted, (11) is the differential equation for the vertical velocity component of a small amplitude stationary perturbation superimposed upon the stratified current U(z), namely

$$Mw_{xx} + w_{zz} - (s + \frac{M'}{M})w_z + [(\sigma + \frac{M'}{M})\frac{g}{U^2} + (s + \frac{M'}{M})\frac{U'}{U} - \frac{U''}{U}]w = 0.$$

The parameters s and σ are the logarithmic vertical gradients of specific volume and potential temperature as defined in (1) and (4). To simplify notations we may instead introduce the composite gradients

(12)
$$S = \frac{d}{dz}\ln(M\alpha) = s + \frac{M'}{M}$$

$$\beta = \frac{d}{dz}\ln(M\theta) = \sigma + \frac{M'}{M}.$$

In terms of these parameters the differential equation becomes

(13)
$$Mw_{xx} + w_{zz} - Sw_z + (\frac{\beta g}{U^2} + \frac{SU'}{U} - \frac{U''}{U})w = 0 .$$

Let now the atmospheric current be bounded below by an arbitrary small amplitude mountain profile at the level z=0, having the form $\zeta_o=\zeta_o(x)$. A stationary flow over the mountain must then satisfy the differential equation (13), the boundary condition at the ground

$$w(z=0) = U_o\partial\zeta_o/\partial x,$$

and the upper condition that the kinetic energy is finite at great heights. The problem of finding this flow is solved by representing the mountain profile as a Fourier integral of sinusoidal components, each of the form $\zeta_o = A(k)\cos kx$, where k denotes the wave number. Since the differential equation (13) is linear, the solution may be represented similarly by an integral, where each component element shall satisfy the differential equation (13) and the lower boundary condition for the corresponding sinusoidal component of the mountain, namely

$$w(z=0) = - U_o k\ A(k)\sin kx.$$

The component solution accordingly is periodic in x at the bottom level and

hence must have the same periodicity at all heights. Therefore we may substitute in (13) for the component solution

$$w = \sqrt{Ma/M_0 a_0}\ \omega(z) \sin kx, \tag{14}$$

where the factor $\sqrt{Ma/M_0 a_0}$ is included to eliminate the w_z- term. The subscript o denotes the values at the ground. From (14), using (12), we get

$$Mw_{xx}/w = - Mk^2$$

$$- S\, w_z/w = - S(\tfrac{1}{2}S + \omega'/\omega)$$

$$w_{zz}/w = (\tfrac{1}{2}S + \omega'/\omega)^2 + (\tfrac{1}{2}S + \omega'/\omega)'$$

and hence

$$(Mw_{xx} + w_{zz} - Sw_z)/w = \omega''/\omega - \tfrac{1}{4}S^2 + \tfrac{1}{2}S' - Mk^2.$$

When this is substituted in (13), we see that the amplitude function $\omega(z)$ of the component solution w with the wave number k must satisfy the differential equation

$$\omega'' + [F(z) - Mk^2]\omega = 0 \tag{15}$$

with

$$F(z) = \beta g/U^2 + SU'/U - \tfrac{1}{4}S^2 + \tfrac{1}{2}S' - U''/U, \tag{16}$$

$$\beta = (\ln M\theta)'; \qquad S = (\ln Ma)'; \qquad M = 1 - (U/C)^2,$$

and the lower boundary condition

$$\omega(z=0) = - U_0 k\, A(k).$$

The general solution of (15) has the form

$$\omega(z) = C_1\omega_1(z) + C_2\omega_2(z),$$

where ω_1 and ω_2 are two linearly independent solutions and C_1 and C_2 are arbitrary constants to be determined by the upper and lower boundary conditions. If the upper boundary condition is applied, one of these constants may be eliminated, and the solution may be written

$$\omega(z) = C_3\omega_3(z),$$

where ω_3 is a linear combination of ω_1 and ω_2 which remains finite at great heights. The constant C_3 is determined by the lower boundary condition, so

$$\omega(z) = - U_0 k\, A(k)\ \omega_3(z)/\omega_3(0).$$

If we return to (14), the vertical velocity of the component solution

has the form

$$w(z) = -\sqrt{\rho_0 a_0/\rho_0 a_0}\, U_0 k\, A(k)\, \omega_3(z)/\omega_3(0) \sin kx. \tag{17}$$

The motion which is stationary relative to an arbitrary mountain is obtained by integrating the component solutions (17) over all wave numbers k in the spectrum of the mountain profile. We then see at once that the character of the resultant motion will be decisively affected by whether or not the component solution $\omega_3(z)$ has a zero at the mountain level for any value of k. If $\omega_3(0)$ is not zero for any value of k, the integral is regular over the entire spectrum, and the stationary flow over the mountain will in this case have the character of a deformation of the streamlines which more or less reflects the shape of the mountain profile below. If on the other hand the component solution $\omega_3(z)$ has a zero at the mountain level for a certain value of k, this means that a stationary free wave with this wave number can exist in the current over level ground. The integral will then have a singularity for this wave number and the main contribution to the integral comes from the small spectral group centered at this wave number. This contribution will have the character of a sine wave with the wave length of a free resonance wave which extends downstream from the mountain crest, so there is a mountain lee wave.

It should be noted that the problem as formulated here as a stationary flow over the mountain profile has no unique solution if a free wave exists. The physical reason for this is obvious. For suppose that we have found one stationary solution by the method just outlined. We can then find another as the resultant of this solution and the free wave with arbitrary amplitude and phase. Mathematically this ambiguity is reflected by the fact that the integral of the component solutions (17) is divergent at the singularity unless the integration through the singularity is specified. Kelvin [1] and Rayleigh [2], who first investigated surface lee-waves mathematically, circumvented this ambiguity by different expedients. Kelvin defines the integration through the singularity by taking the principal value of the integral, which results in a solution which is symmetric relative to the mountain crest consisting of sine waves in opposite phase upstream and downstream separated by a central fringe. He then adds a free wave in opposite phase to the upstream wave and interprets the resulting lee-wave solution as the correct one. Rayleigh avoids the singularity by introducing a small artificial friction proportional to the velocity. This method gives the same lee-wave solution as Kelvin's method when in the end result the coefficient of friction approaches zero. Lyra [3] and Queney [4], who investigated lee waves in a simple atmospheric model which will be described in the next section, adopted both of the above methods in their derivation of the lee-waves.

Hoiland [5] pointed out that the ambiguity disappears and the solution becomes unique if the problem is formulated as an initial value problem, and he proved this for surface waves. Wurtele [6] and Palm [7] independently extended the proof to the Lyra-Queney model. Finally Eliassen and Palm [8] showed that the stationary solution becomes unique if the additional requirement is introduced that the mountain is the only source of energy. These results have put the mathematical theory of lee-waves on a sound foundation. In the models which have been investigated, if the flow over the mountain i. started from initial rest and quickly attains a constant mean value U, the motion as a whole approaches asymptotically a steady state with a lee-wave extending downstream from the mountain if a free wave exists. The flow pattern of this asymptotic state is identically the same as in the stationary

solution derived by Kelvin's and Rayleigh's method. If reasonable atmospheric values of the various parameters in the problems are used, the time required for the motion to attain approximately its permanent value near the mountain is of the order of a few hours.

The mathematical labor is much more formidable in the initial value approach than in the steady state formulation of the lee-wave problem. Therefore, unless we are concerned with transient changes of the flow pattern which are associated with time variations of the basic flow, the steady state approach as outlined above, with Kelvin's method to attain uniqueness, represents the simplest mathematical procedure for the derivation of the mountain lee-waves. The problem is then to find the solutions $w(z)$ of the basic mountain-wave equation (15) for all values of the wave number k, and then evaluate the Fourier integral of the corresponding component solutions in (17). If the stratification and shear of the basic flow are arbitrary functions of height, the corresponding function $F(z)$ in (16) is also an arbitrary function of height and no method is available to find the solutions of (15) in this general case. However, in recent years several investigators have derived solutions which reflect many of the characteristic features of observed mountain lee-waves by considering special simplified atmospheric models for which F is either a constant or a simple function of height. In the following the theory of some of these models will be briefly reviewed.

2. Model with constant stability and constant wind. (The Lyra-Queney model) - The mathematically simplest atmospheric model is an isothermal current with no shear in the basic flow. The speed of sound (or the coefficient of pietzotropy) is then independent of height and hence the parameter M in (9) is a constant. In terms of the temperature gradient, $\gamma = -dT/dz$, the gradients of specific volume and potential temperature are

$$s = \frac{d}{dz} \ln \alpha = (g/R - \gamma)/T$$

(18)

$$\sigma = \frac{d}{dz} \ln \theta = (g/c_p - \gamma)/T.$$

For an isothermal atmosphere $\gamma=0$ so both these are constant. The function $F(z)$ in (16) therefore reduces to a constant, namely

(19) $$F = \alpha g/U^2 - \tfrac{1}{4}s^2 = k_s^2.$$

The wind speed in atmospheric flows is usually an order less than the speed of sound, so no great error is made by replacing M by unity in the last term in the wave equation (15). This approximation is of course not necessary since M is a constant and hence may be absorbed in the definition of k^2. The wave equation for the isothermal current with no shear is therefore

(20) $$w'' + (k_s^2 - k^2)w = 0,$$

where k_s^2 is the constant in (19).

The isothermal atmosphere has a much greater stability than the

values actually observed in the troposphere. However, the equation (20) is approximately applicable to any atmosphere with a constant lapse rate of temperature when the appropriate mean values of the parameters σ and s in (18) are substituted in the expression for k_s^2. Typical mean tropospheric values, $\gamma = 0.006^{\circ}m^{-1}$ and $\bar{T} = 250^{\circ}K$ give $s = 1.2 \times 10^{-4}\ m^{-1}$, $\sigma = 1.6 \times 10^{-5}\ m^{-1}$. If the flow has the speed $U = 20\ ms^{-1}$, the critical wave number is $k_s = 0.6\ km^{-1}$, and hence the critical wave length (see below) is about 10 km. The critical wave length increases with increasing wind speed and decreasing stability, but 10 km appears to be a reasonable average atmospheric value. Note that the term $\frac{1}{4}s^2$ in (19) is less than one per cent of the term $g\gamma/U^2$ for the usual values of the wind speed and may for practical purposes be ignored.

The free-wave solutions of (20), for which ω is zero at the ground, are

$$\omega = \sinh \sqrt{k^2-k_s^2}\, z; \qquad k > k_s$$

(21)

$$\omega = \sin \sqrt{k_s^2-k^2}\, z; \qquad k < k_s$$

The short wave solutions, $k > k_s$, approach infinity at great heights, so these must be rejected. However, the long wave solutions are physically possible free waves for every wave number $k < k_s$. They are internal gravity waves with equidistant horizontal nodal planes separated by the vertical half wave length $\frac{1}{2}H$, given by

$$H^2(k_s^2 - k^2) = 4\pi^2.$$

Substituting here $k_s = 2\pi/L_s$ and $k = 2\pi/L$, we get the following relation between the vertical and horizontal wave length

$$(\frac{L}{L_s})^2 = \frac{H^2 + L^2}{H^2}, \qquad (22)$$

which leads to a simple physical interpretation of these supercritical internal gravity waves. Since they are stationary waves, they are all propagated against the current with the same constant phase velocity U. Superposition of two such waves with equal wave length and amplitude propagating in opposite directions results in standing oscillations relative to the fluid in rectangular cells with vertical and horizontal side-lengths $\frac{1}{2}H$ and $\frac{1}{2}L$. The period of these oscillations is

$$T = L/U.$$

As the wave length is made shorter, the period decreases until in the limit as $L \to L_s$ the period approaches the minimum value, obtained from (19), namely

$$T_s = L_s/U = 2\pi/\sqrt{\sigma g}$$

when the small term $\frac{1}{4}s^2$ is ignored. Comparing these with (22) we see that

$$\frac{T}{T_s} = \frac{L}{L_s} = \frac{D}{H} = \cos\theta,$$

where $\frac{1}{2}D = \frac{1}{2}\sqrt{L^2+H^2}$ is the diagonal of the cell, and θ is the slope angle of the diagonal. Long and shallow cells oscillate slowly, short and deep cells rapidly, which is just what should be expected. The shortest cell compatible with the given phase velocity U has the horizontal wave length L_s, and hence $H = D = \infty$. The oscillations are here strictly vertical and the period is the well known limiting period of vertical gra oscillations.

It is then quite evident that the subcritical waves shorter than L_s cannot have a phase velocity as large as U and hence cannot appear as stationary free waves. But all the supercritical waves longer than L_s are possible free waves and will appear as lee waves behind the mountain in the resultant flow pattern. These waves will interfere and cancel some distance downstream from the mountain crest, and the resultant flow will be non-periodic.

Queney [9] has worked out the details for a symmetric mountain range with the profile

$$(23) \qquad \zeta_o = h[1 + (x/a)^2]^{-1} = ha \int_0^\infty \exp(-ak) \cos kx \, dk,$$

where h is the height of the crest and a is a measure of the width of th mountain. The Fourier components of this profile have the amplitudes $A(k) = ha \exp(-ak)$, and it is therefore evident that only components who wavelengths are comparable to the width of the mountain ($2\pi a$) contribute appreciably to the resultant profile. Therefore only these mountain components will excite appreciable wave components in the resultant stationary flow over the mountain. The general aspects of the flow pattern are determined largely by the width of the mountain ($2\pi a$) as compared to the critical wave length of the current. The simplest flow patterns occur when the mountain is either much narrower or much wider than the critical wave length.

(i) If the mountain is much narrower than the critical wave leng the "active" mountain components have wave numbers $k \gg k_s$. The solutions of (20) for these components are approximately $\omega = \exp(-kz)$, and the corresponding wave components (17) are

$$w = -\sqrt{a/a_o}\, Uk\, ha \exp(-ka) \exp(-kz) \sin kx.$$

The vertical displacements ζ of these components, since $w = U\partial\zeta/\partial x$, are

$$\zeta = \sqrt{a/a_o}\, ha \exp(-ka-kz) \cos kx,$$

and hence the vertical displacements in the resultant flow are approximately

$$\zeta = \sqrt{a/a_o}\, ha \int_0^\infty e^{-k(a+z)} \cos kx \, dx = \sqrt{a/a_o}\, \left(\frac{ha}{a+z}\right)\left[1 + \left(\frac{x}{a+z}\right)^2\right]^{-1}.$$

All the streamlines have symmetric deformations which reflect the shape of the mountain profile below, and the crest line coincides with the vertical of the mountain crest. Since the critical wave length is of the order of 10 km, this solution applies to narrow hills whose width is about 1 km or less.

(ii) If the mountain is much wider than the critical wave length ($2\pi a \gg L_s$), the active mountain components have wave numbers $k \ll k_s$, and the solutions of (20) for these components are approximately $\omega = \cos$ (or $\sin$) $k_s z$. The corresponding wave components in (17) are

$$w = -\sqrt{a/a_0}\, Uk\, ha \exp(-ka) \sin(kx \pm k_s z),$$

or in terms of the vertical displacements

$$\zeta = \sqrt{a/a_0}\, ha \exp(-ka) \cos(kx \pm k_s z).$$

The solutions with the negative sign represent waves which transport the energy downward toward the mountain and must be rejected to attain uniqueness. The vertical displacements of the resultant flow are therefore approximately

$$\zeta = \sqrt{a/a_0}\, ha \int_0^\infty \exp(-ka) \cos(kx + k_s z)\,dk$$

$$= \sqrt{a/a_0}\, h \left(\cos k_s z \quad \frac{x}{a} \sin k_s z\right)\left[1 + \left(\frac{x}{a}\right)^2\right]^{-1}.$$

This solution is periodic along the vertical with the vertical "wave length" L_s. It is nonperiodic in the horizontal direction but has a characteristic asymmetry relative to the mountain as may be seen in figure 12.1 (reproduced from Queney's paper) which shows the flow pattern over a mountain whose width ($2\pi a$) is 10 critical wave lengths. At low levels the streamlines have a pronounced crest immediately upwind from the mountain crest and a weak trough on the lee-side of the mountain. Higher up the upwind crest becomes weaker and the lee trough more intense, while both are gradually shifted backwards against the wind. At the level one quarter of the critical wave length above the ground the crest and trough have equal strengths and are located symmetrically relative to the mountain crest above the points where the mountain has the steepest slope. At the level of one half the critical wave length above the ground the upwind crest has disappeared, the trough has maximum strength and has been shifted back to the mountain crest. The streamline is here an inverted image of the mountain profile. The same trend is repeated in the next half wave length layer with the trough on the upwind side and the crest on the lee side of the mountain. At the elevation of a full critical wave length the trough has disappeared far upwind and the streamline is identical to the mountain profile. (The factor $\sqrt{a/a_0}$ in the streamline amplitude, which increases uniformly with height, has been ignored in figure 12.1.) This theoretical model should apply to relatively broad mountain ranges (50 to 100 km wide), and it does in fact show some of the characteristic features which are observed in cross-mountain flow over such ranges as the Sierras and the Alps. The speed of the flow may be judged in the diagram from the width of the streamline channels, and since the flow is assumed adiabatic, the streamlines are also lines of constant potential temperature. The model has strong warm downslope winds (foehn) at low levels beteen the mountain crest and the lee-side trough, and much weaker cold upslope winds on the upwind side of the mountain crest. This is in complete agreement with the observed conditions in a typical Alpine foehn situation 3 October 1941 described by Hoinkes [10] and further discussed by Bjerknes [11]. In the Sierras the strong foehn wind down the lee slope of the mountain is usually very pronounced, as may be judged from typical situations 30 January 1952 (figure 3.22) and 16 February (3.28).

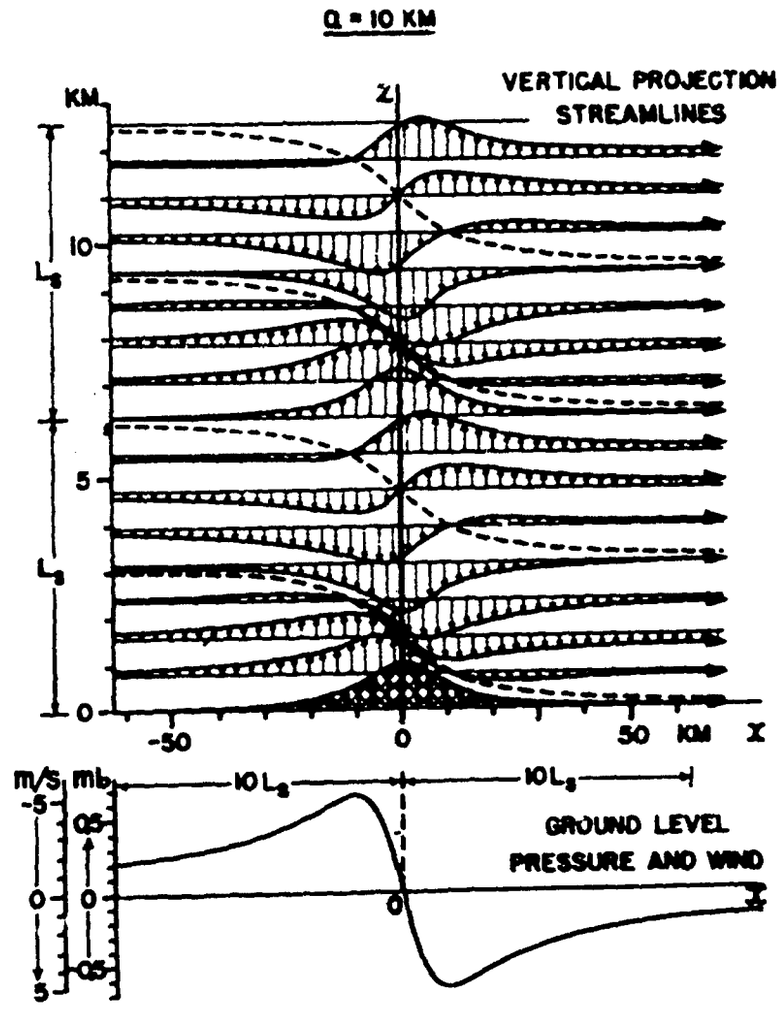

Fig. 12.1 - Flow over a symmetric mountain profile whose width is ten critical wave lengths. (Queney)

The clouds, which form on the upwind side and cover the divide as a dense wall, dissolve in a characteristic "cloud-water fall" along the lee slope of the mountain. The observed flow over the Sierras also usually shows a backward tilt of the lee-side trough at low levels near the mountain crest. But higher up the observed tilt seems to be very slight, certainly much smaller than in Queney's theoretical model. The model fails to predict the lee-waves which are observed downwind from the Sierra crest. Neither is the vertical periodicity in the model borne out by observations.

(iii) If the width of the mountain is about the same as the critical wave length, the active mountain components will excite both subcritical wave components of the type in model (i) whose amplitude decreases exponentially with height, and supercritical components of the type in model (ii) which can exist as stationary free waves in the current. The corresponding Fourier integral is then not quite so simple as in the earlier models, but still it may be evaluated by standard methods. The result of the computation for a mountain which has exactly the width of the critical wave length ($2a = L_s$) is shown in figure 12.2 which is reproduced from Queney's paper. The flow pattern shows some similarity to the wide-mountain model in figure 12.1, but also some significant differences. The entire disturbed part of the flow has been shifted downwind toward the lee-side of the mountain and contains a fairly well developed system of lee-waves with a wave length a little longer than the critical wave length. This is just what should be expected: the main contribution comes from the free super-critical resonance waves with those close to the critical wave length predominant. These wave components are in phase near the mountain, but increasingly out of phase downstream. So already the second resultant wave downstream from the mountain has a much smaller amplitude than the first. Similarly to the wide-mountain model in figure 12.1, the lee-wave trough has a strong backward tilt extending obliquely upward against the wind, and the whole wave system has the same tilt. The strongest downslope foehn winds are located some distance above the ground in this model. In the Sierras the strongest winds are usually found immediately above the ground on the lee slope. This discrepancy may be due to the lack of symmetry in the Sierra profile. A mountain which has some similarity to the Sierra profile is obtained by solidifying the streamline whose mean elevation is one quarter of the critical wave length. The flow over this profile, as copied from figure 12.2, is shown in figure 12.3. The Sierra profile is shown in the lower part of the figure. This model agrees rather well in the lower layers with the observed flow patterns on January 31 and February 16, 1952 (figures 3.22 and 3.28). The strong foehn winds are located immediately above the ground on the lee slope. The isentropes are closely packed, indicating a stable layer, immediately above the mountain crest. But the structure of the observed lee-wave system at higher level is quite different from the model in figure 12.3. The observed lee-waves usually have maximum amplitude at low levels. They have very small if any tilt with height, and they are repeated downstream without appreciable change in amplitude.

It is evident therefore that the theoretical model needs modification in order to account for the distinct lee-waves which are observed. Effective alterations of the model, leading to distinct resonance waves, have been proposed by several investigators.

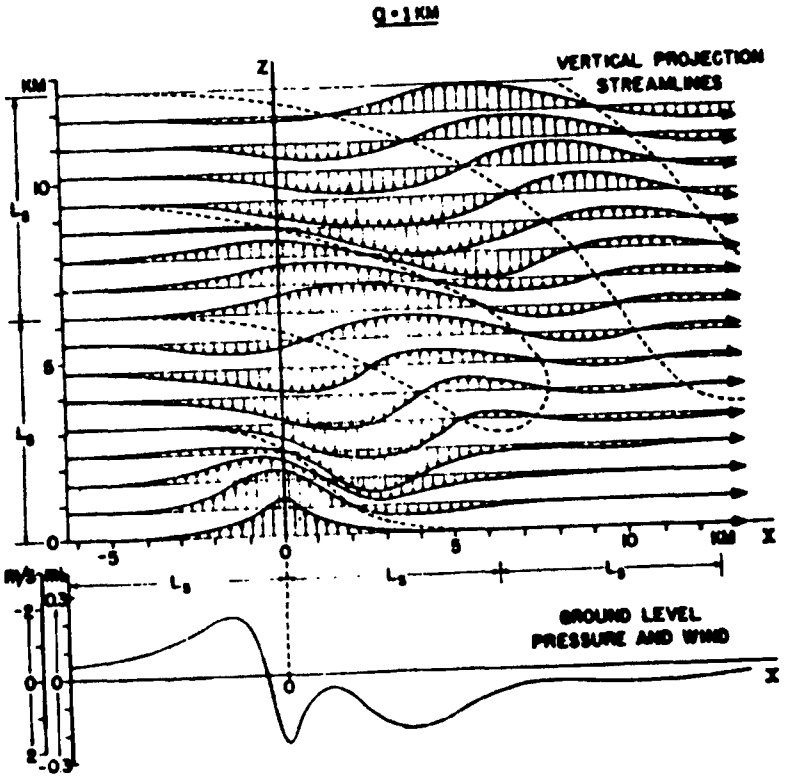

Fig. 12.2 - Flow over a symmetric mountain profile whose width is one critical wave length. (Queney)

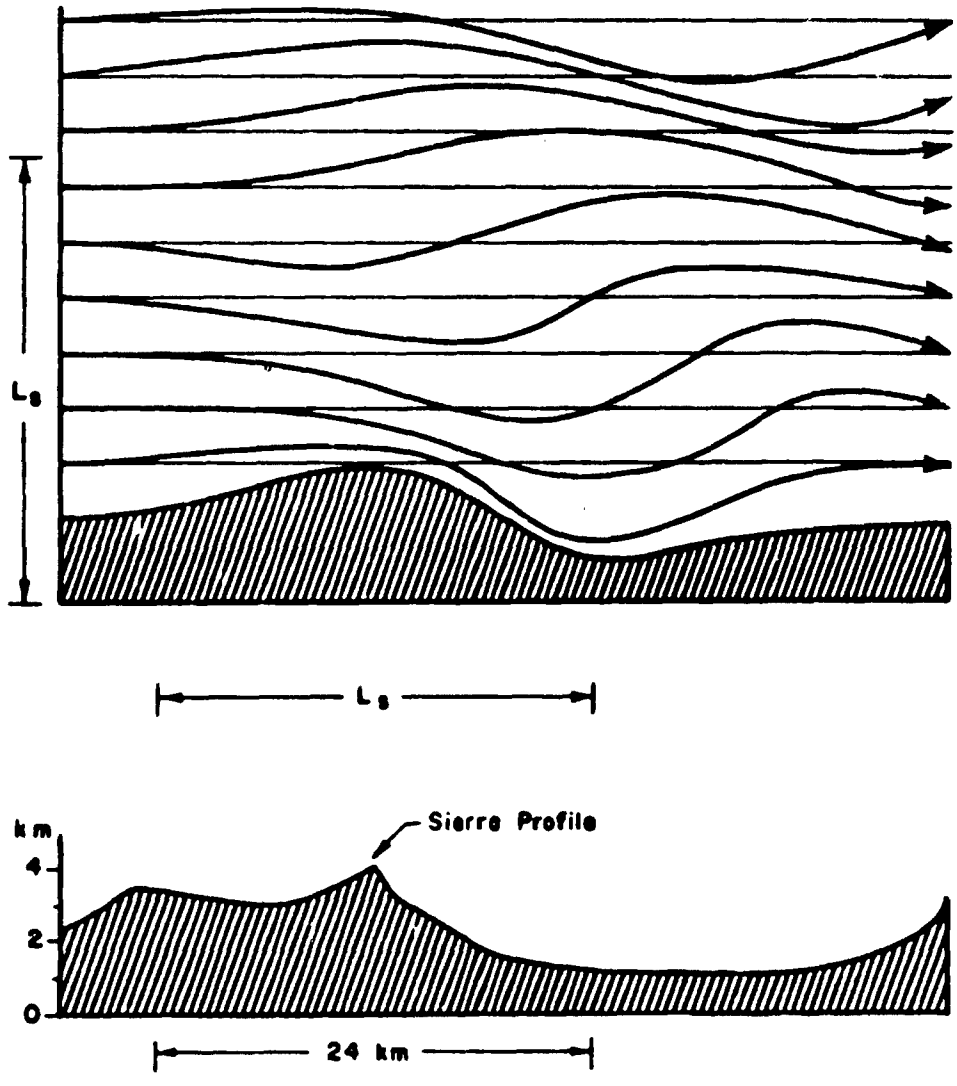

Fig. 12.3 - Flow over an asymmetric mountain profile which resembles the Sierra profile, obtained from Figure 12.2 by solidifying the streamline whose mean elevation is one quarter of the critical wave length.

3. Two-layer model with constant F-parameter in each layer. (Scorer's model). If we return to the complete wave equation in (15), with the value of the F-parameter specified in (16), it is immediately evident that several simplifications can be made without changing the essentials if we consider the normally occurring values of wind and stratification in the atmosphere. The wind is usually much smaller than the speed of sound, so no great error is introduced if we replace M by unity and hence the composite gradients β, S by the simple gradients σ, s. It has already been pointed out that $\frac{1}{4}s^2$ rarely exceeds one per cent of $\sigma g/U^2$. Under normal conditions the terms sU'/U and $\frac{1}{2}s'$ are also much smaller than $\sigma g/U^2$. If all these terms are ignored the wave equation reduces to

$$\omega'' + [F(z) - k^2]\omega = 0 \tag{24}$$

with

$$F(z) = \sigma g/U^2 - U''/U. \tag{25}$$

All the models which have been studied so far are derived by considering this simplified version of the wave equation. The models are specified by choosing vertical distributions of temperature and wind similar to observed condition, but at the same time such that the function F in (25) becomes as simple as possible.

Scorer [12] has proposed a simple two-layer model with constant values of F within each layer, see figure 12.4 reproduced from Scorer's paper. The numerical values below are those of the numerical example in the figure. The upper unbounded layer has a constant strong wind ($U_s = 15$ ms^{-1}) and a constant weak stability ($\gamma_s = 8^o$ km^{-1}). So the parameter F has here a relatively small constant value

$$F_s = \sigma_s g/U_s^2 = k_s^2; \qquad (L_c \approx 11 \text{ km}).$$

The lower layer consists of two layers, both having the same constant value of F which is larger than the upper layer value. Dynamically these two layers act as one layer. The bottom layer has a constant weak wind ($U_o = 10$ ms^{-1}) and a constant stability greater than the upper layer ($\gamma_o = 4^o$ km^{-1}), so F has here the constant larger value

$$F_o = \sigma_o g/U_o^2 = k_o^2; \qquad (L_o \approx 4 \text{ km}).$$

The central layer has a constant stability and a wind profile which is a smooth continuation of the winds above and below, increasing continuously from the value U_o at the bottom to U_s at the top in such a way that the F-parameter has the constant value F_o of the bottom layer. This velocity profile may be evaluated numerically by proper adjustment of the depth of the layer. The profile has a point of inflection, $U'' = 0$, somewhere in the middle of the layer, and here $\sigma g/U^2 = \sigma_o g/U_o^2$. Since $U > U_o$ it follows that the central layer has greater stability than the bottom layer ($\gamma \approx 1^o$ km^{-1}).

The wave equation (25) respectively in the upper and lower layer of this model has the forms

Upper layer: $\omega'' + (k_s^2-k^2)\omega = 0,$

Lower layer: $\omega'' + (k_0^2-k^2)\omega = 0.$

If the lower layer is sufficiently deep, this model has a distinct stationary free wave over level ground with a wave length L_r somewhere in the interval $L_0<L_r<L_s$. All waves in this interval are subcritical ($k>k_s$) in the upper layer and supercritical ($k<k_0$) in the lower layer. With the origin at the interface, the solution of (24) in the two layers which is continuous at the interface is therefore

(26)
$$\text{Upper layer:} \quad \omega = \exp(-\lambda z), \qquad \lambda = \sqrt{k^2-k_s^2}.$$
$$\text{Lower layer:} \quad \omega = \cos \mu z - (\lambda/\mu) \sin \mu z, \qquad \mu = \sqrt{k_0^2-k^2}.$$

with an arbitrary amplitude factor left out. If H denotes the depth of the lower layer (bottom layer + central layer), the boundary condition for a free wave over level ground is $\omega(-H) = 0$, and hence

(27) $$\mu \cot \mu H = -\lambda.$$

The solution of this equation is found graphically by plotting both sides as functions of k. The intersections of the graphs, if any, determine the wave numbers k_r of the free resonance waves. If H is too small there is no intersection of the curves and hence no free waves. In his numerical example Scorer chose H = 2.7 km. The curves have then one intersection which determines the free resonance wave L_r = 6 km. When (27) is used, the lower layer solution for the free wave may be written

(28) $$\omega = A \sin \mu_r(z+H).$$

Since this is a smooth continuation of the exponential decrease in the upper layer, it is evident that the lower layer must include more than a quarter vertical wavelength of this sine curve, so $H>\frac{1}{2}\pi/\mu_r$. From (26) μ_r is less than $(k_0^2-k_s^2)^{\frac{1}{2}}$. If the depth of the lower layer is less than $\frac{1}{2}\pi(k_0^2-k_s^2)^{-\frac{1}{2}}$ there is no free wave in the interval k_0-k_s.

In his numerical example Scorer has taken a mountain with the profile in equation (23) with a width (2a) about equal to the length of the free wave. This mountain excites the corresponding distinct resonance wave to about its maximum amplitude. It appears as a train of lee waves extending downstream from the mountain, starting with a lee trough immediately down wind from the mountain crest. The lee waves have no tilt with height. The vertical velocity amplitude (26) increases from zero at the ground to a maximum value a little above the middle of the lower layer and then decreases uniformly higher up. (Again, as in figure 12.1, the amplitude factor $\sqrt{a/a_0}$ has been ignored in figure 12.4.)

The remaining contribution to the resultant cross-mountain flow pattern comes mainly from the long wave components $L>L_s$ which are supercritical in both layers. We recall that all these supercritical waves are possible free waves, and they appear as a continuous spectrum of lee-waves downstream from the mountain. Their amplitude is independent of height. They are in phase at the mountain and increasingly out of phase downstream. Their resultant contribution is quite similar to Queney's

wide-mountain model (figure 12.1). In the upper layer these supercritical wave components have the phase $kx \pm \lambda z$, with $\lambda = \sqrt{k_s^2 - k^2}$. Both these wave types may be combined with lower layer solutions which satisfy the boundary condition at the ground. However, the waves with the phase $kx - \lambda z$, which propagate obliquely upwards through the air, transport the energy downward since the vertical group velocity is negative in these waves, $d(Uk)/d\lambda = -U\lambda/k$. To obtain uniqueness these physically unrealistic waves must be rejected in the practical solution, just as in Queney's model. In figure 12.4 Scorer has used these wave components and has rejected the waves with the phase $kx + \lambda z$ which transport the energy upwards. As a consequence his flow pattern is wrong in this respect, particularly at high levels. If he had used the correct components, the high-level streamline crest would lie downstream from the mountain crest where it is usually observed.

This model represents the first successful theoretical attempt to account for the observed lee-waves which are repeated periodically downstream with large amplitude at low levels and no tilt with height. The model clearly exhibits the main dynamic prerequisite for such waves, that the dynamic parameter F in the wave equation has a smaller value at high levels than at low levels. The decrease of F with height is primarily due to the increase of the wind speed. We are therefore led to the simple qualitative rule that a necessary condition for a distinct periodic lee-wave is a sufficient increase of the wind speed from low to higher levels. Scorer's model is the simplest theoretical model which satisfies this requirement. The practical applicability of the model is limited by the fact that it calls for a sudden decrease of the F-parameter at some intermediate level. Observations in the Sierra region indicate that the F-parameter usually decreases rather uniformly with height. Models with this property have been discussed by Wurtele [13], Palm [14], and Zierep [15]. Zierep's model appears to be less adaptable to conditions in the Sierras than the other two, and will not be discussed in this report.

4. Model with constant stability and constant wind shear. (Couette flow) - This model was examined by Wurtele in 1953. It has mainly theoretical interest since the wind speed increases to unrealistically large values at great height. However it serves as a useful introduction to Wurtele's practical two-layer model which will be discussed in the next section.

At the ground level this model has the F-parameter

$$F_0(\text{ground level}) = \sigma g/U_0^2 = k_0^2. \qquad (L_0 \approx 6 \text{ km})$$

If the wind speed at the ground is 10 ms^{-1} and the constant lapse rate of temperature is 7° km^{-1}, the critical wave length L_0 is about 6 km, as indicated. It is convenient to measure the height z in this model from the level (below the ground) where the speed would be zero if the Couette flow were extended downward. Let h_0 denote the depth of this reference level below the ground. The constant wind shear in the model is then $U' = U_0/h_0$, the wind speed at the level z is

$$U = U'z = U_0(z/h_0),$$

and the approximate F-parameter in (25) is

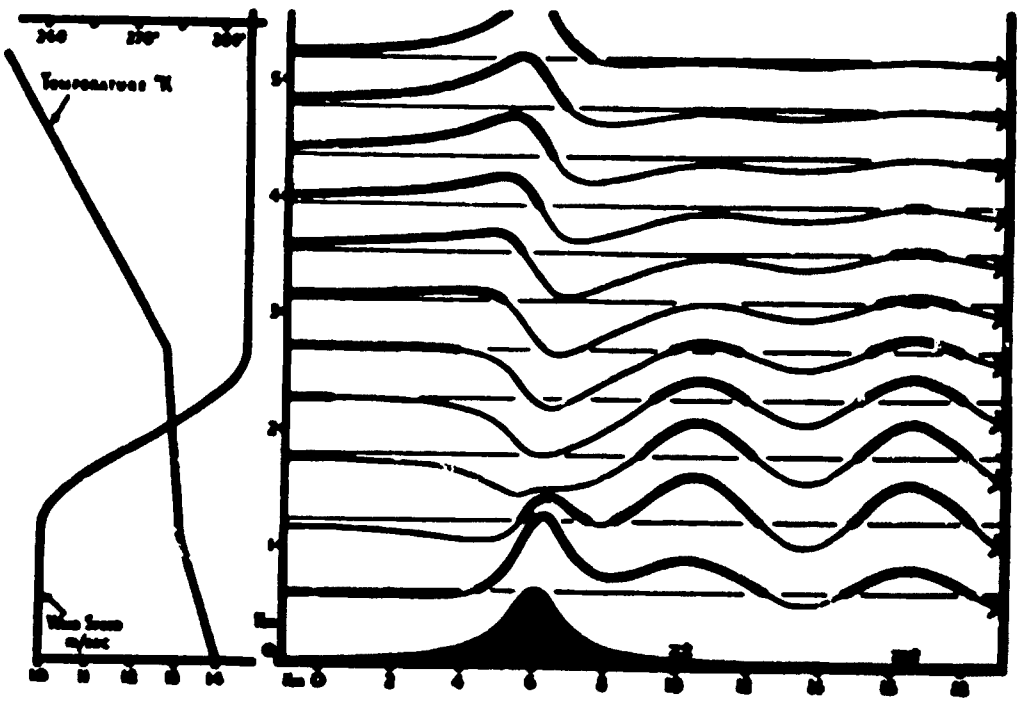

Fig. 12.4 - Flow over a symmetric mountain profile in a two-layer model with constant P-parameter in each layer. (Scorer)

(29) $$F(z) = \sigma_g/U_o^2 \, (h_o/z)^2 = (k_o h_o/z)^2.$$

It decreases uniformly with height from the maximum value k_o^2 at the ground. Ultimately at very great heights it drops down to the same order as the two terms which have been ignored, sU'/U and $\frac{1}{4}s^2$. So the approximation in (29) is not valid here. However, even for extreme atmospheric values of stability and shear the approximation is good well beyond the region of practical interest.

The practical wave equation for this model is accordingly

(30) $$\omega'' + [(k_o h_o/z)^2 - k^2]\omega = 0.$$

At high levels the first term in the bracket is negligible, so here the bounded solution approaches the asymptotic value $\omega \sim \exp(-kz)$. The expression in the bracket changes sign at the level, $z = h_o(k_o/k)$, and the solution is oscillatory below that level. The short waves $k > k_o$ have this level below the ground, so the vertical velocity amplitude of these subcritical wave components is non-oscillatory all the way down to the ground, as in Queney's and Scorer's models. They can not appear as stationary free waves over level ground and hence not as lee-waves. However, the supercritical wave components $k < k_o$ become oscillatory above the ground and a discrete set of them, which have a zero at the ground level, are possible free waves and will appear as distinct lee waves behind the mountain.

To find these free waves, substitute in (30) $\omega = z^{\frac{1}{2}}\bar{\omega}$, which gives

$$z^2\bar{\omega}'' + z\bar{\omega}' - [(kz)^2 - \nu^2]\bar{\omega} = 0$$

with

(31) $$\nu^2 = (k_o h_o)^2 - \tfrac{1}{4} \approx (k_o h_o)^2.$$

This equation is satisfied by the Bessel functions of imaginary argument and imaginary order $n = i\nu$. These Bessel functions have been tabulated by Morgan [16], who used the notations F_ν and G_ν for them. The general solution of (30) is

(32) $$\omega = z^{\frac{1}{2}}[A \, F_\nu(kz) + B \, G_\nu(kz)]$$

where A and B are arbitrary constants. At high levels $F_\nu(kz) \sim z^{-\frac{1}{2}} \exp(kz)$. In order that the solution shall remain bounded, $A = 0$, so the bounded solution is

$$\omega = z^{\frac{1}{2}} \, G_\nu(kz)$$

which at high levels approaches the asymptotic value $\exp(-kz)$. The free waves satisfy the boundary condition $\omega(h_o) = 0$ at the ground. The wave numbers of the free waves are therefore the values of k for the zeros of the Bessel function $G_\nu(kh_o)$. From (31)

$$\nu \approx k_o h_o = 2\pi h_o/L_o \approx h_o(\text{in km})$$

if we take L_0 = 6 km. For a fixed value of the surface wind speed (U_0 = 10 ms^{-1}) h_0 is inversely proportional to the wind shear. The values usually observed in the Sierra region lie in the range 2.5 km<h_0<5 km. The following table gives the wave lengths L_r of the shortest resonance waves for various values of the wind shear when the surface wind is 10 ms^{-1} and the lapse rate 7° km^{-1} (L_0 = 6 km). The longer resonance waves correspond to zeros beyond the range of Morgan's tables.

h_0(km)	Free wave lengths (shorter than 10 h_0) in km.							
10	9.5	13	20	27	38	52	70	94
8	10	16	25	37	55	82		
6	12	21	36	60				
4	15	34						
3	18							
2.4	23							

The first column gives the shortest resonance wave which has no nodal plane above the ground. The second column gives the next longer resonance wave with one nodal plane, and so on. If the wind shear is very strong (h_0 = 2.4) the shortest resonance wave is much longer than the critical wave length L_0. As the shear decreases the shortest resonance wave comes closer to the critical value and the number of resonance waves within any given spectral interval increases. Ultimately as the shear approaches zero the shortest resonance wave in the limit becomes the critical wave L_0 with a continuous spectrum of supercritical resonance waves beyond this limit.

This model clearly exhibits the dynamic effect of the wind shear on cross mountain flow. The wind shear causes the continuous spectrum of supercritical resonance waves in the Lyra-Queney model to be broken up into a discreet set of distinct resonance waves which become more widely separated the larger the shear.

Consider now a mountain which is effectively a little wider than the critical wave length. If the wind shear is small there are a large number of distinct lee-waves whose wave length are comparable to the mountain width. They are in phase near the mountain and increasingly out of phase downstream. The resultant flow will be similar to Queney's model, figure 12.2. If the shear is strong there is only one or two lee-waves comparable to the width of the mountain. The shorter of the two has no nodal plane. It has a maximum amplitude at a relatively low level and decays rather rapidly higher up. The longer lee-wave has a nodal plane at some intermediate height and its amplitude has a slower decay beyond the second maximum above the nodal plane. The resultant flow pattern should therefore have either one distinct lee-wave or at the most two, with the shorter dominating at low levels and the larger dominating higher up. This is actually what Wurtele found in a numerical example with a very strong wind shear, h_0 = 2.5.

5. Two-layer model with constant stability and constant wind in the stratosphere, constant stability and constant wind shear in the troposphere. (Wurtele's model) - The stratosphere is assumed isothermal, having the constant temperature T_s and the constant wind speed U_s. The F-parameter in the wave equation has here the constant value

$$F \text{ (stratosphere)} = k_s^2 = \sigma_s g/U_s^2 = g^2/(c_p T_s U_s^2).$$

The corresponding critical wave length is

$$L_s = 2\pi U_s \sqrt{c_p T_s}/g = (0.3\ U_s \text{ in } ms^{-1})km.$$

The troposphere is the same as the one layer model in the previous section. Using the same notations, the F-parameter at the ground is

$$F_o(\text{ground level}) = \sigma_o g/U_o^2 = k_o^2$$

and, as in (29), at an arbitrary tropospheric level

$$F \text{ (troposphere)} = (k_o h_o/z)^2.$$

The interface (the tropopause) is located at the height H above the ground, or at the height $h_s = h_o + H$ above the reference level. The depth h_o of this reference level below the ground is given by the tropospheric wind shear

$$U' = (U_s - U_o)/H = U_o/h_o = U_s/h_s.$$

The wave equation respectively in the stratosphere and the troposphere of this model has the forms

(33)

$$\text{Stratosphere:} \quad \omega'' + (k_s^2 - k^2)\omega = 0$$

$$\text{Troposphere:} \quad \omega'' + [(k_o h_o/z)^2 - k^2]\omega = 0$$

At the tropopause the boundary conditions require continuity of vertical velocity and pressure. Since the density is continuous the latter condition may be replaced by an equivalent condition as follows: the tropopause is a vorticity discontinuity in the basic flow, so any displacement of it represents the addition of the vorticity U' within the areas between its equilibrium level and its displaced position. This vorticity increment is equivalent to a sliding vorticity at the tropopause which, by Stokes theorem, has the value

$$\Delta u = U'\zeta = U_s\zeta/h_s.$$

Here Δ denotes the difference between the values over and under the tropopause, and ζ its vertical displacement. Application of individual time differentiation $D/Dt = U_s\partial/\partial x$, gives

$$\Delta u_x = w/h_s.$$

We have already ignored the compressibility in the dynamic equations (33) so we may write $u_x = -w_s$. Thus, recalling the kinematic condition $\delta w = 0$, we have the combined boundary condition at the tropopause.

$$-h_s \Delta(\ln \omega)' = 1 \tag{34}$$

Returning now to the wave equations in (33), we note that the short waves $L<L_0$ are subcritical in both layers. Their amplitude decreases exponentially in the stratosphere and is non-oscillatory in the troposphere, and therefore none of them can exist as stationary free waves over level ground.

In the intermediate spectral interval $L_0<L<L_s$ the waves are subcritical in the stratosphere and supercritical (oscillatory) below a certain level in the troposphere. So there is at least a possibility for lee-waves in this interval, just as in Scorer's model. The solutions here are

Stratosphere: $\omega = C \exp(-\lambda z)$, $\qquad \lambda = \sqrt{k^2 - k_s^2}$.

Troposphere: $\omega = z^{\frac{1}{2}}[A F_\nu(kz) + B G_\nu(kz)]$. $\qquad \nu \approx h_0 k_0$.

The combined boundary condition at the tropopause (34) gives

$$(\lambda h_s - \tfrac{1}{2})[A F_\nu(kh_s) + B G_\nu(kh_s)] + kh_s [A F_\nu'(kh_s) + B G_\nu'(kh_s)] = 0$$

where the accent denotes differentiation with reference to the argument. If the solution is a free wave over level ground, its boundary condition at the ground is $\omega(h_0) = 0$, or

$$A F_\nu(kh_0) + B G_\nu(kh_0) = 0$$

Elimination of A and B gives the following equation for the determination of the wave numbers of the free resonance waves,

$$G_\nu(kh_0)[(\lambda h_s - \tfrac{1}{2})F_\nu(kh_s) + kh_s F_\nu'(kh_s)] \qquad \lambda = \sqrt{k^2 - k_s^2}. \tag{35}$$

$$= F_\nu(kh_0)[(\lambda h_s - \tfrac{1}{2})G_\nu(kh_s) + kh_s G_\nu'(kh_s)]. \qquad \nu \approx k_0 h_0$$

This equation corresponds to equation (27) in Scorer's model, and may be solved graphically in the same way when the values of the basic parameters are specified. It is fairly clear that the necessary condition for the existence of a resonance wave is that the spectral interval $L_0 \to L_s$ is sufficiently wide. And further, since the zeros of F_ν and G_ν are more widely separated the larger the wind shear, the interval needed to include a free wave must increase with the shear. Wurtele found that a sufficient condition for a lee wave is that the ratio L_s/L_0 exceeds a certain number which is a function of the wind shear (or more precisely a function of $\nu \approx 2\pi h_0/L_0$).

If a free wave exists in the $L_0 \to L_s$ interval, it will appear as a distinct resonance lee-wave down wind from the mountain starting with a lee trough at the mountain. It will be most strongly excited if its wave length is comparable to the effective mountain width. The remaining contribution

to the flow pattern comes mainly from the long wave components $L>L_s$ which are supercritical in the upper layer and hence a continuous spectrum of possible free waves. To attain uniqueness the components whose phase in the upper layer is kx+lz are used, as in Queney's and Scorer's models.

Palm [14] solved (35) graphically for several numerical examples which were chosen to resemble observed conditions over the Sierras on days with well developed lee-waves:

(i) December 18, 1951 (See figures 3.11 and 3.14.) The height of the tropopause above the ground was about 8 km. In the troposphere the wind could be roughly approximated by a constant wind shear with $U_0 = 10$ ms^{-1} at the ground level increasing to $U_s = 50$ ms^{-1} at the tropopause. The average tropospheric lapse rate was about 7° per km. These values give

$$L_s = 15 \text{ km}, \qquad L_0 = 6 \text{ km}, \qquad h_0 = 2 \text{ km}, \qquad \nu = 2.1.$$

The L_s-L_0 interval is just wide enough to include a resonance wave. The graphical solution of (35) gave $L_r = 14.7$ km which is near the upper end of interval. This agrees rather well with the wave-length of the observed lee-wave which was a little longer (between 15 and 16 km). The lee-wave was strongly developed from early morning till late afternoon, with vertical velocities in excess of 15 ms^{-1}. It persisted with considerable intensity well into the stratosphere. One sailplane rose to 11.5 km above the valley floor at about 10 a.m., and another to 10 km at 4 p.m. The strong development was probably caused by the combination of two effects: (a) The resonance wave length is comparable to the "effective" width of the Sierra profile (see figure 12.3) and is therefore excited to considerable amplitude. (b) The resonance wave length is very close to the critical wave length in the stratosphere, so $\lambda = \sqrt{k^2-k_s^2}$ is very small. The amplitude therefore decreases very slowly with height in the stratosphere. The contributions from the supercritical components near L_s may also be quite significant in this case, particularly in the stratosphere where their amplitude is independent of height. A model with the same wind distribution and stronger stability in the troposphere has a smaller value of L_0 and therefore a wider L_s-L_0 interval. For example, a lapse rate of 5° per kilometer gives $L_0 = 4.4$ km, and the resonance wave length is $L_r = 13.3$ km, well inside the interval.

(ii) January 30, 1952. (See figures 3.22 and 3.24) The tropopause was also on this day located about 8 kilometers above the floor of the Owens Valley. The wind increased from $U_0 = 7$ ms^{-1} at the ground level to $U_s = 30$ ms^{-1} at the tropopause, and the average lapse rate was about 7° per km. These values give

$$L_s = 9 \text{ km}, \qquad L_0 = 5 \text{ km}, \qquad h_0 = 2.4 \text{ km}, \qquad \nu = 3.1.$$

Again the L_s-L_0 interval is just wide enough to include a free resonance wave, namely $L_r = 8.8$ km. As shown in figure 3.22, the observed resonance wave consists of a well developed train of lee waves extending down wind from the Sierra crest with nearly uniform wave length and amplitude. The observed wave length is about 8 km, which again agrees very well with the value predicted by the theoretical model. The observed amplitude is smaller than on December 18, probably because the resonance wave is

so much shorter than the effective width of the mountain.

(iii) February 16, 1952. (See figures 3.28 and 3.30) The 2100Z-sounding from Merced shows the tropopause at 9 km above the Owens Valley floor with a temperature lapse rate of 7.3° per kilometer in the troposphere. The ra-wind sounding at Merced shows a practically uniform wind shear of 6.6 ms^{-1} per kilometer as far as it went. Extrapolation upward with the same shear gives the wind speed U_s = 67 ms^{-1} at the tropopause. The speed at the level of the Owens Valley is U_o = 7.7 ms^{-1}. These values give a model with

$$L_s = 20 \text{ km}, \quad L_o = 4.9 \text{ km}, \quad h_o = 1.2 \text{ km}, \quad \nu = 1.4.$$

The $L_s \rightarrow L_o$ interval is rather wide, but not wide enough to include a free resonance wave since the value of ν is so small in this case. Equation (35) is not satisfied for any wave in the interval. The linear extrapolation of the wind profile in the upper troposphere probably gives an overestimate of the wind at the tropopause. The analysis of the geostrophic wind field and the thermal wind on the upper level maps suggests a much smaller wind shear as indicated by the dotted extrapolation of the wind profile in figure 3.30. This extrapolation gives U_s = 50 ms^{-1} and a smaller value for the mean tropospheric wind shear, so we get a model with

$$L_s = 15 \text{ km}, \quad L_o = 4.9 \text{ km}, \quad h_o = 1.6 \text{ km}, \quad \nu = 2.1.$$

The model is in fact rather similar to that of December 18 in (i). But (35) gives no free resonance wave in this case. The observed flow pattern in figure 3.28 shows a strongly developed lee-wave with a wave length of 21 km. According to the interpretation of the theoretical two-layer model this wave can not be a distinct resonance wave which is repeated periodically downstream. Rather it must be the resultant of a continuous spectral band of supercritical wave components with $L > L_s$. Since the critical wave length is nearly the same as the effective width of the Sierra profile in this case (see figure 12.3), we should expect that the shortest of the supercritical components near L_s are most strongly excited. The observed flow pattern agrees rather well with this interpretation. We also note that the amplitude of the observed wave persists with practically undiminished intensity at high levels, which is a feature characteristic of the supercritical wave components.

6. Multiple-layer model with constant stability and constant wind shear in each layer (Palms model). - Let the interfaces be labeled consecutively upwards by the numbers n = 1, 2, 3. .. As in the earlier models n = 0 represents the ground level. Let U_n denote the speed at the n^{th} interface γ_n the constant temperature lapse rate in the layer above it, and H_n the thickness of this layer. The F-parameter is discontinuous at the interface because of the change in lapse rate. Its value on the upper side of the n^{th} interface is

$$F_n = \sigma_n g / U_n^2 = k_n^2 .$$

The wind at the level z in the layer above is

$$U = U'z = U_n(z/h_n),$$

with z measured from a reference level at the depth h_n below the n^{th} interface where the speed of the extended layer is zero. (This reference level is different for each layer.) The corresponding F-parameter in the layer, as in (29), is

$$F(z) = \alpha_n g/U_n^2 \, (h_n/z)^2 = (k_n h_n/z)^2$$

and, as in (30), the wave equation is

$$\omega'' + [(k_n h_n/z)^2 - k^2]\omega = 0$$

which has the general solution in (31), namely

$$\omega = z^{\frac{1}{2}}[A_n F_\nu(kz) + B_n G_\nu(kz)] \tag{32}$$

with

$$\nu^2 = (k_n h_n)^2 - \tfrac{1}{4} \approx (k_n h_n)^2.$$

The sliding vorticity at the n^{th} interface is

$$\Delta u = - \zeta \Delta U' = -\zeta(U_n/h_n - U_{n-1}/h_{n-1})$$

where again Δ denotes the difference between the values over and under the interface. Application ofindividual time differentiation and subsequent substitution of $u_x = -w_z$ gives the boundary conditions at the n^{th} interface

$$\begin{gathered} -(h_{n-1} + H_{n-1})\,\Delta(\ln \omega)' = 1 - (h_{n-1} + H_{n-1})/h_n \\ \Delta\omega = 0. \end{gathered} \tag{36}$$

When the difference Δ is evaluated, it must be remembered that different reference levels z = 0 are used in the solutions (32) above and below the interface if the wind shear is discontinuous at the interface. In the upper solution the n^{th} interface lies at $z = h_n$. In the lower solution it lies at $z = h_{n-1} + H_{n-1}$.

In an n-layer model there are two boundary conditions (36) at each of the n-1 interfaces. These together with the boundary conditions at the ground and at infinity give a system of 2n homogeneous linear equations for the determination of the 2n constants A_n, B_n in the n solutions (32). The vanishing of the determinant of this system gives the equation which determines the wave numbers of the free resonance waves, if any.

Any observed distribution of stability and wind along the vertical may in principle be approximated as accurately as desired by choosing a sufficient number of layers. However, the equation which determines the resonance waves must be solved graphically, and the numerical labor becomes almost prohibitive for a model with too many layers.

As a first test of the multiple layer model above, Palm considered

a four layer approximation of the situation on December 18, 1951, the situation which was compared with the two layer model in example (i) in the preceding section. The 0700 P - sounding at Merced (Fig. 3.14) shows a pronounced inversion layer a short distance above the mountain crest. This appears to be a rather typical feature of situations with lee-waves in the Sierras. To take account of it, the troposphere was represented by the following three layers:

Bottom layer:	$H_0 = 1.5$ km,	$\gamma_0 = 8^\circ$ km^{-1},
Inversion layer:	$H_1 = 0.5$ km,	$\gamma_1 = -5^\circ$ km^{-1},
Third layer:	$H_2 = 6$ km,	$\gamma_2 = 7.8^\circ$ km^{-1}.

These give the average temperature lapse rate 7° per kilometer for the entire troposphere which was used in the two layer model. The model is otherwise the same as the earlier two layer model. The dynamic parameters at the bottom of each layer are

$h_0 = 2$ km,	$L_0 = 7.4$ km,	$\nu_0 = 1.6$
$h_1 = 3.5$ km,	$L_1 = 4.7$ km,	$\nu_1 = 4.7$
$h_2 = 4$ km,	$L_2 = 13.3$ km,	$\nu_2 = 1.8$
$h_s = 10$ km,	$L_s = 15$ km,	$\nu_s = \infty$.

For $L<L_s$ the solution is $\omega = \exp(-\lambda z)$ in the stratosphere, and it is given by (32) in each of the three tropospheric layers. The combined boundary condition at the troposphere is $-h_s\delta(\ln \omega)' = 1$, as in (34). At the two tropospheric interfaces bounding the inversion layer, since the wind shear is continuous, the boundary conditions are $\Delta\omega = 0$ and $\Delta\omega' = 0$. For a free wave the boundary condition at the ground is $\omega(h_0) = 0$. These give six homogenous equations which determine the constants A_n, B_n of the solutions (32) in the three tropospheric layers. The vanishing of the determinant of the system determines the wave number of the free resonance wave. Solving this equation graphically, Palm found $L_r = 13.3$ km. We recall that this is the same as in the two-layer model if the average tropospheric lapse rate is changed from 7° to 5° per kilometer. The inversion layer appears in this respect to have the same dynamic effect as an increase of the tropospheric stability.

Palm tried out a further improvement of this four level model by assuming that the wind decreases linearly with height in the stratosphere. Since no wind observations were available from the stratosphere on December 18, 1951, he arbitrarily chose a wind shear of -2.5 ms^{-1} per kilometer, that is, one half of the tropospheric value. Aside from this feature the model was the same as the four level model above. The solution of the wave equation is now given by (32) in all four layers. The reference level $z=0$ for the three tropospheric solutions is at the depth $h_0 = 2$ km below the ground as before. For the stratospheric solution the reference level is 20 kilometers above the tropopause and $\nu_s = 8.3$. If a smaller wind shear had been chosen the reference level would be higher up and ν_s would be larger (beyond the range of Morgan's tables). The solution has an oscillatory singularity at the reference level where the basic flow is zero. The supercritical wave components $L>L_s$ remain oscillatory all the way down

to the tropopause. But the subcritical wave components become non-oscillatory some distance above the tropopause.

The vorticity discontinuity at the tropopause is 50% greater in this model, so the boundary condition is now $-h_s\Delta(\ln \omega)' = 1.5$. The other boundary conditions are the same as before. The graphical solution of the equation which determines the free resonance waves gave two values, namely a subcritical resonance wave with $L_x = 13.2$ km and a supercritical resonance wave with $L_x = 20$ km. The first is the same as in the four layer model without shear in the stratosphere. The supercritical resonance wave is due to the stratospheric wind shear. The continuous spectrum of supercritical resonance waves in the models with constant wind in the stratosphere is replaced by one single supercritical resonance wave in this model with decreasing wind in the stratosphere.

Palm evaluated the contribution to the resultant flow over the Sierras from these two resonance waves if the Sierra profile is approximated by the curve

$$\zeta_o = -(h/\pi)\tan^{-1}(x/a), \tag{37}$$

which represents a smooth downwind slope from a plateau to a level plain. A rough fit of the Sierra profile was obtained by choosing for the height of the plateau h = 2 km, and the effective "width" of the slope $2\pi a = 6$ km, (see Figure 12.3). The vertical velocity down this mountain slope is

$$w_o = U_o\frac{\partial \zeta_o}{\partial x} = -\frac{U_o h}{\pi a}\left[1 + \left(\frac{x}{a}\right)^2\right]^{-1} \tag{38}$$

which has the Fourier integral representation in (23). The wind speed at ground level on December 18, 1951 was about 10 ms^{-1}, which gives a maximum vertical downdraft half way down the slope (at x=0) of about 7 ms^{-1}. The contribution to the vertical velocity from the two resonance waves is shown in Fig. 12.5, reproduced from Palm's report. The short wave dominates at low levels. It starts with a lee trough half way down the slope and has maximum vertical velocities in excess of 6 ms^{-1} about one kilometer above the mountain top. This is the region where the maximum vertical updraft was encountered on the sailplane flight 2006 at the time 0900-1200P, see Figure 3.11. But the observed vertical velocities were much greater than the values predicted by the theoretical model. The long supercritical resonance wave predominates at higher levels, which also seems to agree in a qualitative way with the observed flow. But again the vertical velocities in the model are much smaller than the observed values.

Palm did not evaluate the contribution to the resultant flow pattern from the remaining part of the spectrum, the Fourier integral being too complicated. The main function of this remaining part of the field is to remove the discontinuity in Fig. 12.5 along the vertical at x = o and give the appropriate downdraft in (38) along the mountain slope. It is rather unlikely that this part of the field would help to account for the discrepancy between the observed and predicted values of the vertical velocity amplitude. A more plausible explanation may be that the curve in (37) is a poor approximation of the Sierra profile. We have already noted that the amplitude of the resonance wave is most strongly excited

when its wave length is comparable to the effective mountain width. It would therefore be of interest to repeat Palm calculation for a profile with a wider slope, say $2\pi a = 12$ km.

Palm evaluated the contribution to the pressure perturbation from the two resonance waves. He found a maximum amplitude of 1.2 millibar at the ground with low pressure under the streamline troughs and high pressure under the crests. The pressure field has a nodal plane at the level of maximum vertical velocity and the horizontal pressure gradient is reversed above this level with low pressure at the streamline crests and high pressure at the troughs. This is of course in agreement with the general results derived earlier in chapter 9. If the amplitude of the resonance wave is augmented by a factor of 3 so as to bring it up to the observed value, the maximum pressure amplitude becomes 3.6 millibars which would mean maximum altimeter errors of about ±30 meters in this very strong lee-wave. This agrees with other numerical estimates of the altimeter errors in chapter 9.

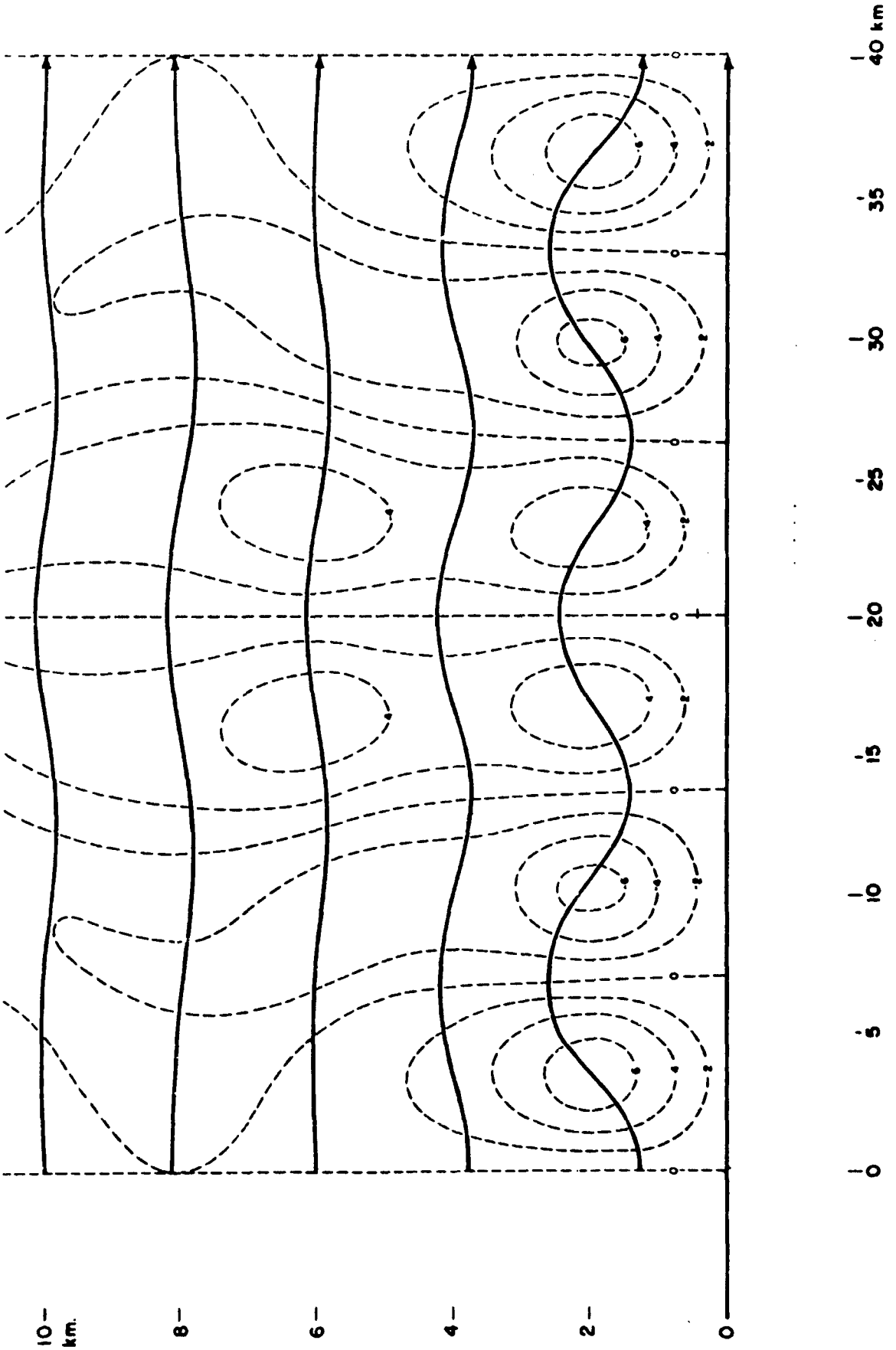

Fig 12.5. The vertical velocity field due to resonant waves and the resultant streamline field. (Units of w: meters/sec.) (Palm)

REFERENCES

1 Kelvin (1886): "On stationary waves in flowing water." Phil. Mag. (5), 22 353-357, 445-452, 517-530.

2 Rayleigh (1883): "The form of standing waves on the surface of running water." Proc. London Math. Soc., 15, 69-78.

3 Lyra, G. (1943): "Theorie der stationären Leevellen-strömung in freier Atmosphäre," Zeit. f. ang. Math. u. Mech, 23, 1-28.

4 Queney, P. (1947): "Theory of perturbations in stratified currents with application to air flow over mountain barriers," The University of Chicago Press, Misc. Report No. 23.

5 Höiland, E (1951): "Fluid Flow over a corrugated bed," Appendix A, Fifth Progress Report, Contract No. AF 19(122)-263. Air Force Cambridge Research Center, Cambridge, Mass.

6 Wurtele, M. (1953): The initial value lee wave problem in an isothermal atmosphere," Scientific Report No. 3, Sierra Wave Project, Contract No. AF 19(122)-263. Air Force Cambridge Research Center, Cambridge, Mass.

7 Palm, E. (1953): "On the formation of surface waves in a fluid flowing over a corrugated bed and on the development of mountain waves," Astrophysica Norvegica, Vol. V, No. 3.

8 Eliassen, A. and Palm, E. (1954): "Energy flux for combined gravitational sound waves," Institute for Weather and Climate Research, Oslo, Publ. No. 1.

9 Queney, P. (1948): "The problem of air flow over mountains: A summary of theoretical studies," Bul. Am. Met. Soc. 29, 16-26.

10 Hoinkes, H. (1950): "Föhnentwicklung durch Höhentiefdruckgebiete," Arch. Meteor. Geophys. u. Bioklimat., ser. A, vol. 2, No. 1, 82-96.

11 Bjerknes, J. (1956): "Dynamic Meteorology and Weather Forecasting, Chap. 16." Carnegie Institution, Waverly Press, Baltimore.

12 Scorer, R.S. (1949): "Theory of waves in the lee of mountains," Quart. J. Royal Met. Soc. Vol. 75, 41-56.

13 Wurtele, M. (1953): "Studies of lee waves in atmospheric models with continuously distributed static stability," Scientific Report No. 4, Contract No. AF 19(122)-263, Air Force Cambridge Research Center, Cambridge, Mass.

14 Palm, E. (1955): "Multiple layer mountain wave models with constant stability and shear," Scientific Report No. 3, Contract No. AF 19(604)-728, Air Force Cambridge Research Center, Cambridge, Mass.

15 Zierep, J. (1952): "Leewellen bei geschichteter Anströmung," Ber. Deutsch. Wetterd. U.S. Zone, No. 35, 85-90.

16 Morgan, S.P. (1947): "Tables of Bessel functions of imaginary order and imaginary argument," California Institute of Technology, Pasadena.

17 Holmboe, J. and Klieforth, H. (1954): Final Report, Contract No. Af 19(122)-263, Air Force Cambridge Research Center, Cambridge, Mass.

APPENDIX A

REDUCTION OF TRACKING DATA

Photo-theodolite tracking data.

Summary. It was the reduction of the tracking data which posed the biggest obstacles to the project and upon which the greatest effort was expended. The attempts to derive useful space positions from the tracking data extended over a period of four years (1951-1955). The many failures and frustrations which preceded eventual success were due primarily to the inherent complexity and novelty of the task, aggravated by a series of unfortunate developments. It had been hoped that the first test flights over the Naval Ordnance Test Station (N.O.T.S.) rocket range near Inyokern in early 1951 would provide a basis for comparison of relative accuracy between Mitchell and Askania photo-theodolites but the Askanias were never used. The later flights of Phase I over the Owens Valley in March and April 1951 were intended in part to furnish data for a sample reduction routine which could be tested and necessary improvements in the techniques completed before the start of the 1951-2 season; the first attempt failed and further efforts were discontinued with the withdrawal of N.O.T.S. from active participation in the Project because of the demands of more urgent research. The loss of the Navy's assistance in data reduction was a serious one since they possessed all the experience and technical knowledge needed for evaluating the tracking data. Later when the computing task was undertaken by the Institute of Numerical Analysis at the University of California at Los Angeles (U.C.L.A.), work was interrupted several times for long periods when the tracking network was re-surveyed, when funds were temporarily unavailable, and when the Institute underwent a change of administration from the Bureau of Standards to become a part of the University as Numerical Analysis Research (N.A.R.). The work was resumed in 1954 by project personnel of the Meteorology Department under the guidance of Dr. Thomas H. Southard of N.A.R. Publications of the Aberdeen Proving Ground and of N.O.T.S. on ballistic trajectory computations from tracking data and results of the 1951 sailplane tracking tests by N.O.T.S. were made available to the project in 1954, having been unknown earlier or unavailable as "restricted" information. In the coding of the problem for the SWAC* electronic computer much credit is due Dr. Southard and Mr. James Dowd.

The method proved to be surprisingly complex. In the following sections are described the raw data from the theodolites, how the cameras were timed and oriented, and the system of coordinates chosen. Evaluation began with the measurement of the position of the image on the film. From this, azimuth and elevation angles were determined after a series of corrections had been applied--compensation for tracking errors, instrument errors, curvature of the earth, the reference system, etc. The space positions were then computed from the corrected angles by triangulation. I.B.M. (International Business Machine) punch cards were used for coding the routine and the data, the computations were performed on SWAC, and the final results giving positions and an estimate of their accuracy were printed in tabular form.

---

*All of the high speed computing machines used in the United States have abbreviated names. SWAC stands for Bureau of Standards Western Automatic Computer.

The photo-theodolite. A photograph of one of the three Mitchell photo-theodolites used in the tracking operation is shown with its crew at one of the stations in Fig. A.1. A schematic drawing of the instrument is presented in Fig. A.2, with the lettered parts corresponding to the following nomenclature:

A stationary horizontal wormwheel

B azimuth handwheel

C movable vertical wormwheel

D elevation handwheel

E telescope eyepiece lens

F telescope crosshairs

G telescope prism

H telescope objective lens

I camera filter

J camera lens

K camera light stop

L camera right-angled mirror or prism

N azimuth and elevation indicator unit

O large prism of indicator optical system

lens of indicator optical system

Q small prism of indicator optical system

R camera shutter

S camera film aperture or mask

T film

The instruments were manually operated in tracking the sailplane. The camera was operated electrically by pulses which at regular 5-second intervals recorded photographically on 35 mm film the image of the sailplane and its vicinity and the frame number and the azimuth and elevation indicators of the optic axis of the theodolite. A sample frame of theodolite film is shown in Fig. A.3.

There are three effects of the optical projection of the sailplane image on the film that are briefly noted here and discussed in more detail below. First, since distances on the film represent various angles in the sky while azimuth refers to the horizon, and elevation to great circles through

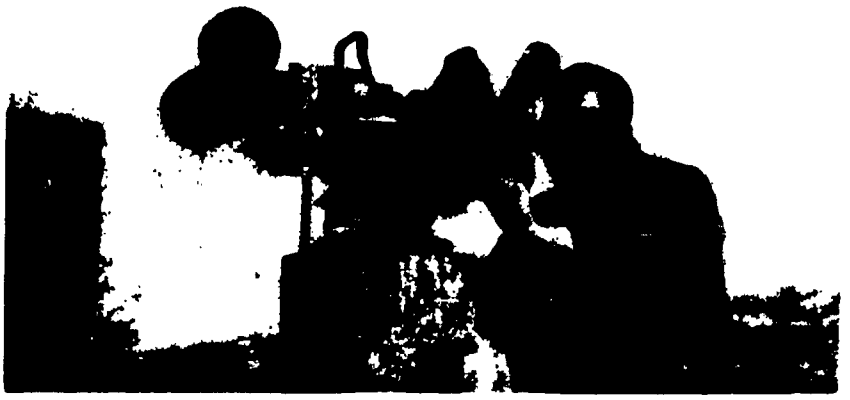

Fig. A.1 - Mitchell photo-theodolite and operator at Ball Park, Independence.

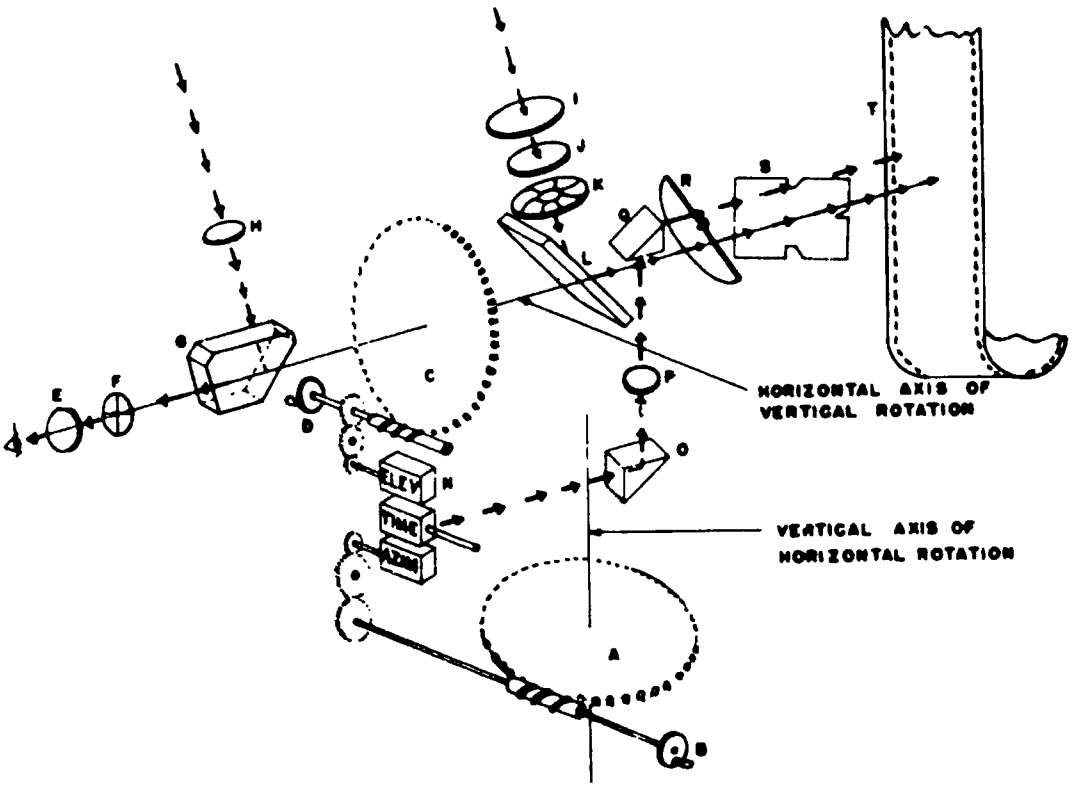

Fig. A.2 - Schematic drawing of Mitchell photo-theodolite.

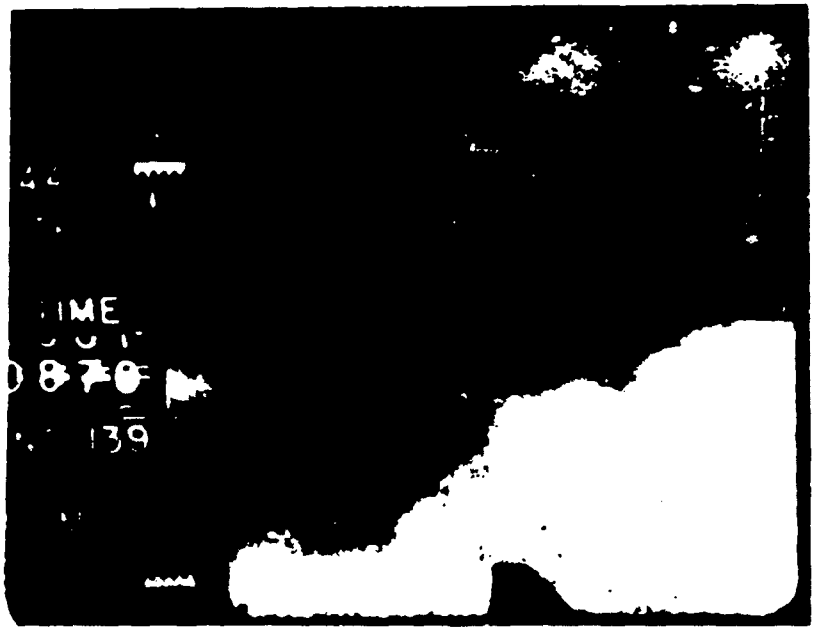

Fig. A.3 - Sample frame of 35 mm theodolite film from flight 2018. Note sailplane (center), and roll cloud.

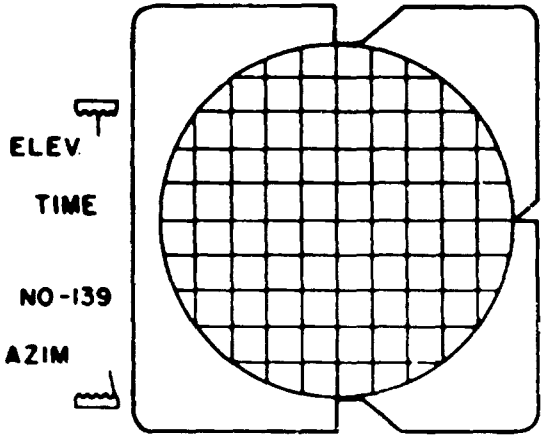

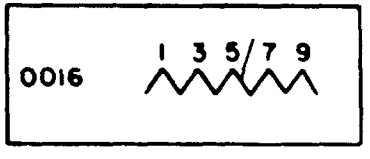

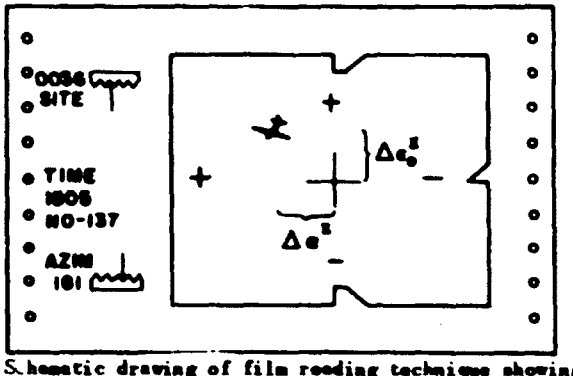

Fig. A.4 - Schematic drawing of film reading technique showing film, grid, sailplane image, dial readings, and unrotated primary tracking corrections.

the zenith, true vertical and horizontal lines with respect to the theodolite were rotated on the film by an amount equal to the elevation angle of the optic axis. Second, "left" and "right" along the true horizontal plane were reversed in the film from their relationship in the sky with respect to the observer. Third, the sailplane which appeared to the observer at some point in the spherical coordinate system of the sky was projected onto the flat plane of the film, thus involving a certain amount of measurable distortion. Consequently, when reading the film and computing the "true" or most probable azimuth and elevation of the sailplane from each theodolite, one had to make allowances and corrections for these effects. These were known as tracking corrections and would all have been obviated had it been possible to keep the sailplane exactly in the center of the crosshairs.

The theodolite network and tracking procedures. On the map in Fig. 1.2 are shown the location of the three photo-theodolites. The station designated Seven Pines (7 P) was at an elevation of 5254 feet, that at the Ball Park (BP) in Independence at an elevation of 3904 feet, and the third at Manzanar (M) at an elevation of 3836 feet. The three stations were connected by wire land lines with each other and with the synchronous-motor timer in the control van at the Manzanar airstrip. Electrical impulses originating at the timer were used to actuate the operating solenoid on each photo-theodolite at 5-second intervals. Intercommunication by radio and telephone was also maintained among the stations for coordination of the tracking effort.

At each of the station sites a stout 16 inch square wooden post was sunk deeply and firmly with its top about 4 feet above the ground (Fig. A.1). Prior to and immediately after the tracking flight, orientation photographs were made at each station by focusing on a signal mirror or light flashed at a reference station in direct line of sight. These recordings of the azimuth and elevation dials were made in both the forward and dumped (reversed) position. From both Ball Park and Manzanar it was possible to see the Seven Pines theodolite and vice versa, so that the operators at the first two made two sets of orientation readings for each flight while the crew at Seven Pines made four sets; the reference station for Seven Pines was Ball Park. Films were identified by flight, date, and station.

During the tracking run, time correlation was maintained by periodic "blackouts" which were effected simultaneously at each station on a count-down from the flight control by placing an object over the telescope lens of the camera.

Some failures and errors of the photo-theodolite tracking method. The limitations and qualifications in the use of photo-theodolites were many, and ranged in order of magnitude from those unfortunate catastrophes and unforeseen circumstances that prevented the securing of any useful data and nullified the entire flight to certain errors which were either so small that they could be neglected or were of such a random and indeterminate nature that they could not be corrected for. Between these extremes in limitations were some errors, many of which were rather large, which could be corrected for in a satisfactory manner. The various defects in these three groups will be considered briefly here.

Of the gross mechanical failures that prevented tracking coverage of whole flights or parts of flights, one that was quite common was the failure

of pulses at one or more of the stations. These were usually a result of the land lines having been severed by predators or by snow removal equipment. Another common reason for no theodolite tracking data, and the only cause not preventable, was the obscuring of the target by intervening clouds or blowing dust. A few operations had to be cancelled for this reason while on many others, parts of the flight paths could not be tracked. Later in the season installation of the electronic "Raydist" system served to overcome these gaps. While black and white film was used generally in the theodolite cameras, color film was employed on the last several flights of the season. It had an advantage over black and white film in making it easier for the film reader to locate the orange sailplane against the sky or clouds, but the serious disadvantage that the dials photographed indistinctly and for large portions of some flights were unreadable. Also a real disaster and cause for anguish occurred when a rather important flight was nullified because the color film was ruined by incorrect processing. The inability of the theodolite operators to remain on target at all times, especially when the sailplane was near the direction of the sun from the station or at low angles, was responsible for some gaps in the theodolite tracking data. Finally, some infrequent "stuttering" of the pulsing mechanism and the consequent exposure of more than twelve frames per minute caused some data to be discarded.

Certain errors which were peculiar to each instrument or which were dependent on the mounting of the theodolite for each flight could be effectively measured and corrected for. These were:

1) Lens collimation correction. This was a constant error of the optical parts of the instrument which affected the measurement of the image on the film. Because of a certain lack of alignment of the optical parts, the "base of the film"--where the film was intersected by the line through the rear nodal point of the lens--did not quite coincide with the center of the frame as defined by the cross hairs imprinted on the film by a pressure plate in the camera and defined by the notches of the mask. These errors were determined from the forward and dumped orientation measurements. The vertical term was a constant correction to elevation while the horizontal term was a varying but systematic correction to azimuth.

2) Zero-point correction in azimuth. The "zero" azimuth reading for both the Ball Park and Manzanar theodolites was along their lines of sight to Seven Pines station while that of the latter was along its line of sight to Ball Park. That this reading was not exactly zero could be corrected from the forward orientation readings in azimuth.

3) Zero-point correction in elevation. Whatever amount the zero reading of the elevation scale was different from that when the instrument was sighted horizontally, was determinable from the orientation readings in elevation corrected for collimation error and the computed elevation of the reference station from survey data taking into account the curvature of the earth and the direction of local gravity.

Those errors which were known to exist or were possible but for which corrections have not been made are listed below. These errors could not be corrected for practically because of their random nature, but they were believed to be small in most cases; all were smaller than estimated film reading errors.

1) Lag or "backlash" occurred when the gears of the wormwheel did not mesh perfectly with those of the counters. Thus the instrument might have moved slightly before the counter moved and this would have given two different readings for the same fixed point depending on the direction of sweep. The occasional difference of one or two mils in the orientation azimuth readings of an instrument suggested this possibility but because of its inconsistencies and infrequency it could also have been caused by a slight "play" in the bolts attaching the metal base to the wooden post. Also a movement of the portable signal light at the reference station by several feet would have caused such a discrepancy.

2) Leveling and gravitational error. Since great care was taken to mount the theodolites by spirit levels and they were believed to be leveled to 0.02 degree (0.35 mil)* maximum error, this systematic but small error was ignored. Variations in the collimation and zero-point corrections to elevation between flights suggest that the leveling error was on the order of ±0.2 mil. This, too, could have been corrected for had there been additional surveyed reference marks for each station. Correlated with the leveling error is the neglect of the variation of the direction of local gravity caused by the proximity of the great rock mass of the Sierra Nevada. Present geophysical data indicate this to be negligible. The corrections for variation of the direction of local gravity associated with the curvature of the earth were made and are treated below.

3) Effect of atmospheric refraction. A correction based on the assumption of a Standard Atmosphere can be applied (McShane, 1942), but calculations have shown this effect to be very small even at low angles which were infrequently recorded. However, since refraction is greatest when sighting along or at a small angle to a temperature inversion, and it is known that lee waves are often associated with a strong inversion which layer partakes of the wave form, it is quite possible that this effect may have been important in certain flights along certain lines of sight. But it could not be solved for, practically, in the routine computations because it depended on knowledge of the temperature field which could only be approximately known after all the sailplane tracking data computations and synthesis had been completed.

Notation. The symbols used below have the following meanings:

α azimuth angle.

α_0 reading of azimuth dial and counter.

α_i corrected azimuth of theodolite i (i = 1, 2, 3)

ε elevation angle.

ε_0 reading of elevation dial and counter.

---

*1600 mils = 90°, or 1° = 17.778 mils.

ϵ_i corrected elevation of theodolite i.

Δa_o^* measured distance on film of sailplane from vertical reference line. + left, - right.

$\Delta \epsilon_o^*$ measured distance on film of sailplane from horizontal reference line. + above, - below.

Δa_o primary tracking correction in azimuth.

$\Delta \epsilon_o$ primary tracking correction in elevation.

Δa final tracking correction in azimuth.

a_T azimuth corrected for tracking error.

ϵ_T elevation corrected for tracking error.

a_R adjusted reference azimuth.

a_T' azimuth measured from reference azimuth, positive clockwise.

A,B,M,N constants for flight or portion of flight.

a_L angle between the reference azimuth of the theodolite and the direction of the origin from the theodolite.

$\overline{a_o}$ azimuth of sailplane from the reference line joining the origin with the theodolite.

c the angle the line joining the center of the earth with the theodolite makes with the line joining the center of the earth with the origin of the reference system.

Δa_c azimuth correction for curvature of the earth.

$\Delta \epsilon_c$ elevation correction for curvature of the earth.

c_a azimuth collimation correction.

c_ϵ elevation collimation correction.

a_L^* angle between the reference line joining the theodolite T_i with the origin O and a north-south reference line from T_i measured in the horizontal plane of O.

ϵ_i elevation corrected for tracking errors, curvature of the earth, and collimation error.

a_i azimuth corrected for tracking errors, curvature of the earth, collimation error, and rotation of the reference line.

O origin of x, y, z coordinate system.

T(X,Y,Z) rectangular coordinates of the theodolite.

P(x,y,z) rectangular coordinates of the sailplane.

$P_i(x_i,y_i,z_i)$	rectangular coordinates of projection of P on ray defined by α_i, ε_i.
a_i,b_i,c_i	direction cosines of ray defined by theodolite.
Z	altitude above mean sea level.
$\underline{r}_i$	vector from T_i to P_i.
r_i	slant range of "sailplane" from theodolite.
$\Delta x_i,\Delta y_i,\Delta z_i$	residual components x_i-x, y_i-y, and z_i-z, respectively, representing the vector between P and P_i.

Film reading and measurement. The films from the photo-theodolites were processed and developed at the Naval Ordnance Test Station, Inyokern. Most of these films were read and recorded by the tracking team in Independence later at U.C.L.A. many of the films were checked and re-read. Reading was done on a Model C Recordak Film Reader. From knowledge of the focal length of the cameras, a circular grid was constructed on a transparent overlay for the viewing screen so that angular distances of the sailplane from the center of the film could be read when the periphery of the grid circle of 50 mils diameter was aligned exactly with the notched references of the projected film frame. This relationship is illustrated in Fig. A.4.

The readings for each frame for each station had five parts: the frame number, the complete azimuth (α_o) and elevation (ε_o) dial readings in mils, and the unrotated primary tracking corrections to these readings ($\Delta\alpha_o^*$, $\Delta\varepsilon_o^*$) consisting of the distances in mils of the sailplane image "right" or "left" and above and below the crosshairs. The grid was scribed in mils and the $\Delta\alpha_o^*$ and $\Delta\varepsilon_o^*$ readings were recorded in mils and tenths of mils, the tenths figure being estimated. The accuracy and reproducibility of the corrections thus depended on the careful adjustment of the film frame and its mask to the grid circle on the screen. The position of the sailplane on the film was defined as the center of the cross formed by the wings and the fuselage.

The azimuth and elevation indicators consisted of two parts which together were the complete "dial" reading. The counter numbers indicated the values in tens of mils while the other part, the sawtooth scale and pointer, indicated mils and tenths of mils. Each tooth represented two mils, so that it could be read to the nearest mil and estimated to the nearest tenth of a mil. Estimated reading accuracy was about $\pm$0.2 mil average. This was attributable not only to the 0.1 mil accuracy in interpolating between lines on the grid but also to the error in alignment of the film mask and the grid, and, perhaps, by slight differences in focal length of the cameras. Reading of the film for the orientation sequences at the beginning and end of each flight required particular care and the accuracies of these readings were probably $\pm$0.1 mil as they were re-read and checked several times. Also, certain selected frames used for sample calculations of positions were treated similarly and read and re-read with extra care.

Recording of data on punch cards. The data for each frame and from each theodolite were recorded on a separate I.B.M. card. On each card were punched 1) an identifying code number giving project, flight, station, and frame numbers; 2) the azimuth and elevation dial readings in mils; and 3) the two tracking corrections in mils. After all the data to be used in position computations had been punched they were listed together with the first and second differences of successive azimuth and elevation dial readings. The latter figures enabled one to detect gross errors caused by 1) misreading the counters--usually by 10 mils as a result of its lag with respect to the pointer; 2) miscounting the sawteeth; 3) wrongly recording the reading, e.g., by transposition; 4) misreading the data sheet; or 5) a mistake in punching.

The reference system. All of the station locations, including the photo-theodolites, the radar set, and the Raydist units, were determined by first-order surveys by the Navy in 1951 and by the U. S. Coast and Geodetic Survey in 1952. The results from the two surveys were quite close; those from the U.S.C.G.S. were used in the computations. The geographic coordinates of the theodolite stations were given to an estimated accuracy of ±1 foot in altitude and ±0.1 foot in latitude and longitude.

The reference system chosen for the reduction problem was one with the origin at a point* in Independence which point was the location of the central unit of the 5-unit Raydist system. A rectangular coordinate system was prescribed such that the (x,y)-plane was tangent to the earth at the origin O with the positive y-axis pointing to true north and the positive x-axis in the east direction. The vertical coordinate z was parallel to the direction of gravity at O.

Geographical constants. In order to compute the space position of the sailplane with respect to the reference system chosen, it was necessary to make appropriate corrections to the measured angles for the effect of the curvature of the earth. This effect can be appreciated upon considering that the theodolites were leveled by spirit levels according to the direction of local gravity, and in the tracking network distances were of the order of five miles. (As an illustration of this, the difference between the absolute values of mutual orientation elevations between 7 P and M was about 2 mils, that from the higher station being the larger since the curvature effect augments a negative angle.) The correction to the measured angles was a varying but systematic one dependent on the constant angle c defined by the theodolite, the center of the earth, and O, and on the azimuth from the station. The accurate computation of c taking into account the eccentricity of the earth's shape is discussed in a special publication of the U.S.C.G.S. (1946). The values for each station are given in Table A.1.

Coordinates of the stations with respect to the origin of the reference system were computed from the U.S.C.G.S. survey results assuming the earth to be a Clark spheroid. Other geographic constants resulting from the definition of the reference system and the geometry of the tracking network and required for the computation problem are certain angles for converting to north-south reference azimuths as defined above in the list of notations and evaluated in the table below.

---

*Latitude 36° 47' 53.935"; Longitude 118° 11' 46.531"; Elevation 3,938 ft.

Table A.1

Station	i	X_i	Y_i	Z_i (ft)
7 P	1	-18,990.943	- 8,629.424	+1305.947
BP	2	- 2,177.706	+ 4,236.982	- 34.639
M	3	+14,779.292	-22,510.819	- 119.056

Station	i	a_L	c	a_L^* (radians)
7 P	1	+0.226,702,7	+0.000,999,9	+1.144,291,2
BP	2	-1.392,351,7	+0.000,228,4	+2.666,829,4
M	3	-0.599,809,3	+0.001,290,9	-0.580,960,1

Determination of flight constants. In order to apply the necessary corrections to the elevation and azimuth dial readings one had to determine the flight constants from the reference readings and assign certain other limits which were prescribed by the geometry of a particular flight. The first group were the flight constants a_R, c_a, and c_ε--the reference azimuth, the collimation error in azimuth, and the collimation correction in elevation, respectively. a_R, c_a, and c_ε were determined from orientation measurements and were constant for each station for each flight. They were computed from the forward (F) and dumped (D) and beginning (B) and end (E) readings in the following manner:

$$\varepsilon = \varepsilon_o + \Delta\varepsilon_o$$

$$a = a_o + \Delta a_o \sec \varepsilon$$

(These were nearly exact since the elevation angles were quite small and hence there was little rotation or distortion of the image on the film.) One computed 4 values of each angle for BF, BD, EF, and ED. The values for ε_{BD} and ε_{ED} were complements as the elevation counter numbers increased as the theodolite was rotated through 180° (3200 mils) or more in elevation to the reversed position.

$$\text{Then } a_R = \tfrac{1}{2}(a_{BF} + a_{EF}) = \bar{a}_F$$

$$c_\varepsilon = -\tfrac{1}{4}(\varepsilon_{BF} + \varepsilon_{EF} - \varepsilon_{BD} - \varepsilon_{ED}) = -\tfrac{1}{2}(\bar{\varepsilon}_F - \bar{\varepsilon}_D)$$

$$c_a = -\tfrac{1}{4}(a_{BF} + a_{EF} - a_{BD} - a_{ED}) = -\tfrac{1}{2}(\bar{a}_F - \bar{a}_D)$$

A further refinement of c_ε to include the zero point correction in elevation was defined by $c_\varepsilon^* = c_\varepsilon + \delta\varepsilon$ where $\delta\varepsilon$ was the difference between the measured reference elevation corrected for collimation error and the angle that should have been measured according to the survey data.

The second set of flight constants A, B, M, and N were required in coding the problem for the SWAC high speed computer so that all angles would be less than 2π radians or 360°. These were also needed to resolve possible ambiguities in the azimuth readings which were in mils. Since 6400 mils corresponded to one revolution in azimuth while the counter readings continued to 9999.9 mils, it was necessary to know whether the instrument approached a given line of sight to the sailplane in a clockwise or a counter-clockwise rotation from the reference azimuth, whether it made more than one revolution in either direction, etc. The constants A, B, M, and N were determined from an approximate plot of the flight path.

Corrections to the measured angles. Many of the necessary corrections to the dial readings--which computations contributed at least half of the complexity to the problem of determining the space positions--have been discussed qualitatively above and are outlined below in terms of their quantitative treatment. They are grouped according to tracking corrections, flight constants, and geometric (geographic) constants. The derivations of these equations are given by Trimble and Weller (1951).

a. The initial (punch card) data. The dial readings ε_o and α_o and the unrotated primary tracking corrections $\Delta\alpha_o^*$ and $\Delta\varepsilon_o^*$ were first converted to radians. In that computation and in all subsequent operations the results were obtained to six decimal places.

b. Tracking corrections. The corrections for the tilt of the true vertical axis on the film were given by the following equations:

$$\Delta\alpha_o = \Delta\alpha_o^* \cos\alpha_o + \Delta\varepsilon \sin\varepsilon_o$$

$$\Delta\varepsilon_o = \Delta\varepsilon_o^* \cos\varepsilon_o - \Delta\alpha \sin\varepsilon_o$$

The smaller effects of converting the position of the sailplane image on the flat plane of the film to its position in the spherical coordinate system of the sky were corrected for by the formulas

$$\tan\Delta\alpha = (\tan\Delta\alpha_o)/\cos(\varepsilon_o+\Delta\varepsilon_o)$$

and $$\alpha_T = \alpha_o + \Delta\alpha$$

$$\sin\varepsilon_T = \sin(\varepsilon_o+\Delta\varepsilon_o)\cos\Delta\alpha_o \quad (0<\varepsilon_T<\pi/2)$$

c. Flight constants. Correction for reference reading:

$$\alpha_T' = \alpha_T - \alpha_R \quad \text{if} \quad A \le \alpha_T - \alpha_R \le B$$

$$\text{otherwise} \quad \alpha_T' = M(\alpha_T - \alpha_R) + N$$

Collimation corrections: c_ε and $c_\alpha/\cos\varepsilon'$ (both added).

d. Geographic constants. Correction to reference line to the origin

$$\bar{\alpha}_0 = \alpha_T' - \alpha_L$$

Correction to N - S reference azimuth: $+ \alpha_L^*$

Corrections for curvature of the earth:

$$\Delta\alpha_c = c \sin \bar{\alpha}_0 \tan \varepsilon_T$$

$$\Delta\varepsilon_c = c \cos \bar{\alpha}_0 \qquad \text{(both added)}$$

e. The corrected angles. The final computations giving the most probable (or best determinable) azimuth and elevation angles measured in the horizontal and vertical planes of the reference system for each frame were:

$$\varepsilon_i = \varepsilon_T + \Delta\varepsilon_c + c_\varepsilon^*$$

$$\alpha_i = \bar{\alpha}_0 + \Delta\alpha_c + \alpha_L^* + c_\alpha/\cos \varepsilon_i$$

where i = 1, 2, or 3 according to whether the station was T P, BP, or M. These equations were specially coded for rapid computation on the electronic computer. A sample calculation for each flight was performed on a hand calculator to check the SWAC routine and the flight constants. In the SWAC computations the decimal data were first converted to binary notation. The flight constants were punched on other cards, coverted to binary form, and inserted in the deck of command cards consisting of the routine and the geographic constants. The values ε_i and α_i were stored for the second phase of the computation, that of obtaining space positions.

Computation of space positions. If there were no errors in measurements, ε_i and α_i would be exact and the determination of the position P(x,y,z) of the sailplane in the reference system could be computed simply and directly from the angles ε_i, α_i of one theodolite and one other angle from another theodolite. In reality, however, there were random errors in the measurements so that the true line of sight and the computed line of sight to the sailplane from each station both lay within a cone-like ray; the computed lines of sight did not intersect in a point except by rare accident. What one wished, then, was to determine the most probable point, a more reliable approximation to the true point, for which a more elaborate computation method was required. The method chosen was one described by Trimble and Weller (1951). The solution is given by two steps:

1. Determine a set of points, one on each of the lines of sight, such that the sum of the squares of the distances from each point determined to every other such point is a minimum.

2. The position of the sailplane is defined by the arithmetic mean of each of the coordinates of the points determined.

As an aid in estimating the reliability of the final result and as a check on the consistency of each theodolite, the residual differences of the coordinates of the point and those on each of the lines of sight were computed.

The procedure for three sets of data was as follows with all computations carried to 6 decimal places:

Given:

$$\alpha_i, \varepsilon_i \qquad (i = 1, 2, 3)$$

$$0 < \alpha_i \leq 2\pi \; ; \; 0 \leq \varepsilon_i \leq \pi/2$$

Computation of direction cosines:

$$a_i = \cos \varepsilon_i \sin \alpha_i$$

$$b_i = \cos \varepsilon_i \cos \alpha_i$$

$$c_i = \sin \varepsilon_i \qquad \text{for } i = 1, 2, 3$$

Computation of $A_{ij} = a_i a_j + b_i b_j + c_i c_j \quad i \neq j$ and $i, j = 1, 2, 3$

thus obtaining A_{12}, A_{13}, and A_{23}.

Computation of $B_i = a_i \left[3X_i - \sum_{j=1}^{3} X_j\right] + b_i \left[3Y_i - \sum_{j=1}^{3} Y_j\right]$

$$+ c_i \left[3Z_i - \sum_{j=1}^{3} Z_j\right]$$ thus getting* B_1, B_2, and B_3.

Solution of the values of the distances r_i from the following set of equations:

$$-2r_1 + A_{12} r_2 + A_{13} r_3 = B_1$$

$$A_{12} r_1 - 2r_2 + A_{23} r_3 = B_2$$

$$A_{13} r_1 + A_{23} r_2 - 2r_3 = B_3$$

Specifically:

$$r_3 = \frac{B_1 (A_{12} A_{23} + 2A_{13}) + B_2 (A_{12} A_{13} + 2A_{23}) - B_3 (A_{12}^2 - 4)}{2 (A_{12}^2 + A_{13}^2 + A_{23}^2 + A_{12} A_{13} A_{23} - 4)}$$

$$r_2 = \frac{2 B_2 - A_{12} A_{13} r_3 + A_{12} B_1 - 2 A_{23} r_3}{A_{12}^2 - 4}$$

$$r_1 = \tfrac{1}{2} (A_{12} r_2 + A_{13} r_3 - B_1)$$

---

*In the computations a scale factor of 25,000 was used to reduce the magnitude of the terms in brackets.

Solution of the set:

$$x_i = X_i + r_i\, a_i$$
$$y_i = Y_i + r_i\, b_i \qquad i = 1, 2, 3$$
$$z_i = Z_i + r_i\, c_i$$

Computation of:

$$x = 1/3 \sum_{j=1}^{3} x_j$$
$$y = 1/3 \sum_{j=1}^{3} y_j$$
$$z = 1/3 \sum_{j=1}^{3} z_j$$

rounding off to one decimal place. The z value is the height above the (x,y) reference plane tangent to the earth at O. To correct for curvature of the earth and to obtain the geometric altitude, Z, above mean sea level, the following corrections were applied:

$$Z = z + 3939.7 + \frac{x^2 + y^2}{41,903,102}$$

For two sets of data, say i = 1, 3, the procedure was:

Given (c_1, s_1) and (c_3, s_3), a_i, b_i and c_i and A_{13} are defined as above

Computation of: $B_1 = a_1(X_1-X_3) + b_1(Y_1-Y_3) + C_1(Z_1-Z_3)$

$$B_3 = a_3(X_3-X_1) + b_3(Y_3-Y_1) + C_3(Z_3-Z_1)$$

Solution of: $-r_1 + A_{13}\, r_3 = B_1$

$$A_{13}\, r_1 - r_3 = B_3$$

by $$r_3 = \frac{B_3 + A_{13}\, B_1}{A_{13}^2 - 1}$$

$$r_1 = A_{13}\, r_3 - B_1$$

x_i, y_i, and z_i were then computed as described above and x, y, and z were computed as means of these with Z determined as above.

For each flight one complete calculation was carried out by hand calculator beginning with the carefully read dial readings and primary tracking corrections for one frame and ending with the space position and residuals. These results were then compared with the same computation made on the SWAC electronic computer. If the results were not the same, the calculations and coded values were checked to locate and correct the errors. A three-dimensional

model of the theodolite tracking system was an aid in studying the relationships of the three rays from the computed position and residuals. Where the latter were large in the sample computation and certain flight constants (c_R, c_a, ε_e^*) were suspected and liable to adjustment, those values were varied experimentally to effect a closer grouping of the points on the rays.

While it required at least one day to compute one space position by hand calculator, the SWAC computations were performed in several seconds per point. Since some of the frames had data from three stations and some from only two stations, a "compare command" was used in the coded routine to allow SWAC to make the proper choice of procedure. The values of x,y,z, and Z and corresponding frame number were listed. By means of an ingenious supplementary coding routine prepared by Dowd, Meteorology Department, U.C.L.A., the residuals, $x_i - x$, etc., were listed in three columns according as they applied to x,y, or z and plotted as numbers i (=1,2,3) according to station. Each number was printed a distance from the center line representing its value plus or minus in units of 5 feet. These differences were quickly and easily graphed, thus providing at a glance the relative accuracy of any position determination.

Evaluation of the reduced data. The overall accuracy of the computations is unknown because of the random errors and the lack of a standard system against which to compare results. However, a very reliable computation of the most probable position and the degree of maximum error involved were obtained by the above procedure. It is reasonable to assume that the probable position of the sailplane so calculated is closer to the indeterminable true value than are the points determined on each ray; certainly this is so in the average. The residuals, then, are extremely conservative as estimates of the accuracy and present the near-maximum error. Large values of the residuals are of the order of 100 feet; some are larger, especially at greater distances from the network. But these are, of course, absolute errors which do not affect the derivatives; the relative errors from point to point are much less and can be nearly eliminated by smoothing. For the horizontal plot of the positions and subsequent determinations of the path and the velocities, the accuracies are entirely satisfactory. For the plot of the altitude in a vertical plane or in a time section, the relative values of Z are generally of sufficient accuracy for most subsequent computations, especially when smoothed curves are drawn, but for certain determinations such as D values, the uncertainty in the absolute value of Z is important and must be considered. The residuals, in all cases, give an estimate of the magnitude of the possible error.

Radar data.

The intended use of radar in the tracking operations was to provide continuity in the measured flight path of the sailplane during those portions of the flights when clouds or dust interfered with optical tracking. It was hoped to have three radar sets as illustrated in Fig. A.5, but only one was provided as there was greater demand for them in military operations elsewhere. Cameras pulsed by the same system of the theodolites recorded the dial readings of time, elevation, azimuth, and slant range. A single radar unit is capable of determining the position in space of an aircraft with a degree of accuracy dependent on the distance of the object and rather more on the recency of the particular model. For any distance from the object tracked, the

Fig. A.5 - Radar unit on the east side of Owens Valley in 1951. The view is toward the east. Mt. Williamson can be seen at the left and the town of Independence on the extreme right. Official photograph, U.S. Navy.

accuracy in slant range was much greater than that in angular measurements of azimuth and elevation. Much difficulty was had by the operators in remaining on target, probably because of the mountainous terrain and the limitations of the model. Perhaps the ineffectiveness of this set could be ascribed to its age. Most of the scanty data obtained when the set was believed to be on target were not useful because the dial readings were indistinct on the film or because the results were doubtful. However, some use was made of the readings recorded manually while tracking the power plane on some of the meteorogram flights. For this reason a brief summary of the reduction procedure is given here.

The notations used are:

t	time
α	azimuth
ϵ	elevation
r	slant range; distance to target along ray described by α and ϵ
s	horizontal distance to target projection in horizontal plane measured along α
H	height above station
h	altitude of station
Z	altitude above mean sea level

Then the required results, knowing the location and reference azimuth accurately, are:

$$s = r \cos \epsilon$$

$$H = r \sin \epsilon$$

$$Z = H + h + \frac{s^2}{41,930,102} \text{ feet}$$

Raydist data.

The Raydist system and data. As a supplement to the theodolite network and as a substitute for unavailable late-model radar sets, a Raydist system was installed in the Owens Valley in January 1952. Raydist is an electronic system consisting of a central recording station, a transmitter carried in the object being tracked, and several receivers placed at various surveyed locations in the tracking region. The central Raydist van was near the Manzanar control van and the five robot units were placed at the locations shown on the map in Fig. 1.2. Signals from the transmitter in the sailplane were received by the five units, pairs of which formed the various baselines. A phasemeter at the master station measured the difference in phase of the signals received at four pairs of receivers and recorded them as sawtooth

traces on a revolving chart. The length of each sawtooth is proportional to the distance travelled by the sailplane along that baseline in the corresponding time interval indicated by the chart; when the sailplane was flying essentially parallel to a baseline the sawteeth were closely spaced and when flying perpendicular to a baseline the trace was essentially a straight line.

During the period from 29 January to 30 March 1952, Raydist was used on 9 tracking flights; some of the data duplicated the theodolite coverage while some of it covered interesting portions of the flight during which the theodolites were off target. The raw Raydist data consist of the brush recordings of sawteeth traces for 3 or 4 baselines, a time-base tracing synchronized with the theodolite pulses to produce "pips" at the same 5-second intervals of theodolite photographs, all supplemented by the notes of the technician in the van giving identity of baselines used, time correlations, approximate positions of the sailplane, power failures, etc.

Reading and measurement of the data. Even more than the reduction of the theodolite data, the Raydist reduction problem required a pioneering approach. Raydist had previously been used for surveying, measuring the speed of ships, and other two-dimensional problems, but was relatively untried in three-dimensional tracking; it had never been used in mountainous terrain or on such an erratic target as a sailplane. The uncertainty concerning the accuracy of this method and the task of deriving and coding a routine for computing space positions were lesser problems than the more basic one of how to obtain relevant numerical data from the brush recordings. Since the Raydist method is based on the measurement of differences, its recordings are relative values or first derivatives and the assignment of absolute values depends upon knowing an initial space position rather accurately.* Hence, one of the limitations of the method is that it is dependent on the results of some theodolite computations and, therefore, the solution of the many Raydist problems had to wait upon the completion of the theodolite computations.

In order to calculate the position in space of the transmitter at a particular time, it was required to know the exact locations of the receivers, the frequency of the transmitter, and a numerical value from each of the four sawteeth traces at the appropriate time. This value consisted of a whole number pertaining to the whole sawtooth and a fractional part determined by the intersection of the time line with the sloping side of the asymmetric sawtooth. The complete figure represented the distance in terms of wave lengths along or parallel to that baseline; the direction of the sloping surface of the tooth indicated whether the sailplane was moving in a positive or negative sense with respect to that baseline. From the values one could obtain slant ranges from each of the receiver stations and eventually the space coordinates with respect to the reference system with its origin at Raydist #1, Independence. Computation of successive positions of the sailplane was dependent on assignment of the correct whole value to the successive sawteeth and the continuity of a distinct trace, i.e., no ambiguity in the identity of an individual tooth because of "noise."

Early attempts to label sawteeth by hand and to compute positions at

*It was attempted to satisfy this requirement by bringing the sailplane to a surveyed reference point on the Manzanar air field at the beginning and end of each flight, but the portion of the Raydist traces recorded at those times were garbled due to the proximity of the terrain.

the Institute of Numerical Analysis (I.N.A.) in 1952-3 failed to give reasonable results. After the completion of most of the theodolite computations in 1954, the Raydist problem was again attacked by the project team. James Dowd undertook to code the routine for computation on SWAC and Robert Cayouette, who had monitored and maintained the Raydist system in the Owens Valley, was hired as a consultant in preparing the routine and in reading the records. By courtesy of the Benson-Lehner Company of Los Angeles, an "OSCAR" (oscillogram analyzer and recorder) data reduction system was loaned to the project. This innovation made possible the recording of the useful Raydist measurements in a very small fraction of the time required by manual methods.

Data chosen for reduction were those for which there was some overlapping with theodolite tracking and for which there was simultaneous sailplane camera data. From several known positions the slant ranges and finally the sawteeth values were computed and the teeth labeled. Often there were disagreements, usually by one count, and those were resolved by choosing the most reliable theodolite fix as the starting point and all teeth labeled consecutively on either side of that time.

Reading was performed by advancing the chart in the "OSCAR" viewer, moving the reference line to the pip marking a theodolite pulse, punching out on the keyboard the "whole count" figures of the sawteeth on each of the four base lines, and, by bringing each of the sloping reference lines of the machine in conjunction with the time and the sawteeth curves, allowing the machine to measure and record the fractional readings. The work proceeded rapidly as the machine automatically recorded the data from the four baselines together with the frame number on a punch card, and simultaneously typed the same information on a sheet of paper for proofreading.

Computation of space positions. The following notation and formulas explain the reduction procedure.

c	speed of transmission = 186,218 miles per second.
f	frequency of signal = 1,742.4 kc.
λ	wave length of the signal = 564.297 feet.
$\lambda/2$	half wave length = 282.148 feet along the baseline.
R_{ij}	phasemeter reading (sawtooth number) along baseline i,j. ($i = 0,1,2,3,4$ and $i \neq j$).
d_{ij}	linear distance (baseline) between two receivers i and j. ($i = 0,1,2,3,4$ and $i \neq j$).
u_{ij}	$= d_{ij} - \lambda R_{ij}$
$P_i(X_i,Y_i,Z_i)$	position of receiver i with respect to receiver 0 at 0 (origin of coordinate system).
$P(x,y,z)$	position of sailplane with respect to 0.

$\bar{x},\bar{y},\bar{z})$ approximate position of sailplane with respect to O.

$= \overline{P_i P}$ = magnitude of position vector (or slant range) of sailplane from receiver i.

baseline to origin O (receiver 0) from station i.

$= \overline{OP}$ = magnitude of position vector of sailplane from origin O.

$= d_i - \lambda R_i = r_i - r_0$.

$\Delta x, \Delta y, \Delta z$ = residuals of $x - \bar{x}$, $y - \bar{y}$, and $z - \bar{z}$.

a_i, b_i, c_i determinants defined in equations below.

With reference to the definition of terms in the above list, the computational steps were:

i. Determination of values R_i from data R_{ij}, the constants λ and d_{ij}, and the geometric constants P_i (X_i, Y_i, Z_i).

ii. $u_i = d_i - \lambda R_i$. (2)

iii. From the law of cosines:

$$(r_i')^2 = (r_0')^2 + (d_i')^2 - 2\, r_0\, d_i' \cos \varphi$$

(where primes indicate projection on the (x,y)-plane), and from the geometry of the problem:

$$r_i^2 = r_0^2 + d_i^2 - 2(xX_i + yY_i + zZ_i)$$

then, from the identity $u_i = r_i - r_0$,

$$xX_i + yY_i + zZ_i + r_0\, u_i - \tfrac{1}{2}\,(d_i^2 - u_i^2) = \Delta F_i$$

If P(x,y,z) were known exactly, i.e., if it represented the true space position of the sailplane, $\Delta F_i = 0$. However, because of inevitable errors in the techniques of measurement, $\Delta F \neq 0$ and the x,y,z values determined in the problem are actually some approximate values $\bar{x},\bar{y},\bar{z}$. So the equation used was:

$$\bar{x}\, X_i + \bar{y}\, Y_i + \bar{z}\, Z_i + \bar{r}_0\, u_i - \tfrac{1}{2}\,(d_i^2 - u_i^2) = \overline{\Delta F_i} \qquad (3)$$

iv. From Maclaurin's Theorem, retaining the first order terms of the series and considering the total differential $dF_i \cong \Delta F_i$:

$$\partial F_i/\partial x\, \Delta x + \partial F_i/\partial y\, \Delta y + \partial F_i/\partial z\, \Delta z = \Delta F_i$$

Now, ΔF_i, Δx, Δy, and Δz exist while $(\bar{x},\bar{y},\bar{z}) \neq (x,y,z)$. Then $\overline{\Delta F_i}$ approximates the change in F_i resulting from addition of increments Δx, Δy, Δz and :

$$(\partial F_i/\partial x)_{\bar{x}}\, \Delta x + (\partial F_i/\partial y)_{\bar{y}}\, \Delta y + (\partial F_i/\partial z)_{\bar{z}}\, \Delta z = \overline{\Delta F_i} \qquad (4)$$

v. Using $\bar{x},\bar{y},\bar{z}$ in (3), solve for $\overline{\Delta F_i}$. The value of $\bar{P}(\bar{x},\bar{y},\bar{z})$ used for the first point is that of a theodolite computation.

vi. In (4) solve for:

$$a_i = (\partial F_i/\partial x)_{\bar{x}} = X_i + u_i\,\bar{x}/r_0$$

$$b_i = (\partial F_i/\partial y)_{\bar{y}} = Y_i + u_i\,\bar{y}/r_0$$

$$c_i = (\partial F_i/\partial z)_{\bar{z}} = Z_i + u_i\,\bar{z}/r_0$$

thus getting four equations with three unknowns in the form:

$$a_i\,\Delta x + b_i\,\Delta y + c_i\,\Delta z = \overline{\Delta F_i}$$

and solving these by the method of determinants.

vii. Then putting $\bar{x} + \Delta x = \bar{\bar{x}}$, etc., the problem beginning with (3) was iterated with $(\bar{\bar{x}},\bar{\bar{y}},\bar{\bar{z}})$ until Δx, Δy, Δz, and $\Delta F_i \longrightarrow 0$. After a sufficient number of iterations the resulting values of x_i, y_i, and z_i were tabulated together with their arithmetic means which values x,y,z were considered to represent the most probable position of the sailplane or nearest possible approximation to the true position. This position was then used as the $\bar{P}(\bar{x},\bar{y},\bar{z})$ for the computation of the next 5-second point, and so on, with a further refinement presently described, to the end of the data.

It was known that there were certain errors in the phasemeter and recording apparatus of the Raydist system that affected the reliability of the recorded data. Further, a possible error in numbering a sawtooth would be propagated through the entire problem thus resulting in serious errors in the positions. Thus it was necessary to have some check on the relative accuracy of the determination as well as some means of correcting for an error in numbering. These requirements made the coding problem especially difficult and involved. Dowd coded an elaborate sub-routine which computed the corrections to be applied to the values R_{ij} in order that $P(x_i,y_i,z_i) \equiv P(x,y,z)$; and applied those corrections to the values R_{ij} of the next 5-second point. The process was repeated for that point, the corrections determined, applied to the next point, etc. The values x,y,z and x_i,y_i,z_i were tabulated together with the flight and frame* number.

Accuracy of results. It was found that the path of the sailplane based on Raydist, and determined by SWAC, differed from that determined by photo-theodolites by 100 to 1000 ft in x or y but by 100 to 3,000 ft or more in Z. It was believed that the large errors in Z were caused by the fact that the hyperboloids, described by the phasemeter readings and treated by the above equations, intersected in a very small angle in the vertical, thus making the determination of Z extremely sensitive to inevitable errors of measurement. Also, the occasional choice of negative values of Z or of an abrupt displacement of the path in the (x,y)-plane appear to be a result of such ambiguities of the computational technique. Gaps in the

*in continuity with theodolite frame numbers for the same flight.

Raydist path appeared where the data could not be recorded because the brush recordings were indistinct. A punching error in the fractional part of the phasemeter (sawtooth) reading resulted in the point being displaced from the smooth curve joining adjacent points and could be corrected for. Where the path was abruptly displaced by 1,000 or 2,000 ft. parallel to itself, the usefulness of the data was relatively unimpaired since it still provided velocity data of a sufficient degree of accuracy. The Raydist data, then, provided two-dimensional* trajectory data that were adequate for position and velocity determination in the (x,y)-plane but not in the vertical plane.

References.

Holmboe, J., and Klieforth, H. (1954): Final Report, Sierra Wave Project. Department of Meteorology, University of California, Los Angeles. Air Force Cambridge Research Center Contract AF 19(122)-263.

McShane, E. (1942): Terrestrial Refraction of Light. Ballistic Research Laboratories Report No. 302. Aberdeen Proving Ground, Maryland.

Southard, T. (1953): Reduction of Sierra Wave Theodolite Data. Numerical Analysis Research, U.C.L.A. 24 pp. (Unpublished).

Sutton, et al (1952): Sierra Wave Raydist Stations. (Coordinates and map of stations locations after N.O.T.S. survey.) BUORD SK 337859, U.S. Naval Ordnance Test Station, Inyokern, China Lake, California.

Titus, J. (1948): Coordinate System for Cine-Theodolite Data. Technical Memorandum RDMA - 30, U.S.N.O.T.S., Inyokern, China Lake, California, 8 pp. (Restricted)

Titus, J., et al (1951): Method of Measurement and Computation to Determine Trajectory Data from Askania Cinetheodolite Records. NAVORD Report 1907, NOTS 433, U.S.N.O.T.S., Inyokern, China Lake, California. 50 pp. (Unclassified)

Trimble, G., and Weller, R. (1951): An Outline of Theodolite Reduction Procedures. Ballistic Research Laboratories Report No. 737, Aberdeen Proving Ground, Maryland. 99 pp. (Restricted)

U.S. Coast and Geodetic Survey (1946): Special Publication 8, p. 93.

U.S. Coast and Geodetic Survey, Department of Commerce (1953): Geographic Positions and Plane Coordinates of Camera Posts and Raydist Stations. (After U.S.C.G.S. survey)

---

*Other useful two-dimensional paths were computed for portions of flights when data from only one theodolite were available. In those cases Z was approximated from the pressure altitude of the airborne measurements and the (x,y)-position computed from that Z and α, ε of the theodolite.

U.S. Geological Survey, Department of the Interior (1951-3): Topographic quadrangles, 15-minute series, scale 1:62,500.

Wilson, C. (1952): Sierra Wave Project. NOTS TM No. 245, U.S.N.O.T.S., Inyokern, China Lake, California. 23 pp. (Restricted)

Wilson, C (1953): Sierra Wave Project Operations 1951-1952. NOTS Technical Memorandum No. 281, U.S.N.O.T.S., Inyokern, China Lake, California. 17 pp. (Unclassified)

APPENDIX B

ALTIMETRY

Introduction.

Appendix B has been added as a background and supplement to Chapter 9. Pressure parameters and the methods of pressure-height computations are discussed with examples. The final section describes the effect of lee waves on radiosonde balloon measurements.

Altimetry.

Standard atmosphere, pressure altitude, and D value. One of the most useful and intuitively satisfying concepts in meteorology is that of a realistic standard atmosphere to serve as a reference for the changing relations among pressure, temperature, and altitude in the vertical. The U.S. Standard Atmosphere is summarized as follows:

Pressure p at mean sea level ($Z_p = 0$) = 1,013.25 mb or 29.92 in.

Temperature T_p at mean sea level ($Z_p = 0$) = + 15°C.

Lapse rate of temperature in troposphere = + 6.5°C per km.

Tropopause at Z_p = 35,332 ft, p = 234 mb, T_p = - 55°C.

Lower stratosphere: T_p = - 55°C (isothermal).

Acceleration of gravity: $g_p = 980.665$ cm sec^{-2} at any ϕ and any Z.

The air is assumed to be a perfect gas, to contain no water vapor, and to be in hydrostatic equilibrium. Pressure altitude, Z_p, is simply the altitude at which a given pressure is found in the U.S. Standard Atmosphere; any pressure is uniquely defined by its pressure altitude and vice versa. A similar one to one relationship exists between standard temperature T_p and either p or Z_p in the troposphere.

Bellamy (1945) has introduced the parameter S*, the "virtual temperature anomoly" defined by

$$S^* = \frac{T^* - T_p}{T_p} \text{ where } T^* = \frac{m_d}{m'} \frac{g_p}{g} T$$

where
m' = molecular weight of air
m_d = molecular weight of dry air
g = acceleration of gravity

By this means the actual height difference or thickness between two isobaric surfaces can be expressed as

$$\Delta Z = (1 + \bar{S}^*)\,(Z_{p_2} - Z_{p_1})$$

Bellamy also introduced the "altimeter correction" or D value defined by $D = Z - Z_p$ to represent the difference between the actual height of a pressure surface at any point in the real atmosphere from its height in the Standard Atmosphere. As such, it is an extremely useful parameter in both meteorological analysis and aircraft flight operations. It simplifies and coordinates three-dimensional pressure analysis: on isobaric charts contour lines of constant Z can be made more meaningful when re-labeled according to their equivalent D values; and in a vertical cross section it is the best representation of the pressure field, contours and isobars both being impracticable. This single parameter, while defining the three-dimensional pressure field, carries in its analyzed pattern of isolines inferences of the temperature and wind fields as well. In this connection the following familiar formulas have been derived by Bellamy:

Hydrostatic equation: $\partial D/\partial Z_p = S^*$ and

$$D_2 - D_1 = \int_1^2 S^*\, dZ_{p_2} = \bar{S}^*\,(Z_{p_2} - Z_{p_1})$$

Geostrophic wind equation: $V_g = -\,(g/2\Omega\sin\varphi)(\partial D/\partial n)_p$

In the horizontal plane or on a constant pressure (isobaric) surface above the friction layer the geostrophic wind blows along the D lines with low values of D to its left (northern hemisphere) and with a speed proportional to the isobaric gradient of D.

In the vertical plane, D increases with height when the mean temperature of the layer is warmer than that of the Standard Atmosphere and decreases with height when the mean temperature of the layer is colder than that of the Standard Atmosphere and at a rate proportional to the difference. Maxima and minima of D in a vertical air column are found where the actual sounding crosses the Standard Atmosphere sounding. The speed of the geostrophic wind component normal to the vertical plane is proportional to the isobaric gradient of D in the plane, and its direction into or out from the plane is determinable from the direction of the isobaric D gradient in the plane.

Two graphs for determining D values from surface and upper air pressure data are shown in Figs. B.1 and B.2. In Fig. B.1 the relationship among surface pressure (p), pressure altitude (Z_p), D value, and altimeter setting (A), at the Bishop Weather Bureau station is plotted in such a way that given any one of the four quantities the other three can be readily found. In Fig. B.2 the D value corresponding to any height of the standard isobaric surfaces can be quickly determined from the coded values of the heights as given in teletype reports.

Gravity variations. At 45° latitude the value of the acceleration of gravity at sea level has been determined equal to 980.616 cm per sec. From the Smithsonian Tables (1951) the following formulas are applicable to the

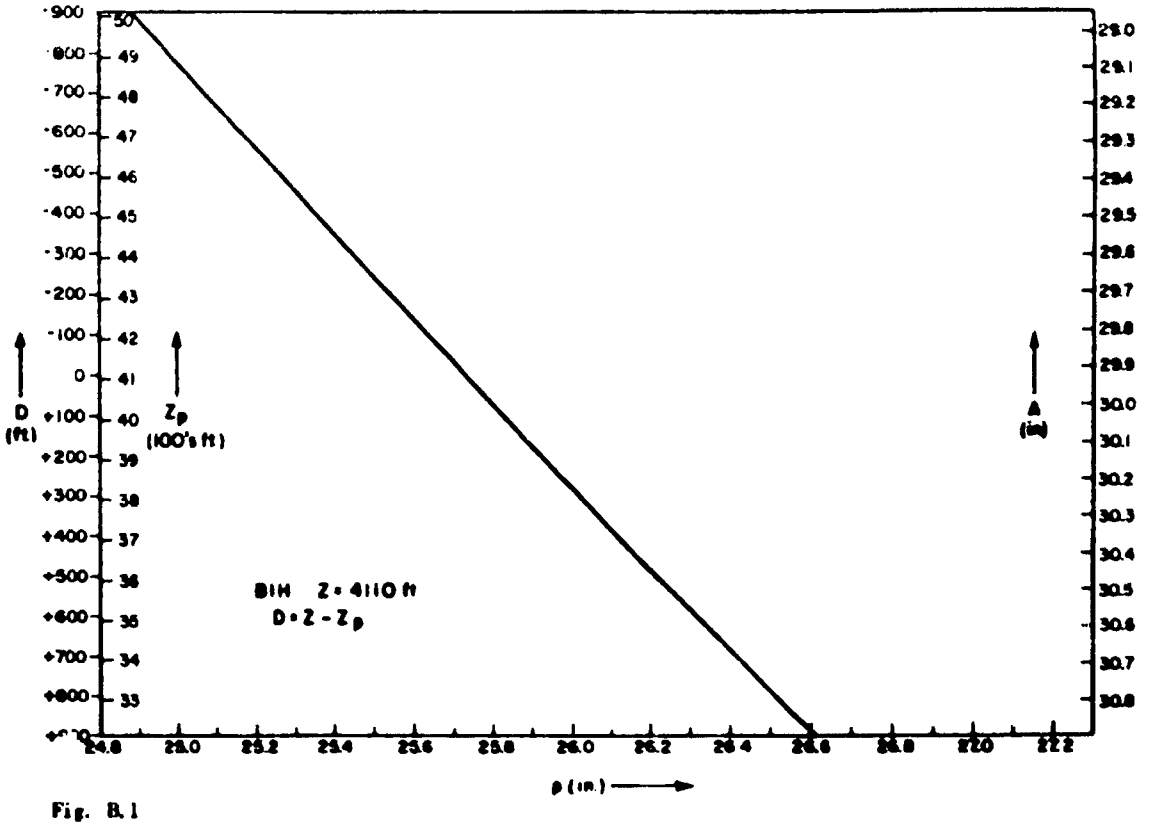

Fig. B.1

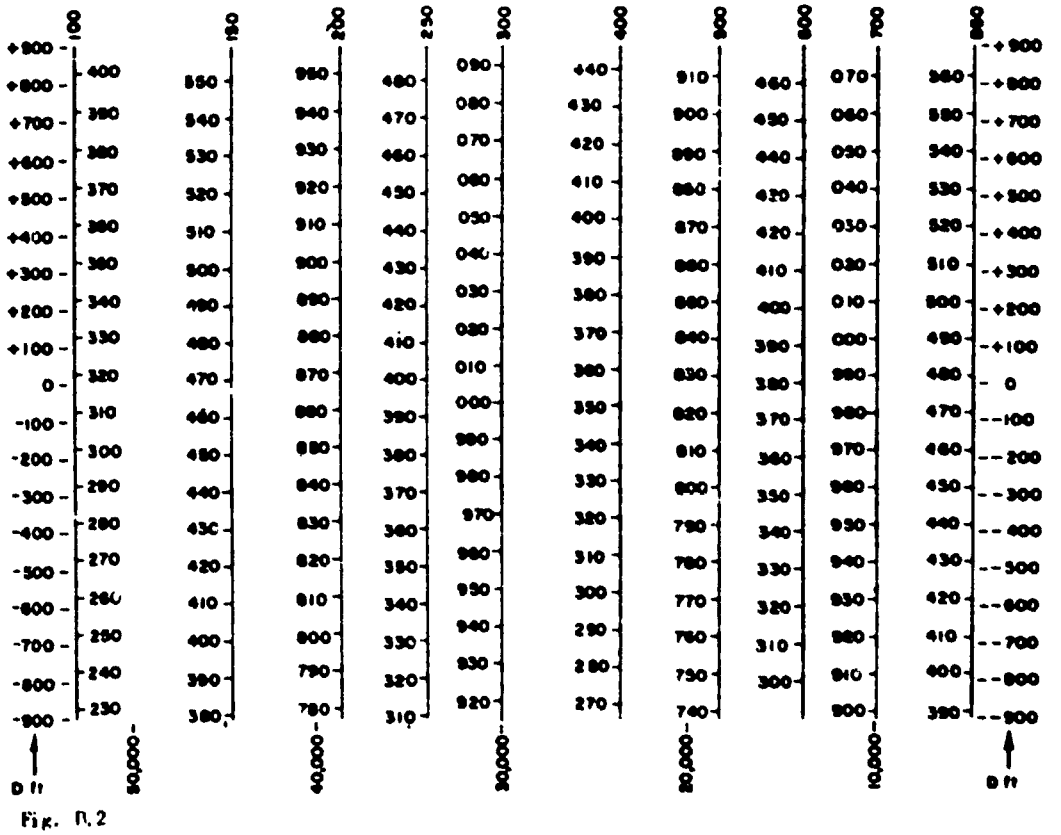

Fig. B.2

In general, $K = R_d/g$ where R_d = specific gas constant for dry air. If g is taken equal to 980 cm s^{-2}, K = 96.09494 geopotential feet per °K.

The use of geopotential units, in which gravity is assumed constant = 980 cm s^{-2} at all latitudes and all elevations, has been adopted by the U.S. Weather Bureau to simplify the calculation of heights from radiosonde data. All contours on upper air isobaric charts are labeled in units of geopotential feet. The relationship between geopotential height and geometric height in meters is given by

$$Z_g = 1/9.8 \int_0^z g \, dz \tag{2}$$

From this equation it can be seen that if g is less than 980 cm s^{-2}, the true (geometric) height is greater than the geopotential height; and if g is greater than 980 cm s^{-2}, the true (geometric) height is less than the geopotential height. As a conservative illustration of this the following relationship, derived from page 222 of the Smithsonian Tables (1951), holds for latitude 37°N, that of the High Sierra region; for comparison purposes, values over the equator and poles are given for the same 5 altitudes:

Table B.1. Geopotential Height vs Geometric Height

	$\phi = 90°$	$\phi = 37°$	$\phi = 0°$
Z_g	Z	Z	Z
gpft	ft	ft	ft
10,000	9,974	10,006	10,023
20,000	19,954	20,022	20,059
30,000	29,944	30,045	30,105
40,000	39,944	40,081	40,158
50,000	49,954	50,125	50,223

Over the United States the differences between geometric and geopotential heights are relatively negligible for all practical purposes, the error due to the variations of g probably being of the same order of magnitude as the error in determining $\bar{T}^*$ from temperature and humidity measurements.

Since pressure altitude in the Standard Atmosphere is actually in terms of a special unit of geopotential (g_p = 980.665 cm s^{-2}) the thicknesses for the Standard Atmosphere are also somewhat different from geopotential (radiosonde) heights and rather more from true (geometric) heights even if the mean temperatures are those of the Standard Atmosphere. To summarize these somewhat trivial differences by means of equation (1) the following formulas are listed:

True or geometric height: $\Delta Z = R_d/g\ \overline{T}^*\ \ln p_1/p_2$

Standard Atmosphere: $\Delta Z_p = R_d/g_p\ \overline{T}_p\ \ln p_1/p_2$

Geopotential or radiosonde: $\Delta Z_g = R_d/9.8\ \overline{T}^*\ \ln p_1/p_2$

The much more important relationship between geometric altitude (or geopotential altitude if g = 980) and pressure altitude can be represented by

(3) $$\Delta Z = (\overline{T}^*/\overline{T}_p)(g_p/g)\Delta Z_p$$

In the real atmosphere the effect of temperature on actual thicknesses between pressure surfaces is far greater than the effect of differences of gravity. Some implications of equations (1), (2), and (3) relevant to aircraft operations and meteorological measurements are:

1. If the true geometric height above sea level of a sailplane or radiosonde balloon were precisely determined by triangulation at latitude 37°N, and altitude 45,000 ft, if furthermore the vertical temperature-pressure sounding from the ground to the sailplane or balloon were precisely known, and if there were no vertical accelerations in the air column, the geometric height would exceed the computed geopotential height by about 102 ft.

2. If in the above example the temperature-pressure curve were exactly that of the Standard Atmosphere the geopotential altitudes and the pressure altitude would be nearly equal (±2 ft) at all levels while the geometric altitude would exceed them by the amounts in Table B.1. Thus the D value at 45,000 ft determined by a tracked radiosonde balloon would be either 0 or +102 ft, depending on whether Z_g or Z were used. (In general practice it is Z_g that is used.)

3. Neglecting the small difference between true gravity and a standard gravity, in equation (3), if the mean temperature of the air column between two isobaric surfaces is warmer (colder) than that of the Standard Atmosphere the geometric or geopotential distance or thickness between those two surfaces is greater (less) than that of the Standard Atmosphere by the same proportion as the respective mean temperatures.

Effects of lee waves on radiosonde ascents. If a radiosonde balloon were released from the east slope of the Sierra into the streamline and temperature fields of a strong lee wave, it would encounter successively a downdraft, a trough, an updraft, a crest, a downdraft, and so on, while generally rising and drifting downstream. The resulting "sounding" would be subject to misinterpretation if considered to be vertical. To see this, one can imagine that in its traverse of the downdraft region the balloon will encounter each successive θ surface at a lower altitude until it reaches the trough and, consequently, the θ ascendant is exaggerated so that the "sounding" appears more stable than is any true vertical sounding in the wave flow. In the balloon's traverse of an updraft region, the reverse is true; each successive θ surface is encountered at a higher altitude until the crest is reached and the "sounding" appears nearer to the adiabatic lapse rate than any true vertical sounding in the flow. The computation of heights of pressure surfaces from these data, however, leads to values which are conservative with respect to those which would result from vertical soundings in either a trough or crest, and therefore would not differ greatly from those of nearby (upwind) stations in undisturbed flow.